THERMOKARST DYNAMICS IN CENTRAL-EASTERN BERINGIA

Insights from permafrost and lacustrine sediment cores

JOSEFINE LENZ *DISSERTATION, November 2016*

ALFRED-WEGENER-INSTITUT
HELMHOLTZ-ZENTRUM FÜR POLAR- UND MEERESFORSCHUNG

Erd- und Umweltwissenschaften
Universität Potsdam

Alfred-Wegener-Institut Helmholtz Zentrum für Polar- und Meeresforschung,
Sektion Periglazialforschung

Universität Potsdam, Institut für Erd- und Umweltwissenschaften

---

Thermokarst dynamics in central-eastern Beringia

– Insights from permafrost and lacustrine sediment cores –

DISSERTATION
zur Erlangung des akademischen Grades
"doctor rerum naturalium"
(Dr. rer. nat.)
in der Wissenschaftsdisziplin Geologie

als publikationsbasierte Arbeit
eingereicht an der
Mathematisch-Naturwissenschaftlichen Fakultät
der Universität Potsdam

von
Josefine Lenz

Eingereicht am 16. Juni 2016
Verteidigt am 25. November 2016

Potsdam

Published online at the
Institutional Repository of the University of Potsdam:
URN urn:nbn:de:kobv:517-opus4-101364
http://nbn-resolving.de/urn:nbn:de:kobv:517-opus4-101364

Für Jakob.

The world can tell us everything we want to know.
The only problem for the world is
that it doesn't have a voice.
But the world's indicators are there.
They are always talking to us.

Quitsak Tarkiasuk, Ivujivik
(1997 Canadian Arctic Resources Committee)

Table of contents

Abstract

Widespread landscape changes are presently observed in the Arctic and are most likely to accelerate in the future, in particular in permafrost regions which are sensitive to climate warming. To assess current and future developments, it is crucial to understand past environmental dynamics in these landscapes. Causes and interactions of environmental variability can hardly be resolved by instrumental records covering modern time scales. However, long-term environmental variability is recorded in paleoenvironmental archives. Lake sediments are important archives that allow reconstruction of local limnogeological processes as well as past environmental changes driven directly or indirectly by climate dynamics. This study aims at reconstructing Late Quaternary permafrost and thermokarst dynamics in central-eastern Beringia, the terrestrial land mass connecting Eurasia and North America during glacial sea-level low stands. In order to investigate development, processes and influence of thermokarst dynamics, several sediment cores from extant lakes and drained lake basins were analyzed to answer the following research questions:

1. When did permafrost degradation and thermokarst lake development take place and what were enhancing and inhibiting environmental factors?
2. What are the dominant processes during thermokarst lake development and how are they reflected in proxy records?
3. How did, and still do, thermokarst dynamics contribute to the inventory and properties of organic matter in sediments and the carbon cycle?

Methods applied in this study are based upon a multi-proxy approach combining sedimentological, geochemical, geochronological, and micropaleontological analyses, as well as analyses of stable isotopes and hydrochemistry of pore-water and ice. Modern field observations of water quality and basin morphometrics complete the environmental investigations.

The investigated sediment cores reveal permafrost degradation and thermokarst dynamics on different time scales. The analysis of a sediment core from GG basin on the northern Seward Peninsula (Alaska) shows prevalent terrestrial accumulation of yedoma throughout the Early to Mid Wisconsin with intermediate wet conditions at around 44.5 to 41.5 ka BP. This first wetland development was terminated by the accumulation of a 1-meter-thick airfall tephra most likely originating from the South Killeak Maar eruption at 42 ka BP. A depositional hiatus between 22.5 and 0.23 ka BP may indicate thermokarst lake formation in the surrounding of the site which forms a yedoma upland till today. The thermokarst lake forming GG basin initiated 230 ± 30 cal a BP and drained in Spring 2005 AD. Four years after drainage the lake talik was still unfrozen below 268 cm depth.

A permafrost core from Mama Rhonda basin on the northern Seward Peninsula preserved a full lacustrine record including several lake phases. The first lake generation developed at 11.8 cal ka BP during the Lateglacial-Early Holocene transition; its old basin (Grandma Rhonda) is still

partially preserved at the southern margin of the study basin. Around 9.0 cal ka BP a shallow and more dynamic thermokarst lake developed with actively eroding shorelines and potentially intermediate shallow water or wetland phases (Mama Rhonda). Mama Rhonda lake drainage at 1.1 cal ka BP was followed by gradual accumulation of terrestrial peat and top-down refreezing of the lake talik. A significant lower organic carbon content was measured in Grandma Rhonda deposits (mean TOC of 2.5 wt%) than in Mama Rhonda deposits (mean TOC of 7.9 wt%) highlighting the impact of thermokarst dynamics on biogeochemical cycling in different lake generations by thawing and mobilization of organic carbon into the lake system.

Proximal and distal sediment cores from Peatball Lake on the Arctic Coastal Plain of Alaska revealed young thermokarst dynamics since about 1,400 years along a depositional gradient based on reconstructions from shoreline expansion rates and absolute dating results. After its initiation as a remnant pond of a previous drained lake basin, a rapidly deepening lake with increasing oxygenation of the water column is evident from laminated sediments, and higher Fe/Ti and Fe/S ratios in the sediment. The sediment record archived characterizing shifts in depositional regimes and sediment sources from upland deposits and re-deposited sediments from drained thaw lake basins depending on the gradually changing shoreline configuration. These changes are evident from alternating organic inputs into the lake system which highlights the potential for thermokarst lakes to recycle old carbon from degrading permafrost deposits of its catchment.

The lake sediment record from Herschel Island in the Yukon (Canada) covers the full Holocene period. After its initiation as a thermokarst lake at 11.7 cal ka BP and intense thermokarst activity until 10.0 cal ka BP, the steady sedimentation was interrupted by a depositional hiatus at 1.6 cal ka BP which likely resulted from lake drainage or allochthonous slumping due to collapsing shore lines. The specific setting of the lake on a push moraine composed of marine deposits is reflected in the sedimentary record. Freshening of the maturing lake is indicated by decreasing electrical conductivity in pore-water. Alternation of marine to freshwater ostracods and foraminifera confirms decreasing salinity as well but also reflects episodical re-deposition of allochthonous marine sediments.

Based on permafrost and lacustrine sediment records, this thesis shows examples of the Late Quaternary evolution of typical Arctic permafrost landscapes in central-eastern Beringia and the complex interaction of local disturbance processes, regional environmental dynamics and global climate patterns. This study confirms that thermokarst lakes are important agents of organic matter recycling in complex and continuously changing landscapes.

Key words: *paleolimnology, permafrost degradation, periglacial landscape evolution, thermokarst processes, carbon cycling, central-eastern Beringia*

Zusammenfassung

Derzeit werden deutliche Landschaftsveränderungen in der Arktis beobachtet, welche sich höchstwahrscheinlich zukünftig v.a. in den Permafrostregionen verstärken, da diese besonders empfindlich auf Klimaveränderungen reagieren. Um derzeitige und zukünftige Entwicklungen einschätzen zu können, ist es wichtig vergangene Umweltprozesse zu verstehen. Ursachen und Wechselwirkungen von Umweltveränderungen können nur bedingt durch instrumentelle Aufzeichnungen erklärt werden, doch Paleo-Umweltarchive können weit in die Vergangenheit reichende Umweltdynamiken aufzeichnen. Seesedimente sind wichtige Archive, die lokale limnogeologische Prozesse, aber auch direkt oder indirekt klimatisch gesteuerte Umweltveränderungen der Vergangenheit aufzeichnen. Ziel der vorliegenden Arbeit ist es, spätquartäre Permafrost- und Thermokarstdynamik im zentral-östlichen Beringia zu rekonstruieren. Beringia umfasst jene terrestrische Landmasse, welche Eurasien und Nord-Amerika zu Zeiten von Meeresspiegeltiefständen verband. Um die Entwicklung, die Prozesse und den Einfluss von Thermokarstdynamik zu untersuchen, wurden mehrere Sedimentkerne von rezenten Seen und ausgelaufenen Seebecken analysiert, um folgende Forschungsfragen zu beantworten:

1. Zu welcher Zeit degradierte Permafrost und wann entwickelten sich Thermokarstseen? Was waren hemmende oder verstärkende Faktoren?
2. Was sind dominierende Prozesse während der Entwicklung von Thermokarstseen und wie spiegeln sich diese in Proxy-Aufzeichnungen wieder?
3. Wie hat Thermokarstdynamik damals und heute zur Bedeutung von organischer Substanz in Sedimenten und im Kohlenstoffkreislauf beigetragen?

Die in dieser Arbeit angewandten Methoden basieren auf einem sogenannten „multi-proxy“ Ansatz, der sedimentologische, geochemische, geochronologische und mikropaläontologische Analysen, sowie die Untersuchung von stabilen Isotopen und die Hydrochemie von Porenwasser und -eis, verbindet. Feldmessungen der modernen Wasserqualität und Beckenmorphometrie komplettieren die Umweltuntersuchungen.

Auf Grundlage der untersuchten Sedimentkerne lässt sich die Degradation von Permafrost und die Dynamik von Thermokarst auf zeitlich verschiedenen Skalen rekonstruieren. Die Analyse eines Sedimentkerns vom GG-Becken auf der nördlichen Seward-Halbinsel (Alaska) zeigt eine vorwiegend terrestrische Akkumulation von Yedoma während des Früh- und Mittel-Wisconsin mit zwischenzeitlich feuchteren Verhältnissen zwischen 44,5 und 41,5 ka BP. Diese frühe Feuchtgebietsphase wurde durch die Akkumulation einer 1 m dicken Tephra-Lage beendet, welche sehr wahrscheinlich von der Eruption des heutigen South Killeak Maar vor etwa 42.000 Jahren stammt. Eine Schichtlücke im Sedimentkern von etwa 22,5 und 0,23 ka BP gibt einen Hinweis auf Thermokarstentwicklung in der Umgebung der Kernlokation, welche bis heute ein Yedoma-Rudiment bildet. Der Thermokarstsee, der GG-Becken formte, entstand 230 ± 30 cal a

BP und drainierte im Frühling 2005 AD. Vier Jahre nach der Drainage war der Talik des Sees in einer Tiefe von 268 cm noch ungefroren.

Ein Permafrostkern vom Mama Rhonda-Becken auf der nördlichen Seward-Halbinsel archivierte eine vollständige limnische Fazies mit mehreren Seephasen. Die erste Seegeneration entstand am Übergang vom Spätglazial zum Frühholozän um etwa 11,8 cal ka BP; das alte Seebecken (Grandma Rhonda) ist bis heute südlich der Kernlokation erhalten. Etwa um 9,0 cal ka BP entwickelte sich ein eher flaches und dynamisches Seesystem mit aktiv erodierenden Ufern und potenziell zwischengeschalteten Flachwasser- oder Feuchtgebietsphasen (Mama Rhonda). Die Drainage vom Mama Rhonda-See etwa 1,1 cal ka BP wurde gefolgt von gradueller Torfakkumulation und einem von oben zurückfrierenden See-Talik Es wurde ein deutlich geringerer organischer Kohlenstoff-Gehalt in Grandma Rhonda-Ablagerungen (TOC im Mittel 2,5 Gew.-%) festgestellt, als in Mama Rhonda Ablagerungen (TOC im Mittel 7,9 Gew.-%). Dies zeigt den bedeutenden Einfluss von Thermokarst auf biogeochemische Kreisläufe, da in verschiedenen Seegenerationen organischen Kohlenstoff durch Permafrost-Tauen im Seesystem mobilisiert wird.

Seesedimentkerne aus der Uferzone und dem zentralen Bereich von Peatball Lake auf der Arktischen Küstenebene von Alaska, ergaben eine junge Thermokarstdynamik von 1.400 Jahren, welche auf der Basis von absoluten Datierungen und Uferexpansionsraten rekonstruiert wurde. Nach der Seeinitiierung als Rest-See eines zuvor ausgelaufenen Seebeckens, vertiefte sich Peatball Lake verhältnismäßig schnell mit zunehmender Sauerstoffanreicherung der Wassersäule, wie aus laminierten Sedimenten und hohen Fe/Ti- und Fe/S-Verhältnissen im Sediment ersichtlich ist. Die Sedimente von Peatball Lake archivierten einen Wechsel des Ablagerungsregimes bei Ausdehnung der Seefläche und einen Wechsel der Sedimentquelle von ursprünglichen, rein terrestrischen Ablagerungen und bereits umgelagerten Sedimenten aus drainierten Seebecken. Angezeigt wird dieser Wechsel durch eine Veränderung im Eintrag organischen Materials in das Seesystem, was wiederum das Potential von Thermokarstseen bei der Aufarbeitung alten Kohlenstoffs aus degradierendem Permafrost im Einzugsgebiet verdeutlicht.

Der Seesedimentkern von der Herschel Insel im Yukon (Kanada) deckt das gesamte Holozän ab. Nach der Seeentstehung um 11,7 cal ka BP und einer Zeit intensiver Thermokarstaktivität bis 11,0 cal ka BP, wird die Phase einer eher kontinuierlichen Sedimentation von einer Schichtlücke um 1,6 cal ka BP unterbrochen. Diese wurde entweder durch die Drainage des Sees oder einer allochthonen Rutschung instabiler Uferlinien verursacht. Die spezielle Situation des Sees auf einer Stauchendmoräne aus marinem Material spiegelt sich auch in dem Seesedimentarchiv wieder. Das Aussüßen des wachsenden Sees wird durch die abnehmende elektrische Leitfähigkeit im Porenwasser angezeigt. Der Wechsel von marinen und Süßwasserostrakoden- und

Foraminiferengemeinschaften bestätigt zum einen die abnehmende Salinität des Sees, aber zeigt zum anderen auch episodische Umlagerung von allochthonem, marinem Sediment.

Auf der Grundlange von Permafrost- und Seesedimentkernen zeigt diese Arbeit Beispiele spätquartärer Entwicklungsgeschichte typischer Arktischer Permafrostlandschaften im zentral-östlichen Beringia. Es werden komplexe Zusammenhänge zwischen lokalen Störungsprozessen, regionaler Umweltdynamik und globalen Klimaveränderungen aufgezeigt. Thermokarstseen spielen dabei eine wichtige Rolle im sich kontinuierlich verändernden Landschaftsbild der hohen Breiten und im Stoffkreislauf bei der Aufarbeitung organischer Substanz.

Stichworte: *Pal olimnologie, Permafrostdegradation, periglaziale Landschaftsentwicklung, Thermokarstprozesse, Kohlenstoffkreislauf, zentral- stliches Beringia*

Abbreviations and nomenclature

Notation	Meaning	Unit (related to SI units if applicable)
%	percent; a number or ratio as a fraction of 100	
~	approximately	
<	less than	
>	greater than	
±	plus-minus-sign; statistical margin of error of a quantity	
≤	less than or equal	
≥	greater than or equal	
©	copyright	
°C	degree Celsius	273.15 °K
°E	longitudinal position in degrees east of the prime median	
°W	longitudinal position in degrees west of the prime median	
µg	micro gram	$1*10^{-9}$ kg
µm	micro meter	$1*10^{-6}$ m
‰	per mille; a number or ratio as a fraction of 1000	
^{14}C	radiocarbon	
^{18}O	stable oxygen isotopes	
a	Latin: annus; year	$3.1536*10^{7}$ s
AD	anno domini (years since the nominal birth of Jesus Christ)	
AHAP	Alaska High-Altitude Photography	
Al_2O_3	aluminium oxide	
AMS	accelerator mass spectrometry	
asl	above sea level	
AWI	Alfred Wegener Institute, Helmholtz Centre for Polar and Marine Research	
BC	before Christ (years before the nominal birth of Jesus Christ)	
BP	before present (present referred to 1950 AD)	
C/N	ratio of total organic carbon and total nitrogen	
$CaCO_3$	calcium carbonate	
cal	calibrated	
CaO	calcium oxide	
CH_4	methane	
Cl	chlorine	
cm	centimeter	$1*10^{-2}$ m
cm bs	centimeter below surface	
CO_2	carbon dioxide	
DOI	digital object identifier	
DTLB	drained thaw lake basin	
e.g.	Latin: exempli gratia; for example	
EC	electrical conductivity	
et al.	Latin:et alii; and others	
etc.	Latin: et cetera; and so on	
F	fluorine	
FeO	iron(II)oxide	
g	gram	
GFZ	German Research Centre for Geosciences	
GG	Guido Grosse	
GIS	geographic information system	
GMWL	global meteoric water line	
Gt	gigatonne	$1*10^{12}$ kg
H_2O_2	hydrogen peroxide	
ha	hectar	10^4 m^2
HCl	with hydrogen chloride	
HTM	Holocene Thermal Maximum	
i.e.	Latin: id est; that is	
ICP	Inner Coastal Plain (North Slope, Alaska)	
K_2O	potassium oxide	
ka	Latin: kilo annus; thousand years	$3.1536*10^{10}$ s

kg	kilogram	1 kg
km²	square kilometer	$1*10^6$ m^2
kV	kilo volt	1000 $kg*m^2*s^{-3}*A^{-1}$
LacCore	National Lacustrine Core Facility	
lat	latitude	
LGM	Last Glacial Maximum	
LIS	Laurentide Ice Sheet	
LMWL	local meteoric water line	
m	meter	1 m
m²	square meter	1 m^2
max	maximum	
mgC	miligram carbon	
MgO	magnesium oxide	
min	minimum	
MnO	manganese(II)oxide	
MS	magnetic susceptibility	
n	sample number	
n.a.	not applicable	
Na_2O	sodium oxide	
NE	northeast	
NW	northwest	
OCP	Outer Coastal Plain	
OS	National Ocean Sciences AMS Facility (NOSAMS)	
P_2O_5	phosphorus pentoxide	
Pb/Cs	ratio of lead and cesium	
PCA	principal component analysis	
pMC	percent modern carbon	
Poz	Poznan Radiocarbon Laboratory	
SC	specific conductivity	
SD	standard deviation	
SE	southeast	
SEM	scanning electron microscope	
SiO_2	silicon dioxide	
sp.	species (plural: spp.)	
SW	southwest	
TC	total carbon	
TiO_2	titanium dioxide	
TN	total nitrogen	
TOC	total organic carbon	
T_{ref} 25 °C	reference temperature of 25 °C	
UCIAMS	UC Irvine Keck- CCAMS facility	
USA	United States of America	
V-PDB	Vienna Pee Dee Belemnite	
wt%	weight pecentage	
XRF	x-ray fluorescence	
$\delta^{13}C_{TOC}$	stable total organic carbon ratio	‰ vs. V-PDB
δD	deuterium, a stable hydrogen isotope	

1 Thesis organization

1.1 Overview of chapters

This dissertation is organized as a cumulative thesis with five manuscript chapters. After the thesis organization overview (Chapter 1), which also indicates the author contribution, the introductory part (Chapter 2) provides scientific background on periglacial landscapes, permafrost degradation and thermokarst features and introduces the study region of central-eastern Beringia. Furthermore, it describes the objectives and the methodical approach of the thesis. The three main chapters (3, 4 and 5) and the appendix (I and II) consist of original research papers that have been published or are under review in international peer-reviewed journals (Table 1.1).

Chapter 3 presents the study of a sediment core from a drained thermokarst lake basin on a yedoma upland on the northern Seward Peninsula. The sediment record archived Mid-Wisconsin to Holocene landscape changes. This study was published in a special issue on "Reconstruction and modelling of paleo-permafrost" in the journal *Permafrost and Periglacial Processes* (Lenz et al. 2016). Chapter 4 presents a study on multiple Lateglacial to Early Holocene thermokarst lake generations based on another drained lake basin core on the northern Seward Peninsula and includes a discussion on carbon degradation following Holocene permafrost degradation in the study area. This research paper is in press in *Boreas* (Lenz et al. in press). Chapter 5 presents a study on Late Holocene sedimentary records from a thermokarst lake on Alaska`s Arctic Coastal Plain and discusses the influence of catchment morphology on lake sediments and organic matter degradation during thermokarst development. The study is in review as a research paper in the journal *Arktos* (Lenz et al. under review). All three chapters are dealing with permafrost degradation and thermokarst lake dynamics on different time scales in the central-eastern part of Beringia. An overarching discussion of the findings in the broader context of this thesis is featured in Chapter 6 where results and implications of the individual chapters are synthesized.

Two additional publications on thermokarst lake records from northwest Canada are also discussed in the synthesis (Chapter 6), while details on these studies are presented in the appendix. Both manuscripts developed from previous studies with key involvement of the thesis author and supplement findings on trans-regional thermokarst dynamics in eastern Beringia. Appendix I presents a study on a thermokarst lake record from Herschel Island, Yukon Territory, Canada and was published as a research paper in *Palaeogeography, Palaeoclimatology, Palaeoecology* (Lenz et al. 2013). Appendix II features a study evaluating a series of proxies of the same lake record to discriminate regional to local environmental changes. This study is in review as a research paper in the *Journal of Paleolimnology* (Fritz et al. under review).

Table 1.1: Overview of publications presented within this thesis.

Chapter	**Publication**
3	Mid-Wisconsin to Holocene Permafrost and Landscape Dynamics based on a Drained Lake Basin Core from the Northern Seward Peninsula, Northwest Alaska **Lenz, J.**, Grosse, G., Jones, B.M., Walter Anthony, K.M., Bobrov, A., Wulf, S. and Wetterich, S. (2016). *Permafrost and Periglacial Processes 27*: 56–75. DOI: 10.1002/ppp.1848 DOI of digital data archive: 10.1594/PANGAEA.845556
4	Evidence of multiple thermokarst lake generations from an 11 800-year-old permafrost core on the northern Seward Peninsula, Alaska **Lenz, J.**, Wetterich, S., Jones, B.M., Meyer, H., Bobrov, A. and Grosse, G. (in press). *Boreas.* DOI: 10.1111/bor.12186 DOI of digital data archive: 10.1594/PANGAEA.859554
5	Impacts of shore expansion and catchment characteristics on lacustrine thermokarst records in permafrost lowlands, Alaska Arctic Coastal Plain **Lenz, J.**, Jones, B.M., Wetterich, S., Tjallingii, R., Fritz, M., Arp, C.D, Rudaya, N. and Grosse, G. (under review). *Arktos*
Appendix I	Periglacial landscape dynamics in the western Canadian Arctic: Results from a thermokarst lake record on a push moraine (Herschel Island, Yukon Territory) **Lenz, J.**, Fritz, M., Schirrmeister, L., Lantuit, H., Wooller, M.J., Pollard, W.H. and Wetterich. S. (2013). *Palaeogeography, Palaeoclimatology, Palaeoecology 381–382*, 15–25. DOI: 10.1016/j.palaeo.2013.04.009 DOI of digital data archive: DOI: 10.1594/PANGAEA.855420
Appendix II	Holocene regional environmental change versus local signal preservation in thermokarst lake sediments: a case study from Herschel Island, Yukon (Canada) Fritz, M., Unkel, I., **Lenz, J.**, Gajewski, K., Frenzel, P., Paquette, N., Lantuit, H., Körte, L., Wetterich, S. (under review). *Journal of Paleolimnology.*

1.2 Author contribution

As a result of the multidisciplinary character of the investigations, several co-authors contributed to the manuscripts of this cumulative thesis with their specific expertise (Table 1.1). As a first author, I initiated the scientific idea, designed the study, reviewed all the relevant literature, conducted all data analyses unless otherwise stated, and wrote and coordinated the manuscripts. All co-authors contributed input to the papers as follows:

Chapter 3: *Mid Wisconsin to Holocene permafrost and landscape dynamics based on a drained lake basin core from the northern Seward Peninsula, Northwest Alaska*.

G. Grosse and B.M. Jones carried out field work and drilled the sediment core. S. Wetterich and G. Grosse provided guidance and help with the framework of the paper and provided, together with B. M. Jones and K. M. Walter Anthony, intellectual feedback throughout the writing process. G. Grosse produced maps for the figures and B. M. Jones conducted spatial analyses. S. Wetterich analyzed ostracods. A. Bobrov carried out analyses on testacea. S. Wulf helped with analyzing and interpreting tephra data. J. Lenz carried out sedimentological, geochemical and hydrochemical laboratory analyses, interpreted the entire dataset, designed and crafted the figures and tables, and wrote the manuscript. Input from all co-authors was received through scientific discussions of subsequent manuscript drafts.

Chapter 4: *Evidence of multiple thermokarst lake generations from an 11 800-year-old permafrost core on the northern Seward Peninsula, Alaska.*

G. Grosse and B.M. Jones carried out field work and drilled the sediment core. S. Wetterich, G. Grosse, B.M. Jones provided guidance and feedback throughout the writing process. G. Grosse produced maps for figures. A. Bobrov carried out analyses on testaceans. H. Meyer provided reference samples and helped with interpretation of isotopic data. J. Lenz carried out sedimentological and geochemical laboratory analyses, interpreted the entire dataset, designed and crafted the figures and tables, and wrote the manuscript. Input from all co-authors was received through scientific discussions of subsequent manuscript drafts.

Chapter 5: *Impacts of shore expansion and catchment characteristics on lacustrine thermokarst records in permafrost lowlands, Alaska Arctic Coastal Plain.*

J. Lenz, B.M. Jones and C.D. Arp carried out field work and drilled the sediment cores. S. Wetterich, G. Grosse, B.M. Jones and M. Fritz provided guidance and feedback in the form of scientific discussions throughout the writing process. B.M. Jones performed calculation of lake expansion rates. N. Rudaya carried out pollen analyses and interpretation. R. Tjallingii performed XRF analyses and helped interpreting the data. J. Lenz carried out sedimentological and

geochemical laboratory analyses, interpreted the entire dataset, designed and crafted the figures and tables, and wrote the manuscript. Input from all co-authors was received through scientific discussions of subsequent manuscript drafts.

Appendix I: *Periglacial landscape dynamics in the western Canadian Arctic: Results from a thermokarst lake record on a push moraine (Herschel Island, Yukon).*

M. Fritz and H. Lantuit carried out field work and drilled the sediment core. M. Fritz, L. Schirrmeister, W.H. Pollard and S. Wetterich provided guidance and feedback throughout the writing process. M. J. Wooller provided feedback to isotopic analyses. J. Lenz carried out sedimentological and geochemical laboratory analyses, interpreted the entire dataset, designed and crafted the figures and tables, and wrote the manuscript. Input from all co-authors was received through scientific discussions of subsequent manuscript drafts.

Appendix II: *Holocene regional environmental change versus local signal preservation in thermokarst lake sediments: A case study from Herschel Island, Yukon (Canada).*

M. Fritz and H. Lantuit carried out field work and drilled the sediment core. J. Lenz performed analyses of pore water which was interpreted by M. Fritz. M. Fritz performed XRF measurements. J. Lenz provided first analyses of XRF data which was further interpreted by L. Körte under supervision of I. Unkel. N. Paquette and K. Gajewski performed pollen analyses and interpretation. P. Frenzel analyzed and interpreted ostracods which were prepared by J. Lenz. Input from all co-authors was received through scientific discussions of subsequent manuscript drafts.

2 Introduction

Environmental changes associated with climate warming were especially significant in northern high latitudes during the last decades (Overpeck 1997, Serreze et al. 2000, Hinzman et al. 2005). Sensitivity to rapid changes of circum-Arctic regions is evident from instrumental and observational data (Pienitz et al. 2004) even though the information only provides temporally limited evidence. To place recent observations into a long-term context and to better project future global changes, it is essential to understand past landscape changes independently from human induced processes by decoding environmental archives on various time-scales (Edwards et al. 2007).

2.1 Scientific background

2.1.1 Arctic environments and permafrost in the study region of Beringia

The Arctic is characterized by generally harsh environmental conditions. Its spatial delineation can be based on geographical, physical, or ecological parameters (Figure 1.1). In natural sciences, the southern boundary of the Arctic is often defined either by the geographic Arctic Circle at 66°33'N, by the July-Isotherm of 10 °C as a climatic characteristic, or by the treeline which roughly corresponds with the isothermal boundary. A characterizing feature for Arctic landscapes is the presence of permafrost and in many regions also ground ice. Permafrost is defined as ground material that remains at or below 0 °C for at least two consecutive years (van Everdingen 2005). It is underlying the majority of the northern terrestrial Arctic not covered by ice sheets and glaciers (Figure 1.1). Although its distribution is also controlled by site-specific factors like thermal conductivity and diffusivity of ground material, topography, topographic aspect, fire, water bodies, vegetation, soil organic layers, and snow cover, the main driving factor for large scale permafrost distribution is climate (French 2007). Consequently, permafrost presence can serve as a climate indicator (Washburn 1980). About 24 % of the modern terrestrial surface of the northern hemisphere is underlain by permafrost (Zhang et al. 2008) and its distribution can be grouped by lateral continuity into continuous, discontinuous, isolated and sporadic permafrost regions (Figure 1.1). The greater surface extent and thickness of up to 1,500 m (Yershov 1998) of Siberian permafrost compared to permafrost in North America reflect differences in its evolution during the Quaternary (French 2007). Whereas eastern Siberian lowlands remained largely ice-free, large portions of Arctic North America were widely covered by ice-sheets during the Last Glacial Maximum (LGM). In North America, extensive postglacial lakes and marine flooding (Murton et al. 2010) additionally reduced the terrestrial surface exposed to low air temperature and subsequent permafrost aggradation (French 2007).

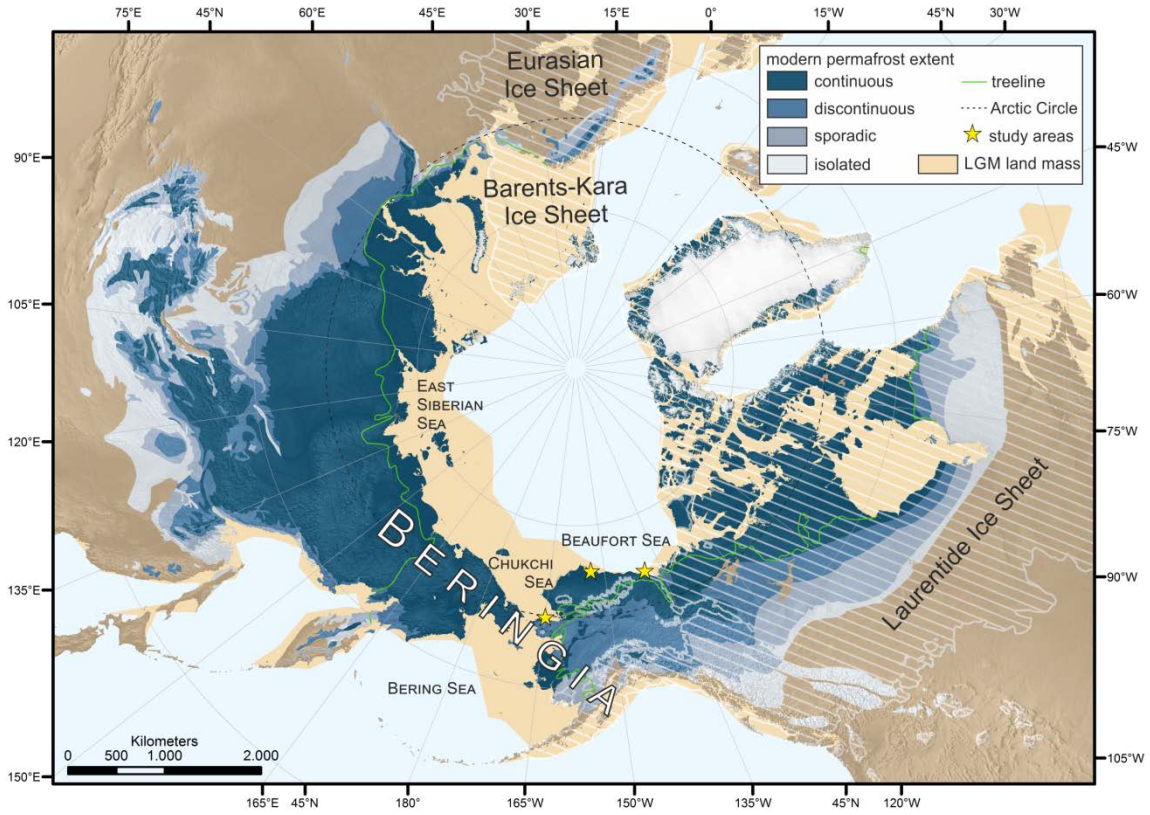

Figure 1.1: Study region of Beringia in the Arctic with extent of ice sheets at 18 cal ka BP (Ice sheets in North-America: Dyke et al. 2003; ice sheets in Eurasia: Hughes et al. 2016), exposed shelves during the LGM delineated by the -120 isobath (Peltier & Fairbanks 2006), modern distribution of continuous, discontinuous, sporadic and isolated permafrost (Brown et al. 1997), and modern treeline (Walker et al. 2005). Study areas are marked with a red star.
Map: Arctic Polar stenographic projection, WGS 1984 (prepared by C. Coch).

Some periglacial features like ice-wedge pseudomorphs, polygonal or sorted patterned ground and cryoturbated soils provide evidence for previous permafrost presence during the Quaternary where it has since disappeared (Washburn 1980). An extensive permafrost zone characterized the mid-latitudes in Eurasia but only a narrow permafrost zone was mapped for North-America for the LGM probably due to different atmospheric circulations and a greater southerly extent of the Laurentide Ice Sheet (Vandenberghe et al. 2014). Thick and extant permafrost in regions with warmer modern climate conditions are referred to as relict and prove colder climate conditions during the Quaternary (Washburn 1980). For paleo-investigations, permafrost can further serve as a climate archive as it can preserve fossils of cold-climate fauna and flora, e.g. tundra pollen taxa or large mammal remains, which are now extinct or were preserved outside their modern distribution (Hopkins 1976, French 2007). Further, cold, sub-aerial conditions supported the development of permafrost on exposed continental shelves during sea level low stands, in particular the East-Siberian shelves and the Bering and Chukchi shelves during glacial periods (French 2007). Most sub-sea permafrost can therefore be considered as relict as it developed during eustatic sea level fluctuations during cold periods of the Quaternary when large water bodies were globally stored in glaciers and ice-sheets. The lowest sea level and correspondent

shoreline during the LGM around 21,000 yr BP was reconstructed to an isobath of about -120 m (Figure 1.1, Peltier & Fairbanks 2006). Vast unglaciated lowlands expanded continuously between the Taymyr Peninsula in central-north Siberia and the Mackenzie River in northwest Canada which were named Beringia (Hopkins 1982). The Bering Land Bridge was of particular importance as it formed a terrestrial corridor in the Bering-Chukchi Sea region during the glacial period of the Late Wisconsin (Hopkins 1982) enabling the migration of flora and fauna (Hopkins 1959a) and the first humans (Morlan & Cinq-Mars 1982) from Eurasia to North America. Beringia was dominated by a continental Arctic climate during the late Pleistocene, resulting in the development of permafrost and widespread periglacial processes (Hopkins 1973, Péwé 1975). The Bering Land Bridge narrowed during the Mid Wisconsin about 35,000 to 25,000 years ago, was restored during the Late Wisconsin about 25,000 to 12,000 years ago until finally sea level rise inundated the land bridge at the end of the Late Wisconsin between 11,000 and 10,000 years ago (Péwé 1975). Since then the Arctic landscape has reorganized with glaciers starting to decay, forests returning to the unglaciated terrain (e.g. in central Alaska) and Pleistocene permafrost starting to thaw (Péwé 1975).

A generally warming trend of upper permafrost in most Arctic regions was recorded for the last decades in accordance with rising air temperatures (Romanovsky et al. 2010). Cold permafrost in northern Alaska recorded severe warming of 5 °C to 7 °C since the Little Ice Age but although warming rates were much lower for warmer permafrost in interior Alaska and on the Seward Peninsula. Warmer permafrost in these regions is more susceptible to degradation and change to discontinuous or sporadic permafrost and in some areas disappearance especially where permafrost thickness is shallow (Romanovsky et al. 2010). A total warming of > 6 °C during the last century was recorded for Prudhoe Bay, Alaska (Osterkamp 2007) where permafrost is reaching modern thicknesses of 650 m and cold temperatures < -7 °C along the coast between Prudhoe Bay and Barrow (Smith et al. 2010). On the northern Seward Peninsula permafrost thickness reaches a maximum of 100 m (Jorgenson et al. 2008) and ground temperatures range from -5 to -2 °C (Smith et al. 2010) leading to a higher vulnerability to degradation compared to colder and thicker permafrost.

2.1.2 Permafrost degradation and its global feedbacks

Permafrost stability, or more specifically the ground thermal regime, is predominately a function of climate. However, as permafrost is not in direct contact with the atmosphere its thermal regime is mediated by topography, hydrology, ground properties (soil, geology and ground ice), vegetation and snow (Jorgenson et al. 2010). As a consequence, the degradation of permafrost is a complex process involving the interaction of all those parameters and a range of both positive and negative feedback mechanisms (Figure 1.2). Fore example, topography affects the amount of solar radiation reaching the ground surface (Jorgenson et al. 2010) as well as surface and ground

water distribution and run-off dynamics. Vegetation cover mediates the impact of solar radiation on the ground surface and insulates the subsurface providing a strong feedback to permafrost resilience in particular in regions with warm, discontinuous permafrost (Viereck et al. 1986). Furthermore, soil organic layer accumulation and snow accumulation are a function of the vegetation type and influence permafrost properties (Jorgenson et al. 2003). At the same time, permafrost conditions influence the patterns of vegetation communities as well as soil development (Jorgenson et al. 2010). Surface and ground water in interaction with topography and ground properties deliver heat into the ground and may enhance permafrost degradation (Hinzman et al. 2005). Drainage networks, run-off volume and timing, as well as sediment and nutrient load are greatly influenced by permafrost degradation, especially in relation to variable topography (Rowland et al. 2010). Ground texture (underlying geology, soil texture, amount and distribution of ground ice) influences the hydrology, e.g. drained organic soils lose heat in winter under frozen conditions due to high thermal conductivities but low summer heat penetration under unfrozen conditions lead to a "thermal offset" between ground surface and permafrost table (Romanovsky & Osterkamp 1995).

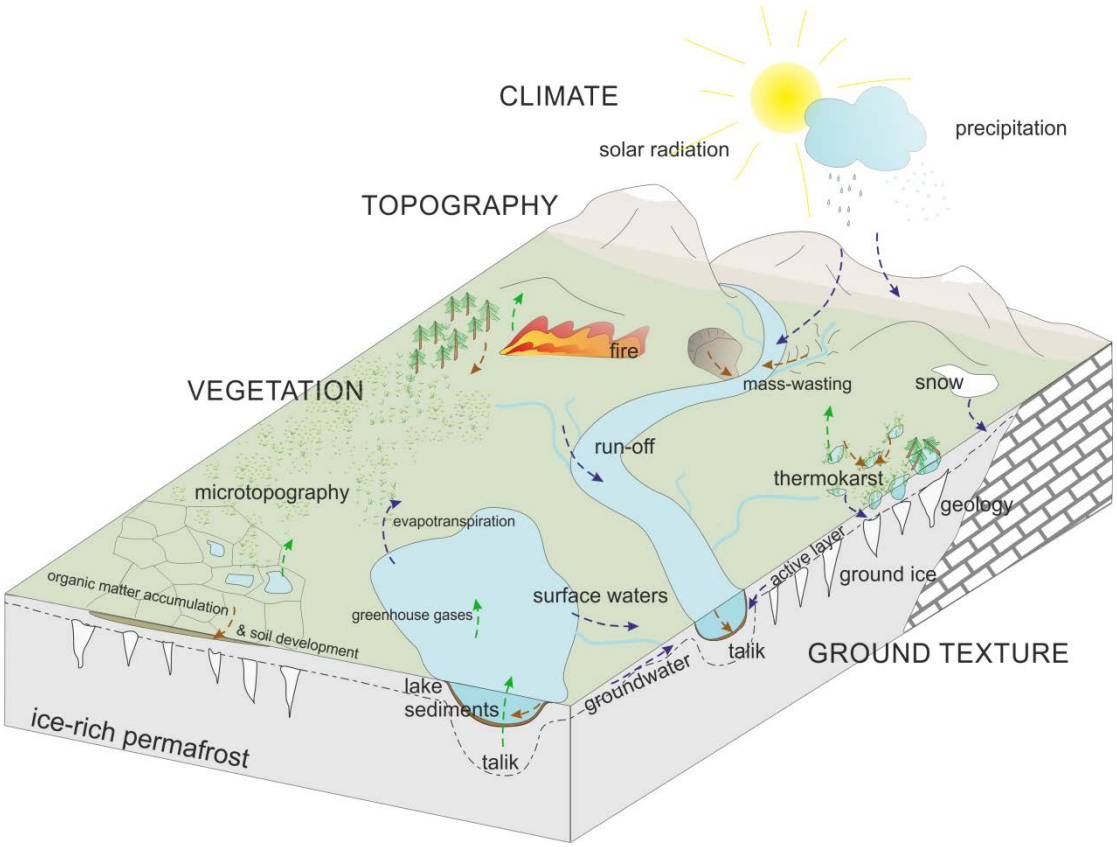

Figure 1.2: Conceptual landscape scheme indicating influence factors for permafrost stability. Arrows indicate fluxes of matter (brown), gas (green) and water (blue).

Also, depth and seasonality of snow have a strong feedback on permafrost thermal regime (Jorgenson et al. 2010). Finally, disturbances such as fires can have a severe and rapid effect on the vegetation, soil and permafrost regimes (Jones et al. 2015, Boike et al. 2016).

Diverse periglacial landforms form through permafrost aggradation and degradation as well as seasonal freeze-thaw cycles. Ice-wedge polygons are the most widespread and characteristic periglacial features (French 2007). Like palsas and pingos, they are associated with permafrost aggradation and are characterized by formation of massive ice bodies in the ground. Upon thaw, ice-wedge polygon landscapes are subject to substantial ecosystem change due to the melt of ground ice, soil volume loss, and heterogeneous surface subsidence. The process by which characteristic landforms result from thawing of ice-rich permafrost is called thermokarst (van Everdingen 2005). Resulting landforms include thermo-erosional gullies (Bowden et al. 2008, Godin & Fortier 2012), retrogressive thaw slumps (Kokelj et al. 2009, Lantuit et al. 2012), thermokarst pits and thermokarst lakes (Jorgenson et al. 2006). The latter are the most typical expression of degrading ice-rich permafrost in Arctic lowlands. Thermokarst lakes are defined as lakes which commonly occupy closed basins formed by ground subsidence following ground ice melt and thaw of ice-rich permafrost (van Everdingen 2005).

Late Pleistocene permafrost started to degrade in the northern mid-latitudes after the LGM (e.g. Vandenberghe & Pissart 1993) and thermokarst lake formation increased in high latitudes in the Early Holocene and intensified during the Holocene Thermal Maximum (HTM, Rampton 1988, Walter et al. 2007). According to three independent estimates from paleo-archives and laboratory incubations by Walter et al. (2007), Northern Hemisphere methane (CH_4) emissions by ebullition from newly initiated thermokarst lakes after the LGM contributed up to 87 % of the boreal contribution to the atmospheric methane concentration recorded in ice cores. CH_4 is released from anaerobic thermokarst lake sediments, unfrozen sediments in lake taliks (defined as layer or body of unfrozen ground in a permafrost area, e.g. formed under lakes that do not freeze to the bottom in winter; van Everdingen 2005) as a result of microbial decomposition of organic matter (Walter et al. 2006; Figure 1.3). On a temporal scale of 100 years, the global warming potential of CH_4 is 24-times higher than that of carbon dioxide (CO_2; Forster et al. 2007). CO_2 is another important atmospheric greenhouse gas that may be produced during thermokarst processes. It results from microbial respiration of labile organic matter under aerobic conditions after thawing of organic-rich deposits. Especially the re-introduction of organic carbon formerly frozen for extended times in permafrost into the carbon cycle has high potential for a positive feedback to climate warming (Zimov et al. 2006, Schuur et al. 2009).

Figure 1.3: Methane ebullition can be observed and quantified in thermokarst lake ice as gas bubbles get trapped in winter lake ice. Other than oxygen or carbon dioxide, methane is ignitable.

2.1.3 Thermokarst lakes and basins as paleoenvironmental archives

Permafrost change can serve as an indicator for climate variations on a larger spatial and temporal scale because its degradation results in mostly irreversible landscape modifications. Present and past landscape changes associated with permafrost degradation (such as development of thermo-erosional gullies, retrogressive thaw-slumps, thermokarst lakes and basins) are imprinted in the periglacial geomorphology. For example, the morphometry and orientation of thermokarst lakes may provide indicators for past water-level regimes and wind directions (Grosse et al. 2013). Furthermore, frozen terrestrial deposits can preserve valuable environmental information to reconstruct past landscape dynamics as shown by studies from Siberia (e.g. Wetterich et al. 2008), Canada (Murton et al. 2005, Fritz et al. 2012) or Alaska (Wetterich et al. 2012, Kanevskiy et al. 2011). Ice-wedges, ice bodies with vertically oriented foliation formed by cyclic frost cracking in winter and seasonal filling of snow melt water (Everdingen 2005), are valuable paleo-archives in ice-rich permafrost areas as their isotopic values can reflect winter season temperatures (Meyer et al. 2010, Meyer et al. 2015). But ice-wedge outcrops are restricted to riverbanks and coastal bluffs so that their use as paleo-archives is spatially limited. Fortunately, Arctic lowlands are characterized by a large number of lakes which react sensitively to ecosystem change (Douglas et al. 2004). With the help of paleolimnology, the study of physical, chemical and biological information stored in lake sediments (Cohen 2003), ecological shifts on millennial time scales can be deciphered in sedimentary records of thermokarst lakes by indirect proxy methods (Pienitz et al. 2004).

2.2 Aims and approaches

The overall objective of this thesis it to improve our understanding of Arctic landscape changes during Late Pleistocene and Holocene periods in central-eastern Beringia. Sediment cores from two drained basins on northern Seward Peninsula and from a thermokarst lake from north of Teshekpuk Lake on the Arctic Coastal Plain, Alaska, were analyzed to answer the following questions:

1. When did permafrost degradation and thermokarst lake development take place and what were enhancing and inhibiting environmental factors?
2. What are the dominant processes during thermokarst lake development and how are they reflected in proxy records?
3. How did, and still do, thermokarst dynamics contribute to the inventory and properties of organic matter in sediments and to the carbon cycle?

To address these research questions, the sediment cores were analyzed with a multi-proxy approach (Table 1.2). The appendix includes two studies from a thermokarst lake in the western Canadian Arctic. Additionally, information and data about the modern lake basin, water quality, and stable isotope of water and ice were documented to characterize and compare the past with the modern environmental setting where suitable. Detailed descriptions of laboratory techniques illustrated in Figure 1.4 are given in each chapter where the methods are used.

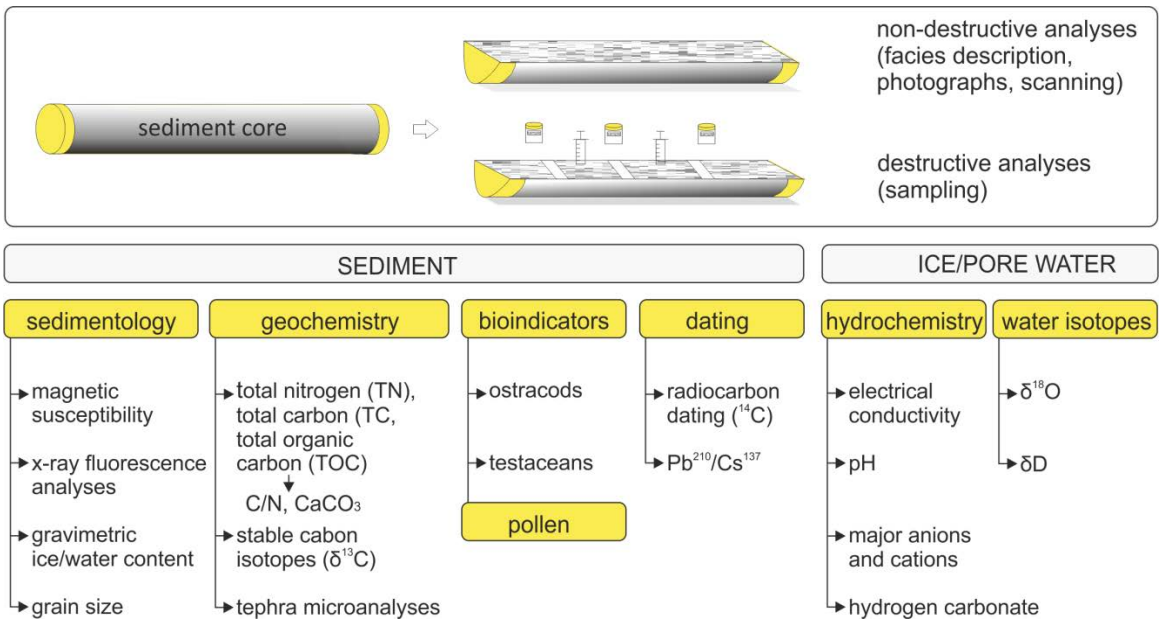

Figure 1.4: Laboratory analyses applied in this thesis on split permafrost and lacustrine sediments cores.

Table 1.2: Overview of studied archives in different locations and applied methods.

Type of archive informal name of lake/ basin (core ID)	Location	Applied laboratory methods	Analyses on modern environmental factors	Chapter
Drained thermokarst lake basin GG basin (Kit-64)	Northern Seward Peninsula, Alaska, USA	Sedimentology: Magnetic susceptibility, gravimetric water content, grain size Geochemistry: TN, TC, TOC, $\delta^{13}C$, geochemical microanalyses on tephra Bioindicators: ostracods testaceans Dating: ^{14}C Pore water: electrical conductivity, pH	Analysis of basin and paleo lake metrics (GIS)	# 3
Drained thermokarst lake basin Mama Rhonda basin (Kit-43)	Northern Seward Peninsula, Alaska, USA	Sedimentology: Magnetic susceptibility, gravimetric water content, grain size Geochemistry: TN, TC, TOC, $\delta^{13}C$, geochemical microanalyses on tephra Bioindicators: ostracods, testaceans Dating: ^{14}C Pore ice: δD, $\delta^{18}O$	Reference water samples: δD, $\delta^{18}O$	# 4
Thermokarst lake Peatball Lake (P1; P2; P3)	Arctic Coastal Plain, Alaska, USA	Sedimentology: Magnetic susceptibility, XRF Geochemistry: TN, TC, TOC, $\delta^{13}C$, $CaCO_3$ Pollen analyses Dating: ^{14}C, Pb^{210}/Cs^{137}	Shoreline expansion rates (GIS)	# 5
Thermokarst lake Lake Herschel (PG1967)	Herschel Island, NWT, Canada	Sedimentology: Radiography, Magnetic susceptibility, gravimetric water content, grain size Geochemistry: TN, TC, TOC, $\delta_{13}C$ Dating: ^{14}C	Modern lake water: EC, pH, temperature Modern lake basin: bathymetry	Appendix I
Thermokarst lake Lake Herschel (PG1967)	Herschel Island, NWT, Canada	Sedimentology: XRF Bioindicators: ostracods, foraminifera Pollen analyses Pore water: pH, EC, major anions and cations, hydrogen carbonate	Reference sediment samples: ostracods, foraminifera	Appendix II

3 Mid Wisconsin to Holocene permafrost and landscape dynamics based on a drained lake basin core from the northern Seward Peninsula, northwest Alaska

Josefine Lenz[1,2], Guido Grosse[1,2], Benjamin M. Jones[3], Katey M. Walter Anthony[4], Anatoly Bobrov[5], Sabine Wulf[6] and Sebastian Wetterich[1]

[1] Department of Periglacial Research, Alfred Wegener Institute, Helmholtz Centre for Polar and Marine Research, Potsdam, Germany

[2] Institute for Earth and Environmental Sciences, University of Potsdam, Potsdam, Germany

[3] Alaska Science Center, US Geological Survey, Anchorage, AK, USA

[4] Water and Environmental Research Center, University of Alaska, Fairbanks, AK, USA

[5] Faculty of Soil Science, Lomonosov Moscow State University, Moscow, Russia

[6] Section 5.2 Climate Dynamics and Landscape Evolution, Helmholtz-Centre Potsdam, GFZ German Research Centre for Geosciences, Potsdam, Germany

Published in: Permafrost and Periglacial Processes 27: 56‐75, DOI: 10.1002/ppp.1848

Key words: Beringia, paleoenvironmental reconstruction, thermokarst lake dynamics, cryostratigraphy, tephra, bioindicators, yedoma

3.1 Abstract

Permafrost-related processes drive regional landscape dynamics in the Arctic terrestrial system. A better understanding of past periods indicative of permafrost degradation and aggradation is important for predicting the future response of Arctic landscapes to climate change. Here, we used a multi-proxy approach to analyze a ~ 4 m long sediment core from a drained thermokarst lake basin on the northern Seward Peninsula in western Arctic Alaska (USA). Sedimentological, biogeochemical, geochronological, micropaleontological (ostracoda, testate amoebae) and tephra analyses were used to determine the long-term environmental Early Wisconsin to Holocene history preserved in our core for central Beringia. Yedoma accumulation dominated throughout the Early to Late Wisconsin but was interrupted by wetland formation from 44.5 to 41.5 ka BP. The latter was terminated by the deposition of 1 m of volcanic tephra, most likely originating from the South Killeak Maar eruption at about 42 ka BP. Yedoma deposition continued until 22.5 ka BP and was followed by a depositional hiatus in the sediment core between 22.5 and 0.23 ka BP. We interpret this hiatus as due to intense thermokarst activity in the areas surrounding

the site, which served as a sediment source during the Late Wisconsin to Holocene climate transition. The lake forming the modern basin on the upland initiated around 0.23 ka BP and drained catastrophically in spring 2005. The present study emphasizes that Arctic lake systems and periglacial landscapes are highly dynamic and that permafrost formation as well as degradation in central Beringia was controlled by regional to global climate patterns as well as by local disturbances.

3.2 Introduction

Climate change has a significant impact on the Arctic terrestrial system (Hinzman *et al.* 2005). Warming and thawing of permafrost has been observed for several decades (Romanovsky et al. 2007, 2010, Grosse et al. 2011. Vaughan et al. 2013) and inferred from numerous paleoecological studies (Mann et al. 2002, Kaufman et al. 2004, Gaglioti et al., 2014). The degradation of permafrost-dominated landscapes influences hydrology, ecology, ground thermal regime and biogeochemical cycles (Rowland et al. 2010, Grosse et al. 2013a, Walter Anthony et al. 2014). Thermokarst lakes represent a particularly widespread mode of permafrost degradation (Jorgenson et al. 2006) and dominate Arctic lowlands in Siberia, Alaska and northwest Canada. They cover up to 40 % (Smith et al. 2007, Grosse et al. 2013a) and drained lake basins up to 70 % (Walter Anthony et al. 2014) of the landscapes surface in some of these lowlands. Thermokarst lakes form by thawing of ice-rich permafrost or melting of massive ground ice followed by ground settlement (van Everdingen 2005). After their initiation as small shallow ponds, these lakes typically experience a succession of growth, shrinkage and gradual or even sudden drainage (Burn & Smith 1990, Jorgenson & Shur 2007, Grosse et al. 2013a, Morgenstern et al. 2013, Lenz et al. 2013, Kanevskiy et al. 2014, Jones & Arp 2015). Thermokarst lake formation and growth is generally associated with periods of warming and wetting in the Arctic, and was especially intense during the Lateglacial and Early Holocene (Kaplina & Lozhkin 1979, Walter et al. 2007). However, the development of specific thermokarst lakes and drained thermokarst lake basins is often triggered by local disturbances (Burn & Smith 1990, Jorgenson et al. 2006). Because of the widespread occurrence of thermokarst lakes during periods of rapid Arctic change, they have a cumulative impact on the carbon and water cycles, climate feedbacks and energy balance of the northern high latitudes (Grosse et al. 2013a). For instance, thawing permafrost releases organic matter for microbial decomposition and in water-saturated, anaerobic conditions below thermokarst lakes methane is produced and emitted to the atmosphere (Walter et al. 2006). However, during their life cycle, thermokarst lakes act as long-term net carbon sinks accumulating organic-rich deposits before and after lake drainage (Walter Anthony et al. 2014).

To understand current and future developments of thermokarst lake dynamics and their feedbacks with landscapes, ecosystems and biogeochemical cycles, it is critical to investigate records of past thermokarst lake processes, driving factors and environmental conditions.

Using lake sediments to reveal past landscape dynamics is of great value because they comprise both minerogenic and organogenic compounds deposited during a specific environment within the lake's lifetime. Few studies have focused on core-based paleoenvironmental reconstructions from thermokarst lakes to reveal permafrost and landscape dynamics (e.g. northwest Canada: Lenz et al. 2013, Siberia: Biskaborn et al., 2013a, 2013b, Schleusner et al. 2015, north Alaska: Gaglioti et al. 2014). In western Alaska, studied lake archives are often of non-thermokarst origin, for example, Imuruk Lake in the center of the Seward Peninsula (Hopkins 1959, 1963, Colinvaux 1964), or undetermined origin as Kaiyak and Squirrel lakes south of the Brooks Range (Anderson 1985, Berger & Anderson 1994) and concentrate mostly on vegetative and climate change. Besides lake sediment cores, natural exposures along lakes, rivers and coasts have been used to study thermokarst lake deposits (e.g. Hopkins & Kidd 1988, Wetterich et al. 2012). Fossil remains recovered from these records such as ostracods, mollusks and testate amoebae (rhizopods) enable the characterization of past ecological conditions during thermokarst lake formation and growth. For example, Wetterich et al. (2012) used these bioindicators as well as pollen and plant macrofossils from a pingo exposure eroded by coastal erosion of the Chukchi Sea to infer a regional signal of late Quaternary landscape dynamics of the northern Seward Peninsula. Paleoenvironmental questions on the northern Seward Peninsula in northwest Alaska were addressed by studies on coastal bluffs along the Chukchi Sea (McCulloch & Hopkins 1966, Matthews 1974, Jordan & Mason 1999, Wetterich et al. 2012), peatlands (Hunt et al. 2013) and the Kitluk paleosol buried under the 18.0 ka BP Devil Mountain Maar tephra (Höfle & Ping 1996, Höfle et al. 2000, Goetcheus & Birks 2001 Kuzmina et al. 2008).

Regional thermokarst dynamics on a modern, decadal timescale with calculated expansion and drainage rates are presented by Jones et al. (2011). However, records of long-term permafrost processes and thermokarst activity from drained lake basins are rare on the northern Seward Peninsula. This region is of particular interest due to its location close to the modern treeline and within the continuous permafrost region but with relatively warm ground temperatures of -5 to -2 °C (Romanovsky et al. 2010, Smith et al. 2010).

We studied a sediment core obtained from a recently drained thermokarst lake basin on a yedoma upland located on the northern Seward Peninsula (Figures 3.1 and 3.2). Here we present a multiproxy record from this basin and discuss the development of a thermokarst lake system on the northern Seward Peninsula in ice-rich yedoma of central Beringia throughout the late Pleistocene and Holocene.

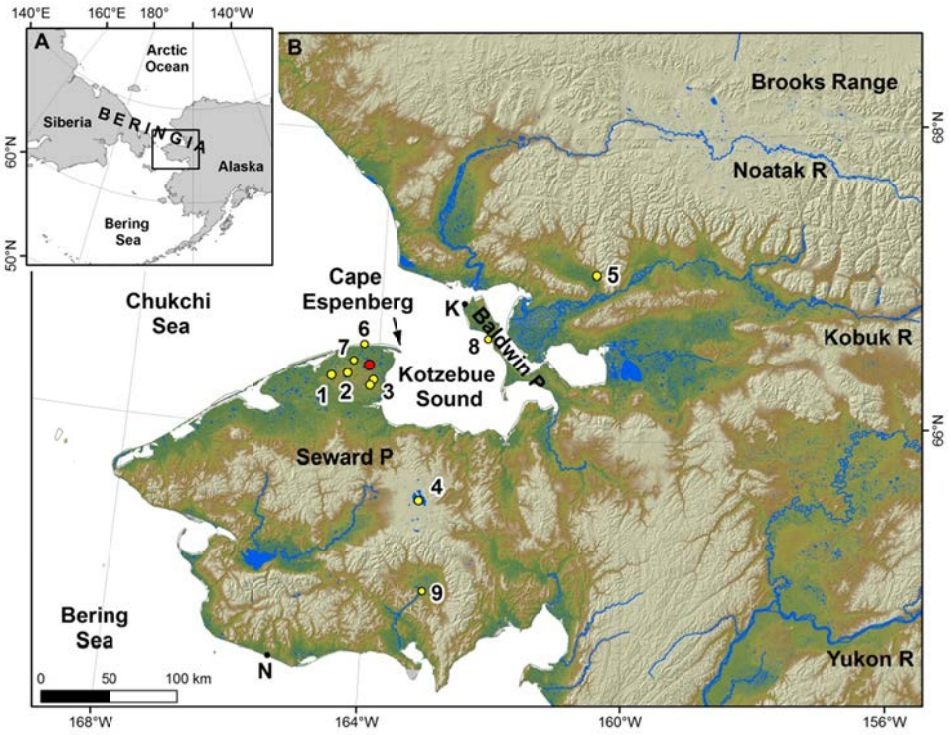

Figure 3.1: Study area of the northern Seward Peninsula as part of the Bering Land Bridge National Preserve (A and B). Red dot=Kit-64 study site; K=Kotzebue; N=Nome; 1=Whitefish Maar; 2=Devil Mountain Maar; 3=North and South Killeak maars; 4=Imuruk Lake (Hopkins 1959, 1963, Colinvaux, 1964); 5=Squirrel Lake (Anderson 1985; Berger & Anderson 1994); 6=Kit-1 Pingo (Wetterich et al. 2012); 7=Tempest Lake (Kuzmina et al. 2008); 8=mammoth site (Hopkins et al. 1976); 9=Niukluk Lake (Hunt et al. 2013).

3.3 Study area

The study region is part of the Bering Land Bridge National Preserve and is located in the central region of Beringia, which remained largely unglaciated during the Last Glacial Maximum (LGM, 26.5–19 ka BP) (Hopkins 1967, Kaufman & Hopkins 1986). The gently northward sloping plain with elevations mostly below 60 m asl is underlain by ice-rich, continuous permafrost (Brown et al. 2001). On the northern Seward Peninsula, permafrost is approximately 100 m thick (Jorgenson et al. 2008). Because of the lower glacial sea level during the LGM and the extensively exposed Bering and Chukchi Sea continental shelves, our study site was located in a central part of the wide Bering Land Bridge and dominated by a continental climate (Hopkins 1967).

The northern Seward Peninsula represents one of the major lake districts in Alaska with extant lakes > 1 ha covering 456 km^2 (7.1 %) (Arp & Jones 2009). Up to 75 % of the landscape is studded with drained thermokarst lake basins demonstrating a dynamic landscape history (Hopkins & Kidd 1988, Jones et al. 2012). The local geomorphology is dominated by thermokarst lakes, drained thermokarst lake basins, remnants of yedoma uplands with ice-rich permafrost, erosional gullies, small streams, pingos and polygonal patterned ground (Jones et al. 2011, Regmi et al. 2012), hence our study site represents a typical landscape feature in this region. While the

yedoma uplands are remnants of the late Pleistocene accumulation surface, most other features are of Holocene age and related to permafrost degradation and re-aggradation processes.

Late Quaternary volcanic landforms are also present in the region including the four large Espenberg Maar lakes, Devil Mountain Volcano and several smaller Quaternary volcanic cone remnants south of the study area (Hopkins 1988, Begét et al. 1996). The Devil Mountain Maar was created by multiple phreatomagmatic eruptions at 17.5 ka BP (Hopkins 1988, Begét et al. 1996) and covers an area of 30 km^2. Its tephra is distributed mostly towards the north and west over an area of about 2500 km^2 (Begét et al. 1996, Höfle et al. 2000). The two maar craters of the North and South Killeak lakes are 12 and 20 km^2 in area, respectively. South Killeak Maar was formed by about 42 ka BP while North Killeak Maar is most likely older than 125 ka (Hopkins 1988). The shallow Whitefish Maar located further west is estimated to be 100–200 ka old, and five small shield volcanoes immediately south appear to be even older than the maars and may have formed prior to permafrost formation on the northern Seward Peninsula (Hopkins 1988).

The study area today is characterized by a subarctic climate with mean annual air temperatures of -6 °C in Kotzebue about 60 km northeast of the study site. The January mean air temperature is -20 °C while the July mean air temperature is 12 °C. Precipitation averages 230 mm a^{-1} with more than half the precipitation falling as rain in summer and early fall (US National Weather Service data, http://www.ncdc.noaa.gov/). The modern vegetation is classified as Bering Tundra (Nowacki et al. 2002). Elevated and better-drained sites are dominated by tussock sedge (*Eriophorum vaginatum*) and dwarf shrubs (*Ledum palustre*, *Vaccinium vitis-idaea*), whereas drier habitats like pingos are occupied by erect shrubs (*Andromeda polifolia*, *Betula nana*, *Spiraea beauverdiana*). Waterlogged acidic sites are characterized by *Drepanocladus* spp. and *Sphagnum* spp. as well as wet sedge-moss communities (*Carex aquatilis*, *E. augustifolium*) (Wetterich et al. 2012).

The shape of the 11.9 ha large study basin suggests that two originally separate lakes coalesced to form the present lake basin (Figures 3.2 and 3.3; Table 3.1). The main basin with a SW-NE extension of 270 m and a NW-SE extension of 330 m is connected at its NW edge over a length of 140 m to a small, round basin of a diameter of 170 m. The lake had no inflow but based on field observations of other similar lake basins in the study area (Jones et al. 2011, Jones et al. 2012); we assume that this lake had a seasonal outflow channel which ultimately became the drainage gully. Remote sensing images suggest that the lake drained catastrophically in 2005. The drainage channel is located south of the basin and leads 275 m through the upland down to the lowland drainage system.

Remnant pools of water are still present in the center of the basin and covered an area of 0.96 ha in the main basin and 0.07 ha in the adjacent basin in September 2011. The main basin floor is elevated about 29 to 31 m asl and moderately flat but pronounced baydzherakhs of about 10m in diameter and up to 1m height are present. Baydzherakhs are conical mounds consisting of ice-wedge polygon centers that are separated by deep troughs from melting of large ice wedges (Soloviev, 1962, cited in French, 1974). Our sediment core was taken from the top of a baydzherakh at 66°27'41''N and 164°8'22''W.

Table 3.1: Metric statistic of GG basin and GG lake derived from satellite images and digital elevation model.

	GG lake (AHAP 1980)	GG basin (Worldview 2011)
Area	7.9 ha	11.9 ha
Elevation yedoma upland	48 m asl	48 m asl
Elevation lake level	40.5 m asl	n.a.
Elevation basin floor	n.a.	28.5 m asl
Average bluff height	7.5 m	19.5 m
Approx. lake depth	12.0 m	n.a.
Total basin depth	n.a.	19.5 m
Volume	712,000 m^3	1,578,000 m^3
Mean slope/Maximum slope	5.8°/24.5°	9.0°/25.7°

AHAP=Alaska High-Altitude Photography; n.a.=not applicable

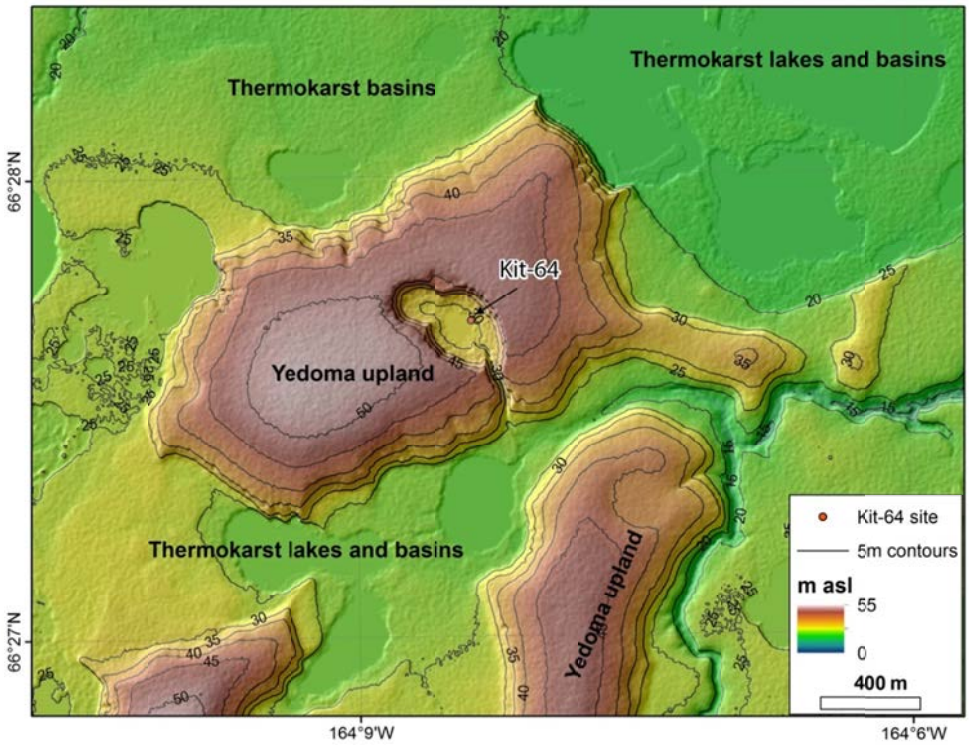

Figure 3.2: Digital elevation model of the drained basin with Kit-64 coring location in a yedoma upland surrounded by thermokarst lakes and basins.

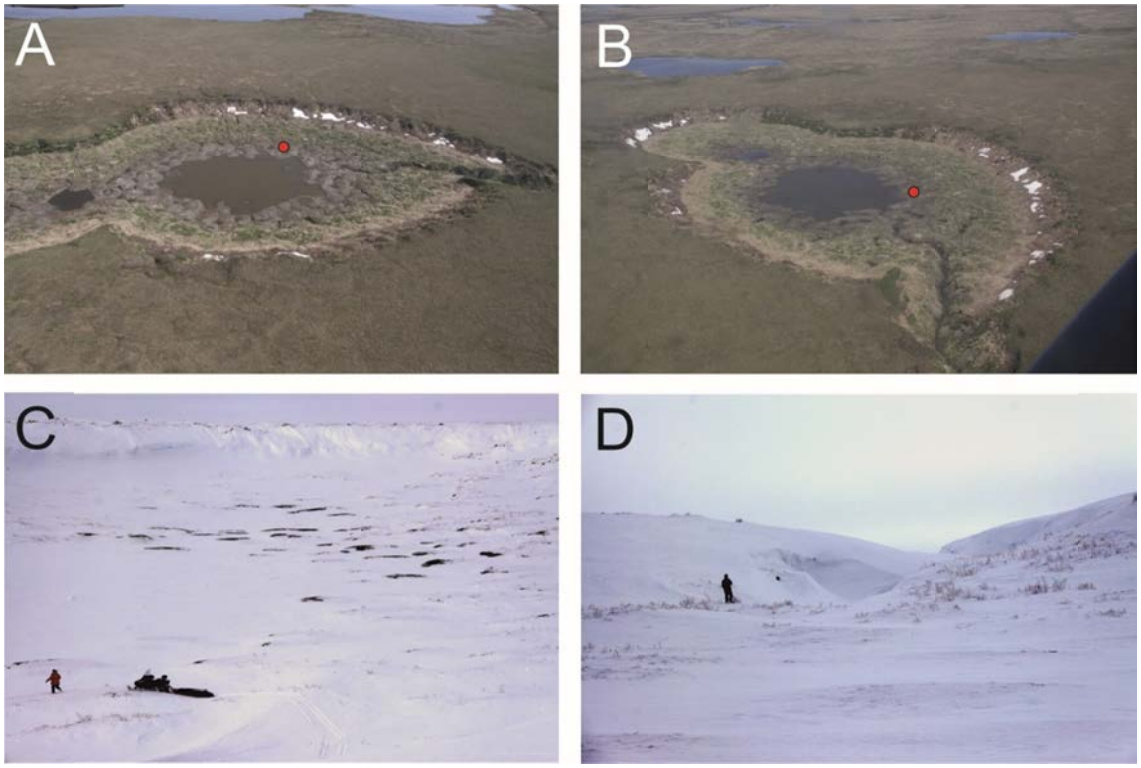

Figure 3.3: Aerial photographs of GG basin with coring location of Kit-64 (red dot). (A) View of the drained basin from southwest to northeast (June 2011); (B) view from south to north; (C) photograph of the southeastern basin margin (April 2009). Note the presence of exposed baydzherakh centers on the basin floor; (D) start of the outflow channel of the basin, which is covered with a large snow drift. Person for scale. See text for abbreviation.

3.4 Material and methods

To reveal the complex landscape history and interaction of land-forming periglacial processes, a multidisciplinary approach was chosen using sedimentological, biogeochemical and paleoecological proxies on a sediment core.

As part of a larger permafrost and thermokarst-focused field campaign on the northern Seward Peninsula in April 2009, a 393 cm core (core ID: Kit-64) was drilled in the thermokarst lake basin described above (informal name: GG basin) (Figures 3.2 and 3.3). The upper frozen sediment section from 0–268 cm was drilled with a SIPRE permafrost corer (Jon Holmgren's Machine Shop, Fairbanks, Alaska, USA). For the unfrozen lower 268–393 cm, a piston hammer corer (Aquatic Instruments, Hope, Montana, USA) was used (all depths are given as centimeters below surface). In the laboratory, both the frozen and unfrozen core segments were cut into halves and high-resolution digital photographs were taken with an optical camera system. A non-destructive analysis of mass-specific magnetic susceptibility (MS) was conducted at the National Lacustrine Core Facility (LacCore) at the University of Minnesota with a Multi-Sensor Core Logger (GEOTEK-MSCL, Daventry, UK). The SI system is used to express MS values in 10^{-6}.

After scanning, core halves were stored frozen or refrigerated, depending on their original field state.

The sediment core was described in detail and subsampled for further analyses at the Alfred Wegener Institute, Helmholtz Centre for Polar and Marine Research in Potsdam, Germany. Pore water was extracted from the frozen core section with rhizon soil moisture samplers (0.2 µm pore diameter, Eijkelkamp, Giesbeek, Netherlands), and electrical conductivity (EC) in µS cm^{-1} (T_{Ref} 25 °C) and pH (both MultiLab 549, WTW, Weilheim, Germany) were measured in fresh water samples. The weight difference between fresh and freeze-dried bulk sediment samples was used to calculate the ice or water content, respectively, which is expressed as weight percentage (wt%). After the removal of organic matter with hydrogen peroxide (H_2O_2, 30%), grain size distribution was measured with a laser particle size analyzer (Coulter LS 200, Krefeld, Germany) according to EN ISO 14688. Particles > 1 mm were dry-sieved for 2 min through 2 mm mesh screens (ATM Sonic Sifter, West Allis, Wisconsin, USA) in order to differentiate gravel.

Total nitrogen (TN), total carbon (TC) and total organic carbon (TOC) were measured in bulk sediments with an elemental analyzer (ElementarVario EL III, Hanau, Germany) with an analytical accuracy of ± 0.1 wt%. The C/N ratio (TOC/TN) was calculated. Values of $\delta_{13}C$ of TOC were analyzed with a Finnigan MAT Delta-S (Bremen, Germany) mass spectrometer equipped with a FLASH elemental analyzer and a CONFLO III (Bremen, Germany) gas mixing system for the online determination of the carbon isotopic composition. Values of $\delta_{13}C_{TOC}$ are expressed relative to the Vienna Pee Dee Belemnite (PDB) standard in per mil (‰) and the standard deviation (1σ) is generally better than $\delta_{13}C_{TOC}$ = ± 0.15 ‰.

Volcanic glass shards in tephra layers were identified on smear slides in glycerin and prepared for geochemical microanalyses in order to identify the source of tephra. Samples were treated with hydrogen peroxide (H_2O_2, 15 %) to remove organic matter, treated with hydrogen chloride (HCl, 10 %) to remove carbonates, wet-sieved through 35 and 125 µm, rinsed in ethanol, dried and embedded in resin on a glass slide. After manual grinding and polishing of samples, the major element glass composition was analyzed by a JEOL JXA-8230 (Munich, Germany) electron microprobe with a voltage of 15 kV, a beam current of 10nA and a beam size of 10 µm. Natural and synthetic minerals and Lipari obsidian were used for instrumental calibration and standardization (Hunt & Hill 1996, Kuehn et al. 2011). Scanning electron microscopy (SEM) images (Zeiss Gemini Ultra+, Jena, Germany) were taken at German Research Centre for Geosciences Potsdam (GFZ) to visualize ash particles.

Paleoecological analyses were carried out to characterize past ecological conditions. Sediment samples with known weight were wet-sieved through 63 and 200 µm mesh screens, dried and examined under a stereo-microscope (Zeiss Stemi 2000-C, Jena, Germany) for species determination of ostracods. Selected ostracod valves were coated with electrically conducting

carbon for SEM images at 40x magnification at the GFZ. Testaceans were identified and counted in glycerin on a glass slide under a light microscope at 100x to 400x magnification (Zeiss Axioskop 2) after subsamples were suspended in purified water and passed through a 500 µm mesh sieve to remove organic and mineral particles. Occasional findings of single diatom algae specimens and ash particles have been recorded.

Accelerator Mass Spectrometry (AMS) radiocarbon age determination of macroscopic plant remains was carried out on wet-sieved (>250 µm) and hand-picked samples. Thirteen samples of plant detritus were dated at the Poznan Radiocarbon Laboratory (Poland) and results were calibrated using CALIB 7.0 with the INTCAL13 data-set (Reimer et al., 2013). The calibration of seven samples was impossible due to old radiocarbon ages extending beyond the calibration data-set. Dates in this study are reported in uncalibrated years before AD 1950, referred to as before present (ka BP), for reasons of unification. Calibrated radiocarbon ages (cal ka BP) are given in Table 3.2.

3.5 Results

3.5.1 Core stratigraphy

The sediment core Kit-64 is characterized by grey, fine grained deposits with organic inclusions and layers (Figure 3.4). Based on lithological descriptions and the analyzed sedimentary, biogeochemical and paleoecological parameters, the sediment core is divided into five lithostratigraphic units:

- Unit A: 393–262 cm
- Unit B: 262–245 cm
- Unit C: 245–146 cm
- Unit D: 146–36 cm
- Unit E: 36–0 cm

Unit A (393–262 cm) comprised the unfrozen sediment section and a small portion of 4 cm of the frozen segment. It was characterized by a dark greyish brown to very dark brown color (Munsell Soil Color Chart (1994), ID 10YR 4/2 to 2/2), unlayered but marbled silt with thick lenses of black (10YR 2/1), well-decomposed organic matter with single pieces of woody remains up to 1 cm long at 386.5 cm and 306 cm. Between 310 and 288 cm, the sediment was interpreted as disturbed since the borehole filled back in at these depths during the drilling process. Unit B (262–245 cm) was a dark olive brown peat (2.5Y 3/2) which was well decomposed at

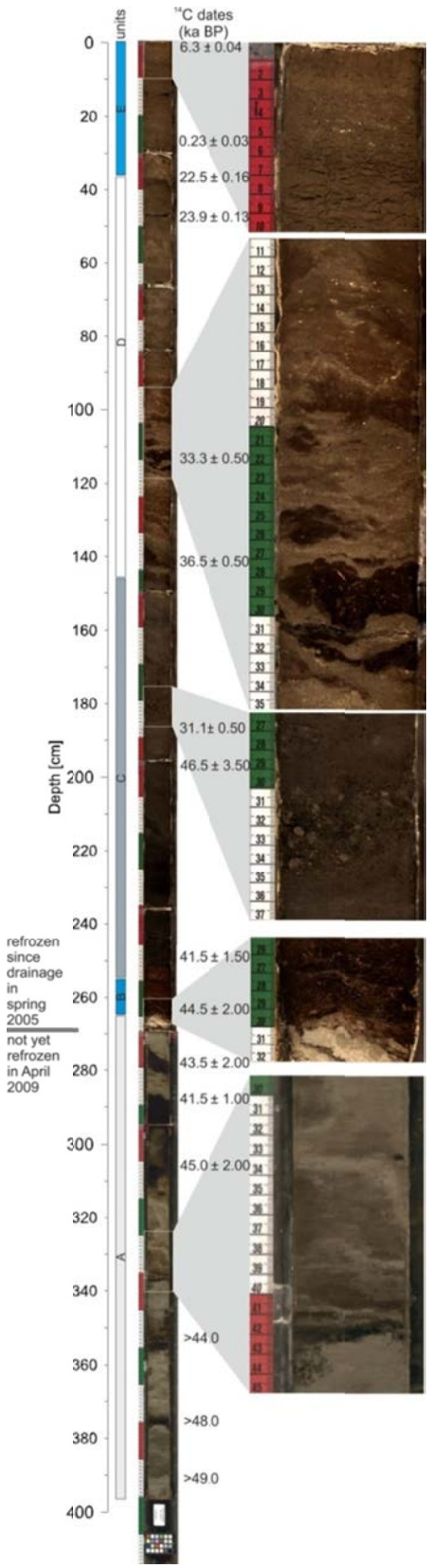

Figure 3.4: Photograph of core Kit-64 and detailed images of each unit. Note the unfrozen state of sediment below 268 cm. Radiocarbon ages are given in uncalibrated years before present.

262–250 cm and poorly decomposed with woody remains of up to 2 cm length at 264–262 cm. Unit C (245–146 cm) was composed of very dark grey (5Y 3/1) to black (2.5Y 2.5/1) minerogenic sediments that were mainly made up of coarse-grained tephra material (grain size up to 7 mm at 182 cm). Unit D (146–36 cm) was olive (5Y 4/4) to dark olive grey (5Y 3/2) in color and characterized by fine-grained sediments with organic-rich inclusions including woody remains at 146–143 cm, 141–137 cm, 117–112 cm and 111–109 cm. From 120 cm, upward slight layering was visible and became more distinct above 64 cm. Unit E (36–0 cm) compromised fine-grained, olive (5Y 4/4) sediments. Here, distinct laminations were visible by color with thicker laminae of about 1 mm at 3–0 cm and thinner laminae of < 0.5 mm at 64–3 cm. Macrofossil plant remains were observed throughout Unit E, and mollusk shells were identified at 25 cm (both valves of 3 mm length), 22 cm and 11 cm.

3.5.2 Cryostratigraphy

The upper part from 266–0 cm (small part of Unit A as well as Unit B to Unit E) was recovered frozen while the lower part from 393–266cm (most part of Unit A) was unfrozen. The mean gravimetric water content of unfrozen Unit A was 26.8wt% (max: 51.1 wt%, min: 14.3 wt%) and a single sample from the uppermost, frozen portion of Unit A yielded an ice content of 19 wt%.

For our cryostructure description, we followed the classification scheme according to Murton and French (1994). The frozen upper 4 cm of Unit A were ice-poor and structureless. Units B and C were also structureless with no visible ice lenses. However, mean ice contents were 55.8 wt% in Unit B and 22.5 wt% in Unit C. The lower section

of Unit D was structureless, but wavy, non-parallel lenticular ice lenses were visible at 152–150 cm and wavy, parallel micro-lenticular ice lenses showed at 93–83 cm. Sub-vertical ice veins of up to 5 cm and 9 cm lengths were identified at 124–115 cm and 83–74 cm, respectively. In the upper section of Unit D, small irregular ice veins were observed at 65–63 cm. Wavy, parallel lenticular cryostructures dominated at 60–44 cm with thin vertical ice veins of up to 11 cm long. Cryostructures at 44–36 cm were structureless again. Mean ice content in Unit D was 32.7wt% with a wide range between 22.3 and 46.7 wt%. The cryostructure of Unit E was parallel micro-lenticular at 36–24 cm and irregular reticulate at 25–6 cm. Parallel lenticular structures with ice lenses of 4 cm length and 2 mm thickness dominated at 6–3 cm, whereas the uppermost 3 cm below the surface were structureless, possibly due to sublimation processes at the exposed drained basin surface during winter. Mean ice content was similar to Unit D with 37.5 wt% and ranged from 44.4 wt% at 11–10 cm to 29.9 wt% near the surface at 2–1 cm.

3.5.3 Grain size distribution

The granulometric results integrated the laminations and general trends in sedimentological variations. According to the nomenclature used by Shephard (1954), the sediment core was dominated by silt with varying proportions of clay and sand (Figure 3.5). A notable exception was the grain size distribution in Unit C and the lower part of Unit D. Here, sand and silty sand were dominating with fractions of gravel mainly in samples at a depth of 181–130 cm (Figures 3.5 and digital appendix figure 3.1). In Units E, D, B and A, mean grain sizes ranged from 5.9 to 6.2 Φ (silt) after Folk and Ward (1957). Unit C is characterized by 2.5 Φ (sand). The sediment of the whole core was poorly to very poorly sorted (2.0 to 2.4 on average after Folk & Ward, 1957).

3.5.4 Magnetic susceptibility

The MS in the core data varied between 0 and 206 (Figure 3.5). In Unit A, MS generally decreased up-core from about 66 to 0 but distinct higher values up to 144 were measured between 298 and 293 cm. In Unit B, MS values increased to 90. The tephra-dominated Unit C exhibited the highest variability of all core units and the highest values of MS of 200 to 206 at about 186–177 cm (average MS of 139). Unit D was less variable (33 on average) with the highest MS value of 78 at the boundary to Unit C and the lowest MS of 15 at 82 cm. Unit E was similar to Unit D with an MS value of 33 on average and a minimum of 23 and maximum of 40.

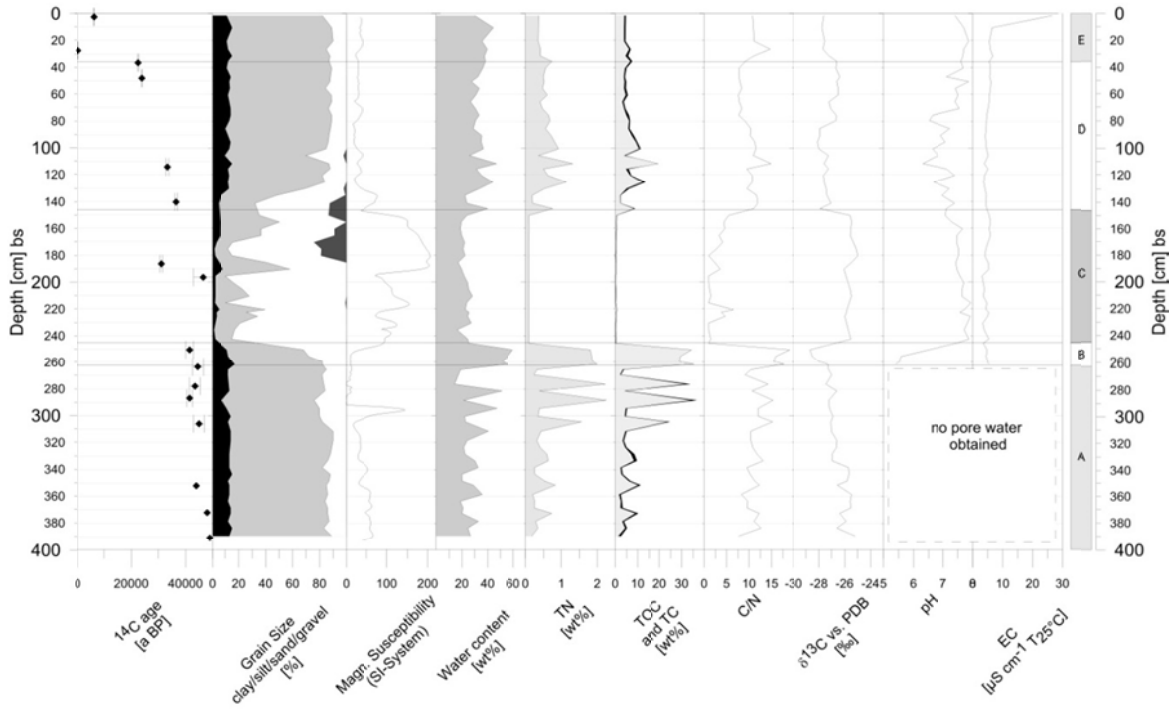

Figure 3.5: Geochronological, lithological and sediment biogeochemical results for core Kit-64: AMS radiocarbon dates, grain size, magnetic susceptibility, water content, total nitrogen (TN), total carbon (TC) and total organic carbon (TOC), C/N ratio, $\delta^{13}C_{TOC}$, pH and electrical conductivity (EC) (only obtained from the frozen core sections). cm bs = Centimeters below surface. Pee Dee Belemnite (PDB).

3.5.5 Biogeochemical characteristics

In Unit A, the TN, TC and TOC were 0.6, 8.5 and 7.6 wt% on average, respectively. A distinct increase in organic carbon content was noted at 305–277 cm. Here, TN_{max} was 2.3 wt%, TC_{max} was 36.6 wt% and TOC_{max} was 34.5 wt% (Figure 3.5). The C/N ratio was relatively steady with 11.3 on average. The $\delta_{13}C_{TOC}$ values in Unit A ranged from -27.5 ‰ to -25.2 ‰ with a clear negative trend towards the top of the core. In Unit B, TN was 1.9 wt%. TOC and TC were nearly the same (32 wt% and 31.5 wt%, respectively) due to the peaty character of this unit. The C/N ratio in Unit B was 17.1 and $\delta_{13}C_{TOC}$ was -28.1 ‰ on average. TN was mostly below the detection limit of 0.1 wt% in Unit C. TC and TOC were also low with 0.4 wt% and 0.3 wt% on average, respectively. This resulted in an average C/N ratio of 2.7. Values of $\delta_{13}C_{TOC}$ were relatively stable at about -25.0 ‰. The biogeochemical properties in Unit C clearly reflected dominance of tephra material in this sediment. In Unit D, biogeochemical parameters varied especially near the transition to Unit C at 146cm and 100 cm (Figure 3.5). Average TN, TC and TOC were 0.6, 6.9 and 6.2 wt%, respectively. The C/N ratio was 9.9. Values of $\delta_{13}C_{TOC}$ ranged between -28.1 ‰ and -26.4 ‰. Unit E exhibited the highest values of TN, TC and TOC at the base of the deposits that decreased upwards until they reached plateau values of 0.4, 4.6 and 4.0 wt%, respectively, in the upper 21 cm. The C/N ratio was 11.3 and $\delta_{13}C_{TOC}$ ranged between -27. ‰ and -26.6 ‰ in Unit E.

3.5.6 Tephra

Unit C consisted of a 1 m thick layer of volcanic air-fall tephra. The geochemical composition of this tephra was analyzed in order to identify the eruptive source and the potential to add tephra geochronological information (Tables 3.2 and digital appendix table 3.1). As displayed in Table 3, all samples between 243 and 155 cm yielded a similar basaltic-trachybasaltic to basaltic andesitic glass composition pointing to a single eruption source for the entire layer. However, differences in particle size indicated different eruption phases of unknown duration. Sharp edges and pronounced vesicles of glass shards indicated a low stage of alteration which in turn pointed to no or only very limited re-deposition processes (Figure 3.6). Radiocarbon dating of lignified shoots and roots in the tephra deposit suggested an age of this layer between 46.5 ± 3.5 ka BP and 31.1 ± 0.5 ka BP. This age range can be further specified by the directly under- and overlying sediments of Units B and D that were dated to 41.5 ± 1.5 ka BP and 36.5 ± 0.5 ka BP, respectively (see Geochronology).

Table 3.2: Results of electron probe microanalyses on glass shards of eight subsamples of the tephra in Unit C of the Kit-64 core from Seward Peninsula. Data are expressed as mean, normalized (volatile-free) values (wt%) and their standard deviations (SD). n=number of single glass shards analyzed. Single non-normalized data of all samples and the Lipari obsidian reference standard are given in digital appendix table 3.1.

Sample	SiO_2	TiO_2	Al_2O_3	FeO	MnO	MgO	CaO	Na_2O	K_2O	P_2O_5	Total	Cl	F
Kit-64, 155-156 cm	51.35	2.76	14.96	9.95	0.15	5.50	9.53	3.91	1.39	0.50	100	0.04	0.00
SD (n=24)	*0.76*	*0.18*	*0.42*	*0.40*	*0.03*	*0.33*	*0.34*	*0.15*	*0.21*	*0.04*		*0.01*	*0.01*
Kit-64, 160-166 cm	51.06	2.44	15.55	9.70	0.15	6.03	9.44	3.88	1.28	0.47	100	0.03	0.00
SD (n=23)	*0.54*	*0.14*	*0.30*	*0.34*	*0.03*	*0.28*	*0.18*	*0.21*	*0.06*	*0.03*		*0.01*	*0.00*
Kit-64, 175-181 cm	51.61	2.59	15.24	9.72	0.14	5.65	9.30	3.85	1.41	0.49	100	0.03	0.00
SD (n=22)	*1.39*	*0.25*	*0.44*	*0.37*	*0.02*	*0.77*	*0.46*	*0.54*	*0.24*	*0.06*		*0.01*	*0.00*
Kit-64, 185-191 cm	51.21	2.51	15.38	9.98	0.15	5.81	9.25	3.83	1.39	0.49	100	0.04	0.00
SD (n=21)	*1.06*	*0.24*	*0.64*	*0.64*	*0.03*	*0.70*	*0.42*	*0.18*	*0.19*	*0.06*		*0.01*	*0.01*
Kit-64, 195-216 cm	51.76	2.55	15.15	9.88	0.16	5.76	9.19	3.75	1.33	0.47	100	0.04	0.00
SD (n=21)	*1.16*	*0.19*	*0.59*	*0.36*	*0.03*	*0.51*	*0.45*	*0.21*	*0.15*	*0.04*		*0.01*	*0.00*
Kit-64, 220-226 cm	49.50	2.77	15.85	9.98	0.15	5.62	9.86	4.15	1.54	0.59	100	0.04	0.00
SD (n=23)	*0.23*	*0.05*	*0.14*	*0.26*	*0.03*	*0.07*	*0.06*	*0.10*	*0.05*	*0.03*		*0.01*	*0.02*
Kit-64, 230-231 cm	51.05	2.83	15.27	9.92	0.15	5.38	9.41	3.94	1.49	0.56	100	0.04	0.00
SD (n=24)	*1.89*	*0.13*	*0.71*	*0.40*	*0.02*	*0.28*	*0.51*	*0.37*	*0.15*	*0.08*		*0.01*	*0.00*
Kit-64, 242-243 cm	51.91	2.80	14.97	9.80	0.16	5.30	9.18	3.92	1.43	0.52	100	0.05	0.00
SD (n=22)	*1.91*	*0.17*	*0.70*	*0.40*	*0.03*	*0.33*	*0.52*	*0.33*	*0.27*	*0.08*		*0.01*	*0.01*

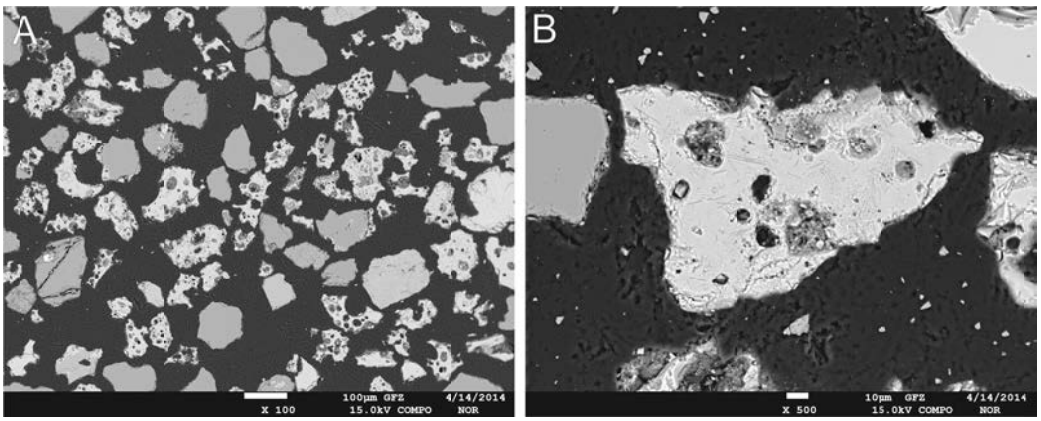

Figure 3.6: Scanning electron microscopy images of polished tephra grains in resin. (A) Tephra particles 100x magnification found at core depth 166-165 cm; (B) tephra particle 500x magnification found at core depth 156-155 cm.

3.5.7 Paleoecology

Lacustrine Environments (pore water and ostracoda)

To characterize past lake conditions, pore water was extracted. No water was obtained from the unfrozen Unit A. An acidic pH of about 5.5 was measured in Unit B, whereas pH was neutral to moderately alkaline in Unit C (pH 7.1-7.9), slightly acid to moderately alkaline in unit D (pH 6.3-7.9) and slightly to moderately alkaline in Unit E (pH 7.4-7.9). The EC of all pore waters was very low with 3–7 µS cm^{-1}. Only the uppermost sample at 2-1 cm yielded increased EC of 26.5 µS cm^{-1}.

A total of 75 samples equally distributed in all units were analyzed for ostracods. Except for the uppermost Unit E, all units lacked fossil remains of ostracods and mollusks pointing either to a non-lacustrine origin of sediments or to unfavorable living or preservation conditions. In Unit E, seven ostracod taxa were identified in four samples representing the uppermost 28 cm of the core (Figures 3.7, Figure 3.8; digital appendix table 3.2). The count numbers of valves per sample range from only six specimens at 28-27 cm up to 794 specimens at 22-21 cm. The species *Cypria ophtalmica*, *Candona ikpukpuensis* and juvenile *Candoninae* (most likely representing juvenile stages of *Fabaeformiscandina protzi*) were found in all four samples. Adult *F. protzi* were observed in the upper 22 cm. Here, single carapaces (both valves attached together) were documented. The findings of intact carapaces point to in-situ preservation of the lacustrine records. Female specimens of *Candona candida* and *F. caudata* are found only at 3–2 cm and 12 cm and *F. pedata* only at 3–2 cm. Male specimens of these three species as well as of *Cypria ophtalmica* were lacking in the record. Both sexes were present for *Candona ikpukpuensis* and *F. protzi*. The species composition was clearly dominated by *F. protzi*; a species known as cold stenothermal that tolerates a wide range of ecological conditions of pH and salinity (Meisch 2000). In modern subarctic and arctic environments, *F. protzi* is so far recorded in the Lena River

Delta (Wetterich et al. 2008a) and the Indigirka Lowland (Schneider et al., 2016) as well as in the Canadian Northwest Territories and the Alaskan Yukon (L. D. Delorme, unpublished data). A broad circumarctic distribution is known for *Candona candida*, a highly tolerant species (e.g. Alm, 1914; Røen, 1962, 1968; Havel et al., 1990; Wetterich et al., 2008a, 2008b; L. D. Delorme, unpublished data) while *F. caudata*, *F. pedata* and *Cypria ophtalmica* show more restricted occurrences in the Canadian subarctic for *F. caudata* (Havel et al. 1990) and in northeastern Siberia for *F. pedata* and *Cypria ophtalmica* (Sars 1898, Wetterich et al. 2008a, Schneider et al. 2016).

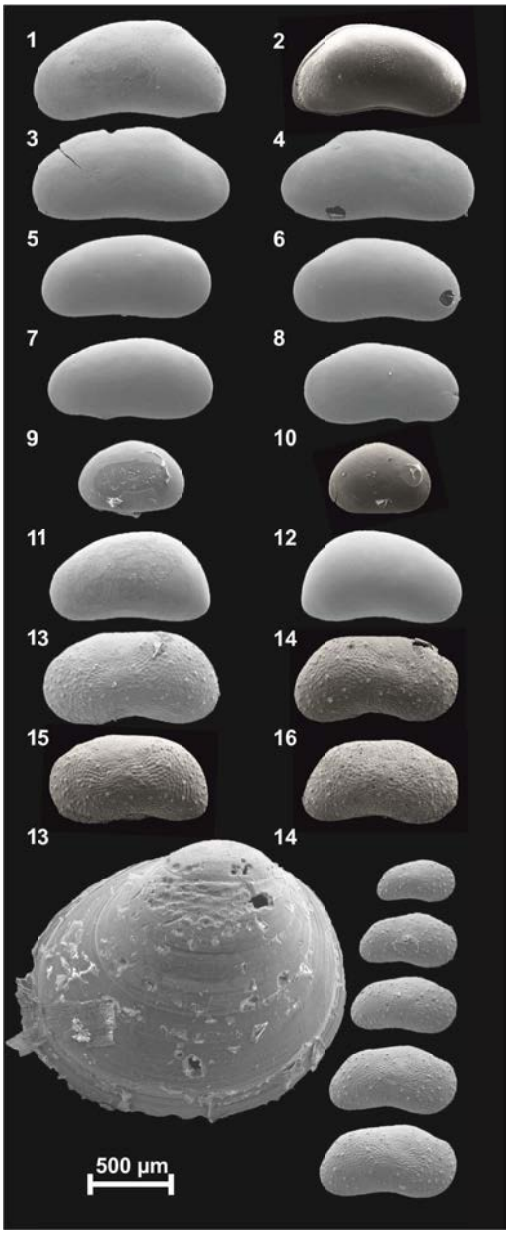

Figure 3.7: Scanning electron microscopy images of fossil ostracod valves and a mollusk shell. *Fabaeformiscandona caudata*: (1) female LV (left Valve), (2) female carapace (RV (Right Valve) view); *F. pedata*: (3) female LV, (4) female RV; *F. protzi*: (5) male LV, (6) male RV, (7) female LV, (8) female RV; *Cypria ophtalmica*: (9) female LV, (10) female RV; *Candona candida*: (11) female LV, (12) female RV; *Candona ikpukpuensis*: (13) male LV, (14) male RV, (15) female LV, (16) female RV; *Pisidia* sp.: valve (17); *Candona ikpukpuensis*: (18) juvenile RVs in five development stages.

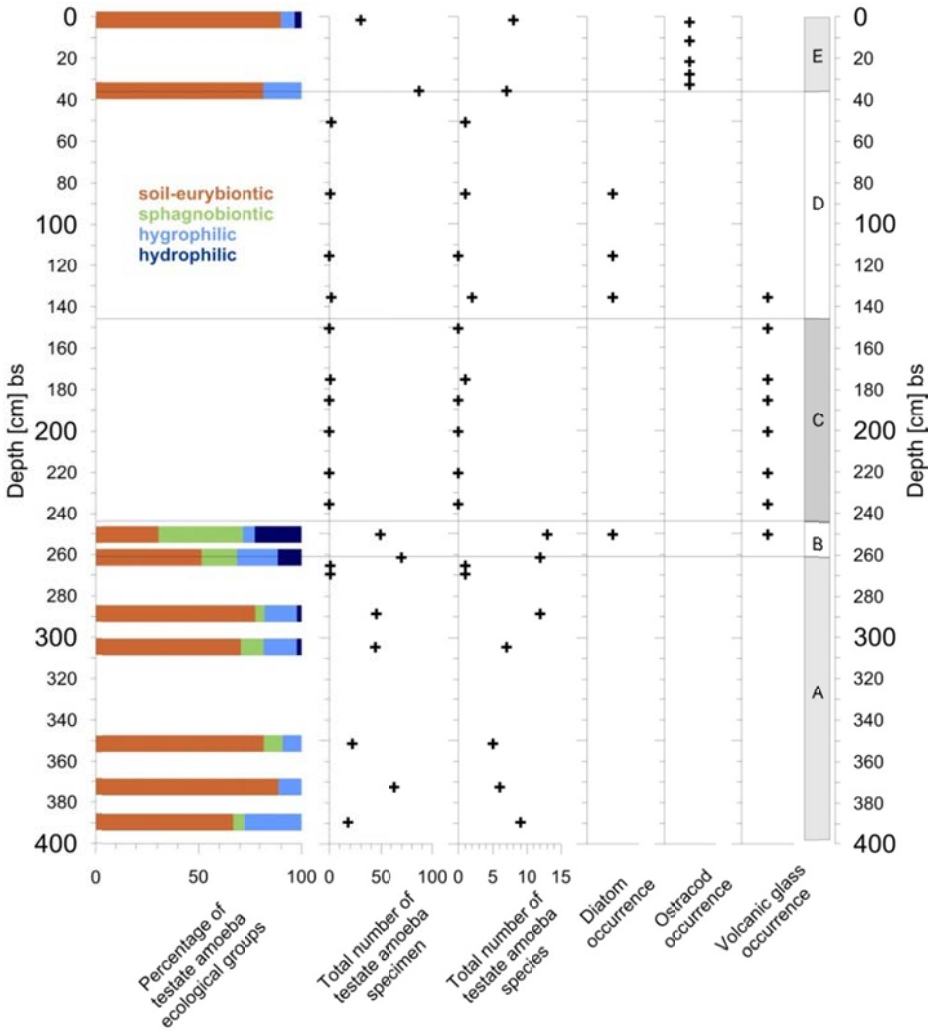

Figure 3.8: Total number of testate amoeba specimens and species, as well as occurrence of diatoms, ostracods and volcanic glass in sediment core Kit-64. cm bs=centimeters below surface.

Modern records *of Candona ikpukpuensis* are only known from the Alaskan Yukon (L. D. Delorme, unpublished data). However, modern ecological reference data on freshwater ostracods is generally still rare in subarctic and arctic regions and therefore of less use for the characterization of Holocene thermokarst conditions. Except for *F. pedata*, fossil records of all species present in Unit E as adult specimens are known from thermokarst deposits of Mid Wisconsin to Holocene age from the Seward Peninsula (Wetterich et al. 2012). Therefore, the ostracod assemblage of Unit E is assumed to represent local shallow-water thermokarst during the Holocene, which was most likely controlled by varying water levels due to summertime evaporation and consequently varying hydrochemical conditions (e.g. increasing ion content because of water loss) during the growing season of ostracods. The high ecological tolerance level of the dominant ostracod species ensured their survival under such conditions.

Testate amoeba

A total of 21 samples were analyzed for the presence of testaceans. Out of these, six samples did not contain any testate amoebae and 15 samples yielded 39 testacean taxa of ten genera (digital appendix table 3.3). Specimen counts per sample varied between single finds and up to 87 (Figure 3.8). Four ecological groups were distinguished based on Chardez (1965) (Figure 3.8): hydrophilic (indicating waterlogged habitats), hygrophylic (indicating moist habitats), sphagnobiontic (typical inhabitants of Sphagnum moss) and soil-eurybiontic species (tolerating a wide range of a particular environmental factor, the specific factor (moisture, pH, etc.) varies between species). The following species were found in three or more samples: *Centropyxis aerophila* v. *major*, *Centropyxis sylvatica*, *Centropyxis sylvatica* f. *major*, *Cyclopyxis eurystoma* and *Plagiopyxis callida* (all soil eurybiontic), *Heleopera petricola* (sphagnobiontic) and *Centropyxis constricta* (hygrophilic).

In Unit A, soil-eurybiontic species of the genera *Centropyxis*, *Cyclopyxis* and *Plagiopyxis* dominated at 390 cm. However, findings of large specimens of the soil-eurybiontic *Centropyxis* aerophila v. major and *Centropyxis sylvatica* f. (*major*) as well as the hydrophilic species *Centropyxis constricta sensu lato* and the sphagnobiontic species *Arcella arenaria* v. *compress* indicated generally moist conditions. At 372–352 cm, sphagnobiontic species were lacking but the species composition still indicated overall moist conditions. At 305 cm, specimen numbers of hydrophilic species *Centropyxis cassis* and *Centropyxis constricta sensu lato* increased indicating a higher degree of moisture. Ecological groups were similar at 289 cm but here also the hydrophilic species Centropyxis gibba occurred. At 270 cm, only single specimen finds of soil-eurybiontic species indicated ecological conditions not favourable for testaceans.

A sharp change in ecological conditions occurred in Unit B. All ecological groups were present and although soileurybiontic species dominated with 50 %, strictly hydrophilic species of the genus *Difflugia* also occurred which indicate very moist conditions. Samples from the tephra-dominated Unit C contained only one observed testacea. In Unit D, only four soil-eurybiontic species with one specimen each were found. In Unit E, high testacean numbers were observed at 36 cm. Here, mainly soil-eurybiontic species from the genera *Centropyxis*, *Cyclopyxis* and *Plagiopyxis* were found but also the hygrophilic species *Centropyxis constricta* and the calceophilic, soil-eurybiontic species *Centropyxis plagiostoma*. *Cyclopyxis kahli* showed moisture enrichment in biophilic elements right above the permafrost table. The same ecological groups but with different species were identified at 2-1 cm.

Other Fossil Remains

In Unit A, a sponge needle occurred at 266–265 cm. Within Unit B, benthic alkaphilic diatoms of the species *Hantzschia amphioxys* and *Navicula elginensis* were found at 251–250 cm. No diatoms were found in samples from Unit C. In Unit D same diatom species were found at 136-135 cm as in Unit A as well as occasional benthic diatom species *N. elginensis* and *Pinnularia brevicostata*. Mollusk remains of *Pisidia* sp. were found in the upper 22 cm of Unit E.

3.5.8 Geochronology

According to the results of 16 AMS radiocarbon determinations, the sediment core covered at least the last 49,000 years (including age inversions and a hiatus between 22.5 and 0.23 ka BP) and allowed a chronological classification of landscape development stages (Figures 3.4 and 3.5; Table 3.3). Out of six-dated plant macrofossils in Unit A, three had infinite ages and two more exceeded the range of current radiocarbon calibration curves. Age inversions in this unit are disregarded due to the large errors of up to 2,000 years and the general limitations of ages close to the methodological limits of radiocarbon dating. An overall age span of > 49 to 44.1 ± 1.0 ka BP was assumed for Unit A, placing this unit most likely into the Early to Mid Wisconsin. According to two radiocarbon dates of 44.5 ± 2.0 ka BP (264-263 cm) and 41.5 ± 1.5 ka BP (251-250 cm), Unit B was dated to the Mid Wisconsin. Unit C provided two radiocarbon ages of 46.5 ± 3.5 ka BP (197-196 cm) and 31.1 ± 0.5 ka BP (187-186 cm) and fell in the Mid Wisconsin. Unit D was dated with four samples and no age inversion between 36.5 ± 0.5 ka BP (141-140 cm) and 22.5 ± 0.16 ka BP (37-36 cm), placing this unit in the transition phase from the Mid to Late Wisconsin. In Unit E, ages included 0.23 ± 0.03 ka BP (28-27 cm) and 6.3 ± 0.04 ka BP (3-2 cm), representing the Holocene deposition of lacustrine sediments and reworking of older organic material from shore erosion processes. An overall age of 290 ± 0.02 cal a BP will be discussed for Unit E. The age inversion in this unit was likely caused by re-deposition of terrestrial organic matter as commonly described in thermokarst lake sediments (Murton 1996, Wetterich et al., 2011, Biskaborn et al. 2013a, Kanevskiy et al. 2014).

Table 3.3: AMS ^{14}C ages from core Kit-64.

Core depth (cm)	Dated plant material	Mass (mgC)	$\delta^{13}C_{TOC}$ (‰)	Uncalibrated ^{14}C age (a BP)	Calibrated 2σ-range (cal a before Christ, BC)	Mean 2σ-age (cal a BP)	Lab. no.
2-3	Rootlets, leaves and shoots, < 1% moss	1.5	-29	6,270 ± 40	5,324-5,205	7,200 ± 60	Poz-49845
27-28	Rootlets of higher plant	0.7	-30	230 ± 30	314-286	290 ± 23	Poz-61951
36-37	Rootlets of higher plants, lignified shoots & leaves	2.3	-27	22,530 ± 160	25,319-24,454	26,800 ± 430	Poz-49846
47.5-48.5	Woody fragments	1.2	-30.7	23,890 ± 130	26,313-25,733	28,000 ± 290	Poz-61952
114	Rootlets of higher plants, lignified shoots and leaves	1.3	-27	33,300 ± 500	36,725-34,323	37,500 ± 200	Poz-49847
140-141	Woody fragments	3.1	-32.1	36,500 ± 500	39,996-38,131	39,100 ± 930	Poz-61953
186-187	Lignified shoots and leaves	0.1	-34.3	31,100 ± 500	34,078-32,171	35,100 ± 950	Poz-49848
196-197	Lignified shoots and leaves	0.4	-34.2	46,500 ± 3,500	[a]	[a]	Poz-49849
250-251	Mostly Carex rootlets and leaves	2.02	-28.1	41,500 ± 1,500	45,889-40,562	45,200 ± ,700	Poz-49851
263-264	Rootlets and leaves, lignified shoots and branches	1.35	-26.3	44,500 ± 2,000	[48,051]-42,682	[a]	Poz-49852
278	Lignified shoots and branches, leaves and rootlets	2.27	-28.3	43,500 ± 2,000	[48,051]-41,885	[a]	Poz-49853
287	Lignified shoots and branches, leaves and rootlets	2.31	-20.3	41,500 ± 1,000	44,713-41,177	44,900 ± ,800	Poz-50096
306	Lignified shoots and branches, leaves and rootlets	2.19	-26.5	45,000 ± 2,000	[48,051]-43,055	[a]	Poz-49855
352	Lignified shoots and branches, rootlets, leaves	1.73	-24.2	>44,000	[a]	[a]	Poz-49856
372	Lignified shoots and branches, rootlets	2.83	-27.6	>48,000	[a]	[a]	Poz-49857
391	Lignified shoots and branches, non-lignified plant remains	2.31	-20.3	>49,000	[a]	[a]	Poz-49866

Calibrated ^{14}C ages were derived using CALIB 7.0 based on the terrestrial radiocarbon age calibration INTCAL13 (Reimer et al., 2013). [a] Calibration was not possible due to old ^{14}C ages.

3.6 Discussion

Our results from core Kit-64 allowed the interpretation of various landscape development stages in the study region for an approximately 50,000 year period (Figure 3.9).

Early to Mid Wisconsin deposition of yedoma and Mid Wisconsin thaw (Unit A)

Fine-grained sediments with interbedded organic-rich material in Unit A represent yedoma deposits that most likely accumulated during the Early to Mid Wisconsin from > 49 to 45 ka BP. Based on the experience that Pleistocene depositional areas in unglaciated regions of Beringia often have long continuous sedimentary records, we assume that Unit A despite the presence of infinite ages is an immediate stratigraphic predecessor of Unit B without hiatus. Although yedoma is a prominent feature of the modern terrestrial unglaciated Arctic of Eurasia and North America (Froese et al. 2009, Kanevskiy et al. 2011, Strauss et al. 2012, Schirrmeister et al. 2013), it only constitutes remnants of the Pleistocene depositional landscape (Grosse et al. 2013b). Here, syngenetic ice-rich permafrost developed concurrently with primarily silt sedimentation under cold and severe climate conditions (Kanevskiy et al. 2011). Although aeolian deposition is assumed to be an important component of yedoma sediment accumulation, other processes such as nival, alluvial and even fluvial and lacustrine processes have contributed to yedoma deposition in the Arctic (Strauss et al. 2012, Schirrmeister et al. 2013). In our record, sediments are dominated by the silty grain size fraction; thus, primary aeolian deposition and secondary re-deposition of aeolian and nival weathering material may have contributed most of the sediment. These processes in turn reflect Beringia's high continentality due to sea-level low stands which resulted in generally cold and dry conditions during this time (Hopkins, 1967; Kaufman and Hopkins 1986). In contrast to the proposed high continentality, less aridity during the LGM was suggested by pollen and insect records from areas adjacent to the Bering Land Bridge (Elias et al. 1997, Ager 2003); steppe-tundra conditions were evident from mammoth remains dated to > 39 ka BP in central Alaska and 27 ka BP on Baldwin Peninsula east of the Seward Peninsula (Hopkins et al. 1976).

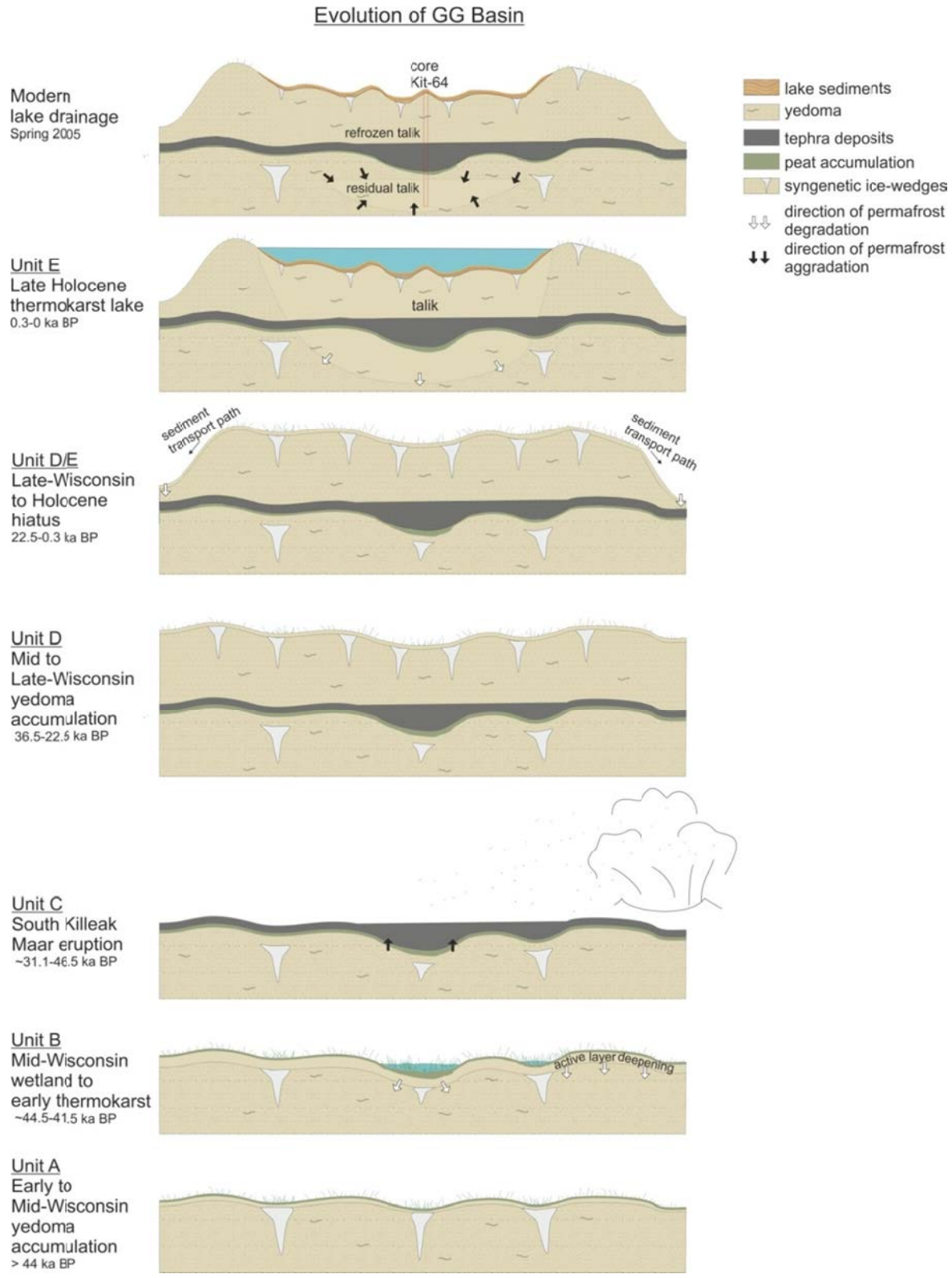

Figure 3.9: Schematic evolution of GG basin. See text for abbreviations.

Organic matter accumulated in permafrost soils under harsh ice age conditions and was only weakly decomposed as it became integrated into permafrost by the seasonally thawing active-layer. Unit A of Kit-64 exhibits a mean TOC of 7.6 wt% which is relatively high compared to the studies of Strauss et al. (2013) (3.0 +1.6/-2.2 wt%), Kanevskiy et al. (2011) (2.8–8.2 % in the active-layer and 0.01-1.7 % in the permafrost) and Zimov et al. (2006) (2–5 %). In Unit A, several organic-rich sections, previously also described for other yedoma sites (Schirrmeister et al. 2008, 2011, 2013), increase the mean TOC value significantly. The inclusions and layers of well-decomposed organic matter contain single pieces of woody remains up to 1 cm in length. These layers have a maximum TOC content of 34.5 wt%, whereas a minimum TOC content of 1.3 wt% is found in the mineral sections of Unit A. The large range indicates the high variability of primary productivity during deposition. In addition, Unit A experienced complete thaw and beginning transformation into a taberite under the former thermokarst lake (Unit E), hence we expect that portions of the originally present carbon were decomposed. However, the TOC data are within the range of previously reported possible values for yedoma (Schirrmeister et al. 2013, from < 1 to > 20 wt% in 700 analyses from 14 Siberian sites). Organic-rich layers in Unit A demonstrate the potential for soil development under Mid Wisconsin conditions. The marbled sediment structure of Unit A points towards soil cryoturbation at the time when the sediment was frozen. Additionally, rhizopods indicate an intermittent wet, but still terrestrial environment since soil-eurybiontic and hygrophilic species dominate but hydrophilic rhizopods are present in the organic-rich layers of the upper part of the unit. Syngenetic freezing of organic-rich sediments resulted in significantly slowed decomposition, forming an effective long-term organic carbon sink (Strauss et al., 2013).

Unit A was recovered almost completely unfrozen (only the uppermost 4 cm of the 125 cm long unit were frozen), indicating the impact of deep thaw under the lake of Unit E and subsequent slow refreezing after this lake drained. Melt out of ground ice including large syngenetic yedoma ice wedges caused a significant loss of volume and ground subsidence. The sediment of Unit A is therefore considered as a diagenetically altered (thaw, compaction in a talik) yedoma deposit also known as taberite (Romanovskii 1993, Walter Anthony et al. 2014).

Mid Wisconsin wetland (Unit B)

The terrestrial yedoma deposition of Unit A is followed by a clear wet phase (Unit B) dated to 44.5 ± 2.0 ka BP to 41.5 ± 1.5 ka BP forming a wetland or shallow pond as indicated by hydrophilic rhizopod communities. Single diatoms were observed, although ostracods were not present. Either ostracods were not preserved in the peaty deposits of Unit B due to acidic conditions as measured in pore-waters with a pH of 5.4-5.6 or living conditions in the Mid Wisconsin were unfavorable. Poor preservation conditions for ostracod calcite in acidic peaty sediments of lacustrine origin were previously reported, for example, by Wetterich et al. (2005).

Higher TOC contents of 29–35.4 wt% in Unit B point to higher bioproductivity, possibly signaling climate amelioration during that part of the Mid Wisconsin. The highest C/N ratio in the core of 19 was calculated for Unit B indicating a low degree of decomposition. In combination with relatively low $\delta^{13}C_{TOC}$ values of -28.7 to -27.3 ‰, it is evident that terrestrial plants from the surrounding catchment are the most likely source of the organic matter (Meyers 1994, Meyers & Lallier-Verges 1999).

Unit B demonstrates intermediate wet conditions allowing the formation of wetlands or initial ponding. Hopkins & Kidd (1988) interpreted lacustrine sequences on exposures along the Seward Peninsula coast as Wisconsin-age thermokarst lakes. Radiocarbon-dated evidence for Mid Wisconsin thermokarst lake development in central Beringia was provided by Wetterich et al. (2012). Here, lacustrine sediments as well as fossils of freshwater mollusks and ostracods indicate that a lake persisted until about 32 ka BP. Various studies in eastern Beringia based on vegetation distribution and summarized by Anderson & Lozhkin (2001) indicate spatially complex but regional warmer temperature conditions during the Mid Wisconsin. For example, herb Betula-Salix low-shrub tundra at 39 ka BP suggesting temperatures warmer than during glacial times but still much cooler than present in the Yukon Territory. However, Beringia was climatically and environmentally heterogeneous due to the effect of boundary conditions like insolation, meteorological conditions, distribution of ice sheets and sea surface temperatures (Anderson & Lozhkin 2001).

South Killeak Maar eruption and tephra fall-out (Unit C)

Because of its age constrain between 46.5 ± 3.5 ka BP and 31.1 ± 0.5 ka BP, we suggest that the Kit-64 tephra most likely coincides with the 42 ka South Killeak Maar eruption (Hopkins 1988, Begét et al. 1996). From this chronological evidence, we exclude a correlation with the much younger Devil Mountain Maar tephra (18.0 ka BP). Unfortunately, we are not able at this stage to strengthen this correlation by the comparison of tephra compositions due to the lack of glass chemical data in the literature. Both, the South Killeak and Devil Mountain Maar tephra are in general described as basaltic air fall products of phreatomagmatic eruptions, which are known to be extraordinarily explosive because frozen (solid) water in permafrost is rapidly transformed to the gas phase (e.g. Hopkins 1988, Begét et al. 1996). Our data provide the first geochemical data-set of the South Killeak Maar tephra (Table 3). Previously, several studies focused on investigations of a paleosol buried by the younger Devil Mountain Maar tephra (Höfle & Ping, 1996, Höfle et al. 2000, Goetcheus & Birks 2001, Kuzmina et al. 2008) but geochemical data of this and other tephra layers have not been reported so far. As tephra layers are important stratigraphic markers, the geochemical glass data of the Kit-64 tephra can be of great value for future paleoenvironmental investigations in the region.

The 1 m thick air-fall tephra associated with the South Killeak Maar eruption at about 42 ka BP interrupted and abruptly terminated the wetland development at our site (Unit B). The abrupt change of facies from Unit B to C is not only evident in the lithology but also in the high MS signals, low biogenic deposition, high accumulation of clastic material greater than 0.063 mm up to occasional 7 mm grain size, as well as isotopic enrichment in $\delta_{13}C_{TOC}$. The absence of rhizopods, diatoms and ostracods points towards unfavorable living conditions or, alternatively, very rapid deposition of the entire unit. It can be assumed that the wetland or initial pond was entirely covered by tephra. Apparently, the South Killeak Maar eruption had a significant influence on the regional wetland and pond development and thus may have substantially changed the local to regional landscape evolution by filling and levelling terrain depressions.

Continued yedoma accumulation during the Mid to Late Wisconsin (Unit D)

The initial Mid Wisconsin wetland or shallow pond did not recover after the fall-out of the South Killeak Maar tephra but terrestrial silty sediment accumulated with intermediate organic layers within a time span of 36.5 ± 0.5 ka BP to 22.5 ± 0.16 ka BP. The sedimentological and biogeochemical properties of these yedoma deposits are similar to those in Unit A. Four findings of a soil-eurybiontic testate amoeba species indicate a generally cold and dry depositional environment. No ostracods but the occasional presence of diatoms were reported which is not unusual in yedoma deposits as proven by molecular biomarkers (occurrence of brassicasterol, J. Strauss, personal communication; detected in Siberian yedoma, Strauss et al. 2014) indicating seasonally wet phases.

Late Wisconsin to Late Holocene hiatus (Transition from Unit D to Unit E)

At 36 cm, a change of facies is noted and its transition was bracketed by radiocarbon dates of 22.5 ± 0.16 ka BP below the boundary and 0.23 ± 0.03 ka BP above the boundary from Unit D to Unit E. We hypothesize that this apparent hiatus of sedimentation may be explained either by a lack of deposition during the Lateglacial and Holocene or by Early Holocene thermokarst-related erosion of surficial deposits at the study site. Both scenarios have been suggested as a responsible mechanism for a depositional hiatus during this period in other studies of yedoma and thermokarst profiles of northern Siberia (Grosse et al. 2007, Andreev et al. 2009).

In our hypothetical scenario, after syngenetic permafrost accumulation during the Mid to Late Wisconsin, a period of massive thermokarst initiated in the region. Deep and widespread permafrost thaw is suggested in various datasets from northwest North America and Siberia which propose strong postglacial warming and peaking at the onset of the Holocene Thermal Maximum (HTM) (McCulloch & Hopkins 1966, Burn et al. 1986, Rampton 1988, Burn & Smith 1990, Burn 1997, Kaufman et al. 2004, Walter et al. 2007, Wetterich et al. 2012, Fritz et al. 2012, Lenz et al. 2013, Morgenstern et al. 2013, Schleusner et al. 2015). Alaska and the western

Canadian Arctic warmed earlier (11.3 ± 1.5 cal ka BP) than continental Canada and the Canadian Arctic Archipelago (7.3 ± 1.6 cal ka BP) due to the cooling influence of the Laurentide Ice Sheet (Kaufman et al. 2004). Although timing of the HTM varied spatially, an increase in mean summer temperature of 1.6 ± 0.8 °C compared to average 20th century is assumed for the North American Arctic (Kaufman et al. 2004). Rapid thermokarst formation in the study region resulted in dissection of the yedoma uplands which is evident from the general geomorphology of the region. Yedoma remnants were carved out and persisted as smaller uplands until modern times while thermokarst lakes now dominate the lowlands (see also Figure 3.2). Kanevskiy et al. (2014) stated that the process of reducing yedoma to isolated remnant hills by thermokarst lake development can take thousands of years. In this case, the yedoma upland of the modern GG basin (Figure 3.2) served as a sediment source and parts of the potentially present Late Wisconsin deposits were eroded. This phase of intense thermokarst activity, indicating warmer and wetter climate conditions in the Late Wisconsin and Holocene, is not resolved in our record by sedimentation but indicated by a depositional hiatus. Thus, neither the LGM nor the prominent Devil Mountain Maar tephra was archived in the record of core Kit-64.

Late Holocene thermokarst lake (Unit E)

A lake phase forming GG basin evidently started about 300 years ago (0.23 ± 0.3 ka BP or 290 ± 0.02 cal a BP at 28-27 cm) as suggested by distinct laminations and mollusk shells as well as a well-preserved ostracod assemblage indicating a cold freshwater, shallow-water ecosystem. The cause for the lake initiation is difficult to access based on a single core alone, but we speculate that local disturbances of the ground thermal regime rather than a broader climatic signal were the most likely cause. The high ecological tolerance of ostracods present allowed them to live in altering hydrochemical conditions during the Late Holocene. At the lower boundary of Unit E, increased bioproductivity of the initiating shallow lake is signaled by higher TN, TC and TOC. A C/N ratio of 14 indicates a poor decomposition of organic matter in the early phase. Testate amoeba point towards a shift from terrestrial wet to aquatic conditions; so does the ratio of $\delta^{13}C_{TOC}$ and C/N ratio. The EC of pore water is as low as in the rest of the frozen core but increased at the sediment surface to 26.5 µS cm^{-1} $T_{25°}$ indicating sublimation processes at the surface which were also evident in the field by a salty crust.

The presence of a thermokarst lake is visible in a series of aerial and satellite images taken in 1950, 1978, 2004 and 2005 (Figure 3.10). In 1980, GG lake had a mean water depth of 12 m and a surface area of 7.9 ha (Table 3.1). Jones et al. (2011) analyzed high-resolution remotely sensed imagery to determine thermokarst lake expansion rates on the northern Seward Peninsula between the early 1950s and mid-2000s. Thermokarst lakes surrounded by yedoma terrain typically have lake bluff heights that range from 6-17 m and erosion rates of 0.15-0.18 m a^{-1} over this time period. Between 1950 and 1978, the lake that formerly occupied GG basin decreased in surface

area by 0.2 ha indicating that the lake may have started to drain slightly during this period. While the shoreline receded around much of the lake perimeter, the lake eroded towards the outlet and eventual drainage gully location at a rate of ~ 0.20 m a^{-1}. The 1978 aerial photograph also revealed substantial erosion (~30 m) along the drainage gully relative to the 1950 aerial photograph. There is a lack of high-resolution remotely sensed imagery following the 1978 image and prior to the drainage of the lake that occupied GG basin. The presence of baydzherakhs on the lake floor (Figures 3.3 and 3.10) indicates that GG lake was a first-generation thermokarst lake. The presence of baydzherakhs also suggests that not much surface sediment was removed during the drainage event. The sediment core, taken from the top of a baydzherakh, had only 36 cm of lake sediment. Cross-sections of thermokarst lake deposits on the Seward Peninsula show highly variable lacustrine sediment thicknesses with thicker sediment packages in the troughs between baydzherakhs and thinner lake sediments on top of baydzherakhs (G. Grosse, unpublished data).

The water volume of GG lake was calculated to about 0.7 million m^3 for the year 1980. With about 12 m water depth in 1980 (Table 3.1), GG lake was deep enough to prevent lake ice grounding. Therefore, this young lake must already have had a substantial thaw bulb or talik which is a body of unfrozen ground due to a local anomaly in thermal, hydrological, hydrogeological or hydrochemical conditions (van Everdingen 2005).

Late Holocene lake drainage and basin development since Spring 2005 AD

Landsat imagery shows that the lake likely drained catastrophically between May and June 2005 (Figure 3.10): On 23 May 2005, the lake was largely ice-free but a residual ice cover was still present in the center of the larger basin. On 24 June 2005, the lake had already drained except for a small remnant pond. Whereas GG basin has mean bluff heights of 7.5 m and maximum heights of 20 m, up to 40 m of thaw settlement were observed for yedoma deposits in central Yakutia (Czudek & Demek 1970). Kessler et al. (2012) described a thermokarst lake system forming in yedoma on the northern Seward Peninsula near our study site with a total thaw settlement of 20-30 m similar to GG basin. Based on the digital elevation model (DEM), about 1.6 million m^3 volume loss was caused by thawing of yedoma during the lake formation of GG basin (Table 3.1). The net surface area of lakes on the northern Seward Peninsula decreased between 1950/51 and 2006/07 by 14.9 % (Jones et al. 2011) due to the drainage of several large lakes. Jones et al. (2012) described a high number of drainage events within the last 4000 years, especially during the medieval climate anomaly.

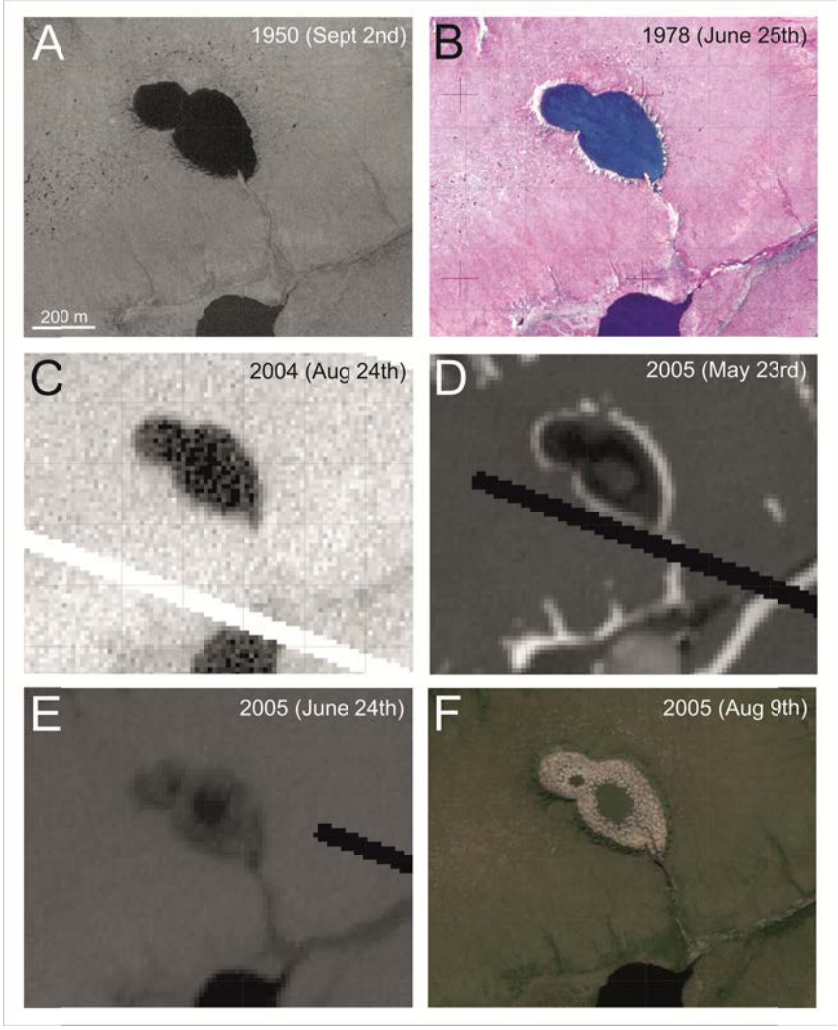

Figure 3.10: Time series of remote sensing imagery of the study area: (A) Black and white aerial image (2 Sep 1950); (B) color infrared aerial image (25 Jun 1978); (C) Landsat Enhanced Thematic Mapper (ETM)+panchromatic satellite image (24 Aug 2004); (D) Landsat ETM+panchromatic satellite image (23 May 2005); (E) Landsat ETM+panchromatic satellite image (24 June 2005); (F) Quickbird satellite image (9 Aug 2005).

Peat most rapidly accumulated with 35.2 g C m^{-2} a^{-1} in the youngest basins which drained 50–500 years ago. In general, thermokarst lake basins in the Cape Espenberg lowlands of the northern Seward Peninsula (covering 76 % of the surface) are thought to store 6.4–6.6 Tg organic carbon in their terrestrial peat (Jones et al. 2012). Drained in spring 2005, no substantial vegetation cover had re-occupied the floor of GG basin in 2009 when coring took place. Post-drainage succession will likely result in vegetation re-occupation of the basin over the next years and possibly will result in slow peat accumulation. However, unlike the very wet lowland basins in our study region described in Jones et al. (2012) or on the Barrow Peninsula by Zona et al. (2010), gross primary productivity might stay low in the well-drained upland of GG basin. Since permafrost redeveloped within 4 years from the surface down to 268 cm in April 2009, it can be assumed that the formation of a new lake is not yet in progress but that the existing ponds are remnants of GG lake. Regmi et al. (2012) stated that the succession of a thermokarst lake in an old drained basin is

dependent not only on climate variability but also basin topography and hydrology, the amount of ice content, the rate of vegetation succession and polygonal development.

Modern permafrost aggradation is discussed in the literature primarily in the context of development after local lake drainage. The prominent Illisarvik lake drainage experiment in 1978 by Ross Mackay revealed evidence for rapid re-aggradation of permafrost (Mackay 1997). The up to 32 m deep talik of Illisarvik lake refroze down to 5-6 m within 2 years after drainage, whereas nearshore sites of ≤ 10 m were already completely refrozen (Burgess et al. 1982). Mean summer subsidence of the Illisarvik basin decreased during the first 8 years from 10 to 3 cm before winter frost heave and summer subsidence stabilized. Here, change in snow depth associated with vegetation growth is assumed to be the dominant control on variation of active-layer depth (Mackay & Burn 2002). Growth of aggradational ice of 0.5 cm a^{-1} has been recorded 20 years after the experiment took place (Mackay & Burn 2002).

Every year approximately 0.3 to two lakes drain in different regions in Arctic North America (northern Seward Peninsula: Jones et al. 2011, North Slope: Hinkel et al. 2007, northwest Canada: Marsh et al. 2009). Lateral drainage can be triggered by a number of geomorphological and hydrological processes such as bank over-topping as a result of heavy precipitation events, gully erosion through ice-wedge networks or tapping by rivers, lakes and coastal erosion (Hinkel et al. 2007, Marsh et al. 2009, Grosse et al. 2013a, Jones & Arp 2015). The lateral drainage of GG lake was likely caused by an increased inflow into the lake from snowmelt and eventually by an overflow at the outlet channel that resulted in down-cutting into the ice-rich permafrost and promoting the drainage of the lake.

3.7 Conclusions

A sediment core record from a drained lake basin allowed us to reconstruct Mid Wisconsin to Holocene landscape dynamics for this region typical of central Beringia. The following conclusions can be drawn:

1. A multi-proxy approach allowed the determination of complex landscape interactions in a changing Arctic system affected by permafrost.
2. Yedoma deposition prevailed throughout the Early to Mid Wisconsin with intermediate wet conditions by about 44.5 to 41.5 ka BP. Here, initial permafrost thaw began as indicated by wetland or potentially shallow pond formation but was terminated by the deposition of a thick air-fall tephra, most likely originating from the South Killeak Maar eruption at about 42 ka BP. A depositional hiatus in our core between 22.5 and 0.23 ka BP was interpreted as a signal of strong landscape changes and local erosion associated with thermokarst development in the areas surrounding our yedoma upland site during the Lateglacial to Holocene. Following this period, our

study site served as a sediment source for surrounding large thermokarst lakes and basins rather than an accumulation area until the formation of a small thermokarst lake on the upland about 300 years ago. This expanding and deepening lake drained catastrophically in spring 2005 as indicated by remote sensing thermokarst lake basin in which permafrost has just started to aggrade again.

3. Permafrost formation, as well as degradation, in our study region in central Beringia over the last 49 ka was controlled by regional to global climate patterns impacting processes (syngenetic permafrost formation during the Early to Late Wisconsin; wetland formation during short warmer and wetter phases of the Mid Wisconsin; Lateglacial and Early Holocene spread of thermokarst development) as well as local disturbances (wetland and pond burial during a Mid Wisconsin tephra deposition event caused by a nearby phreatomagmatic maar lake eruption; thermokarst lake formation during the Late Holocene; sudden lake drainage in 2005).

Acknowledgements

We thank the National Park Service (NPS) for permitting research in the Bering Land Bridge National Preserve and L. McFadden for help in the field. We thank L. Farquharson, A. Myrbo and other colleagues from the National Science Foundation (NSF)-sponsored LacCore facility at the University of Minnesota for facilitating core splitting and GEOTEK scanning. Further, we would like to thank H. Kemnitz, I. Schäpan and O. Appelt (GFZ) for facilitating the SEM imaging as well as the geochemical analyses of tephra. R. Zibulski helped with the determination of radiocarbon-dated plant macrofossils. Laboratory assistance was provided by U. Bastian, A. Eulenburg, L. Schönicke and H. Meyer. Diatom species identification was thankfully undertaken by L. Pestryakova (North-eastern Federal University Yakutsk, Russia). We thank Jones for reviewing the manuscript. The study contributes to the Arctic Ecological Network (Arc-EcoNet) funded by the German Federal Ministry of Education and Research (BMBF Grant No. 01DJ14003). Funding was provided by the NSF (ARC0732735), the NASA (NNX08AJ37G), the Western Alaska Landscape Conservation Cooperative (LCC) (WA2011-02) and a doctoral stipend by the University of Potsdam awarded to J. Lenz. Any use of trade, product, or firm names is for descriptive purposes only and does not imply endorsement by the US Government. We thank Jef F. Vandenberghe, Mark Bateman and all guest editors of the special issue Reconstruction and modelling of paleo-permafrost as well as two anonymous reviewers who helped to improve the manuscript.

4 Evidence of multiple thermokarst lake generations from an 11,800-year old permafrost core on the northern Seward Peninsula, Alaska

Josefine Lenz[1,2], Sebastian Wetterich[1], Benjamin M. Jones[3], Hanno Meyer[1], Anatoly Bobrov[4] and Guido Grosse[1,2]

[1] Department of Periglacial Research, Alfred Wegener Institute, Helmholtz Centre for Polar and Marine Research, Potsdam, Germany

[2] Institute for Earth and Environmental Sciences, University of Potsdam, Potsdam, Germany

[3] Alaska Science Center, US Geological Survey, Anchorage, AK, USA

[4] Faculty of Soil Science, Lomonosov Moscow State University, Moscow, Russia

In press in: Boreas, DOI: 10.1111/bor.12186

Key words: Permafrost dynamics, Thermokarst processes, Paleoenvironment, Central Beringia, Lateglacial and Holocene, Carbon cycling

4.1 Abstract

Permafrost degradation influences the morphology, biogeochemical cycling and hydrology of Arctic landscapes over a range of time scales. To reconstruct temporal patterns of early to late Holocene permafrost and thermokarst dynamics, site-specific paleo-records are needed. Here we present a multi-proxy study of a 350-cm-long permafrost core from a drained lake basin on the northern Seward Peninsula, Alaska, revealing Lateglacial to Holocene thermokarst lake dynamics in a central location of Beringia. Use of radiocarbon dating, micropaleontology (ostracods and testaceans), sedimentology (grain-size analyses, magnetic susceptibility, tephra analyses), geochemistry (total nitrogen and carbon, total organic carbon, $\delta^{13}C_{TOC}$) and stable water isotopes ($\delta^{18}O$, δD, d excess) of ground ice allowed the reconstruction of several distinct thermokarst lake phases. These include a pre-lacustrine environment at the base of the core characterized by the Devil Mountain Maar tephra (22.8 ± 0.28 cal ka BP, Unit A), which has vertically subsided in places due to subsequent development of a deep thermokarst lake that initiated around 11.8 cal ka BP (Unit B). At about 9.0 cal ka BP this lake transitioned from a stable depositional environment to a very dynamic lake system (Unit C) characterized by fluctuating lake levels, potentially intermediate wetland development, and expansion and erosion of shore deposits. Complete drainage of this lake occurred at 1.1 cal ka BP, including post-drainage sediment freezing from the top down to 154 cm and gradual accumulation of terrestrial peat (Unit D), as well as uniform

upward talik refreezing. This core-based reconstruction of multiple thermokarst lake generations since 11.8 cal ka BP improves our understanding of the temporal scales of thermokarst lake development from initiation to drainage, demonstrates complex landscape evolution in the ice-rich permafrost regions of Central Beringia during the Lateglacial and Holocene, and enhances our understanding of biogeochemical cycles in thermokarst-affected regions of the Arctic.

4.2 Introduction

Understanding past environmental change is important for assessing the potential impact of future climate variability on permafrost-influenced landscapes in the Arctic. Permafrost plays a key role in the Earth System because it withdraws a large amount of carbon from the carbon cycle by long-term sequestration into perennially frozen soils (Hugelius et al. 2014). However, permafrost, and thus the preservation of frozen carbon, is vulnerable to thaw due to increasing air temperatures, creating the potential for extensive permafrost degradation and the formation of thermokarst landforms (Romanovsky et al. 2010, Grosse et al. 2011).

Thermokarst lakes form in depressions that result from thawing ice-rich permafrost and melting ground ice (van Everdingen 1998). Widespread thermokarst lake initiation appears to have coincided with the onset of the Holocene as a result of warmer and wetter conditions relative to the Pleistocene (Rampton 1988, Walter et al. 2007). Since then, the expansion, shrinkage, coalescence and drainage of thermokarst lakes in ice-rich Arctic coastal lowlands has created a complex periglacial landscape of varying-aged lakes and drained lake basins (Hopkins & Kidd 1988, Jones et al. 2012). The potentially cyclical nature of thermokarst lakes forming, draining and reforming in arctic coastal lowlands has been a topic of discussion for several decades (Billings & Peterson 1980, Harry & French 1983, Jorgenson & Shur 2007). While thermokarst lake dynamics have been studied in various permafrost regions with satellite imagery and field observations (e.g. in Alaska: Hinkel et al. 2007, Jones et al. 2011, Jones & Arp 2015, NW Canada: MacDonald et al. 2012, Olthof et al. 2015, Siberia: Morgenstern et al. 2013, Séjourné et al. 2015), observations of site-specific thermokarst lake dynamics occurring over long time scales are scarce. A number of lake sediment records have been studied previously to better understand thermokarst processes (Alaska: Jones et al. 2012, Gaglioti et al. 2014, Lenz et al. 2016, Farquharson et al. 2016, northwestern Canada: Michel et al. 1989, Lenz et al. 2013, Siberia: Kaplina & Lozhkin 1980, Biskaborn et al. 2013a,b, Schleusner et al. 2015) while a few studies have focused on the characteristics, evolution and role of vegetated drained lake basins with respect to carbon storage and biogeochemical cycling in Arctic coastal lowlands (Hinkel et al. 2003, Bockheim et al. 2004, Zona et al. 2010, Jones et al. 2012, Fritz et al. in press). However, observations of multiple thermokarst lake generations within a Lateglacial-Holocene

paleoenvironmental record have not been reported so far even though significant effects on e.g. carbon cycling can be expected.

Here we present a multi-proxy record from a permafrost core taken in a drained thermokarst lake basin located on the northern Seward Peninsula (northwest Alaska) to investigate the complex dynamics in spatially overlapping thermokarst lake generations and the vertical chronosequence of thermokarst lake deposits. The northern Seward Peninsula is of particular interest because of its unique location in Central Beringia, the former non-glaciated land bridge between Eurasia and North America, which not only allowed human migration and population of America during the last deglaciation until about 11,000 years ago (Hopkins 1959) but also enabled long-term permafrost development in a continental climate (French & Millar 2014, Vandenberghe et al. 2014). In this region, thick syngenetic permafrost of the Late Pleistocene ice-rich yedoma suite has accumulated (Kanevskiy et al. 2011), while deglacial to Early Holocene warming and sea-level rise shifted the environmental setting from highly continental to more maritime. Thermokarst lakes formed in this region due to thaw of ice-rich yedoma permafrost (Hopkins & Kidd 1988, Lenz et al. 2016) and numerous drained basins characterize the modern morphology of the northern Seward Peninsula (Jones et al. 2012). Remote sensing studies of spatially overlapping drained lake basins in conjunction with radiocarbon dating of basal ages indicate that such cycling over longer time scales resulted in up to seven overlapping generations of lake basins (Jones et al. 2012, Regmi et al. 2012). This spatial overlap and the vertical chronosequence of lacustrine and terrestrial phases probably have profound implications for local stratigraphy and biogeochemical cycling in these lakes (Walter Anthony et al. 2014). In particular, there is the potential for lacustrine deposits of different lake generations, interspersed by terrestrial deposits, to be preserved on top of each other in lake-basin cores. In this paper, we address the following research questions: (I) how are maturation of permafrost landscapes and thermokarst dynamics reflected in sedimentary, paleontological and geochemical proxy data?; (II) what are the implications of lake development on the northern Seward Peninsula for carbon cycling and large-scale environmental change during the Lateglacial and Holocene?

4.3 Study area

The study is based on a 350-cm-long sediment core taken in April 2009 from the centre of a drained thermokarst lake basin located on the Cape Espenberg lowlands, northern Seward Peninsula, NW Alaska (latitude 66°33'57''N, longitude 164°28'53''W, Figure 4.1). The northern Seward Peninsula is part of the Bering Land Bridge National Park and Preserve and one of the major lake districts in Alaska, where 7.1 % of the surface area is covered with extant lakes > 1 ha in area (Arp & Jones 2009). More than 75 % of the Cape Espenberg lowlands have been reworked by the formation and drainage of thermokarst lakes (Jones et al. 2012). Our drained lake basin (informal name: Mama Rhonda) core site (Kit-43) is located 600 m inland from the Chukchi Sea coast and lies 7.4 m above sea level (m asl., Figure 4.1). An extant thermokarst lake, Rhonda Lake, whose area is 80 ha and whose average depth is ~ 1 m, is located to the south and east of the Kit-43 coring location.

Figure 4.1: (A) Study area and coring location of Kit-43 as well as location of Kit-1 (Wetterich et al. 2012) and Kit-64 (Lenz et al. 2016) on the northern Seward Peninsula (©SpotImage Planet Action), which is shaped by numerous drained thermokarst lake basins (yellow circles, see Jones et al. 2012) and located in (B) central-eastern Beringia (exposed shelves down to –120 m below modern sea level during the LGM shown in green colors; Peltier & Fairbanks 2006). (C) Aerial photograph of the study site from northeast to southwest shows modern Lake Rhonda and coring site Kit-43 (white dot).

Due to a lower sea level during the Last Glacial Maximum (LGM, 26.5–19.0 ka BP), the continental shelves of the Bering and Chukchi Sea were widely exposed and our study site was located in the center of a wide Bering Land Bridge (Hopkins 1967, Kaufman & Hopkins 1985). Continental climate allowed continuous permafrost to develop, which today is approximately 100 m thick (Jorgenson et al. 2008) with a mean annual ground temperature that ranges from -5 to -2 °C (Smith et al. 2010). Besides remnants of Late Pleistocene yedoma uplands, the local morphology is shaped by Holocene periglacial landscape features like thermo-erosional gullies, pingos and polygonal patterned ground, as well as thermokarst lakes and drained thermokarst lake basins (Hopkins 1967, Jones et al. 2011, Regmi et al. 2012, Wetterich et al. 2012). Non-thermokarst lakes of late Quaternary volcanic origin are also present on the northern Seward Peninsula: The Devil Mountain Maar Lakes located about 16 km south of the coring location were created during multiple phreatomagmatic eruptions at 21.5 cal ka BP (Hopkins 1988, Begét et al. 1996). The Devil Mountain Maar tephra is distributed over an area of about 2,500 km² and buried the excellently preserved LGM Kitluk paleosol (Höfle et al. 2000, Goetcheus & Birks 2001, Kuzmina et al. 2008). The two South and North Killeak Maar lakes formed about 42 and > 125 ka BP, respectively, whereas Whitefish Maar is assumed to be 100,000–200,000 years old (Hopkins 1988).

Based on observations from Kotzebue (90 km northeast of the study site), the modern climate is classified as subarctic, with a mean January air temperature of -20 °C, a mean July air temperature of +12 °C and a mean annual air temperature of -6 °C. Average annual precipitation is 230 mm a^{-1}, with more than half of the precipitation falling as rain in summer and early autumn (US National Weather Service data, http://www.ncdc.noaa.gov/).

The region is classified as Bering Tundra (Nowacki et al. 2002) and modern vegetation is characterized by *Drepanocladus* spp. and *Sphagnum* spp. as well as wet sedge-moss communities (*Carex aquatilis*, *Eriophorum augustifolium*) in waterlogged acidic habitats, tussock sedge (*Eriophorum vaginatum*) and dwarf shrubs (*Ledum palustre*, *Vaccinium vitis-idaea*) on elevated, better-drained sites and erect shrubs (*Andromeda polifolia*, *Betula nana*, *Spiraea beauverdiana*) in drier locations (Wetterich et al. 2012).

4.4 Material and methods

A 350-cm sediment core (core ID: Kit-43; all depths are given as cm below surface, cm b.s.) was recovered with a SIPRE permafrost corer (Jon Holmgren's Machine Shop, Fairbanks, AK) in April 2009 from the approximate center of Mama Rhonda basin (Figure 4.1). A multi-proxy approach was applied including sedimentological, geochemical and paleoecological analyses of the sediment as well as isotope geochemical analysis of the intra-sedimentary ice (pore ice and segregated ice).

The frozen core segments were split lengthwise and high-resolution digital photographs were taken with an optical camera system. Mass-specific magnetic susceptibility (MS) was measured at 1-cm intervals at the National Lacustrine Core Facility (LacCore, University of Minnesota) with a multi-sensor core logger (GEOTEK, Bartington-MS2C loop sensor; SI system is used to express MS values in 10^{-6}). The sediment core halves were then described and stored frozen until subsampling. Subsampling was generally carried out at a 5-cm sampling interval but adapted according to changes of sediment facies.

Pore-water was extracted from thawed intra-sedimentary ice with rhizon soil moisture samplers (0.2 µm pore diameter, Eijkelkamp). The hydrogen (δD) and oxygen ($\delta^{18}O$) stable isotope composition of intra-sedimentary ice was analyzed with a Picarro L2120i water isotope analyzer (as well as with Finnigan MAT Delta-S mass spectrometers for validation, if sample size allowed both measurement techniques). Additional samples taken in the study area in July 2008 from an ice-wedge, a snow patch, rainwater, active-layer groundwater, Kitluk River water and a small thermokarst lake close to the Kit-43 coring site were analyzed to compare modern seasonal signals from different water sources to the isotopic composition preserved in the Kit-43 core. The δD and $\delta^{18}O$ values are given as per mil (‰) difference from Vienna Standard Mean Ocean Water (V-SMOW), with internal 1σ errors of < 0.8 and < 0.1 ‰ for δD and $\delta^{18}O$, respectively (Meyer et al. 2000). The deuterium excess (d excess) is calculated according to: $d = \delta D - 8\ \delta^{18}O$ (Dansgaard 1964) and is indicative of secondary non-equilibrium fractionation processes and conditions in the initial moisture source regions.

The gravimetric ice content was measured as the weight difference between fresh and freeze-dried bulk sediment samples and is expressed as a weight percentage (wt%). The grain-size distribution was measured with a laser particle size analyzer (Coulter LS 200) according to EN ISO 14 688 after organic matter was removed with hydrogen peroxide (H_2O_2, 30 %). Particles > 1 mm were dry sieved through 1 and 2 mm mesh screens for 2 min (ATM Sonic Sifter) in order to differentiate the coarse sand fraction and the gravel-size clasts. Total nitrogen (TN), total carbon (TC) and total organic carbon (TOC) were measured on bulk sediments with an elemental

analyzer (ElementarVario EL III; analytical accuracy of ± 0.1 wt%) and the C/N ratio (TOC/TN) was calculated. To determine the carbon stable isotope composition, $\delta^{13}C_{TOC}$ was analyzed with a Finnigan MAT Delta-S mass spectrometer equipped with a FLASH elemental analyzer and a CONFLO III gas mixing system. Values of $\delta^{13}C_{TOC}$ are expressed relative to the Vienna Pee Dee Belemnite (VPDB) standard in ‰ and the standard deviation (1σ) is generally better than ± 0.15 ‰.

Volcanic glass shards in tephra layers were identified on smear slides in glycerine and prepared for geochemical microanalysis in order to identify the source of the tephra (detailed sample preparation described in Lenz et al. 2016). The major element glass composition was analyzed with a JEOL JXA-8230 electron microprobe with a voltage of 15 kV, a beam current of 10 nA and a beam size of 10 µm. For standardization and instrumental calibration, natural and synthetic minerals and the Lipari obsidian were used (Hunt & Hill 1996, Kuehn et al. 2011). To visualize the ash particles, scanning electron microscope (SEM) images were taken (Zeiss Gemini Ultra+) at the German Research Centre for Geosciences Potsdam (GFZ).

For ostracod species determination, sediment samples (sampling interval mostly 5-7 cm in core depth of 350-185 cm and 10-20 cm in core depth of 180-0 cm) with known weight normalized to 15 g of dry sediment were wet-sieved through 63 and 200 µm mesh screens, dried and examined under a stereo-microscope (Zeiss Stemi 2000-C, Carl Zeiss Microscopy GmbH, Jena, Germany). For testacean species, material was subsampled at intervals of 2-26 cm to take account of changes in sediment facies, suspended in purified water and wet-sieved through a 500-µm screen to remove organic and mineral particles. Testaceans were identified and counted in glycerine on glass slides under a light microscope at 100-400x magnifications (Zeiss Axioskop 2, Carl Zeiss Microscopy GmbH).

Ten samples were wet-sieved (> 250 µm) and handpicked to obtain macroscopic plant remains for accelerator mass spectrometry (AMS) radiocarbon dating. Three initial samples were sent to the National Ocean Sciences AMS Facility, NOSAMS (USA), and seven additional samples of plant remains, taken later to refine the chronology, were dated at the Poznan Radiocarbon Laboratory (Poland). All dates of this study shown in Table 4.1 are reported in calibrated radiocarbon years before present (cal a BP) as derived from age-depth modelling with the Bacon (Bayesian accumulation histories) modelling routine in Rstudio software (Blaauw & Christen 2011; applying the calibration data set INTCAL13 according to Reimer et al. 2013). The age modelling method divides the sediment core into 71 sections of 5 cm thickness and estimates the accumulation rate of each section through millions of Markov chain Monte Carlo iterations. The core basal age was calibrated using CALIB 7.0 with the INTCAL13 data set (Reimer et al.

2013). Three additional dates from outcrops along the Lake Rhonda shoreline are reported in Table 4.1 for geochronological comparison.

Table 4.1: AMS radiocarbon age determinations from the Kit-43 core with modelled and calibrated ages derived from CALIB 7.0 and the Bacon modelling routine in R (Blaauw & Christen 2011). Poz = Poznan Radiocarbon Laboratory; OS = National Ocean Sciences AMS Facility (NOSAMS); UCIAMS = UC Irvine Keck- CCAMS facility; pMC = percent modern carbon.

Lab. no.	Core depth (cm bs)	Dated plant material	Mass (mg C)	$\delta^{13}C_{TOC}$ (‰)	pMC	AMS age (a BP)	AMS age range, Calib 7.0 (cal a BP, 2 sigma)	Bacon model age range (cal a BP)	Bacon model median age (cal a BP)
Kit-43									
Poz-49858	5	Remnants of roots and shoots and mosses	1.11	-31.8	153.34 ±0.37	-3,435 ±19[1]	186-220	-860-359	-342.7
Poz-49859	38	Remnants of roots, *Carex*, lignified shoots, leaves of *Sphagnum* mosses	1.32	-28.0	86.12 ±0.28	1,200 ±26	1,182-1,059	872-1,125	1,026
OS-83573	50	Wooden remains	n.a.	-25.8	n.a.	1,160 ±30	1,176-1,045	1,031-1,204	1,137
OS-83574	55	Bulk sedge peat	n.a.	-26.8	n.a.	1,130 ±30	1,090-962	1,076-1,273	1,173
Poz-49861	143	Remnants of *Carex* and mosses	1.39	-25.8	64.22 ±0.27	3,557 ±33	3,930-2,135	3,668-4,096	3,868
Poz-49862	182	Remnants of moss and *Carex* remains	0.99	-27.3	45.6 ±0.23	6,308 ±40	7,317-7,165	5,155-7,359	7,007
Poz-49863	276	Remnants of shoots and mosses	0.69	-29.2	38.57 ±0.22	7,653 ±45	8,544-8,381	8,295-11,324	8,788
Poz-49864	310	Remnants of *Carex* and higher plants	1.44	-19.7	26.94 ±0.18	10,535 ±53	12,689-12,379	9,473-12,758	10,074
OS-83575	313	Wooden remains	n.a.	-26.7	n.a.	8,890 ±30	10,188-9,888	9,715-12,818	10,138
Poz-49865	347	Non-lignified shoots and branches	1.30	-27.4	9.52 ±0.13	18,891 ±109	23,032-22,475	-	-
Kit-7									
UCIT21189	240	Wood	n.a.	-28.0	n.a.	10,375 ±25	12,421-12,020	Brosius et al. (2012)	
Kit-75									
OS-83579	112.5	Charcoal, wood	n.a.	-25.5	n.a.	8,170 ±50	9,010-9,270	Jones et al. (2012)	
Kit-10									
UCIAMS-70597		Wood	n.a.	-24.8	n.a.	1195 ±15	1,176-1,069	Jones et al. (2012)	

[1]Excluded from the age model.

4.5 Results

4.5.1 Geochronology

AMS radiocarbon dates in the Kit-43 sediment core covered the full Holocene period. Ten samples were AMS radiocarbon-dated (Table 4.1) and one major age inversion was identified. A sample at 310 cm, located in a reliable lithological context, consisted of sedges and higher plants mixed with aquatic plant material ($\delta^{13}C_{TOC}$ of -19.7 ‰, Table 4.1) and dated to 10.54 ± 0.053 ka BP. A younger age of 8.89 ± 0.030 ka BP at 313 cm, immediately below the older sample, originated from an organic inclusion with wooden remains. Contamination with young material during the permafrost drilling process can be excluded for this sample. Accordingly, neither of the two dates could be a priori excluded. The samples at 38, 50 and 55 cm were of almost the same age and age inversions were negligible because they were within the range of error. The uppermost sample at 5 cm was of modern age with 153.34 ± 0.37 percent modern carbon (pMC) and was therefore the only radiocarbon date that was manually excluded from the age model. When applying the Bacon modelling routine (Figure 4.2), eight out of nine dates were situated within the 95 % confidence interval; the oldest age of 18.89 ± 0.11 ka BP at 347 cm within the tephra layer was outside the likely age range. Figure 4.2 displays a reliable age-depth relationship for 0–182 cm but below 182 cm it shows a high discrepancy between the weighted mean (blue line) and the median (red line) of the age-depth model. In the following, the statistical median is used for applying a chronology to the Kit-43 core as it better reflects the fact that the Bacon age modelling routine considered the 8.89 ± 0.030 ka BP at 313 cm to be more reliable than the 10.54 ± 0.053 ka BP at 310 cm.

The Bacon modelling routine in R calculated a basal age for the full sediment record of 12.8 cal ka BP with a mean sedimentation rate of 0.03 cm a^{-1} (with a maximum sedimentation rate of 0.05 cm a^{-1} at 276–182 cm and minimum sedimentation rate of 0.01 cm a^{-1} at 182–143 cm, Figure 4.2). The basal age of the lacustrine sediment is 11.8 cal ka BP.

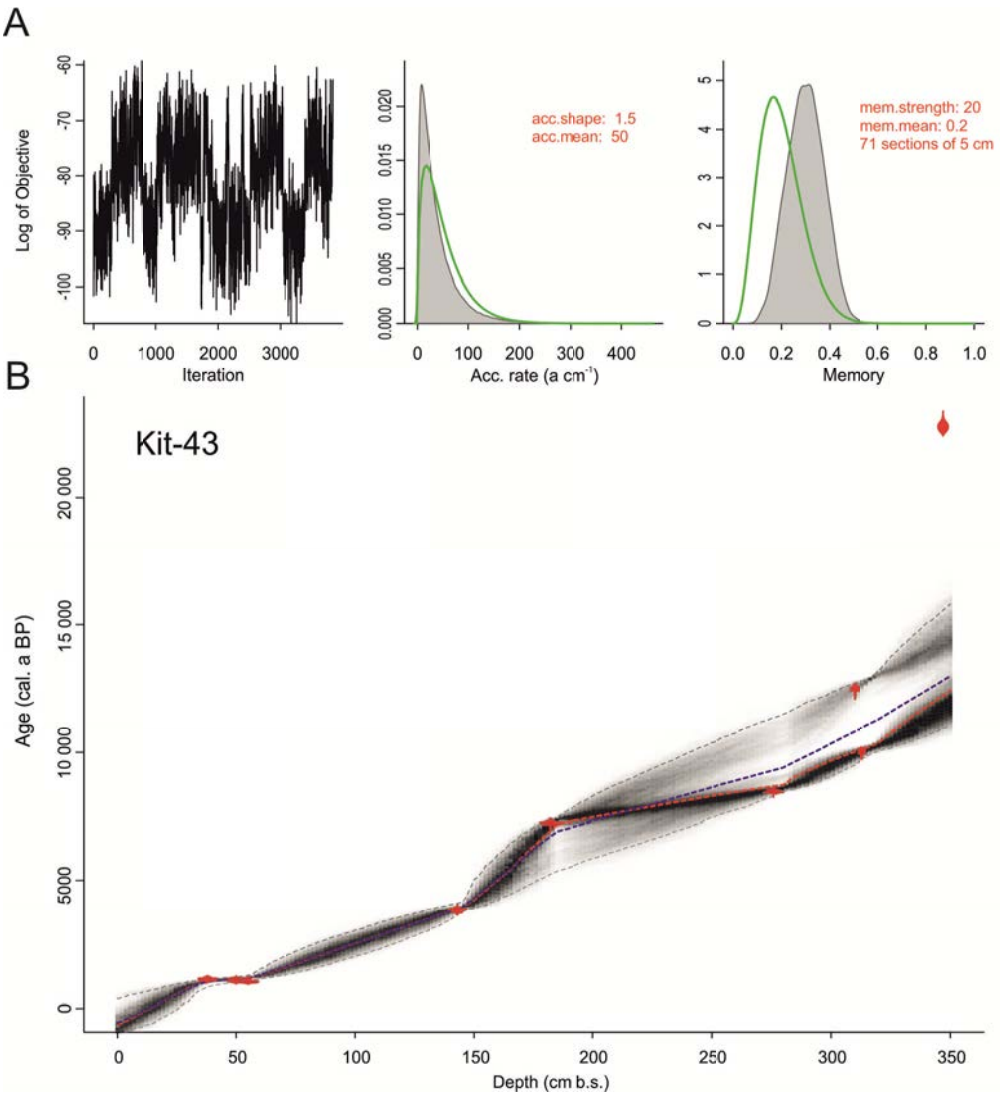

Figure 4.2: Bacon modelling routine output graph of age-depth model of core Kit-43 based on radiocarbon dates (Table 4.1). (A) Markov chain Monte Carlo iterations, prior (green curves)/posterior (grey histograms) distributions of accumulation rate and memory R of Kit-43 core. (B) Calibrated radiocarbon dates (red) and age-depth model (darker greys indicate more likely calendar ages; grey dashed lines show 95 % confidence intervals; blue curve shows single 'best' model based on the weighted mean age for each depth, red curve shows single 'best' model based on the median age for each depth).

4.5.2 Cryolithological description

Based on the lithological description and analysed sedimentological, geochemical and paleoecological parameters (digital appendix table 4.1), the Kit-43 permafrost core was divided into four lithostratigraphical units:

- Unit A: 350–336 cm, > 11.8 cal ka BP
- Unit B: 336–283 cm, 11.8–9.0 cal ka BP
- Unit C: 283–40 cm, 9.0–1.06 cal ka BP
- Unit D: 40–0 cm, 1.06 cal ka BP–today

The core was mainly composed of dark olive grey (Munsell Soil Color Chart, ID 5Y 3/2) (Munsell Color Company 1994), greyish-brown (2.5YR 5/2) to dark-greyish-brown (2.5YR 3/1) fine-grained sediment. A 40-cm-thick layer of alternating poorly and well-decomposed, strong brown-to-black (7.5YR 5/6 to 2.5/1) peat characterized Unit D at the top of the core (Figure 4.3). Intermediate dark-brown (7.5YR 3/2) peaty layers alternate with minerogenic deposits in Unit C whereas Unit B is characterized by more homogenous sediment deposits. Coarse-grained tephra deposits of about 14 cm thickness dominate Unit A at the base of the core from 350 to 336 cm as well as different overlying sections; these observations were also supported by grain-size analyses. Whereas Unit B and C are dominated by silt with varying proportions of clay and sand, coarse sand and gravel-size clasts up to 5 mm characterize tephra layers in Unit A and deposits at 239–226, 202–178 and 163–138 cm (Figure 4.4). The coarse grain size and described tephra deposits in Unit A are also reflected in the sediment core MS (Figure 4.4). MS increased down-core from 0 (within the first meter from the top; Unit D and part of Unit C) to 47 at 335 cm with high values up to 88 in Unit A and pronounced peaks of 192 at 238–228 cm and 140 at 200–192 cm within Unit C where tephra layers were identified.

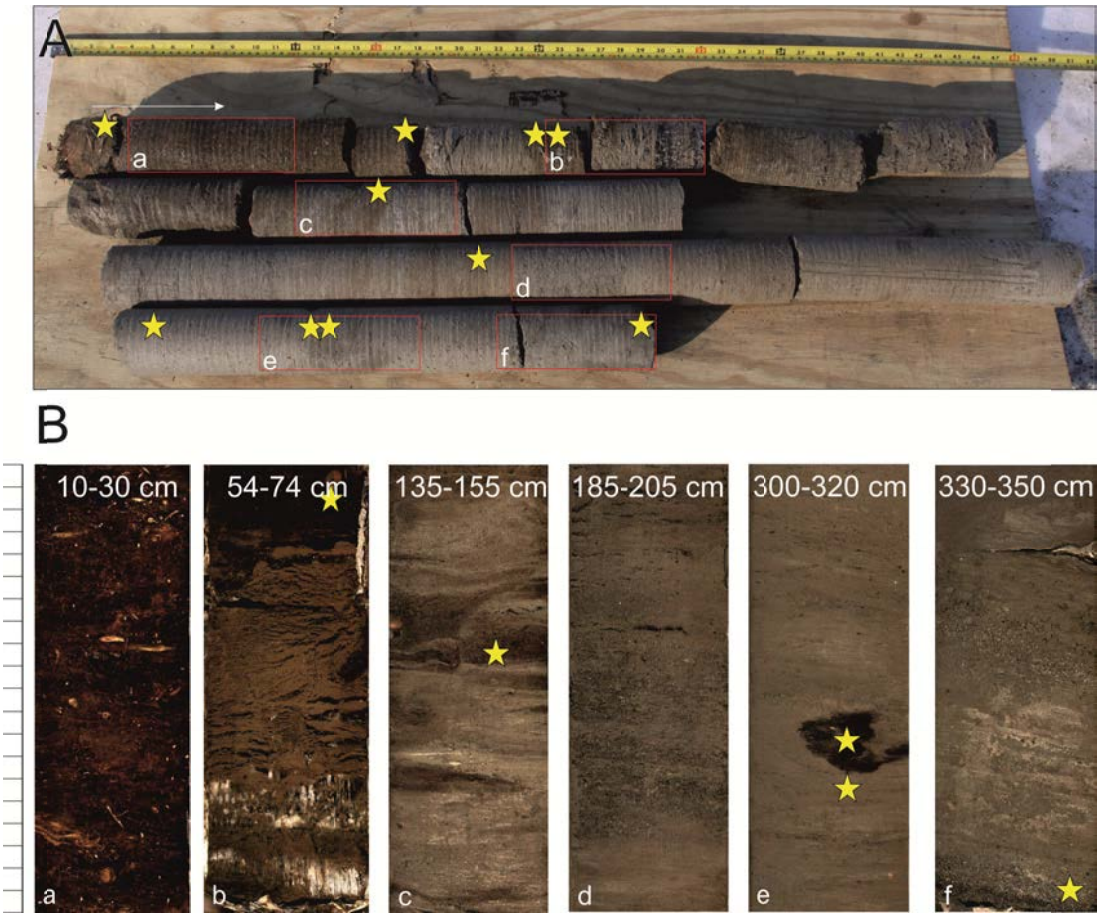

Figure 4.3: (A) Core Kit-43 as recovered in the field in April 2009; yellow stars mark radiocarbon samples, core segments from left (top) to right (bottom). (B) Close-up of high-resolution photographs of different sections; vertical scale is cm.

Following French & Shur (2010), the cryostructure of Kit-43 was characterized as predominantly structureless below 156 cm (Unit A, B and part of Unit C), whereas ice lenses up to 5 mm thick, ice veins up to 10 mm thick, and wavy parallel lenticular layers were prevalent in the upper part from 156 to 0 cm (Unit D and part of Unit C); transparent ice structures with bubbles were noted in Unit C at 88–87 and 74–66 cm (Figure 4.3). The gravimetric ice content ranged from 77.7 wt% at 70–69 cm in Unit C to 8.8 wt% at the core bottom (Unit A) with a decreasing trend down-core, although stable values around 26 wt% were measured between 343 and 282 cm in Unit B (Figure 4.4).

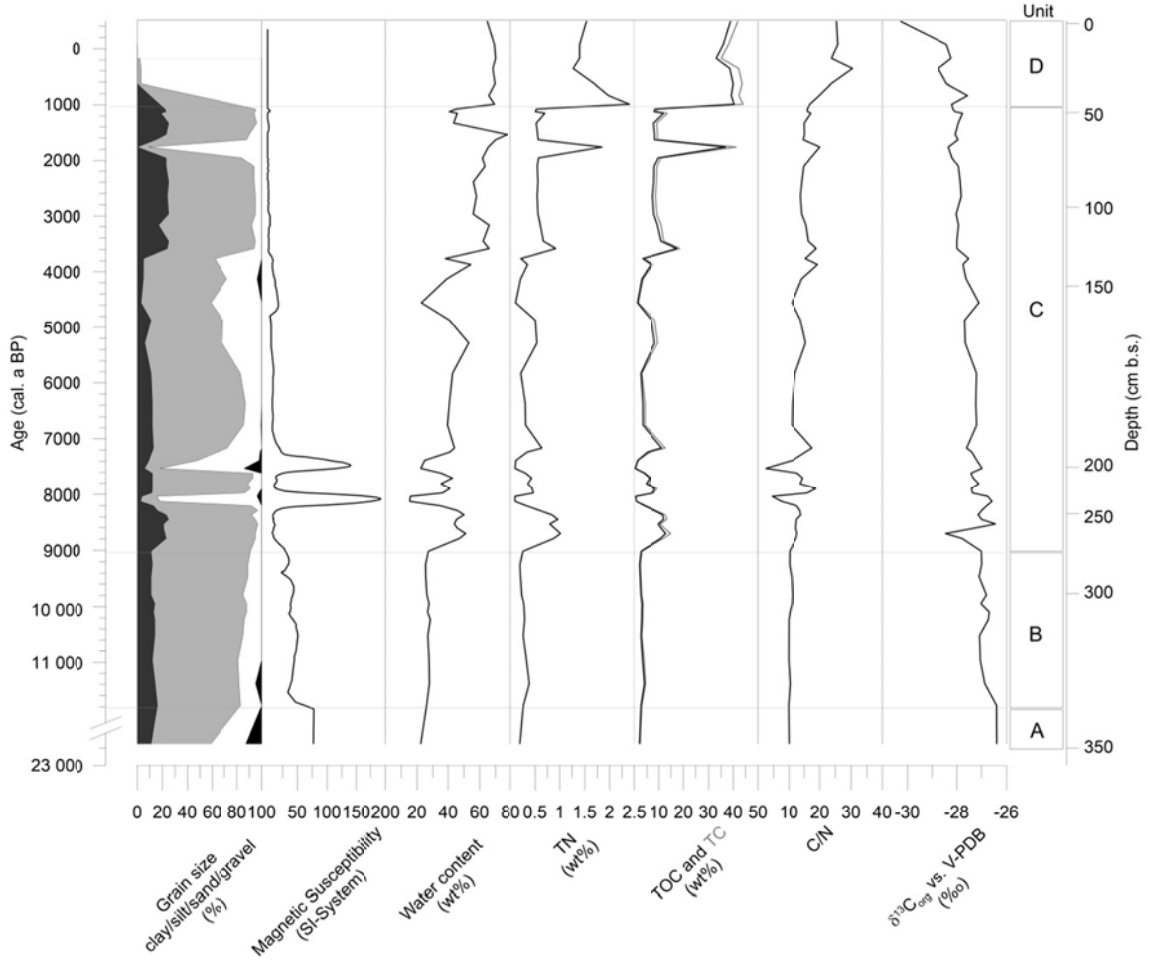

Figure 4.4: Lithological and geochemical results of core Kit-43 according to calibrated and modelled ^{14}C ages: Grain size, magnetic susceptibility, water content, total nitrogen (TN), total carbon (TC, in grey), total organic carbon (TOC), C/N ratio and $\delta^{13}C_{TOC}$ vs. V-PDB (proxy values are given in the digital appendix table 4.1).

4.5.3 Geochemical results

All geochemical analysis results are displayed in Figure 4.4. The average TN of Kit-43 core sediments was 0.59 %. TN was below detection limits in layers described as tephra (in Unit A) and was highest in the terrestrial surface peat (Unit D). A TN_{max} of 2.4 % occurred within Unit D at 35–34 cm. Average TC was 11.1 %; TC_{min} of 0.4% was found in Unit A and in tephra layers in Unit C, and the highest TC values occurred within the peat in Unit D (TC_{max} of 44 % at 35–34 cm). TOC followed a similar pattern, with a TOC_{min} of 0.2 % in tephra layers (Unit A and parts of Unit C), the highest TOC in the terrestrial surface peat in Unit D (TOC_{max} of 40 % at 35–34 cm), and an average core TOC of 10 %. The C/N ratio generally decreased down-core from about 30–2. Values of $\delta^{13}C_{TOC}$ increased core-downwards from -30.3 to -26.5 ‰ (-27.5 ‰ on average); a pronounced negative peak of -28.45 ‰ was measured at 271–270 cm in Unit C.

Tephra analyses of 24 and 23 glass shards at depths of 349–348 cm (Unit A) and 201–200 cm (Unit C), respectively, yielded similar geochemical compositions. These values were similar to results obtained from tephra at a depth of 243–155 cm from the Kit-64 core of a drained lake basin (Lenz et al. 2016) and tephra found in a nearby pingo outcrop (Wetterich et al. 2012) (Table 2, digital appendix table 4.2). SEM images visually showed rather sharp tephra particles at the depth of 349–348 cm in Unit A compared to rounded particles at the depth of 201–200 cm in Unit C (Figure 4.5).

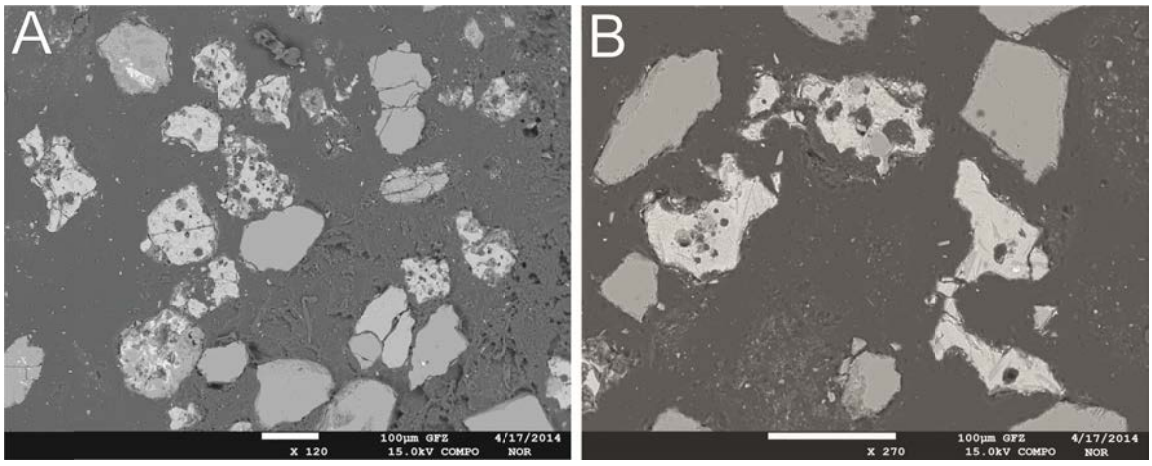

Figure 4.5: SEM images of polished tephra grains in resin. A. Tephra particles at 120x magnification found at 200–201 cm core depth. B. Tephra particles at 270x magnification found at 348–349 cm core depth.

Table 4.2: Electron probe analyses of glass shards from different tephra samples from the Seward Peninsula. Data are expressed as normalized mean (volatile-free) values (wt%), number of single glass shards analysed and their standard deviations (SD). Single non-normalized data of all samples and the Lipari obsidian reference standard are given in the digital appendix table 4.2.

Sample	SiO_2	TiO_2	Al_2O_3	FeO	MnO	MgO	CaO	Na_2O	K_2O	P_2O_5	Total	Cl	F
Kit-43, 201-200 cm	51.08	2.57	15.12	10.17	0.15	5.95	9.57	3.74	1.18	0.45	100	0.04	0.00
SD (n=23)	*0.42*	*0.52*	*0.02*	*0.49*	*0.25*	*0.31*	*0.27*	*0.10*	*0.42*	*0.52*		*0.02*	*0.01*
Kit-43, 349-348 cm	51.39	2.47	15.01	10.11	0.16	6.16	9.61	3.58	1.09	0.39	100	0.04	0.00
SD (n=24)	*0.42*	*0.40*	*0.02*	*0.50*	*0.44*	*0.15*	*0.17*	*0.05*	*0.42*	*0.40*		*0.04*	*0.00*
Kit-64, 243-155 cm	51.20	2.66	15.30	9.86	0.15	5.61	9.38	3.89	1.41	0.51	100	0.04	0.00
SD (n=8)	*0.73*	*0.14*	*0.28*	*0.11*	*0.01*	*0.23*	*0.21*	*0.12*	*0.08*	*0.04*		*0.01*	*0.00*
Kit-1, 6 cm (Pingo)	51.22	2.81	14.95	10.06	0.16	5.39	9.66	3.88	1.35	0.50	100	0.03	0.00
SD (n=24)	*0.23*	*0.17*	*0.39*	*0.44*	*0.02*	*0.36*	*0.34*	*0.15*	*0.35*	*0.04*		*0.01*	*0.01*
Kit-1, 13 cm (Pingo)	51.05	2.48	15.21	10.52	0.17	5.70	9.72	3.60	1.19	0.04	100	0.40	0.00
SD (n=24)	*0.51*	*0.18*	*0.28*	*0.42*	*0.02*	*0.47*	*0.39*	*0.19*	*0.17*	*0.02*		*0.05*	*0.00*

4.5.4 Bioindicators

Three species of ostracods were identified in 47 Kit- 43 core samples (Figure 4.6). *Cypria ophtalmica* was identified in all samples where ostracods were present, except for one sample at 3–2 cm depth in Unit D. Here, a single carapace of *Candona elliptica* was identified. *Cyclocypris ampla* was identified in Unit A at depths of 339–338 cm, as well as in Unit B at 332–331, 323–321 and 294–276 cm depth; a single carapace was found at the depth of 159–158 cm in Unit C. Specimen counts per sample varied from single finds up to a maximum of 234 valves (*Cypria ophtalmica*) at 271–270 cm in Unit C. Ostracods were absent in layers where tephra was noted (i.e. 350–343, 237–231 and 202–194 cm), but two ostracod valves were documented within the tephra layer at 339–338 and 337–336 cm in Unit A.

A total of 34 samples was analysed for testaceans (Figure 4.6). Eleven samples did not contain any testaceans and 23 samples yielded 56 testacean taxa including subspecies and varieties of 15 genera. Specimen counts per sample varied from single finds to 47 counts per sample in the surface peat layer of Unit D. Higher specimen counts correlated positively with a larger number of ecological groups in the core. Whereas varying proportions of eurybiontic species (tolerating a wide range of a particular environmental factor, e.g. pH or soil moisture) and hygrophilous species (indicating moist habitats) were present in the core, sphagnobiontic species (typical inhabitants of Sphagnum moss) were present throughout Unit C and Unit D. Hydrophilous species, indicating waterlogged habitats, were only documented at depths of 306–305 and 256–255 cm (Unit B), 158–157 cm (Unit C) and at the top at 2–1 cm (Unit D).

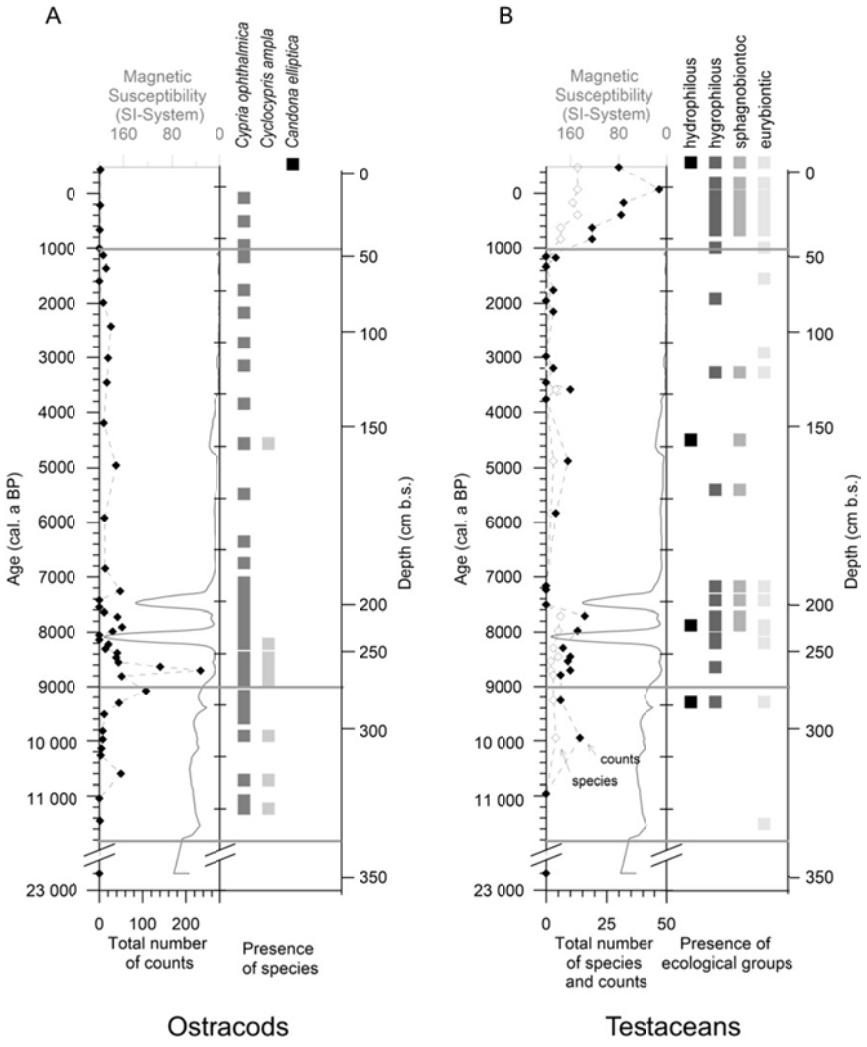

Figure 4.6: (A) Ostracod individual counts and species. (B) Testacean individual counts, number of species, and ecological groups. Both graphs also show magnetic susceptibility as an indicator of tephra layers in the Kit-43 core.

4.5.5 Characteristics of intra-sedimentary ice and comparison with modern waters

The isotopic composition of intra-sedimentary ice allows us to distinguish five hydrological units in the Kit-43 core that are independent of the lithostratigraphical units described above because they represent the post-drainage hydrology and freezing at the study site:

- Hydrological Unit I: 0–42 cm
- Hydrological Unit II: 42–82 cm
- Hydrological Unit III: 82–154 cm
- Hydrological Unit IV: 154–343 cm
- Hydrological Unit V: 343–350 cm

The isotopic composition of the intra-sedimentary ice from the Kit-43 core ranged between -13.9 and -10.6 ‰ for $\delta^{18}O$ and from -108.6 to -83.8 ‰ for δD. A pronounced heavier isotopic composition was observed at 349–348 cm (Hydrological Unit V; $\delta^{18}O$ = -11.6 ‰ and δD = -92.3 ‰), at 70–69 cm ($\delta^{18}O$ = -10.6 ‰ and δD = -86.2 ‰) and at 42–41 cm (transition between Hydrological Units I and II; $\delta^{18}O$ = -11.8 ‰ and δD = -90.9 ‰). The d excess varied from -2.3 to +8.1 ‰ and reached its lowest levels at the $\delta^{18}O$ maxima. In general, the isotopic composition was more variable in the upper part of the core (Hydrological Units I, II, III) and became more stable from 154 cm down-core (Hydrological Unit IV). Furthermore, to compare past and modern isotopic characteristics of pore-waters in the core and from the surrounding landscapes, six types of waters were analyzed (Table 4.3). Isotope data from groundwater in the modern active-layer as well as samples from open waters, such as from the Kitluk River, are similar to Kit-43.

Table 4.3: Isotope composition of intra-sedimentary ice in permafrost core Kit-43 compared to modern waters.

Type of sample		**$\delta^{18}O$ (‰)**	**δD (‰)**	**d excess (‰)**
Lake water	n = 2	-9.20	-80.9	-7.3
(modern surface water)	Sd	0.01	0.01	0.1
Kitluk River	n = 2	-12.08	-99.1	-2.4
(modern surface water)	Sd	0.03	0.12	0.13
Rain water	n = 12	-15.61	-127.5	-2.6
(modern summer precipitation)	Sd	2.9	17.7	6.5
Activ- layer water	n = 4	-14.74	-109.6	+8.3
(modern groundwater)	Sd	0.4	1.9	1.4
Snow patch	n = 20	-20.89	-161.2	+5.9
(modern winter precipitation)	Sd	0.7	4.8	1.0
Ice-wedge	n = 38	-23.80	-183.5	+6.8
(past winter precipitation)	Sd	0.6	5.9	2.9
Kit-43				
Hydrological Unit I (0-42 cm)	n = 8	-12.31	-92.7	5.9
	Sd	0.6	4.0	1.5
Hydrological Unit II (42-82 cm)	n = 7	-12.17	-95.9	1.5
	Sd	0.8	4.7	2.4
Hydrological Unit III (82-154 cm)	n = 11	-13.46	-106.2	1.5
	Sd	0.4	2.4	1.2
Hydrological Unit IV (154-343 cm)	n = 37	-13.04	-104.5	-0.2
	Sd	0.2	1.0	1.0
Hydrological Unit V (343-350 cm)	n = 1	-11.64	-92.3	0.8

4.6 Discussion

The analytical results from the Kit-43 sediment core are used to reconstruct the evolution of a thermokarst lake system on the northern Seward Peninsula of Alaska extending from 11.8 cal ka BP to present. The application of an age-depth-model allows the determination of the timing of sediment facies changes associated with past landscape dynamics. The magnetic susceptibility of the sediment record reflects changes in grain size or content of magnetic minerals and therefore indicates input of allochthonous material into the lake (Thompson et al. 1975), which is most likely to be tephra in the Kit-43 record. The tephra layers in core Kit-43 were geochemically

analyzed for comparison with tephra in other studies and to estimate its value as a chronostratigraphical marker. The geochemical proxies of TN and TC indicate nutrient supply and past bioproductivity in the lake (Cohen 2003, Lamoureux & Gilbert 2004) whereas TOC content gives a signal for autochthonous productivity and for allochthonous organic input into the lake system (Lamoureux & Gilbert 2004). The TOC content is probably also related to the magnitude of decomposition of organic matter in unfrozen lake sediments, in which older layers had more time to decompose and thus should be depleted in TOC relative to younger lake sediments. The C/N ratio can be used as an indicator of different states of mineralization of organic matter in core Kit-43 and in combination with $\delta^{13}C_{TOC}$ it may be used to discriminate organic matter sources (Meyers 1997, Meyers & Takemura 1997).

Paleoecological analyses of ostracods and testaceans were able to differentiate lake stages and terrestrial phases, and to describe past ecological conditions. Finally, the isotopic composition of the intra-sedimentary ice reflects the situation after the drainage of Mama Rhonda Lake and, in comparison to modern waters, allows study of the changes in permafrost conditions after drainage. Our interpretations of lake stages and associated landscape changes based on all analyzed proxies are described in detail below and a conceptual schematic is presented in Figure 4.7.

4.6.1 Thermokarst lake dynamics

Pre-lake environment: > 11.8 cal ka BP (Unit A)

Ice-rich permafrost was present prior to lake formation at the study site. The Bering Land Bridge tundra was drier than present during the Lateglacial, and fossil insect remains indicate an arctic climate (Elias et al. 1997). A cold permafrost environment of at least -8 to -6 °C mean annual air temperature or colder was reconstructed for the LGM from ice-wedges underlying the Kitluk paleosol as well as from blocky soil structures indicating the formation of ice nets and ice lenses within the paleosol (Washburn 1980, Höfle et al. 2000). A chronology for the Devil Mountain Maar tephra was established using radiocarbon dates from the Kitluk paleosol. The Devil Mountain Maar eruption occurred around 18.0 a BP (21.5 cal ka BP) and covered about 2,500 km^2 of the northern Seward Peninsula with a tephra layer of varying thickness (Begét et al. 1996). Two radiocarbon dates have been published for the tephra originating from a Lake Rhonda bluff outcrop: 17.42 ± 0.26 ka BP (Begét et al. 1996) and 19.63 ± 0.11 ka BP (Höfle et al. 2000).

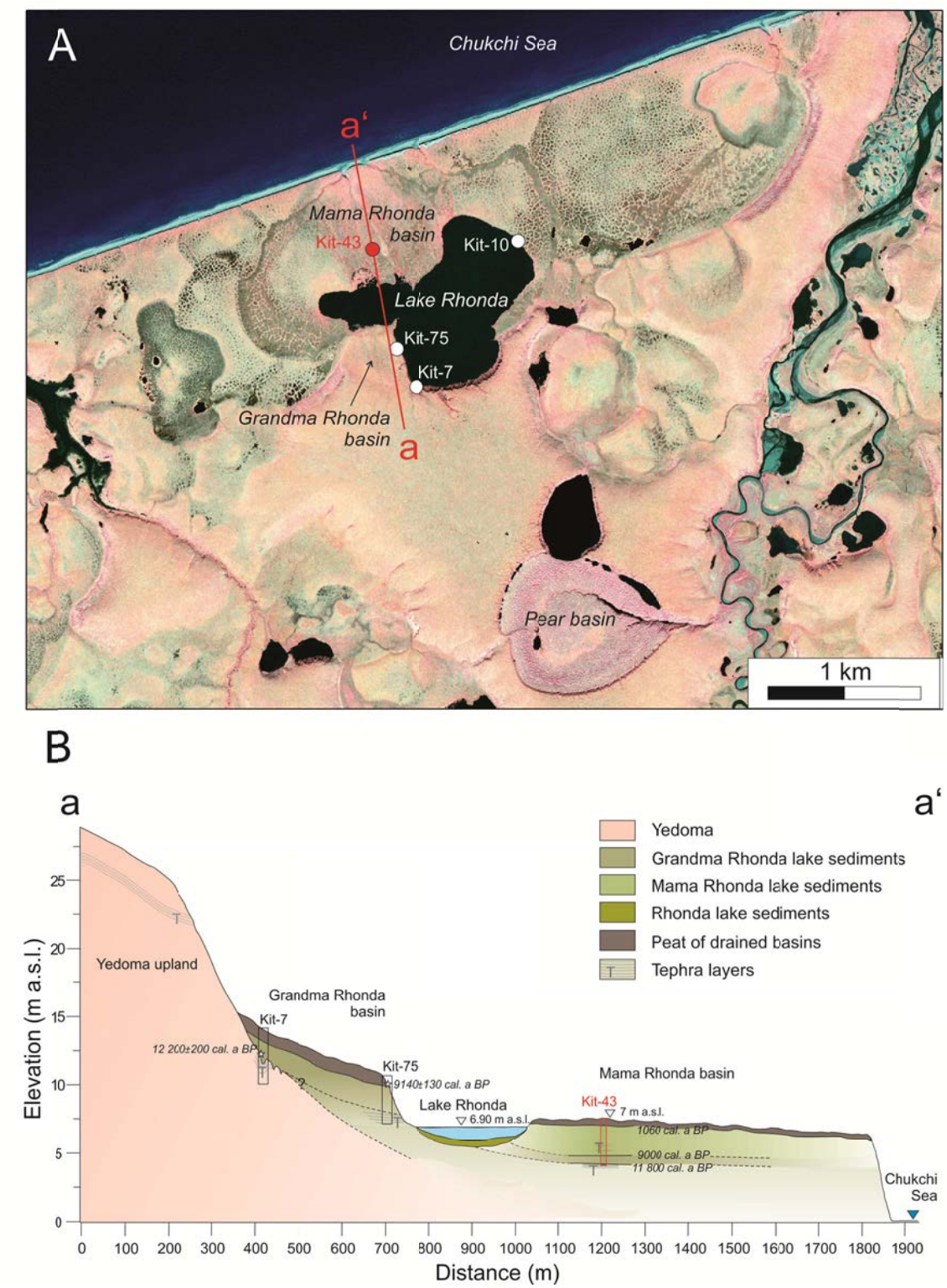

Figure 4.7: (A) Spot satellite image (©SpotImage) of the study region and (B) cross-section of Mama Rhonda basin and neighboring Grandma Rhonda basin and Lake Rhonda. Surface elevations along the cross-section were derived from a high-resolution digital elevation model. Dashed lines give the hypothetical extent of sediment packages. Chronological correlations described in the text are noted in outcrops at the shore of Lake Rhonda. Note the strong height exaggeration of the cross-section.

The tephra layer at the base of the Kit-43 core was dated to 18.89 ± 0.11 ka BP (22.8 ± 0.28 cal ka BP) and is in chronological agreement with the Devil Mountain Maar tephra. Thus, the results from this study align well with the existing chronology of landscape evolution in this region. The geochemical composition of the tephra layer is very similar to that of the much older South Killeak Maar tephra detected 19 km to the southeast in the Kit-64 drained lake basin core (Lenz et al. 2016; Figure 4.1) and in the Kit-1 pingo outcrop east of the Rhonda basins (Wetterich et al. 2012; Figure 4.1, Table 4.2). We argue that the geochemical similarity of these different tephra layers with their evidently different ages is due to these phreatomagmatic maar eruptions originating in the same geological setting of the Cape Espenberg maars and thus producing very similar geochemical signatures.

Subsequent thermokarst lake formation in ice-rich permafrost resulted in a vertical displacement of tephra in Unit A during thaw subsidence. As illustrated in Figure 4.7B there is a more than 15 m elevation difference between in situ Devil Mountain Maar tephra in the adjacent yedoma upland vs. the tephra in Unit A of core Kit-43. Although substantial horizontal transport processes can be ruled out because the tephra particles evidently are still characterized by sharp edges (Figure 4.5), thaw subsidence and compaction influenced the stratigraphical bedding of terrestrial deposits including the tephra layer during lake formation.

Lake development (Grandma Rhonda lake phase): c. 11.8–9.0 cal ka BP (Unit B).

Lacustrine sediment accumulated on top of terrestrial deposits, as is clearly indicated by a sedimentological change to silty deposits and the occurrence of the two ostracod species *Cypria ophtalmica* and *Cyclocypris ampla*. Little variability in geochemical parameters in Unit B suggests that the coring location was distant from a dynamic shoreline of a large water body. This is supported by grain-size analyses that show a decrease in the sand and increase in the silt fraction from 11.8 to 9.0 cal ka BP. Decreasing MS indicates a lower input of tephra from eroding shores, thus indicating that the lake area expanded or the lake deepened such that the core site was deeper than the wave base. According to the age-depth model, the initiation of the studied lake basin was at about 11.8 cal ka BP. This coincides with the end of the Younger Dryas (c. 12.8–11.5 cal ka BP; Kokorowski et al. 2008, Kaufman et al. 2010), which was triggered by changes in ocean-water circulation in the North Atlantic and showed spatially complex paleoclimatic patterns (Kokorowski et al. 2008). Whereas southern Alaska seems to have been very susceptible to changes in atmospheric circulations, some studies have also recorded simultaneous cooling in northern Alaska (e.g. Mann et al. 2010, Meyer et al. 2010). For interior Alaska, several studies have suggested uniform climate or even warming during the Younger Dryas (Kokorowski et al. 2008). Bigelow & Edwards (2001) observed a shift from low lake levels and sparse herbaceous

tundra vegetation to higher lake levels and shrub tundra around 11.8 ka BP (c. 13.6 cal ka BP) in eastern Beringia. On the southern part of the Seward Peninsula, in turn, Hunt et al. (2013) reported the presence of *Picea* spp. and *Larix laricinia* in peatlands from 13.5 to 12.1 cal ka BP, indicating a warm regional climate, followed by a cold and dry interval from 12.1 to 11.1 cal ka BP. The Younger Dryas seemed to be absent in records from e.g. Imuruk Lake (Colinvaux 1964) and Cape Deceit (Matthews 1974). Kaufman et al. (2004) summarized an interval of warmer-than-present Holocene temperatures in Alaska between 11.5 and 9.0 cal ka BP with an initiation of the Holocene Thermal Maximum (HTM) in central-eastern Beringia at 11.3 ± 1.5 cal ka BP but also highlighted the complex spatial pattern of highly variable temperature during that time (Kaufman et al. in press).

Our sediment core records the early onset of thermokarst dynamics at the Lateglacial to Holocene transition during a time when the Bering Land Bridge was rapidly narrowing. By 11.0 cal ka BP the Land Bridge was closed due to postglacial sea-level rise and the June and July solar insolation started to reach its maxima at 65°N latitude (Elias 2001). The Kit-43 record captures the initial landscape shifts from a continental-climate-dominated accumulation plain to a warming and wetter environment under increasing maritime influence. At the same time, model simulations of thermokarst lakes on the northern Seward Peninsula demonstrate that lake expansion is not necessarily climate-driven but is strongly related to topography (Kessler et al. 2012). As the HTM was not yet fully developed during lake initiation and early lake development, stable shoreline slope conditions may have contributed to the development of a surprisingly stable lake system at the Kit-43 site.

Radiocarbon ages from outcrops along the shore of Lake Rhonda provide additional context for the chronological relationship of lake generations. A radiocarbon age (Table 4.1) of an ice-wedge cast (Kit-7, Figure 4.7) containing basal lake sediments suggests that the associated lake basin (informal name: Grandma Rhonda lake basin) initiated around 12.2 ± 0.2 cal ka BP. Considering the large error of 200 years for the Kit-7 date and wide 95 % confidence interval ranging from 10.5 to 14.7 (with the median at 11.8) cal ka BP for this time period in the age-depth model of Kit-43 (Figure 4.2), it is possible that the initiation of the first lake generation detected in Kit-43 coincides with the initiation of Grandma Rhonda lake. As the Grandma Rhonda lake site at Kit-7 and the Kit-43 site are < 800 m apart, these older deposits in both records may thus well belong to the same lake system (Figure 4.7); hence, we term this lake phase the 'Grandma Rhonda lake phase'. Furthermore, there is geochronological evidence that not only Grandma Rhonda lake initiation (transition Unit A/B) is preserved in the Kit-43 core, but also Grandma Rhonda lake drainage. According to the nearby Kit-75 exposure (Figure 4.7), which preserves at least 160 cm of lake sediments with reworked tephra deposits overlain by 112.5 cm of terrestrial peat (G.

Grosse, unpublished data), the Grandma Rhonda lake drainage was radiocarbon dated in Kit-75 to 9140 ± 0.13 cal ka BP (Jones et al. 2012). At about the same time at 9.0 cal ka BP, core Kit-43 shows a drastic transition from stable proxies to strongly variable proxies (TN, TC, TOC, water content, and even testacean and ostracod counts; see below). Due to the spatial closeness of these sites it is very likely that the drainage event recorded in Kit-75 is coincident with the event causing the depositional change in our core. We suggest that the first generation of Grandma Rhonda lake either did not drain completely or that a second lake generation rapidly developed at the study site.

Lake modification (Mama Rhonda lake phase): c. 9.0–1.06 cal ka BP (Unit C).

An abrupt change of facies was detected in core Kit-43 at around 9.0 cal ka BP. Here, all geochemical proxies become more variable than in Unit B, pointing towards an alternating lake level with the potential for intermediate wetland development; the generally increased contents of nitrogen, carbon (in particular organic carbon) and water in the sediments indicate a higher input of organic matter. In addition, the average C/N ratio in Kit-43 is elevated from 10.4 in Unit B to 14.6 in Unit C (excluding tephra layers with extremely low TN, TC and TOC contents), pointing towards enhanced input of terrestrial matter due to shoreline erosion. The maximum Unit A ostracod count at 8.7 cal ka BP, dominated by the cosmopolitan species *Cypria ophtalmica*, indicates optimal ecological conditions in a large but generally shallow freshwater lake at the beginning of the Mama Rhonda lake phase.

Pronounced peaks in MS, coarse grain-size fractions and a change in geochemical parameters at about 230 and 200 cm depth, as well as a high sedimentation rate of 0.053 cm a-1 at 276–182 cm, indicate rapid input of tephra from the catchment. The tephra particles are of the same geochemical composition as the tephra at the core base (Table 4.2) but no volcanic eruption in the Cape Espenberg lowland area is known after the Devil Mountain Maar eruption around 21.5 cal ka BP (Begét et al. 1996). The tephra in Unit C is most probably reworked because the particles are more rounded than the tephra particles at the core base, which subsided vertically in place (Unit A), suggesting at least some horizontal aquatic transport of sediments in Unit C (Figure 4.5). Such a dynamic ecosystem implies unfavorable living conditions for aquatic organisms such as ostracods, which have a variable abundance in this unit (Figure 4.6). Absence of ostracods gives evidence for rapid transportation and deposition of tephra particles. The low occurrence of testaceans as a general terrestrial indicator (with varying proportions of hydro- and hygrophilous as well as sphagno- and eurybiontic species throughout the core; Figure 4.6) points towards a dynamic depositional environment but possibly also intermediate wetland development in the catchment and input of peaty deposits from shore erosion.

Mama Rhonda lake probably started as a small residual lake of Grandma Rhonda lake that gradually grew and persisted with oscillating lake levels over much of the Holocene. Kaufman et al. (in press) summarized that lake levels were consistently lower during the Early Holocene and started to raise around 9.0 cal ka BP in northern and interior Alaska. During that time re-organization of the periglacial landscape may have been a result of rapidly expanding thermokarst lakes. Coalescence with other remnant lakes would have caused renewed sediment input and changing lake levels that, in turn, caused the observed high variability of lithological and geochemical proxies in the Kit-43 core. Remnant lakes in the center or on the margins of drained lake basins have been frequently observed in the study region (e.g. Hopkins & Kidd 1988, Jorgenson & Shur 2007, Jones et al. 2011, Lenz et al. 2016). Additionally, new lakes may form following complete drainage along basin margins where sufficient ground ice is still available, as well as in the center of a basin following sufficient accumulation of post-drainage ground ice (Jorgenson & Shur 2007, Jones et al. 2011). A similar setting can be observed in Pear basin, a large, deep, drained lake basin about 2 km south of Lake Rhonda (Figure 4.7).

For the second lake phase (Mama Rhonda lake), the period of more than 8,000 years seems to be rather long for persistence of a thermokarst lake on the northern Seward Peninsula. It is possible that several lake cycles are represented by Unit C. Even if they are not clearly identifiable in the sediment core, they might be indicated by changes in sedimentation rate e.g. at 8.7, 7.0 and/or 3.9 cal ka BP (Figure 4.2). Another possibility for Mama Rhonda lake is that it developed rather slowly after the HTM with ongoing Holocene cooling and drying. Hopkins & Kidd (1988) suggested that the life span of thermokarst lakes on the northern Seward Peninsula is typically as short as 2,500–3,000 years but that larger lakes may persist for 4,000–5,000 years. In environments with deep ground ice (> 20 m), like the northern Seward Peninsula, basins of > 100 m diameter and depths of about 20 m may form in c. 5,000 years (West & Plug 2008), but also as rapidly as in 300 years (Lenz et al. 2016). If Mama Rhonda lake did not comprise several lake phases, it would have been one of the exceptional old lakes before it drained. The longevity of this lake phase may be explained by a general cooling trend throughout the Holocene (Kaufman et al. 2004). Old thermokarst lakes are known e.g. in the Northwest Territories, Canada: the prominent experimental Lake Illisarvik initiated about 9.5 cal ka BP (with maximum lake expansion at 6.0 cal ka BP and shrinkage to its pre-drainage size by 2.0 cal ka BP; Michel et al. 1989) before it was artificially drained in AD 1978 (Mackay 1997). In the Yukon Flats upland, deep thermokarst lakes also prevailed throughout the Holocene (Edwards et al. 2016).

Lake drainage (Mama Rhonda drained thermokarst lake basin phase): c. 1.1 cal ka BP to present (Unit D).

Finally, in the Late Holocene, Mama Rhonda lake drained at about 1.06 cal ka BP, as indicated by the abrupt transition from lacustrine sedimentation to a terrestrial peat. The number of testacean counts significantly increased to 47 individuals per sample, dominated by mainly hygrophilous and sphagnobiontic species. Hydrophilous testacea dominate only at 2–1 cm, indicating modern summer water-logged conditions. Occasional occurrences of the ostracod species *Cypria ophtalmica* at 27–26 and 17–16 cm and the unique presence of *Candona elliptica* at 3–2 cm were noted for this predominantly terrestrial phase of thermokarst basin development.

The drainage of Mama Rhonda coincides with the Medieval Warm Period, which previously has been connected to increased aeolian activity and dune expansion from 1.05 to 0.55 cal ka BP in northwest Alaska (Mann et al. 2002b). Mann et al. (2002b) concluded that dune expansion in the Kobuk valley was primarily controlled by the regional moisture balance, which, in turn, is most probably related to late-summer storms. In the case of Mama Rhonda lake, summer storms could have enhanced wave activity on the lake as well as lake shore and coastal erosion, which then may have triggered the drainage event. A basal peat age of 1.13 ± 0.05 cal ka BP (Kit-10, Table 4.1) < 1 km east of the study site (Figure 4.7) indicates coinciding drainage events in the vicinity, which probably would have affected the local hydrological regime in the surroundings of the Kit-43 site.

The isotopic compositions of intra-sedimentary ice as well as river and lake waters cluster in the heavy part of the $\delta^{18}O$ - δD diagram. Kit-43 samples taken in April 2009 display similar, but slightly heavier isotope compositions relative to rainwater, representing the modern summer signal. In contrast, the isotopic signatures of a snow patch and an ice-wedge in the study area are lighter (more negative) and both represent a winter signal (Figure 4.8). Kit-43 intra-sedimentary ice samples plot slightly below the Local Meteoric Water Line (LMWL, $\delta D = 7\delta^{18}O - 11$) of Barrow (Figure 4.8B), which indicates some alteration of the isotope composition by secondary fractionation processes (i.e. evaporative enrichment) compared to local modern winter and summer signals; these paleo-winter signals both correspond well with the LMWL and Global Meteoric Water Line ($\delta D = 8\delta^{18}O + 10$; Craig 1961). The Kit-43 samples from the sediment surface down to 42 cm represent the modern active-layer (with a slope of 6.2 in the co-isotope plot). The position of these sample series in the co-isotope plot (Figure 4.8B) indicates that the active-layer has been saturated by summer precipitation rather than by snow-melt. A similar pattern is noticeable at 82–42 cm with a slightly lower d excess (slope of 5.7).

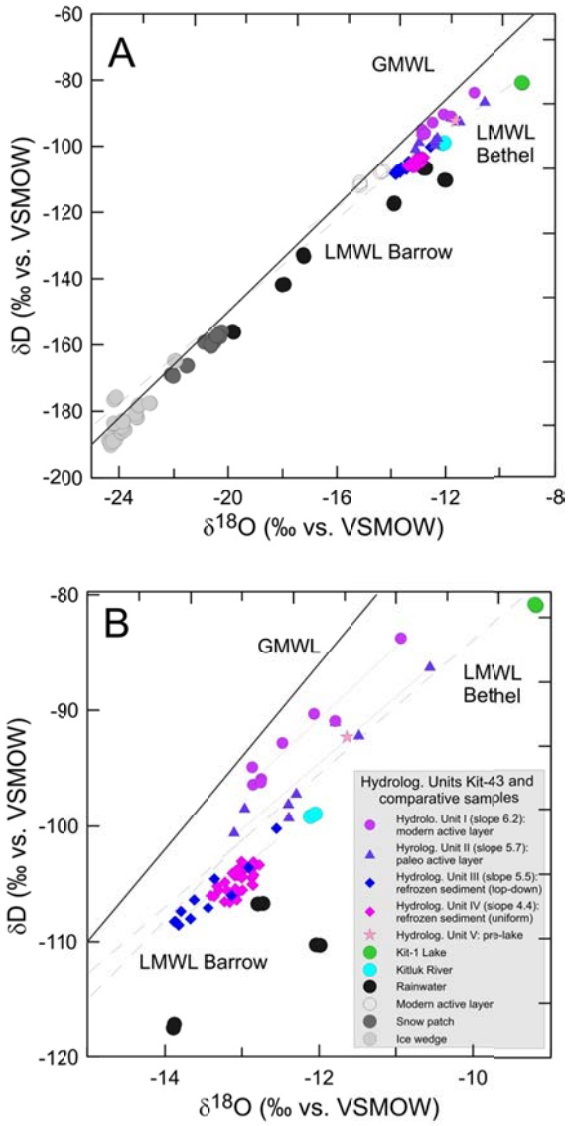

Figure 4.8: (A) $\delta^{18}O$- δD diagram of samples from permafrost core Kit-43 (in purple) compared to different types of ice and water (in grey, blue and green). (B) Close-up of same diagram with focus on Kit-43 core samples. GMWL = global meteoric water line; LMWL = local meteoric water line for Barrow and Bethel (http://www-naweb.iaea.org/napc/ih/IHS_resources_gnip.html).

Based on these very similar patterns we assume that the position of a paleo-active-layer related to the period prior to peat formation is preserved. After the lake drained at 1.06 cal ka BP, and before the peat accumulated on top of the drained lake sediment surface, the terrain surface was probably in direct atmospheric exchange.

The difference in the isotopic composition of the modern and paleo-active-layers suggests a change in the active-layer dynamics and characteristics due to build-up of a post-drainage peat layer. Heavy hydrogen and oxygen isotope compositions and low d excess are visible at the boundary between the modern and paleo-active-layers and the permafrost table where water migrated toward the freezing front (first ice during fractional freezing). Below 82 cm, the trend

from heavy to lighter isotopic composition indicates that the talik refroze from top to bottom. Below 154 cm, intra-sedimentary ice was described as structureless and oxygen isotope values and d excess were relatively uniform at -13 and 0 ‰, respectively. This points to a uniform water source (i.e. the adjacent lake) and no significant secondary isotope fractionation processes related to evaporation and/or melting/freezing. A similar situation has been found near Lake El'gygytgyn, where lateral contact with the adjacent lake and open system freezing have been suggested to explain uniform isotope composition over large parts of a permafrost core (Schwamborn et al. 2014). Hence, we assume a complex talik system next to our coring location due to the presence of Lake Rhonda until the present time.

4.6.2 Regional lake dynamics and global environmental change

From lake initiation in the Lateglacial at 11.8 cal ka BP to final drainage in the Late Holocene at 1.06 cal ka BP, different lake generations were archived in the Kit-43 core. Superimposed sets of thermokarst lake generations were previously assumed on the northern Seward Peninsula based on field observations and remote sensing. Hopkins & Kidd (1988) described sediment sequences in exposures with up to three thermokarst generations; Jones et al. (2012) detected assemblages of up to six partially overlapping lake generations with remote-sensing studies. Wetterich et al. (2012) investigated a pingo exposure (Kit-1, about 10 km east of Kit-43) and found cyclic permafrost aggradation and degradation over stadial–interstadial and glacial–interglacial time periods. At Kit-1, following a late mid-Wisconsin thermokarst lake, polygonal shallow water deposits were described for the late Wisconsin, before a thermokarst lake re-initiated in the Early Holocene around 9.4 cal ka BP and drained again in the Mid Holocene. The Early Holocene lake formation in Kit-1 therefore nearly overlaps with the transition from the Grandma Rhonda lake phase to the Mama Rhonda lake phase shown in Kit-43 at 9.0 cal ka BP, which also corresponds with the end of the HTM on the Seward Peninsula (Kaufman et al. 2004) and rising lake levels in interior and northern Alaska (Kaufman et al. in press).

Regional thermokarst lake formation in the Lateglacial and Early Holocene may have been predominantly caused by a warming and wetter climate. Such trends are indicated by a variety of evidence: invasion of *Populus* (Nelson & Carter 1987, Mann et al. 2002a, Ager 2003), occurrence of fossil beaver dams and beaver-gnawed wood beyond the modern presence of beavers (McCulloch & Hopkins 1966, Hopkins et al. 1981, Kaufman & Hopkins 1985) and buried ice-wedge casts on the Seward Peninsula (McCulloch & Hopkins 1966), as well as increased shrub cover, paludification of the landscape in northern Alaska (Detterman 1970, Oswald et al. 1999, Mann et al. 2002a, 2010, Jones & Yu 2010, Hunt et al. 2013) and fossil beetle assemblages indicative of climate amelioration (Nelson & Carter 1987, Elias 2000); all of these proxies indicate increased moisture availability and warmer-than-present temperatures in northwestern

and northern Alaska during that time. Climate models suggest that warm and moist air masses coming from the North Pacific (Bartlein et al. 1998) were responsible for rising lake levels (Edwards et al. 2001, Mann et al. 2002a, Abbott et al. 2010). Some other studies suggest cooler temperatures in the new coastal settings due to marine transgression and extensive seasonal sea ice (Sancetta & Robinson 1983, Ager 2003). Our study demonstrates the onset of thermokarst lake development and therefore permafrost degradation as early as the Lateglacial with continued lake evolution and changes throughout the Holocene.

4.6.3 Carbon cycling

Thermokarst lake dynamics and maturation of the periglacial landscape at our study site had a direct influence on carbon availability and storage. The first lake generations expanding into yedoma can cause substantial methane emissions from freshly thawed late Pleistocene permafrost (Walter et al. 2006, Kessler et al. 2012). Such lakes may have contributed, in turn, to climate warming at the Pleistocene–Holocene transition (Walter et al. 2007). Grandma Rhonda lake developed under a Lateglacial climate and eroded into Pleistocene yedoma deposits, which at that time were most probably not yet covered with a significant organic layer or peat; hence, comparably little organic matter entered the lake as indicated by an average TOC content of only 2.7 % in Unit B. The internal bioproductivity of the lake was dominated by algae (C/N of 10.4 in Unit B), possibly related to still rather cold climate conditions. Throughout the warmer Holocene submerged water plants were probably more abundant in Mama Rhonda lake and a thicker soil organic layer accumulated in the catchment of the developing thermokarst lake, resulting in an accelerated input of terrestrial organic matter into Mama Rhonda lake as a result of eroding shorelines (C/N of 14.6 and TOC of 8.6 % in Unit C, excluding the tephra layers). Thus, TOC in Holocene Mama Rhonda lake sediments exceeds TOC in Lateglacial Grandma Rhonda lake sediments by a factor of 3 (or 3.2 when excluding tephra layers in Mama Rhonda lake sediments). In contrast, Walter Anthony et al. (2014) found in 40 drained refrozen thermokarst basins in Siberia, on average, a 1.6 times larger carbon accumulation in Holocene thermokarst lake sediments than in late Pleistocene deposits. Because the Grandma Rhonda lake sediments remained unfrozen below Mama Rhonda lake, decomposition and release of carbon over a long time period probably additionally reduced the carbon stock in Grandma Rhonda lake sediments.

Like most lake basins after drainage (Hinkel et al. 2003, Bockheim et al. 2004, Jones et al. 2012, Regmi et al. 2012), the waterlogged soils of Mama Rhonda basin most probably became vegetated within the first 5–10 years and began to accumulate peat after 20–100 years had elapsed (Jones et al. 2012). At the Kit-43 coring site, terrestrial peat accumulated at a rate of 0.46 cm 10 a^{-1} to a total thickness of 40 cm. The organic carbon content of 38 % highlights the carbon storage capacity of drained basins. The area of modern Lake Rhonda is expanding with a mean rate of

0.53 m a^{-1} and maximum erosion rates of up to 2.6 m a^{-1} at its northern shore (Jones et al. 2011), so Mama Rhonda lake sediments and post-drainage peat are continuously incorporated into the next thermokarst lake and geochemical cycle.

4.7 Conclusions

Our study confirms previous observations of permafrost degradation and thermokarst development in Central Beringia in the Lateglacial and Early Holocene. For the first time, multiple lake and basin generations were documented in a permafrost core. The main conclusions of this study are:

1. Thermokarst lake initiation with thaw subsidence of in situ Devil Mountain Maar tephra occurred in the Lateglacial at 11.8 cal ka BP.
2. Intensive thermokarst processes in the Lateglacial and Early Holocene enabled the development of a rapidly expanding lake system. While sediments of this lake system (Grandma Rhonda lake phase) were preserved in the bottom of the Kit-43 core, a small remnant of this older lake basin is preserved at the southern margin of our study basin, including an ice-wedge cast with Grandma Rhonda lake sediments at Kit-7.
3. An abrupt change in the depositional environment around 9.0 cal ka BP as recorded in the Kit-43 core indicates a shift to a rather shallow and more dynamic lake system (Mama Rhonda lake phase), temporally coinciding with the Grandma Rhonda lake drainage event recorded in the Kit-75 exposure south of our study site. This drainage was, most probably, partial, resulting in wetland peat accumulation at Kit-75; our site was still occupied by a smaller remnant lake (Mama Rhonda lake) that subsequently started expanding again and was affected by multiple Holocene lake-level changes due to coalescence with neighboring lakes.
4. Drainage of Mama Rhonda lake and subsequent peat accumulation in the Late Holocene started with the Medieval Warm Period at 1.1 cal ka BP. The isotopic composition of intra-sedimentary ice preserved the paleo-active-layer and top-down aggradation of permafrost after drainage. Uniform isotopic composition shows missing secondary isotope fractionation processes below a depth of 154 cm, which may indicate an open freezing system i.e. as a result of the vicinity of an adjacent lake. Both paleo- and modern active-layers were filled by summer precipitation.

Overall, the Kit-43 sediment record preserves intensive environmental change in a periglacial lowland of Central Beringia that contains ice-rich permafrost. Newly forming thermokarst lakes in Late Pleistocene yedoma had profound impacts on biogeochemical cycling by thawing and mobilizing previously frozen organic carbon and nutrients into aquatic environments. This study

also emphasizes that later generation lakes have a higher potential to accumulate and decompose organic matter from erosion of organic-rich Holocene deposits if they persist in the landscape over long time periods and that peat layers developing after drainage are an important carbon source for future thermokarst lakes.

Acknowledgements

Fieldwork was supported by NSF (ARC-0732735), NASA (NNX08AJ37G) and the US National Park Service. Additional funding was provided by the German Federal Ministry of Education and Research (BMBF Grant No. 01DJ14003), the Western Alaska Landscape Conservation Cooperative Project (WA2011-02), RFBR (#16-040045-a) and the ERC (#338335). J. Lenz was supported by a Christiane Nüsslein-Volhard-Foundation grant, a dissertation stipend from the University of Potsdam, and the Helmholtz Graduate School for Polar and Marine Research (POLMAR), and acknowledges an invitation by S. Mischke to the Faculty of Earth Sciences (University of Iceland) for a research visit to finalize this study. We thank K. Walter Anthony and L. Farquharson for field support and discussions, and A. Myrbo and L. Farquharson for assisting with core splitting, imaging and GEOTEK scanning at the LacCore facility at the University of Minnesota. Further, we would like to thank H. Kemnitz, I. Schäpan, S. Wulf and O. Appelt (GFZ) for facilitating SEM imaging as well as geochemical analyses of tephra. We thank L. Farquharson, S. Lauterbach and one anonymous reviewer for providing helpful comments that improved the manuscript. Any use of trade, product or firm names is for descriptive purposes only and does not imply endorsement by the US Government.

5 Impacts of shore expansion and catchment characteristics on lacustrine thermokarst records in permafrost lowlands, Alaska Arctic Coastal Plain

Josefine Lenz[1,2], Benjamin M. Jones[3], Sebastian Wetterich[1], Rik Tjallingii[4], Michael Fritz[1], Christopher D. Arp[5], Natalia Rudaya[6,7,8], Guido Grosse[1,2]

[1] Department of Periglacial Research, Alfred Wegener Institute, Helmholtz Centre for Polar and Marine Research, Telegrafenberg A43, 14473 Potsdam, Germany

[2] Institute of Earth and Environmental Science, University of Potsdam, Karl-Liebknecht-Str. 24-25 14476 Potsdam, Germany

[3] Alaska Science Center, US Geological Survey, 4210 University Drive, Anchorage, AK, USA

[4] Section 5.2 Climate Dynamics and Landscape Evolution, Helmholtz Centre Potsdam, GFZ German Research Centre for Geosciences, Telegrafenberg C, Potsdam, Germany

[5] Water and Environmental Research Center, University of Alaska Fairbanks, 306 Tanana Loop, 437 Duckering, Fairbanks, AK, USA

[6] Institute of Archaeology and Ethnography, Ac. Lavrentiev Ave, 17, SB RAS, 630090 Novosibirsk, Russia

[7] Novosibirsk State University, Pirogova St. 2, 630090, Novosibirsk, Russia

[8] Kazan Federal University, Kremlevskaya Street, 18, 420008, Kazan, Russia

Under review in: Arktos

Key words: Permafrost degradation, carbon cycle, paleoenvironment, sedimentology, Arctic lakes, North Slope

5.1 Abstract

Arctic lowland landscapes have been modified by thermokarst lake processes throughout the Holocene. Thermokarst lakes form as a result of ice-rich permafrost degradation and they may expand over time through thermal and mechanical shoreline erosion. We studied proximal and distal sedimentary records from a thermokarst lake located on the Arctic Coastal Plain of northern Alaska to reconstruct the impact of catchment dynamics and morphology on the lacustrine depositional environment and to quantify carbon accumulation in thermokarst lake sediments. Short cores were collected for analysis of pollen, sedimentological and geochemical proxies. Radiocarbon and $^{210}Pb/^{137}Cs$ dating, as well as extrapolation of measured historic lake expansion rates, were applied to estimate a minimum lake age of ~ 1,400 calendar years BP. The pollen record is in agreement with the young lake age as it does not include evidence of the "alder high" that occurred in the region ~ 4.0 cal ka BP. The lake most likely initiated from a remnant pond in a drained thermokarst lake basin (DTLB) and deepened rapidly as evidenced by accumulation of laminated sediments. Increasing oxygenation of the water column as shown by higher Fe/Ti and Fe/S ratios in the sediment indicate shifts in ice regime with increasing water depth. More recently, the sediment source changed as the thermokarst lake expanded through lateral permafrost degradation, alternating from redeposited DTLB sediments, to increased amounts of sediment from eroding, older upland deposits, followed by a more balanced combination of both DTLB and upland sources. The characterizing shifts in sediment sources and depositional regimes in expanding thermokarst lakes were therefore archived in the thermokarst lake sedimentary record. This study also highlights the potential for Arctic lakes to recycle old carbon from thawing permafrost and thermokarst processes.

5.2 Introduction

Permafrost degradation influences hydrology, ecology, biogeochemical cycles, and terrain stability in Arctic lowlands (Rowland et al. 2010, Grosse et al. 2013a, Walter Anthony et al. 2014). In particular, ground subsidence following thaw of ice-rich permafrost or melting of massive ground ice, known as thermokarst (van Everdingen 2005), has been observed and monitored during the last several decades (Jorgenson et al. 2006, Romanovsky et al. 2007, 2010, Grosse et al. 2011, Jones et al. 2015). Typical thermokarst and thaw-related landforms include retrogressive thaw slumps (Kokelj et al. 2009, Lantuit et al. 2012), thermo-erosional gullies (Bowden et al. 2008, Godin & Fortier 2012), thermokarst pits (Jorgenson et al. 2006), as well as thermokarst lakes and drained lake basins which are the most ubiquitous features of lowland Arctic permafrost landscapes (Hinkel et al. 2005, Grosse et al. 2013a).

Thermokarst lake landscapes are modified by lake formation, expansion, coalescence, shrinkage, drainage and/or re-initiation, resulting in a complex topography where thermokarst basins constitute important depositional environments archiving landscape dynamics (French 2007). Aside from other permafrost paleo-records such as ice-wedges (Siberia: Meyer et al. 2015, Alaska: Meyer at al. 2010) and terrestrial deposits (e.g. Siberia: Wetterich et al. 2008b, Canada: Murton et al. 2005, Fritz et al. 2012b, Alaska: Wetterich et al. 2012, Kanevskiy et al. 2011), thermokarst lake sediments are important paleo-archives for reconstructing environmental changes on millennial time scales. Numerous studies have focused on general paleolimnological investigations of Late Quaternary lake sediments by using various sediment and biogeochemical proxies (Lenz et al. 2013, diatoms: Biskaborn et al. 2013a, plant macrofossils: Gaglioti et al. 2014). Some studies have concentrated on investigating thermokarst and geomorphological processes (Siberia: Biskaborn et al. 2013b, Morgenstern et al. 2013, Schleusner et al. 2015, Canada: Coloumbe et al. 2016, Fritz et al. under review, Alaska: Farquharson et al. in press), reconstructing lake generations (e.g. Jorgenson & Shur 2007, Jones et al. 2012, Lenz et al. in press) and carbon cycling (carbon accumulation rates: Klein et al. 2013, ^{14}C age offsets: Gaglioti et al. 2014, carbon degradation: Lenz et al. in press, methane production potentials: Heslop et al. 2015).

On the Arctic Coastal Plain of northern Alaska, paleo-ecological lake sediment investigations are scarce aside from Wooller et al. (2012) who reconstructed past methane availability from chironomids and cladocerans for a lake near Atqasuk. Most studies have focused on mapping and classifying thermokarst lakes and drained lake basins (Sellmann et al. 1975, Frohn et al. 2005, Hinkel et al. 2005, Farquharson et al. under review) or modern lake processes and dynamics. Here, scientific progress was achieved by research on thermokarst lake hydrogeomorphology (Arp et al. 2011), lake orientation (Black & Barksdale 1949, Carson & Hussey 1962), geomorphic controls on lake bathymetry (Hinkel et al. 2012), lake thermal regimes (Brewer 1958), lake ice regime shifts (Arp et al. 2012), thermal talik modeling (Ling & Zhang 2003), and catastrophic lake drainage (Jones & Arp 2015). Under scenarios of even modest climate warming, 10-30 % of the lowland landscapes of the Arctic Coastal Plain will be affected by thermokarst (Jorgenson et al. 2006), which could potentially impact the distribution of thermokarst lakes on the landscape. The highly dynamic nature related to the formation and drainage of thermokarst lakes in this region is particularly evident (Hinkel et al. 2003). In this region, paleo-environmental archives are scarce and it is important to investigate past thermokarst processes and lake dynamics using sedimentary records to assess potential future landscape changes.

The specific objectives of this study are:

1. to reconstruct the interaction of a late Holocene thermokarst lake with the surrounding landscape on the Arctic Coastal Plain based on analysis of sediment cores and shoreline expansion rates;
2. to assess how catchment dynamics and morphology impact the lacustrine depositional environment by comparing sediment records proximal and distal from shores;
3. to characterize and quantify how organic carbon accumulation and degradation in lacustrine thermokarst settings may be influenced by these dynamics.

5.3 Study area

The Arctic Coastal Plain of northern Alaska has been subject to several marine transgressions during the Quaternary (Brigham-Grette & Carter 1992, Brigham-Grette & Hopkins 1995) and is divided into the older, Inner Coastal Plain (ICP) to the south which is dominated by aeolian sand and the younger, Outer Coastal Plain (OCP) to the north, which is characterized by ice-rich marine silt (Hinkel et al. 2005, Williams et al. 1978). The northern Teshekpuk Lake Special Area is situated in the low-lying younger OCP, within the zone of continuous permafrost, where an average volumetric ground ice content of 77 % has been documented in near-surface permafrost (Kanevskiy et al. 2013) and where permafrost reaches thicknesses of at least 410 m (Jorgenson et al. 2008). However, excess ice is substantially lower in sediment deeper than 4 m (Sellmann et al. 1975), which limits the water depths of most thermokarst lakes to about 2.5 m and causes relatively uniform lake basin morphometries on the OCP (Hinkel et al. 2012). Holocene permafrost degradation and lacustrine succession associated with erosion, thaw and drainage processes have widely shaped the modern landscape (Hinkel et al. 2003, Jorgenson & Shur 2007). Today, lakes cover 22.5 % of the younger OCP north of Teshekpuk Lake, whereas DTLBs occupy 61.8 % (Jones & Arp 2015).

Peatball Lake (informal name; 70°42.4'N, 153°55.5'W; 3 m asl, above sea level) is located to the northwest of the largest lake on the Arctic Coastal Plain, Teshekpuk Lake (Figure 5.1). Peatball Lake is informally named for peculiar and abundant fibric peat spheres (up to ~ 5 cm diameter) that form in this lake and accumulate along a sandy shelf of the western shoreline. Peatball Lake is subcircular, has a surface area of 1.18 km², and is 1,300 m in diameter. The maximum water depth is 2.5 m. Lake ice covers the lake for ~ 9 months of the year on average during the past 4 years of monitoring and maximum ice thickness is typically 1.5 to 2.0 m over the same period (Arp et al. 2015). Water quality parameters monitored for different seasons and years (2012-2015) are summarized in table 5.1. Water temperatures ranged from about 5 to 14 °C

in August to about 0 to 1 °C below the ice cover in April. Uniform temperature, pH and specific conductivity (SC) in different depths confirm a well mixed water body of the shallow lake in summer and are indicative for a cold-monomictic lake circulation. SC is up to four times higher under the lake ice in April because ion content increases in the remaining liquid phase during the freezing. Lake water conditions are oxic in summer and can become hypoxic in winter, e.g. 0.2 mg L-1 in April 2012 (Table 5.1). Chlorophyll-a, an indicator for algal biomass, points towards an oligo- to mesotropic lake system although it is highly variable throughout the year (1-15 mg/L) and essentially higher under the winter lake ice.

The study area is dominated by high- and low-centered polygonal tundra. The cover is characterized by wetland vegetation with wet graminoids and moss communities (Raynolds et al. 2005). The modern regional climate is characterized by mean annual air temperatures of -12.2 °C ($T_{January}$ -27.5 °C, T_{July} +4.3 °C) and low average precipitation of 113 mm a^{-1} in Barrow (120 km northwest of Peatball Lake) (www.climate-data.org).

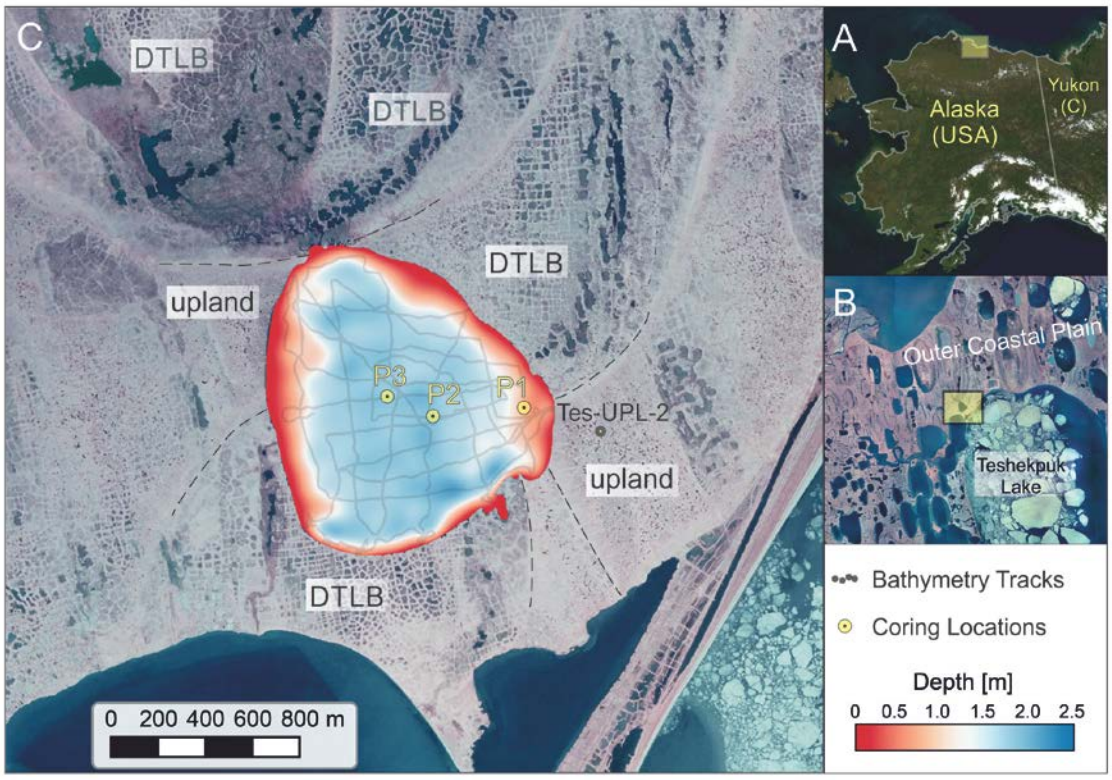

Figure 5.1: Study area of (A) Alaska (B) and the northern Teshekpuk Lake Special Area on the Outer Coastal Plain and (C) location of Peatball Lake indicating coring sites (P1, P2, P3) and core Tes-UPL-2 (Jock, unpublished data). Background of main map: Color infrared aerial orthoimage mosaic, 2002. Note the presence of drained thaw lake basins (DTLB) and upland remains as well as the abundance of ice-wedge polygonal landforms with high ground ice contents in near surface permafrost.

Table 5.1: Hydrochemical characteristics of Peatball Lake in different water depths and from different seasons (*CALON project:* http://www.arcticlakes.org/).

Month	Year	Water depth [m]	pH	Specific conductivity [µS/cm]	Temperature [°C]	Dissolved oxygen [mg/L]	Dissolved oxygen [%]	Chlorophyll-a [mg/L]
April	2012	2.3	-	3,170	1.1	0.2	2	-
August	2012	0.5	7.07	712	13.7	10.6	103	7.07
August	2012	1.3	7.04	712	13.7	10.4	101	7.04
April	2013	2.0	-	1,780	-0.2	15	-	14.9
August	2013	1.0	-	744	10.4	11.7	105	1.2
August	2013	2.0	-	744	10.4	11.7	105	2.1
April	2014	2.0	6.69	2,113	0.2	17	6.7	4.7
August	2014	0.5	7.14	704	5.3	12.6	100	2.9
April	2015	2.0	7.07	-	0.0	6	6.9	-
August	2015	-	-	667	9.3	-	-	-

5.4 Material and methods

Three short cores were recovered from Peatball Lake by using a piston corer (Aquatic Research Instruments, Hope, ID, USA) operated from the lake ice (April 2014) or inflatable coring platform (August 2014): Two cores of 49 and 100 cm length were obtained from the lake center (core ID P3 in April and core ID P2 in August 2014) and one core (core ID P1 in August 2014) of 50 cm length was recovered near-shore (Table 5.2).

Table 5.2: Meta data of the three cores from Peatball Lake.

Core ID	location	Core length [cm]	Water depth [cm]	Coordinates	Date of coring
P1	Near-shore	50	148	70°42.349'N, 153°54.527'W	15 August 2014
P2	Center	100	215	70°42.328'N, 153°55.133'W	15 August 2014
P3	Center	49	230	70°42.368'N, 153°55.454'W	20 April 2014

Split sediment cores were visually described and photographed at the German Research Centre for Geosciences Potsdam (GFZ). Magnetic susceptibility (MS) was measured every 0.1 cm with a split core logger (scl-2.3) developed at GFZ that was equipped with a Bartington MS2E sensor in combination with a MS2 control unit (Nowaczyk et al. 2013). The geochemical sediment composition was acquired by X-ray fluorescence (XRF) core scanning using an ITRAX core scanner (Croudace et al. 2006). The XRF core scanner was operated with a Cr X-ray source

(30 kV, 300 uA, 10 s) and provides element intensities. Element intensities are non-linear functions of element concentrations due to physical sediment properties (e.g. water content), the sample geometry, and XRF absorption and enhancement effects (Tjallingii et al. 2007). However, down-core variations in physical properties and sample geometric effects can be minimized by using (log-)ratio of the intensity data (Weltje & Tjallingii 2008).

The cores were subsampled at 1 cm intervals for geochemical analyses. Total nitrogen (TN), total carbon (TC), and total organic carbon (TOC) were measured on bulk sediments with an elemental analyzer (ElementarVario EL III; analytical accuracy of ± 0.1 wt%) and the C/N-ratio (TOC/TN) was calculated. To determine the stable carbon isotope composition, $\delta^{13}C$ of TOC was analyzed at GFZ with a Carlo-Erba CN2500 attached to a stable isotope ratio mass spectrometer (DELTAplusXL, Finnigan). Values of $\delta^{13}C_{TOC}$ are expressed relative to the Vienna Pee Dee Belemnite (V-PDB) standard in per mill (‰) and the standard deviation (1σ) is generally better than ± 0.02 ‰. The water content was calculated using the weight difference between fresh and freeze-dried bulk sediment samples and is expressed as weight percentage (wt%).

A total of 24 pollen samples were processed in an average interval of 4 cm from core P2, each consisting of 2-3 g of dry sediment. Sample preparation followed common protocols (Fægri & Iversen 1989, Moore et al. 1991, Beug 2004*)* including the addition of *Lycopodium* spore tablets (Batch number 1031; n=20848) to calculate total pollen and spore concentration. The bulk samples were processed with hydrochloric acid, potassium hydroxide, and hydrofluoric acid (40 %). Afterwards, samples were treated to three minutes of acetolysis, for staining the pollen grains and an ultrasonic bath (max. 30 seconds, mesh size 7 µm) was applied to remove small pollutants. Pollen residues mounted in glycerol were analyzed under the light microscope with a 400× magnification. Identification of pollen and spores was performed using reference pollen collections and regional pollen atlases (e.g. Reille 1988, 1992).

Accelerator mass spectrometry (AMS) radiocarbon dating was performed at the Poznan Radiocarbon Laboratory (Poland) on three samples of core P1, ten samples of core P2 and four samples of P3. Samples were wet-sieved through > 250 mm mesh screens and hand-picked for macrofossil remains, except for two samples at the base of core P2 which were dated as bulk samples. Results were calibrated using the CALIB 7.1 with the IntCal13 data-set (Reimer et al. 2013) and reported in calibrated years before 1950 AD, referred as before present (cal a BP).

Dried sediment samples from core P2 were analyzed in an interval of 0.5 cm for ^{210}Pb, ^{226}Ra, and ^{137}Cs by direct gamma assay in the Liverpool University Environmental Radioactivity

Laboratory using Ortec HPGe GWL series well-type coaxial low background intrinsic germanium detectors (Appleby et al. 1986). ^{210}Pb was determined via its gamma emissions at 46.5 keV, and ^{226}Ra by the 295 keV and 352 keV γ-rays emitted by its daughter isotope ^{214}Pb following 3 weeks storage in sealed containers to allow radioactive equilibration. ^{137}Cs was measured by its emissions at 662 keV. The absolute efficiencies of the detectors were determined using calibrated sources and sediment samples of known activity; corrections were made for the effect of self-absorption of low energy γ-rays within the sample (Appleby et al. 1992).

Erosion rates for Peatball Lake were determined by comparing the lake shoreline in aerial photography acquired in 1955 and 2002. The 2002 orthophotography (2.5 m resolution) served as the base in which to georegister the 1955 photography to a resolution of 2.5 m. The mean RMS error associated with the georegistration of the 1955 photography was 0.78 m using 13 ground control points and a 3rd order polynomial transformation. The lake shoreline was manually digitized in both images and then erosion rates calculated using the USGS Digital Shoreline Analysis System add-on for ArcMap (Thieler et al. 2008). While this method is intended for measuring coastal shoreline erosion, it has also been successfully used to quantify thermokarst lake expansion previously (Jones et al. 2011, Arp et al. 2011). Thus, lake expansion rates were measured at 10 m transect intervals along the lake shoreline between 1955 and 2002 to help further constrain the age of Peatball Lake.

5.5 Results

Sediment parameters were analyzed in order to characterize the past depositional environment of Peatball Lake. The combination of visual sediment core description with MS and XRF core scanning results provide a detail characterization of the core lithology and sediment facies. In the sediments of Peatball Lake, magnetic minerals are restricted to siliciclastic sediments that originate from input of allochthonous material into the lake. Additional information on the origin or grain-size of siliciclastic sediments is obtained by variations of the K/Ti XRF scanning record. The Fe/Ti and Fe/S ratios provide information on relative changes of the oxygenation in the lake, which is linked with water depth in Peatball Lake. Geochemical analyses of TN and TOC indicates past bioproductivity, allochthonous input of organic material into the lake system but also reflects preservation conditions of organic matter (Cohen 2003, Lamoureux & Gilbert 2004). As $CaCO_3$ is presumably produced only autochthonously in lakes and is not present in the terrestrial terrain on the younger OCP, it indicates deposition of lacustrine biogenic carbonates. $CaCO_3$ and TOC may vary due to a dilution effect of the other. The C/N ratio characterizes the degree of decomposition of organic material but can also be used to discriminate sources or

organic matter by using the ratio of $\delta^{13}C_{TOC}$ and C/N (Meyers 1997, Meyers & Takemura 1997). Changing abundance and taxa composition of pollen grains in the sediment gives evidence for regional vegetation composition but is also influenced by changing sources of sediment into the lake.

5.5.1 Sedimentological results of near-shore core P1 (PG2370)

Core P1 was dominated by homogenous minerogenic sediment composed of dark gray (Munsell Soil Color Chart, ID 2.5Y 4/1) fine sands (Figure 5.2). A peat inclusion of 1.5 cm in diameter was described in 17 cm depth as well as organic layers (2.5Y 3/2) of 2 mm thickness in depth of 36 to 46 cm. The base of the core was composed of a 4 cm thick, black organic deposit (2.5Y 1.5/1), which was poorly decomposed and included a root of 7 mm length. The MS of the core ranged from 5 to 103 with distinct changes combined with up-core increasing MS at 45 cm, 31 cm and 20 cm. The K/Ti record shows some variation but no obvious trend in core P1. In contrast, Fe/Ti and Fe/S was low and showed no variation in most of the sediment core, but high values occur at the black organic deposit of the basal part of the core.

TN was 0.2 wt% on average (TN_{min} below detection limit of 0.1 wt% mainly in 13-34 cm depth, TN_{max} 0.6 wt% at the core base) and TOC was on average 1.6 wt% (TOC_{min} below detection limit of 0.1 wt% at 15-22 cm depth, TOC_{max} 13.3 wt% at the core base). The C/N-ratio was calculated to an average of 8.7 with presumably low C/N where TN and TOC reached the detection limit and a maximum of 25.4 at the core base. $CaCO_3$ calculated from TIC was 4.5 % on average with $CaCO_{3min}$ of 2.9 % and $CaCO_{3max}$ of 11.8 %. A narrow $\delta^{13}C_{TOC}$ range of -28.2 to -27.2 ‰ was measured for core P1.

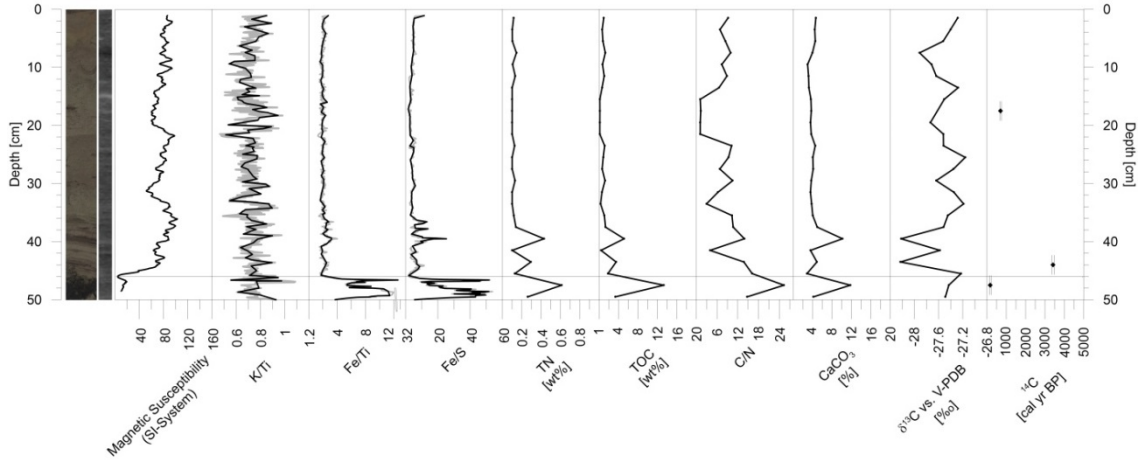

Figure 5.2: Core photograph, radiographic image, lithological and geochemical results, and radiocarbon dates of core P1 according to core depth.

5.5.2 Sedimentological and palynological results of lake center-cores P2 (PG2371; and P3 (PG2372))

Sediments of core P3 from the lake center are covering the same facies as the upper half of the 100 cm long core P2 from near the lake center. Subsequently, we will therefore concentrate on core P2 (Figure 5.3, for analytical details of core P3 see digital appendix table 5.1).

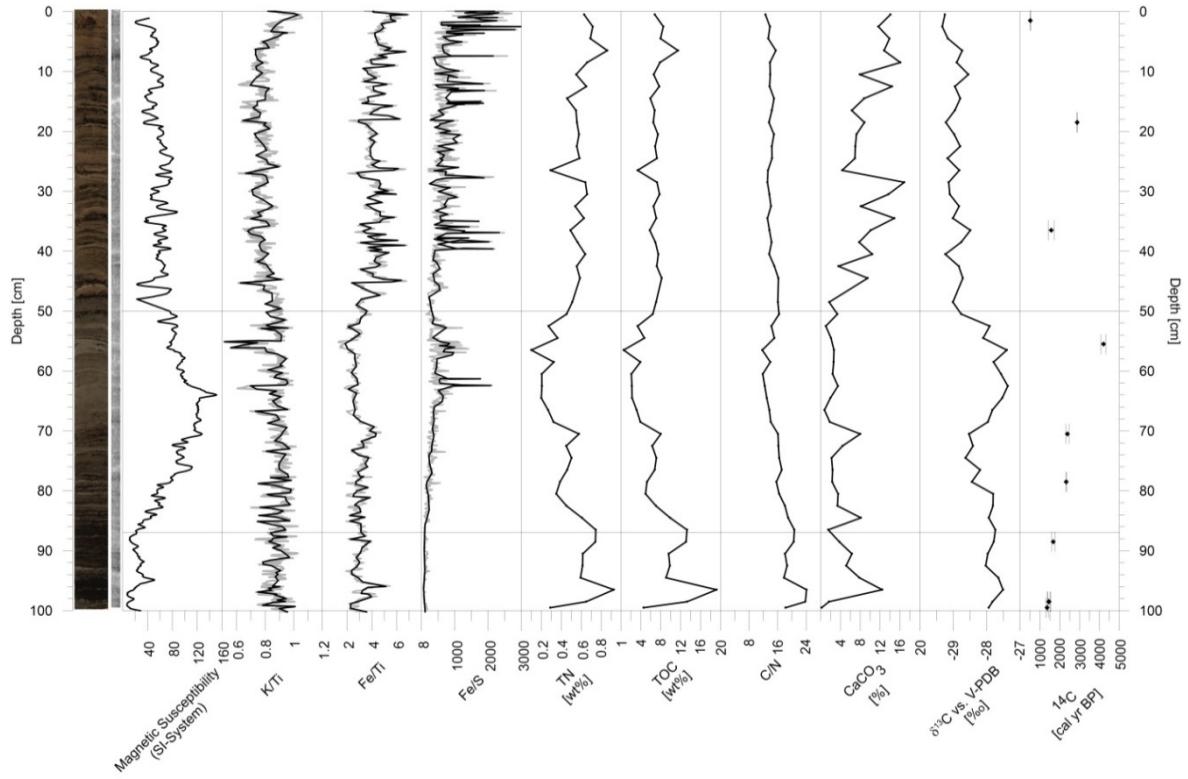

Figure 5.3: Core photograph, radiographic image, lithological and geochemical results, and radiocarbon dates of core P2 according to core depth.

Core P2 was mostly well-laminated with alternating dark grayish brown (2.5Y 4/2), silty minerogenic sediments and black (2.5 Y 2.5/1) organic layers of up to 5 mm thickness. Minerogenic deposits without visible organics and no clear laminations characterize core P2 between 71 and 87 cm. Thinner laminae were observed in depths of 87 to 99 cm. The base of the core P2 was composed of a very dark gray (2.5Y 3/1) and fairly decomposed peat layer. Core P3 differed only in its thickness of organic (1 to 10 mm) and minerogenic layers (2-30 mm) and presence of a bivalve mollusk of 4 mm length at 31 cm depth. The MS of the sediment core P2 ranged from 7 to 151 (36 to 94 in core P3) with a pronounced change to increasing MS from 87 to 64 cm and decreasing MS from 64 cm to 50 cm.

Similar to core P1, the K/Ti record was highly variable but showed no trend within core P2; except for a narrow K/Ti ratio shown at 55-56 cm (Figure 5.3). The Fe/Ti ratio showed low

variation in depths of 100 to 50 cm and higher variation and ratio with slightly increasing trend in depth of 50 to 0 cm. Similarly, the Fe/S ratio was very low at 87-100 cm and increased up-core with high variations in depth of 0 to 38 cm.

TN was on average 0.5 wt% (TN_{min} below 0.1 wt% only at 61-62 cm, TN_{max} 0.93 wt% at 96-97 cm) and TOC was on average 7.0 wt% (TC_{min} 0.53 wt%, TOC_{max} 19.1 wt% at 96-97 cm), both with lowest values between 52 and 69 cm. The C/N-ratio was decreasing up-core from a maximum of 24 at 96-97 cm to a minimum of 12 at 60 cm and remained stable around 14 in 0-60 cm depth. $CaCO_3$ varied between 1.4 and 16.8 % with $CaCO_{3min}$ < 4 % between 48 and 69 cm. The $\delta^{13}C_{TOC}$ ranged between -29.3 and -27.4 ‰ in core P2 with highest $\delta^{13}C_{TOC}$ of ≥ -28 ‰ in depth of 54 and 69 cm.

Pollen analysis revealed high pollen concentration (Figure 5.4) that allowed counting up to 300 grains in each sample. Two pollen zones (PZ) were identified in the pollen diagram of core P2 based on changing pollen taxa composition and abundances (Figure 5.4): PZ I (101-72 cm) was characterized by almost equal percentages of Poaceae and Cyperaceae. The abundance of planktonic green algae remnants (*Botryococcus*, *Pediastrum* and *Zygnema*) increased in PZ I. PZ II (72-0 cm) was characterized by dominance of Cyperaceae over Poaceae and a decrease of planktonic green algae. Arboreal pollen of *Betula*, *Alnus* and *Salix* dominated over *Picea* and Pinaceae in both pollen zones PZ I and PZ II.

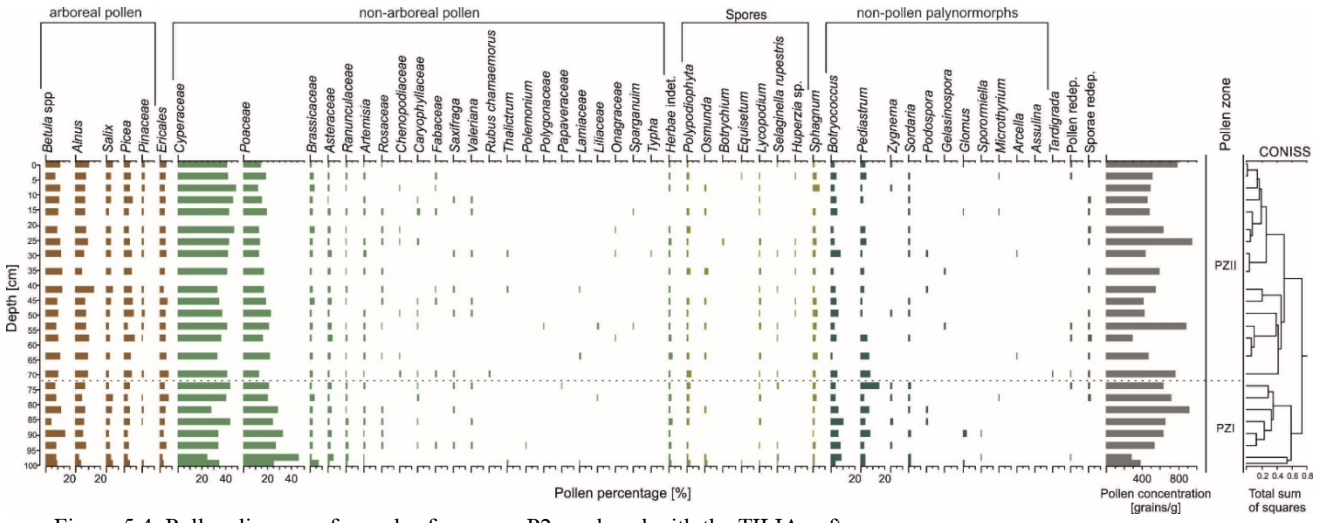

Figure 5.4: Pollen diagram of samples from core P2 produced with the TILIA software.
The visual definition of pollen zones is supported by cluster analysis with the program CONISS (Grimm 1987).

5.5.3 Lake age estimation

Calibrated ages ranged between 180 and 3,420 cal a BP for core P1; between 530 and 4,200 cal a BP for core P2; and between 1,300 and 3,180 cal a BP for core P3, but did not show a clear age-depth relationship (Table 5.3). While the near-surface date (1-2 cm) in core P2 had the youngest age of the geochronological record, the second youngest date in this core was obtained at the core base. Here, three samples (bulk and plant remains) yielded similar radiocarbon age between 1,370 and 1,470 cal a BP.

Table 5.3: AMS radiocarbon age determinations of three cores (P1, P2 and P3) with calibrated ages derived from CALIB 7.1 (Poz = Poznan Radiocarbon Laboratory, pMC = percent modern carbon).

Core ID	Lab ID	Depth [cm]	Dated material	$\delta^{13}C_{TOC}$ [‰ V-PDB]	pMC	AMS age [a BP]	Calibrated ^{14}C age [cal a BP]
P1	Poz-68412	17-18	moss remains, Cyperaceae remains	-36.7	90.74	780 ± 30	710 ± 40
P1	Poz-68413	43.5-44.5	moss remains, small wooden remains, remains of leaves	-31.0	67.17	3,195 ± 35	3,420 ± 60
P1	Poz-68414	47-48	wood, single moss remains, roots, some Cyperaceae remains	-27.5	97.98	165 ± 30	180 ± 50
P2	Poz-68415	1-2	moss remain	-36.6	93.69	525 ± 30	530 ± 25
P2	Poz-68417	18-19	Cyperaceae remains, moss leflets	-32.1	71.82	2,660 ± 30	2,880 ± 30
P2	Poz-68664	36-37	mollusk shell	-21.0	79.90	1,690 ± 70	1,580 ± 160
P2	Poz-68418	55-56	moss remains, wooden remains, single seeds	-32.0	62.30	3,800 ± 35	4,200 ± 125
P2	Poz-68479	70-71	Cyperaceae remains, moss remains	-30.6	74.65	2,350 ± 30	2,390 ± 70
P2	Poz-68480	78-79	Cyperaceae remains, moss remains	-31.2	75.17	2,295 ± 30	2,330 ± 25
P2	Poz-68481	88-89	Cyperaceae remains, moss remains	-31.3	80.18	1,775 ± 30	1,680 ± 70
P2	Poz-68482	98-99	moss stems and moss leaves, wooden remains, seed	-30.2	82.45	1,550 ± 30	1,450 ± 75
P2	Poz-70802	98-99	bulk sediment	-23.1	82.23	1,571 ± 30	1,470 ± 70
P2	Poz-70804	99-100	bulk sediment	-26.9	82.86	1,510 ± 30	1,370 ± 50
P3	Poz-68483	15-16	moss remains, Cyperaceae remains, aquatic plant remains	-34.3	68.74	3,010 ± 35	3,180 ± 85
P3	Poz-68484	33-34	moss remains, Cyperaceae remains, roots, aquatic plant remains	-34.7	69.82	2,890 ± 40	3,000 ± 120
P3	Poz-68485	42-44	moss, aquatic plant remains	-36.3	84.29	1,375 ± 30	1,300 ± 70
P3	Poz-68486	46-47	moss remains, Cyperaceae remains	-32.4	78.16	1,980 ± 30	1,930 ± 60

Total ^{210}Pb activity significantly exceeded the supporting ^{226}Ra in the uppermost 3 cm of core P2. The measured ^{210}Pb inventory of the core corresponds to a mean ^{210}Pb supply rate of 9 Bq m^{-2} a^{-1}. Although being very low, the ^{210}Pb supply rate lies within the expected range for this region given the very low mean annual rainfall at this site (< 200 mm a^{-1}). The ^{137}Cs concentrations in P2 were significant in the uppermost 3 cm of the core P2. Although there was no discernible sub-surface peak, the results do suggest that the 1963 fallout maximum from the atmospheric testing of nuclear weapons is recorded in sediments lying between 1 and 2.5 cm depth, with a mid-point of the fallout inventory at 1.5 cm. Low sedimentation rates of 0.04 cm a^{-1} (0.021 g cm^{-2} a^{-1}) were

calculated from the ^{210}Pb concentration. An age of 2,100 years was calculated for the base of core P2 when assuming a constant sedimentation rate.

A third independent age estimation of Peatball Lake is based on determining the shoreline expansion rates (Figure 5.5) and inverting the expansion with the assumption of stable rates to retrieve the potential timing of lake initiation. A maximum shoreline erosion of 1.36 m a^{-1} was calculated at the upland bluff to the southeast and the modern outflow to the north of Peatball Lake; a minimum of 0.02 m a^{-1} was determined at the western shoreline. Applying the mean shoreline expansion rate of 0.46 m a^{-1} to the lake radius of about 650 m and assuming a constant radial lake expansion from a central point, a lake initiation around 1,400 years ago is calculated (650 m/0.46 m a^{-1} = 1,413 a). This calculation provides an independent, yet crude assessment for limiting the initiation age of Peatball Lake.

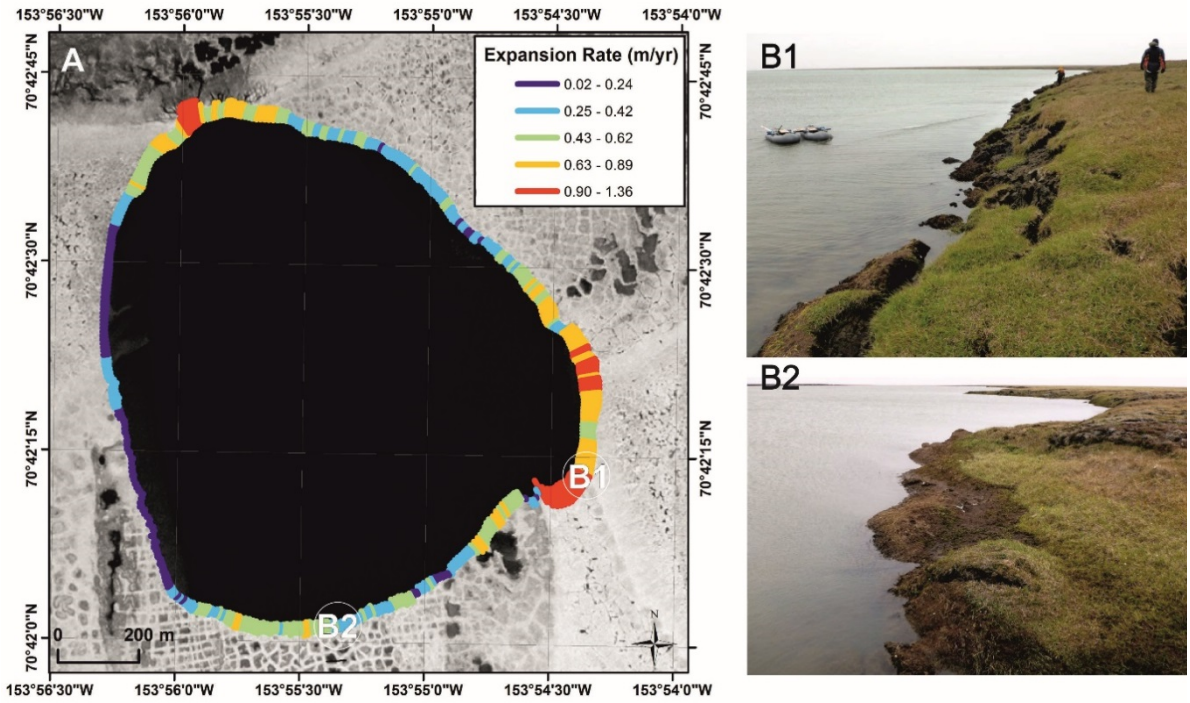

Figure 5.5: (A) Expansion rates of Peatball Lake between 1955 and 2002 at 10 m increments. (B1) Upland bluff to the SE and (B2) lowland along the SSW of Peatball Lake.

5.6 Discussion

5.6.1 Thermokarst lake development

The development of Peatball Lake can be reconstructed from the sediment cores and the calculated shoreline expansion rates. Deriving a clear age-depth relationship for sediments in Peatball Lake is challenging but the lake initiation is set to a minimum age of 1,400 years based on the following arguments: Triplicate radiocarbon measurements of different materials (bulk sediment and plant macrofossils) at slightly different depths in core P2 generated similar calibrated radiocarbon ages of about 1,400 cal a BP. $^{210}Pb/^{137}Cs$ dating yielded a maximum age of about 2,100 a BP for the core base when assuming a constant sedimentation rate of 0.04 cm a^{-1}. However, constant sediment accumulation is not realistic in dynamic thermokarst lake environments where intermittent rapid lake expansion can cause slumping and mass deposition (Biskaborn et al. 2013b, Lenz et al. 2013, Fritz et al. in press). Therefore, a minimum age of core P2 of 1,400 a BP seems reasonable and is supported by the modern mean shoreline expansion rate of 0.46 m a^{-1} (for 1955-2002 AD) leading to a lake initiation age of around 1,400 years before today. The pollen record suggests that major shifts in vegetation did not occur (Figure 5.4). The typical mid-Holocene increase of alder usually reported in this region, e.g. by Colinvaux (1964), Anderson & Brubaker (1994) and Eisner et al. (2005) is not observed, pointing towards a young depositional environment for our record of < 4.0 cal ka BP.

The initial Peatball Lake basin likely deepened rapidly with laminated lake sediments accumulating early on above the preserved wetland peat at the base of the central core P2 (Figure 5.6, Phase A) and aquatic algae preserved in the sedimentary record (Figure 5.4). The initial pond may have evolved at the intersection of ice-wedges where degradation and impoundment of water at troughs can lead to the formation of small but > 1.5 m deep ponds (Jorgenson & Shur 2007). Ice-wedge networks are present in the modern catchment (Figure 5.1) and their high ground ice content is crucial for deeper thawing and thermokarst development (Hopkins & Kidd 1988). Previous studies have shown that the depth of ice-wedges is generally limited to a maximum of 6 to 8 m in areas affected by multiple thermokarst lake cycles (Hopkins & Kidd 1988). It is even more likely that the early Peatball Lake initiated from a remnant pond located in one of the drained thermokarst basins (DTLBs) situated in the catchment of the modern Peatball Lake basin. A shallow lake has either persisted in the DTLB or a secondary, new thermokarst lake developed. Secondary thermokarst lakes are typically (1) small and shallow ponds at the low-lying margins or (2) slightly deeper and larger lakes in the basin center created by thawing into ice- and organic-rich lacustrine material of a drained primary thermokarst lake (Jorgenson & Shur 2007).

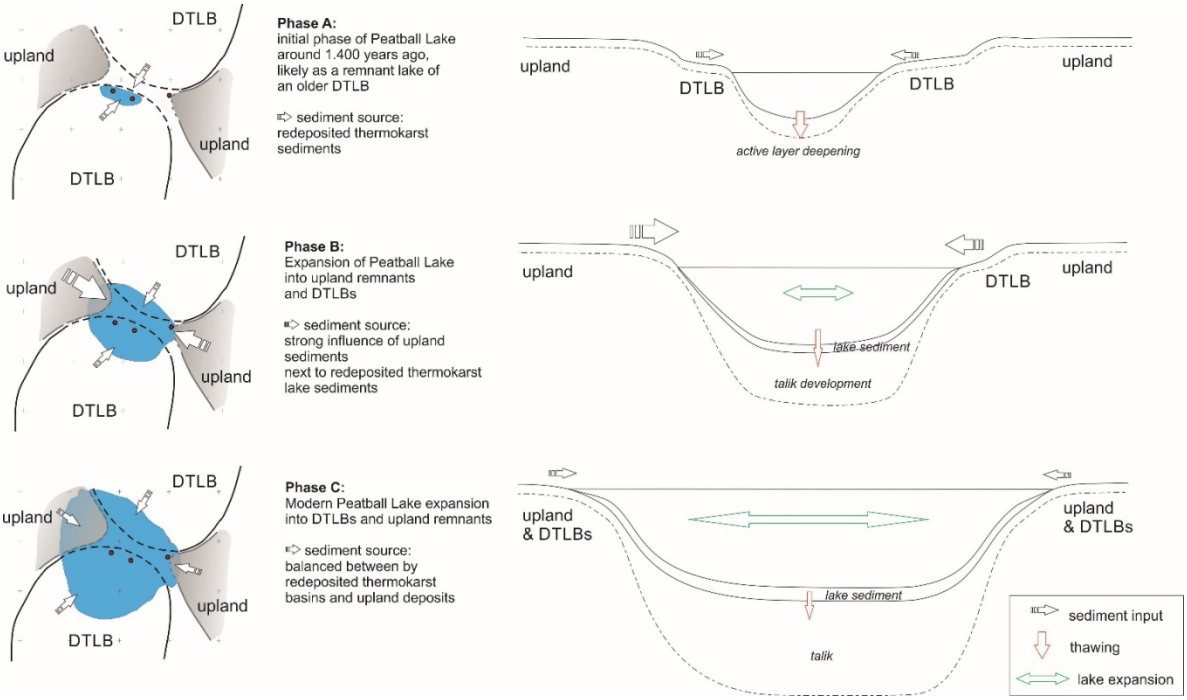

Figure 5.6: Development of Peatball Lake and indication of changing sediment sources: Phase A – Initial lake development and deep thawing around 1,400 years ago as a remnant of a former thermokarst lake and redeposited lacustrine sediments as predominant sediment source. Phase B – Lateral lake expansion into upland deposits and talik development. Phase C – Expansion of Peatball Lake into DTLBs and upland remains.

Both have been observed in recent basins (Hopkins & Kidd 1988, Jorgenson & Shur 2007, Jones et al. 2011, Lenz et al. 2016) or interpreted in paleo-records (Lenz et al. in press) in other continuous permafrost regions in Alaska. In the early stage of Peatball Lake development, the winter lake ice cover apparently has not disturbed the sediment layering. Increasing oxygenation at the central part of the lake was derived from a high Fe/Ti and Fe/S ratio in core P2. Oxygenation in Arctic lakes is not only an indicator for increased water depth but also is dependent on winter lake ice thickness which reduces the water volume over lake sediments. In Peatball Lake, increased oxygenation indicates a shift in ice cover from bedfast ice to floating ice conditions with increasing water depth. Low Fe/Ti and Fe/S ratios in core P1 reflect predominantly anoxic conditions for the near shore zone reasoned by bedfast ice in shallow waters. However, Fe/Ti and Fe/S ratios at the core base of P1 are surprisingly high and most likely indicate in-situ terrestrial peat which deposited under atmospheric conditions before the lake expanded into the P1 coring site. This signal is less obvious in the Fe/Ti and Fe/S records of the central core P2.

After its initiation and deepening, Peatball Lake predominately expanded laterally through thermal and mechanical erosion (Figure 5.6, Phases B and C). The larger the lake surface area, the longer the wind fetch and the greater the shoreline erosion due to mechanical wave action (Jorgenson & Shur 2007). Additionally, water depth exceeding the maximum lake ice thickness in winter has been linked to higher rates of shoreline erosion (Arp et al. 2011). Although the modern shoreline expansion rate of Peatball Lake ranges from 0.02 m a^{-1} to 1.36 m a^{-1}, the lake likely enlarged radially which is typical for most thermokarst lakes (Hopkins & Kidd 1988), but does not follow the typical pattern of north-south lake elongation observed in most of the Teshekpuk Lake Special Area (Carson & Hussey 1962, Hinkel et al. 2005, Arp et al. 2011). The formation of oriented lakes is still not yet fully understood but it seems widely accepted that sublittoral shelves form by near-shore wind-driven currents, which are perpendicular to the prevailing easterly and westerly winds, protecting subsequently the eastern and western lake shores from thawing and erosion due to lower wave height and energies in shallow waters (Carson & Hussey 1962). In Peatball Lake, a sublittoral shelf is clearly evident from the bathymetry on the western shore and is present, although less clear, at the eastern shore (Figure 5.1) suggesting an increasing elongation for Peatball Lake`s future development. This could include tapping and drainage into the older DTLB to the north or into Teshekpuk Lake to the south in the future.

5.6.2 Impact of catchment genesis and morphology on the lake sediment record

During the lake expansion process the eroding shorelines intersected sediment sources of different genesis and morphology. A homogenous, clastic dominated sediment facies in 71 to 87 cm depth of the otherwise layered central core P2 points towards alternating deposition conditions. In this section, low accumulation of organic matter indicates rapid deposition of clastic material and high magnetic susceptibility indicates a change of external sediment sources in the catchment. Old radiocarbon dates of up to 4,200 ± 125 cal a BP in in this section of core P2 (Table 5.3) indicate the influence of a different sediment source which likely is associated with the neighboring upland remains dated to at least 6,840 ± 100 cal a BP (in depth of 156-159 cm, Poz-74869, core ID Tes-UPL-2, Figure 5.1, S. Jock, unpublished data). The sediment record hence archived the history of a growing Peatball Lake which initiated in a DTLB (Phase A) and subsequently expanded laterally into upland remnants and also DTLBs (Phase B and C, Figure 5.6). When shore erosion reached the uplands, higher sediment fluxes with occasional thaw slumping were likely due to the steeper geomorphological gradient of several meters between lake and upland. Biskaborn et al. (2013b) reconstructed different states of slope stability, including

slumping events from ice-wedge structures, in the sedimentary record of a Siberian thermokarst lake in a less heterogeneous catchment with higher relief energy. In Peatball Lake, the relief energy is lower but the sediment source suddenly changed from lacustrine, reworked deposits od DTLBs in Phase A to predominately upland deposits in Phase B, and gradually to a mixture of both DTLB and upland deposits in Phase C.

The nearshore core P1 is situated close to the today's upland in the eastern catchment and confirms a similar depositional environment like Phase B in core P2: Rapid, event-like deposition is indicated by radiocarbon ages as young as 180 ± 50 cal a BP in 48 cm depth, a step-like increase of magnetic susceptibility at 45 cm, 31 cm and 20 cm and low organic matter content. C/N as well as $\delta^{13}C_{TOC}$ is more variable in near-shore sediments indicating a dynamic organic matter accumulation of different quality and origin. The XRF-based ratio of K/Ti points to a generally constant clastic sediment source for the near-shore and lake center, which is explained by short transport paths of redistributed sediments of initially the same origin.

5.6.3 Carbon degradation

The variability of AMS radiocarbon ages in all three Peatball Lake cores highlights that old permafrost carbon is continuously recycled and redeposited in thermokarst landscapes the Alaskan Arctic Coastal Plain. When located in thawed sediments, the old reworked carbon is affected by ongoing decomposition by microbial communities and the response to warmer temperatures is a key factor for changes in local carbon cycling (Kao-Kniffin et al. 2015). Average organic carbon content of sediments in the central part of Peatball Lake ($TOC_{average}$ = 7 wt% in P2 and P3) were 4 times lower and near-shore deposits ($TOC_{average}$ = 1.6 wt% in P1) were even more than 18 times lower than upland deposits from the eastern catchment ($TOC_{average}$ = 30 wt% in a 190 cm upland permafrost core Tes-UPL-2, Jock, unpublished data). Similar relationships were investigated for total nitrogen which was 3 times lower in central Peatball Lake sediments ($TN_{average}$ = 0.5 wt% in P2 and P3) and 7 times lower than in near-shore deposits ($TN_{average}$ = 0.2 wt % with TN under detection limit of 0.1 wt% in large parts of P1) than in terrestrial upland deposits ($TN_{average}$ = 1.4 wt% in Tes-UPL-2, S. Jock, unpublished data). Old organic matter is significantly affected by permafrost degradation during the process of thawing and decomposition (Mueller et al. 2015). The degraded organic material is relocated by thermokarst erosion and accumulated in the lake basin. Rapid near-shore deposition of degraded material and low primary production under Arctic climate and anoxic conditions in shallow waters result in nutrient-poor sublittoral sediment deposition as reflected in sediment core P1.

Finer sediments were relocated and accumulated in the deeper basin where a vertically mixed water body enhanced primary production in summer and enrichment of lacustrine organic matter in the sediment (Cohen 2003). Aquatic algae were present throughout the full sediment record of P2 (namely *Botryococcus* and *Pediastrum*, Figure 5.7) giving evidence for sufficient primary production in the short growing season. Oxic water conditions allowed good preservation conditions during sediment deposition in Phase C of the Peatball Lake development (Figure 5.6, Table 5.3). Further on, nitrogen becomes relatively enriched as carbon decomposition is presumably higher in oxic water conditions. A higher rate of decomposition due to longer residence times in unfrozen lake sediments result in lower C/N ratios. The on average 3 times lower C/N ratio in near-shore sediments (on average 7 in P1 ranging from close to 0 where TOC and TN is below the detection limit to 22) than in upland deposits (22 in Tes-UPL-2, Figure 5.1, S. Jock, unpublished data) highlights the high degree of decomposition. The generally wide range of C/N in core P1 (Figure 5.7) points at a wide range of organic matter sources from typically terrestrial land plants to lacustrine algae, whereas the central core P2 shows a similar signature with less variability. However, it is possible that inorganic nitrogen from marine sands and silts also have reduced the C/N ratio derived from total nitrogen.

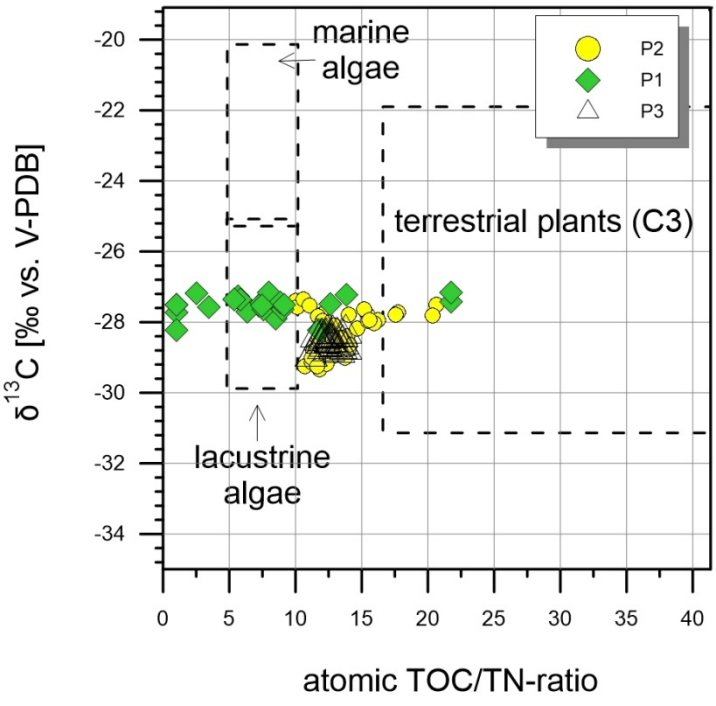

Figure 5.7: Ratio of $\delta\,^{13}C_{TOC}$ and TOC/TN of all Peatball Lake cores (P1, P2, P3) demonstrating a wide range for P1 and P3 representing P2.

Mueller et al. (2015) have shown that large amounts of labile organic carbon is stored in deposits of drained lake basins on Barrow Peninsula (42 ± 5 kg m^{-3} in young basins < 50 years old and up to 62.5 ± 14 kg m^{-3} in old basins 300-2000 years old) and confirmed a major carbon stock in the active-layers as previously described by Bockheim et al. (1999). It is also evident that the largest amounts of organic carbon (> 25 kg m^{-2}) are stored as easy degradable organic matter in carbohydrates and only ~ 10 kg m^{-2} are stored as mineral associated, thus more stable, organic matter (Mueller et al. 2015). Although we have no samples of DTLBs in the catchment of Peatball Lake for comparison, it can be assumed that the organic matter content is lower in thermokarst affected terrain where unfrozen organic matter was potentially recycled repeatedly during several lake generations like shown in previous studies from the northern Seward Peninsula (Lenz et al. in press).

5.7 Conclusions

Our study of lake expansion and sedimentary records of Peatball Lake on the Alaska Arctic Coastal Plain reflects the landscape and sediment dynamics of typical ice-rich permafrost lowlands affected by thermokarst activity. The main conclusions of the study are:

1. The development of a late Holocene thermokarst lake on the Arctic Coastal Plain was delineated by sedimentary records and remotely sensed imagery. Radiocarbon dating in this periglacial environment is problematic due to input of organic matter into the lake from permafrost deposits along eroding lake shores. However, $^{210}Pb/^{137}Cs$ and multiple ^{14}C dating together with the calculation of the lake expansion rates of the last 47 years allow an estimation of a minimum lake age of 1,400 years. As derived from lithological, geochemical and vegetation data, Peatball Lake likely initiated as a remnant lake from DTLBs (Phase A), deepened rapidly and expanded radially into surrounding DTLBs and uplands remains (Phase B and C).

2. Sedimentological analyses of the cores show lake-internal variability in sediment deposition and reflect the impact of landscape morphology and genesis in the catchment of thermokarst lakes on sedimentation dynamics. As derived from lithological and geochemical proxies the sediment source has changed during lake expansion from predominantly redeposited, thermokarst sediments from DTLBs (Phase A) to a sudden input of older, not yet, relocated upland deposits (Phase B), to a mixture of upland and DTLBs as sediment source (Phase C).

3. The sedimentary record highlights that old carbon is being recycled by permafrost thaw and thermokarst processes. Organic matter content was significantly lower in lake sediments than in neighboring organic-rich, peaty upland deposits. Near-shore sediments showed very low average TOC of 1.6 wt% and TN of 0.2 wt% and had indications for a wide range of lacustrine to terrestrial organic matter sources.

The sedimentary records of Peatball Lake demonstrate the high complexity of depositional environments in thermokarst lakes due to the spatio-temporal changes in lake morphology as well as in the surrounding landscape. Re-shaping of permafrost regions by multiple lake generations generate a diversity of catchment situations that may affect depositional patterns within lakes differently. This needs to be taken into account when interpreting thermokarst lake cores and implications for biogeochemical cycling and carbon stocks of Arctic thermokarst landscapes.

Acknowledgements

This research was primarily supported by a PhD stipend of the University of Potsdam and a grant by the Christiane Nüsslein-Volhard-Foundation awarded to J. Lenz, and a grant of the European Research Council (#338335) awarded to G. Grosse. Field work was enabled through the CALON project (www.arcticlakes.org) and the Teshekpuk Lake Observatory (www.teshekpuklake.com). We wish to thank C. Baughman (USGS) and Jim Webster (Webster's Flying Service) for help in the field, I. Nitze for bathymetric measurements and map preparation, N. Nowaczyk (GFZ) for MS measurements, J. Thom and S. Jock for help in the lab, J. Wolter for macrofossil determination for radiocarbon dating and B. Niemeyer for pollen preparation. The study contributes to the Arctic Ecological Network (Arc-EcoNet; Federal Ministry of Education and Research Grant No. 01DJ14003). N. Rudaya performed this study according to the Russian Government Program of Competitive Growth of the Kazan Federal University. Any use of trade, product, or firm names is for descriptive purposes only and does not imply endorsement by the US Government.

6 Synthesis

This thesis aimed at deriving new insights into complex thermokarst dynamics and permafrost development in central-eastern Beringia. Detailed sedimentological, geochemical and paleontological analyses of permafrost and lacustrine sediment cores revealed landscape dynamics on different time scales. Understanding these past environmental changes and processes is important to assess potential future changes of Arctic landscapes which are highly sensitive to global climate warming.

The synthesis of the thesis summarizes the environmental pre-conditions of the investigated paleo-archives and compares similarities and differences of the studied regions within central-eastern Beringia. In the following sub-chapters the research questions defined in the introductory chapter 2.2 are answered. The synthesis is followed by an evaluation of potentials and limitations of thermokarst lakes as paleoenvironmental archives and concludes with an outlook on further research needs.

6.1 Study sites in central-eastern Beringia: Similarities and differences

The region of Beringia is of particular interest to study past thermokarst dynamics as it represents a landmass characterized by continuous permafrost since the LGM. The study regions in central-eastern Beringia (Figure 6.1) contrast between relatively warm permafrost with mean annual ground temperatures of -5 to -2 °C on the northern Seward Peninsula (Chapter 3 and 4) and relatively cold permafrost with a mean annual ground temperature of -10 to -5 °C on Alaska's Arctic Coastal Plain (Chapter 5) and Herschel Island, Canada (Appendices I and II) (Smith et al. 2010). The thickness of permafrost varies from only ~100 m on northern Seward Peninsula to at least 410 m on the OCP of Alaska (Jorgenson et al. 2008). For Herschel Island, a similar permafrost thickness can be expected along the Yukon Coastal Plain where permafrost depths of 238 m (near Blow River) and 148 m near Roland Bay are known from boreholes (Smith & Burgess 2002). Another important difference between the study sites is the landscape evolution and genesis of the geological underground: Whereas Seward Peninsula was a central part of the Bering Land Bridge on which widespread yedoma deposits accumulated (Kanevskiy et al. 2011), the OCP of northern Alaska is characterized by silty deposits that originated from several marine transgressions and also terrestrial deposition (Hinkel et al. 2005, Williams et al. 1978). Herschel Island, in contrast, is a Pleistocene push moraine formed by ice-thrusting of the Laurentide Ice Sheet and is mostly composed of beds of shell-bearing and marine sands, silts, and silty clays (Mackay 1959, Burn, 2009). Although characterized by different geological origin, all study regions are dominated by fine-grained frozen sediments which are able to develop ice-rich permafrost under cold-climate conditions (Kanevskiy et al. 2013).

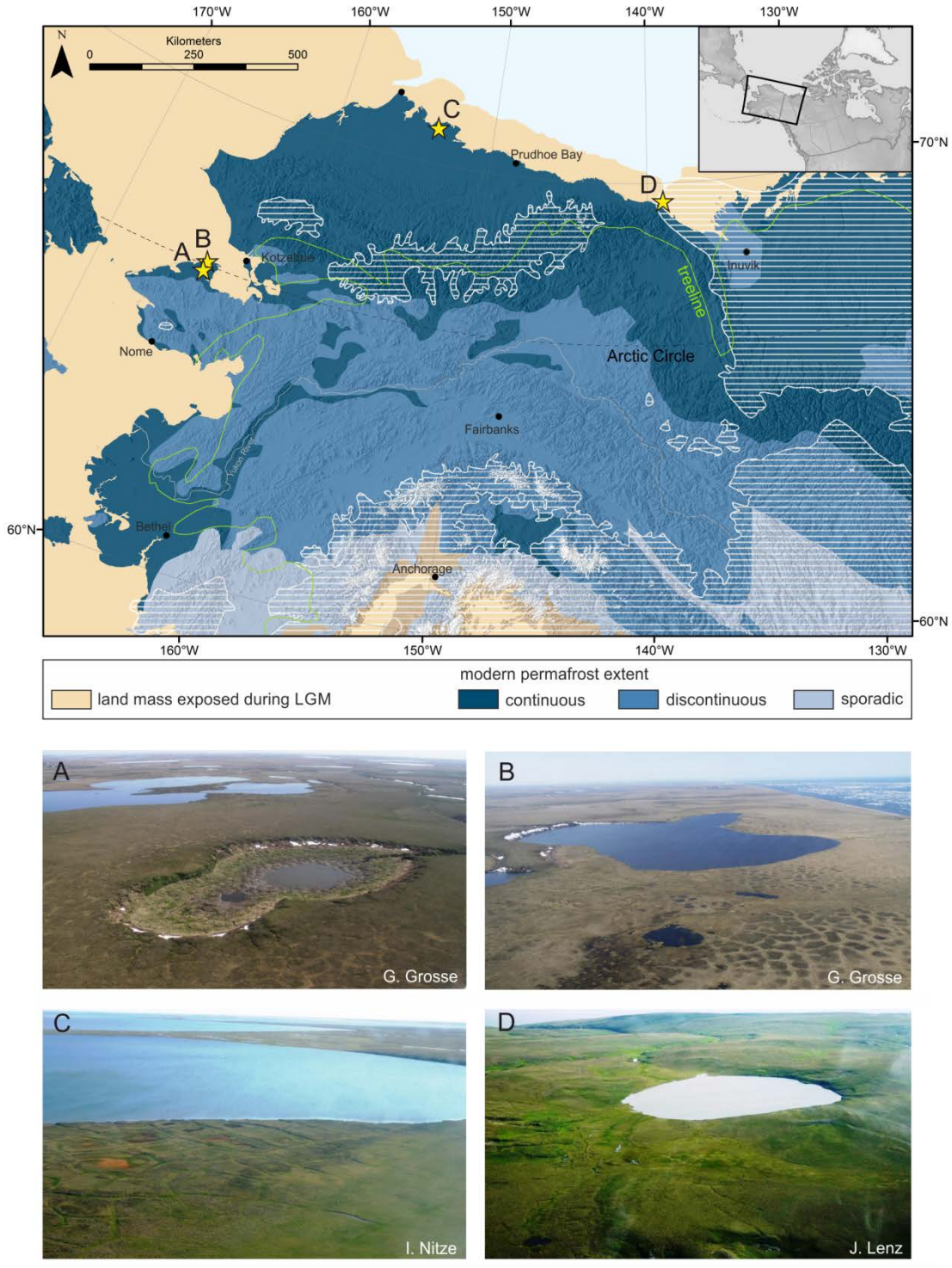

Figure 6.1: Study area of central-eastern Beringia with modern permafrost distribution (Brown et al. 1997), glacial limits at 18 cal ka BP (Dyke et al. 2003), exposed shelves during the LGM delineated by the -120 m isobath (Peltier & Fairbanks 2006), and field sites marked with a red star. Aerial photographs show the field sites (A) GG basin (chapter 3) and (B) Mama Rhonda basin (chapter 4) on the northern Seward Peninsula, (C) Peatball Lake (chapter 5) on the Arctic Coastal Plain of Alaska (USA) and (D) Lake Herschel (appendices I and II) on Herschel Island, Yukon (Canada). Map: Transverse mercator projection, NAD83 UTM Zone 7N (prepared by C. Coch)

The yedoma on the northern Seward Peninsula is very ice-rich with 70–90 % ground ice by volume (Shur et al. 2009). The younger OCP also has high volumetric ground ice content of 77 % in near-surface permafrost (Kanevskiy et al. 2013). Near-surface ground ice constitutes up to 60–70 % of Herschel Island (Pollard 1990) and the presence of massive buried glacial ice bodies is reported (Fritz et al. 2011). Ice-wedge polygons indicating these near-surface ice-rich conditions are apparent in all studied regions (Figure 6.1).

Ice-rich permafrost creates greatest loss in volume by thawing (even though gradual thawing takes longer due to low heat transfer of ice) and warm permafrost is more likely to degrade than colder permafrost (Calmels et al. 2015). Although thicker permafrost will take longer to degrade completely, major thermokarst processes over a longer time period can be expected (Calmels et al. 2015). In fact, more severe warming of cold permafrost like on the OCP or Herschel Island was recorded during the last decades compared to warmer permafrost like on the Seward Peninsula. Warmer and shallower permafrost like on northern Seward Peninsula is most likely to degrade first (Romanovsky et al. 2010). Therefore, our studied sites are of high relevance to assess environmental changes on different time scales.

6.2 Permafrost degradation and thermokarst development in central-eastern Beringia

6.2.1 Timing of thermokarst development

Thermokarst lake initiation and expansion in northern high latitudes are largely associated with periods of warming and wetting which were particularly prevalent during the Pleistocene-Holocene transition (Kaplina & Lozhkin 1979, Walter et al. 2007). For the HTM, Kaufman et al. (2004) suggested mean summer temperatures of 1.6 ± 0.8 °C above the 20th century average for the North American Arctic. However, the onset of the HTM was time-transgressive, with an earlier warming occurring in Alaska and the western Canadian Arctic at 11.3 ± 1.5 cal ka BP than in continental Canada and the Canadian Archipelago at 7.3 ± 1.5 cal ka BP (Kaufman et al. 2004).

The paleoenvironmental records presented in this thesis are in agreement with these findings as they demonstrate thermokarst lake initiation on northern Seward Peninsula around 11.8 cal a BP (Mama Rhonda Lake; Chapter 4) and around 11.7 cal ka BP on Herschel Island in the western Canadian Arctic (Lake Herschel, 11.5 cal ka BP; Appendix I; revised to 11.7 cal ka BP; Appendix II). However, Kaufman et al. (2016) revised their previous temperature reconstructions and suggested that temperatures were much more variable and showed a less clear spatial pattern of warming. Thermokarst as well as peatland initiation peaked between 11.0 and 10.0 cal ka BP in eastern Beringia, most likely in response to changing seasonality rather than solely increased

summer temperatures (Kaufman et al. 2016 and references herein). Furthermore, Kaufman et al. (2016) summarized that simultaneous low lake levels during the Early Holocene, which seems to contradict evidences of lake and peatland formation at that time, point towards the major role of seasonal distribution of precipitation: Low winter precipitation may have decreased lake levels and increased peatland development by paludification while high summer precipitation promoted peatland development.

Although climate-induced thermokarst initiation cannot be fully resolved with the presented records, they indeed highlight wetting during glacial periods. A record from a drained lake basin (GG basin; Chapter 3) preserved wetland formation on a yedoma accumulation surface which was dated to 44.5 to 41.5 ka BP (Mid Wisconsin). Lacustrine sediment sequences of Mid Wisconsin age were also reported for the Seward Peninsula by Hopkins & Kidd (1988) and Wetterich et al. (2012). The latter study was able to reconstruct thermokarst lake persistence until 32 ka BP from freshwater mollusks and ostracods. Although general warm temperatures peaked between 35 and 33 ka BP, high regional variability was recorded in western and eastern Beringia (Anderson & Lozhkin 2001). In fact, several climate fluctuations were reconstructed for the Mid Wisconsin in eastern Beringia between 80 and 30 ka BP with conditions warmer than present (Schweger & Matthews 1985). In this context, the record of GG basin on the northern Seward Peninsula supports evidence of regional wet conditions during glacial periods.

The records presented in this thesis show thermokarst activity throughout the Holocene. The permafrost record from a drained lake basin (Mama Rhonda, Chapter 4) not only recorded multiple thermokarst lake generations starting around 11.8 cal ka BP but also fluctuating lake levels with potential temporary wetland development from 9.0 to 1.1 cal ka BP. In interior and northern Alaska, other studies suggest mostly rising lake levels after 9 cal ka BP (Kaufman et al. 2016). Consequently, thermokarst dynamics must have contributed to the hydrological re-organization of Mid Holocene landscapes.

A depositional hiatus in the sediment core of GG basin between 22.5 and 0.23 ka BP was interpreted as an indirect signal of general intense thermokarst development in the surrounding area of the upland site which served as a sediment source and therefore did not preserve Late Glacial to Holocene deposits. The actual thermokarst lake which shaped the modern GG basin formed only recently about 0.29 ± 0.02 cal ka BP and signals permafrost degradation by local disturbances rather than a broader climate signal (Chapter 3).

Finally, our record from Alaska's North Slope on the younger OCP with a minimum lake age of 1,400 years also reflects Late Holocene thermokarst development (Chapter 5). Even though there is little reference in the literature for lake initiation on the Arctic Coastal Plain, it can be assumed that a variety of thermokarst lake age classes are present as concluded from the age

range of drained lake basins (as terminal stage of a thermokarst lake) from younger than 50 years to up to 5,500 years (Hinkel et al. 2003). In summary, thermokarst lake initiation was especially pronounced during the Early Holocene in central-eastern Beringia as shown by our and other studies but thermokarst activity in ice-rich permafrost regions has also been proven during interstadial periods and throughout the Holocene.

6.2.2 Environmental factors supporting and inhibiting thermokarst

Climate warming has a dominant impact on permafrost and its degradation because permafrost is part of a very complex geo-ecological system with positive and negative feedback mechanisms (Jorgenson et al. 2010, Shur & Jorgenson 2007). Stable permafrost conditions, groundwater recharge and obviously thermokarst are the factors that support an increasing lake area, whereas talik drainage, surface water evaporation and desiccation are the most inhibiting factors affecting fine-scale heterogeneity of lake area (Roach et al. 2011). Significant decline in lake area was observed in burned areas, on well-drained, coarser catchments and far away from rivers (Roach et al. 2013). However, regional climate is very important as e.g. shallow lakes in the Arctic may freeze solid in winter and do not develop a talik but shallow lakes in boreal regions may develop a deep talik which even extends laterally several meters below the surficial permafrost banks (Jorgenson et al. 2008, Kokelj & Jorgenson 2013). In addition, ground-ice content has a large influence on rates of thermokarst development.

On a larger scale, Shur & Jorgenson (2007) distinguished five patterns of lowland permafrost formation and degradation in relation to climate and ecosystems: climate-driven, climate-driven/ecosystem-modified, climate-driven/ecosystem-protected, ecosystem-driven, and ecosystem-protected. This concept highlights that different zonal and regional types of permafrost have different sensitivities to change by climate warming. High sensitivity to thermokarst initiation is common in climate-driven/ecosystem-modified permafrost (Shur & Jorgenson 2007). Here, the rather simple type of climate-driven permafrost is transforming into a complex system where vegetation and soil organic horizons become important for permafrost stability (Shur & Jorgenson 2007). Those different types may develop zonal but permafrost stabilizing or destabilizing factors, or rather thermokarst supporting or inhibiting environmental factors, as specific periglacial landforms vary on a regional to local scale.

For example, airfall tephra on the northern Seward Peninsula did halt initial wetland development during the Mid Wisconsin which may otherwise have resulted in an early thermokarst lake (Chapter 3). Here, a 1-meter-thick volcanic tephra, most likely of the South Killeak Maar eruption at about 42.0 ka BP, was documented on top of peat which accumulated from about 44.5 to 41.5 ka BP. The wetland or initial shallow water body must have been entirely covered by tephra so that the barren surface changed the permafrost system from climate-

driven/ecosystem-modified to climate-driven/ecosystem-protected where the tephra layer not only leveled the terrain but its poor insulation properties also allowed deeper freezing of the underlying permafrost. Although this example is mostly of regional importance, it shows how thermokarst development is influenced by local changes. The drainage of GG lake in spring 2005 AD, which developed at the site only 0.29 ± 0.02 cal ka BP, again changed the system to ecosystem-driven. No substantial vegetation cover had developed yet in 2009 AD and permafrost started to aggrade from the surface down to 266 cm four years after the drainage event. The drainage was likely related to site-specific geomorphological and hydrological processes like overflow at the outlet channel as a result of increased snow melt run-off and down-cutting into ice-rich permafrost.

The study of multiple thermokarst lake generations on the northern Seward Peninsula (Chapter 4) shows that even more complex environmental settings may develop under a regime of continued thermokarst dynamics. The first thermokarst lake generation of Grandma Rhonda lake formed during the Lateglacial to Holocene transition and was a result of initial landscape shifts from a continental-climate-dominated terrain of Beringia to a warming and wetting environment of the closing Bering Land Bridge. The following lake modification from the Grandma Rhonda lake phase to the Mama Rhonda lake phase by lateral expansion and thermal and mechanical erosion was supported by the presence of ice-rich permafrost and ice-wedges in the catchment. Mama Rhonda's drainage around 1.1 cal ka BP may be related to the Medieval Warm Period, when sand dunes expanded in the nearby Kobuk Valley which in turn has been linked to increased summer storm activity (Mann et al. 2002b). It is possible that wave activity due to summer storms have intensified lakeshore erosion which has triggered the drainage of Mama Rhonda lake. Another possibility is that enhanced wave activity increased coastal erosion which led to the drainage of Mama Rhonda lake. Thus, a combination of climate-induced, and local disturbance processes were responsible for substantial landscape modification. In this record, the drainage event was followed by vegetation succession and aggradation of permafrost that developed in organic-rich soil. These circumstances provided an ecosystem-protected permafrost environment. Modern polygonal patterned ground gives evidence for the underlying ice-rich permafrost.

Similar to the lake succession of Grandma/Mama Rhonda on northern Seward Peninsula, Peatball Lake developed in a periglacial landscape which was pre-shaped by thermokarst processes (Chapter 5). Inherited structures of the paleo-relief, i.e. pre-existing DTLBs, promoted path-dependent thermokarst processes. The initiation of Peatball Lake as a remnant pond in a drained lake basin is a typical situation for periglacial lowland landscapes where lakes expand, coalesce, shrink, drain partially and re-initiate (French 2007). Thus, the evolution of landscapes by repetitive lake formation is one of the most important controlling environmental factors for Late Holocene landscape development.

The initiation of Lake Herschel on the Yukon Coastal Plain (Appendices I and II) was most likely climate-driven during the HTM, as described above. A depositional hiatus indicates an interruption in the steady sedimentation by around 1.6 to 1.0 cal ka BP which led to two hypotheses: (1) Either the lake drained or dried out which caused a hiatus in sedimentation or (2) allochthonous slumping disturbed the continuous sediment accumulation. Although the reason for the hiatus has not been fully resolved, the Lake Herschel record demonstrates that site-specific disturbance processes are leaving their imprint in the sedimentary record.

In summary, the studies presented in this thesis describe some important interactions of global climate patterns, regional environmental dynamics and local disturbance processes for thawing ice-rich permafrost at different temporal scales. Active thermokarst processes were documented in contrast to other investigations e.g. in the southern marginal uplands of the Yukon Flats in interior Alaska where ice-poor near-surface permafrost, forest cover, and a negative regional moisture balance resulted in a stabilization of thermokarst lakes that formed during the Early Holocene (Edwards et al. 2016).

6.3 Processes of thermokarst lake development and their imprint in proxy records

Thermokarst lakes in Arctic lowlands are dynamic and their life cycle is commonly characterized by expansion or shrinkage. The evolution of thermokarst lakes and basins, as described by Jorgenson & Shur (2007), involves complex processes of (1) initial flooding or ponding forming the first lake generation, (2) lateral and vertical growth by shore erosion and permafrost thaw (talik formation), (3) lake drainage, (4) differential ice aggradation in sandy margins and silty centers, (5) the formation of the second lake generation along margins of DTLBs and heaved centers of ice-rich basins, and (6) stabilization of the thermokarst lake basin. Within this cycle, thermokarst lakes frequently coalesce or drain partially which may complicate landscape reconstruction from single sediment cores (Chapter 4). Some of these processes and their impact on permafrost are illustrated in Figure 6.2. Repetition of the thermokarst lake cycle can result in spatially overlapping lake generations like shown for the northern Seward Peninsula where up to seven overlapping drained basin generations were identified (Jones et al. 2012, Regmi et al. 2012). The lake shore erodes over the course of lake expansion by processes of mass wasting through thaw slumps (Kokelj et al. 2009, Plug & West 2009), wave action and thermomechanical erosion of lake banks (Tedrow 1969), block failures by over-steepening of lake banks (Kokelj & Jorgenson 2013), ice-jam and mechanical erosion during ice break-up which also removes vegetation and soil (Chen et al. 2014), or incorporation of ice-wedge ponds into the lake (Billings & Peterson 1980); as partially illustrated in Figure 6.3.

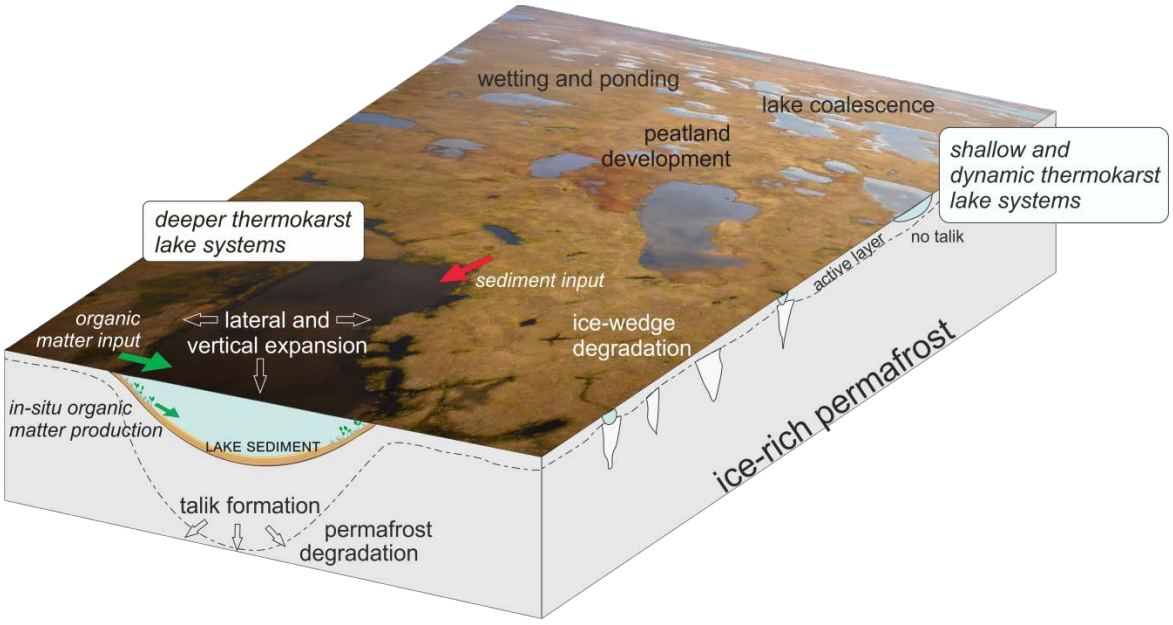

Figure 6.2: Thermokarst processes in permafrost lowlands. Ice-wedge degradation can lead to ponding/wetting and peatland development in Arctic landscapes; the lateral and vertical growth of thermokarst lakes may result in lake coalescence (drainage or partial drainage is not illustrated in this figure). Permafrost is degrading and a talik of unfrozen sediment is forming when water depth exceeds winter ice thickness. Arrows indicate organic (green) and sediment input (red) into the lake system.

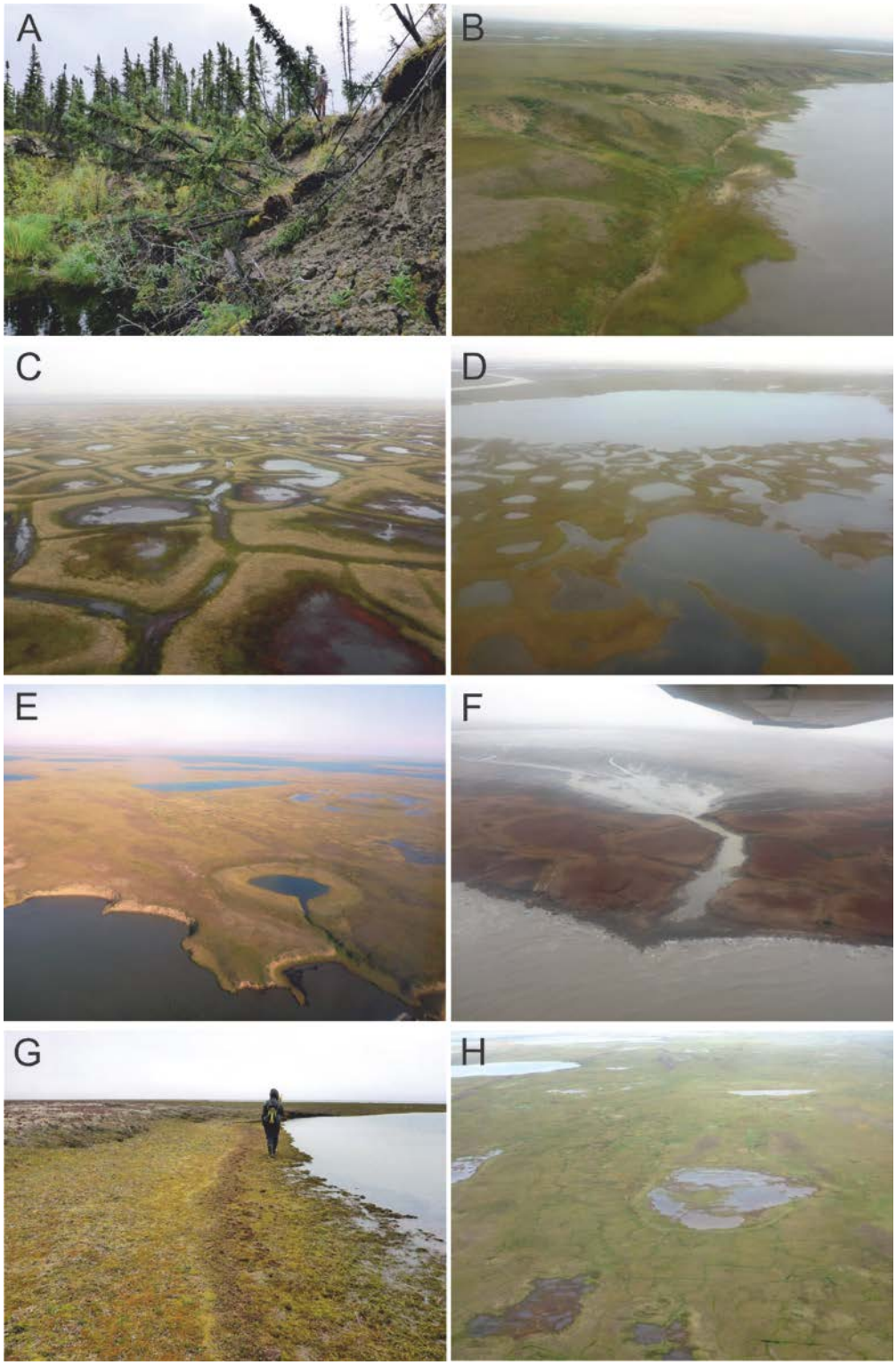

Figure 6.3: Examples of thermokarst lake processes in Alaska. (A) Eroding bluffs and toppling trees in the boreal zone, Vault Lake, Interior Alaska; (B) Mass wasting processes through slumps into a thermokarst lake near Inigok, Inner Coastal Plain; (C) Degrading ice-wedges with wetting and ponding in polygon centers and troughs; (D) Seasonal flooding and incorporation of ice-wedge ponds; (E) Partial drainage of a thermokarst lake into another, expanding thermokarst lake; (F) Full drainage of thermokarst lake L195 into the Arctic Ocean, documented by Jones & Arp (2015); (G) Evidence of lake level change and (H) potential re-initiation of a thermokarst lake in a DTLB (all Outer Coastal Plain, Alaska, unless otherwise stated; photographs taken in August/September 2014).

The thermokarst lake phase in the sedimentary record of GG basin on the northern Seward Peninsula (Chapter 3) was relatively short and too low in resolution (accumulation of 36 cm in 0.29 ± 0.02 cal ka BP) to investigate processes of thermokarst lake development in the record. Thawing of ice-wedges in the remaining yedoma upland as a dominant process is indicated by the presence of baydzherakhs in the basin which were not removed by the drainage event. An accumulation rate of 0.12 cm a^{-1} can be calculated by assuming constant sedimentation rates.

The sedimentation of the Grandma/Mama Rhonda record (Chapter 4) was calculated from the age-depth model with a mean accumulation rate of 0.03 cm a^{-1} (with a maximum and minimum ranging between 0.05 and 0.01 cm a^{-1}). However, changing catchment morphology during the life span of about 2,800 years of Grandma Rhonda lake and about 7,940 years of Mama Rhonda lake with levelling by thermokarst processes most likely changed the depositional environment. Lake expansion of Grandma Rhonda was preserved in the sedimentary record by decreasing tephra input from increasingly distant eroding shores (indicated by decreasing magnetic susceptibility). Lake water level change during the Mama Rhonda lake phase is indicated by high variability in geochemical proxies (TC, TN and TOC) and rapid input of reworked tephra (shown by pronounced peaks in magnetic susceptibility and coarse-grain size fractions). Enhanced input of terrestrial organic matter by shoreline erosion is evident from higher C/N ratios. The drainage of Mama Rhonda as part of the thermokarst lake cycle (Jorgenson & Shur 2007) was archived by the isotopic composition of the intra-sedimentary ice which preserved the paleo-active layer directly after drainage and indicated top-down aggradation of permafrost. The terrestrial surface peat was characterized by a dominance of hygrophilous and sphagnobiontic testaceans and only occasional occurrence of ostracods.

The sedimentary records of Peatball Lake highlight thermokarst dynamics in a complex periglacial environment (Chapter 5). The relatively young lake of about 1,400 years expanded into different landscape units and the altering intersection with upland remains and younger re-deposited DTLBs sediment were imprinted in the sedimentary record. The lithostratigraphic character, geochemical proxies (TN and TOC) and mixed radiocarbon ages gave evidence for this altering sediment source although the siliciclastic sediment signal remained constant as derived from XRF-ratios of K/Ti. Thus, the changing organic input rather than the mineral input is imprinted in the sedimentary record of Peatball Lake. The deepening, and therefore oxygenation of the lake sediments, is reflected by higher Fe/Ti and Fe/S ratios. Magnetic susceptibility and young radiocarbon ages as well as variable C/N and $\delta^{13}C_{TOC}$ of near-shore sediments of Peatball Lake further on indicate rapid, event-like deposition near an upland during lateral lake expansion.

Sediments of Lake Herschel recorded a special situation of thermokarst dynamics because the lake developed on a push moraine of up-thrusted marine sediments (Appendices I and II). The

expanding lake and increasing water volume resulted in a continuous desalinization of lake water as recorded by decreasing electrical conductivity and XRF-derived Sr/Ca ratio. Increased freshwater input is further supported by decreasing (Na+K)/(Ca+Mg) and Cl/HCO_3 ratios in pore-water. The coexistence of marine, brackish and freshwater ostracoda and foraminifera throughout the record is partly explained by past oligohaline to mesohaline water chemistry but also reflects re-deposition of specimens of Pleistocene origin from the catchment of marine deposits. Thus, the faunal assemblage recorded inputs of allochthonous material by local catchment disturbances like slumping, shoreline erosion or active-layer detachment. The sediments which originated from a disturbance at the depositional hiatus at 1.6 to 1.0 cal ka BP are organic-poor, coarse-grained and show little authigenic carbonate production as derived from high Mn/Fe and low Sr/Ca ratios.

Investigating past processes of thermokarst development by using sedimentary records is essential to understand past landscape dynamics but also to assess the carbon budget and release of carbon in permafrost environments, e.g. the mobilization of carbon by lake expansion or accumulation as peat in DTLBs.

6.4 Contribution of thermokarst dynamics to the carbon cycle

Permafrost deposits (Zimov et al. 2006) and thermokarst lakes (Kling et al. 1992) have been identified as important sources of atmospheric greenhouse gases, carbon dioxide (CO_2) and methane (CH_4). Strauss et al. (2013) confirmed a substantial pool of frozen organic carbon of 57 to 371 Gt in yedoma and frozen thermokarst deposits in Siberia and Alaska. A large amount of atmospheric CO_2 will be produced upon thaw of organic-rich permafrost under aerobic conditions. Thermokarst processes and in particular thermokarst lake expansion results, predominantly, in subaerial permafrost degradation. Secondly, anaerobic microbial decomposition of organic matter at thermokarst lake bottoms produces CH_4 which additionally contribute to the current atmospheric carbon budget (Walter et al. 2006). The pace of permafrost carbon decomposition is largely uncertain. For example, a 12-year incubation experiment of a permafrost soil from Greenland has shown that 50-75 % of the initial carbon was lost under aerobic, laboratory conditions (Eberling et al. 2013) but other incubation experiments show even faster carbon decomposition in particular of mineral soils (Schädel et al 2014). Greenhouse gas emissions from permafrost degradation and thermokarst dynamics could create a potential feedback loop resulting in further atmospheric warming during the Anthropocene (Schuur et al. 2015).

Degradation pathways of organic matter are largely unknown. Even though only punctual, the studies presented in this thesis add important data on carbon storage and degradation patterns in thermokarst lake systems summarized in Table 6.1.

Table 6.1: Mean TOC content, C/N ratio and stable carbon isotopes of lacustrine units in studied sediment cores.

Chapter	Study region	Site	Core ID, depth range of lacustrine sediment	mean TOC (wt%)	C/N ratio	$\delta^{13}C$ (‰)	Characteristics
# 3	Northern Seward Peninsula, Alaska	GG basin	Kit-64, 0-36 cm	4.9	11.3	-27.4	Active-layer
			Sd (n=6)	1.1	1.7	0.4	
# 4	Northern Seward Peninsula, Alaska	Grandma Rhonda	Kit-43, 283-336 cm	2.7	9.6	-26.8	First lake generation
			Sd (n=14)	0.8	2.2	0.3	
		Mama Rhonda	Kit-43, 41-283 cm	7.9	14.0	-27.5	Second lake generation
			Sd (n=43)	5.8	3.4	0.5	
# 5	Outer Coastal Plain, Alaska	Peatball Lake	P1, 0-50 cm	1.6	7.4	-27.5	Near-shore sediments
			Sd (n=25)	2.7	4.7	0.3	
			P2, 0-100 cm	7.0	13.2	-28.4	Central lake sediments
			Sd (n=50)	3.2	2.3	0.6	
			P3, 0-49 cm	6.9	13.6	-28.6	Central lake sediments
			Sd (n=24)	0.8	0.7	0.2	
Appendices I and II	Herschel Island, NWT, Canada	Herschel Lake	PG1967, 0-726 cm	2.2	10.7	-26.4	Central lake sediments
			Sd (n=73)	1.2	2.0	0.3	

The lacustrine sediment unit at depths of 0-36 cm in core Kit-64 (GG basin, chapter 3) is situated in the active-layer. The mean TOC content of 4.9 wt% may be reduced due to seasonally unthawed conditions and microbial activities within the active-layer. However, no substantial vegetation cover has developed 4 years after drainage but wetland plant communities are expected to establish and develop first peatlands in the near future which will result in enhanced carbon accumulation.

Interestingly, stratigraphically stacked thermokarst lake generations also reflect different carbon degradation stages on the northern Seward Peninsula (Chapter 4). Grandma Rhonda lake developed under Lateglacial climate conditions and eroded into yedoma deposits which were at that time likely not yet covered with a significant soil organic layer. This could be one reason why significantly lower TOC contents were identified in Grandma Rhonda lake sediments (mean TOC of 2.7 wt%) than in Mama Rhonda lake sediments (mean TOC of 7.9 wt%) which accumulated under a warmer Holocene climate 9.0 to 1.1 cal ka BP. Another likely reason for a reduced carbon stock in Grandma Rhonda lake sediments is the decomposition of these older sediments over a longer time period within the talik of Mama Rhonda lake. The higher C/N ratio and lower $\delta^{13}C_{TOC}$ in Mama Rhonda sediments compared to Grandma Rhonda sediments points towards enhanced input of allochthonous, terrestrial matter by shoreline erosion.

Furthermore, much lower organic carbon contents were identified in near-shore sediments than in sediments in central parts of Peatball Lake (Chapter 5). This is most likely a result of event-like deposition of predominantly clastic material in the near-shore zone and longer transport path of finer, more organic-rich deposits in the deeper, central part of the lake. Organic matter may have been additionally increased by enhanced primary production in the deeper part of the basin where water depth was greater than winter ice thickness. An average C/N ratio below 10 indicates predominately aquatic sources of organic matter in the near-shore but the high standard deviation also shows the altering terrestrial and aquatic organic matter deposition.

Lake Herschel provided a different setting with higher inorganic carbon storage in the catchment of marine origin. A $CaCO_3$ content of up to 10 % (mean 6.7 %) is recorded for the core of 726 cm. Mean TOC is only 2.2 wt% but mean total inorganic carbon (TIC) is 0.8 wt%. The carbon record therefore reflects the authigenic carbonate productivity of the thermokarst lake. C/N and $\delta^{13}C_{TOC}$ reflect mostly aquatic origin of deposited organic matter.

Examples of carbon stocks and their origin in different units of thermokarst deposits presented in this thesis highlight the potential of carbon recycling by permafrost degradation and thermokarst processes.

6.5 Potentials/limitations of thermokarst lake archives and outlook

Paleoenvironmental records from Arctic regions are scarce and underrepresented compared to mid and low latitudes. With our investigations we were able to extract specific paleoenvironmental information from thermokarst lakes. Thermokarst lakes are abundant features in Arctic lowlands where other environmental archives are absent or spatially limited (Pienitz et al. 2004). As shown in this thesis, proxies in lake sediments preserve valuable environmental information for periods that date well back before instrumental observations and cover mostly the

Holocene since thermokarst onset during the Lateglacial warming events. Regional to local processes were imprinted in the investigated deposited sediments.

A multi-proxy approach seems to be most suitable to reconstruct processes of thermokarst development since a single parameter would not have been able resolve the investigated landscape dynamics. However, studies from Peatball Lake (Chapter 5) and Herschel Lake (Appendix II) suggest that quantitative climate reconstruction based on pollen is not recommended for thermokarst lakes for several reasons: Despite general chronological uncertainties in radiocarbon dating of thermokarst lake sediments due to re-deposition of old organic matter, old pollen also gets reworked by shoreline erosion. Since transport pathways are rather short, reworking might not be clearly identified in analytical data. Further, local vegetation might be over-represented in small catchments, and lake sediments may record local rather than regional signals affected by microtopography, nutrient availability and soil moisture which in turn are largely regulated by local permafrost conditions. In general, further research is needed to develop new proxies (e.g. in the field of microbiology) that better reflect past climate conditions. Investigations on bioindicators should be developed further, e.g. *Daphnia* eggs indicating planktivorous fish abundance (Jeppesen et al. 2002) may be a good indicator of lake ice regime shifts (a function of lake depth and lake ice thickness which turn is a function of permafrost thawing, seasonality and winter temperature). The impact of lake ice cover on the sediment surface of shallow lakes is an unknown field in limnology; the influence of ice pressure on the sediment column should be tested in laboratory experiments for a better understanding in paleolimnological investigations.

The geochronological control of thermokarst lake sediments by radiocarbon dating is often limited due to (1) lower bioproductivity during shorter growing seasons in the Arctic and therefore paucity of terrestrial plant remains and (2) high preservation potential of old organic matter in frozen permafrost deposits which enter the lake system by thermokarst erosion. Further, ^{210}Pb and ^{137}Cs inventories are rather low in remote Arctic sediments, especially when annual precipitation is low. A number of studies from glacial lakes applied varve-chronologies based on annual laminations (e.g. Hughen et al. 2000, Lamoureux & Gilbert 2004, Francus et al. 2008, Bird et al. 2009). This dating control is likely not applicable in thermokarst lakes with actively eroding shorelines where laminations do not necessarily reflect seasonal in-situ production but altering allochthonous and autochthonous deposition, some of which is event-driven (e.g. shore slumping). In the challenging dating situation of sediments of Peatball Lake, shoreline expansion rates with long-term remote sensing data were used to estimate the lake age (Chapter 5). This indirect approach of lake age estimation should be further tested on a larger set of lakes with similar character to validate whether this method can be used as indirect tool in challenging dating

situations. In general, developing a more accurate geochronological control seems necessary for reliable interpretation of paleo-records.

Effectively, sediment cores provide one-dimensional information of the column of sediment and a limited perspective on the sedimentary archive is given even with a collection of several cores (Cohen 2003). The coring location, the sampling strategy (e.g. resolution), as well as the choice of analyzed proxies play a critical role in paleoenvironmental research and depend on the research questions to be answered. Preceding geophysical applications can help in finding the most suitable coring location but Arctic field and weather conditions often have a decisive influence. Further, paleolimnological investigations should be expanded to exposures along lakes, rivers and coastal shores to better understand spatial variability of sedimentation processes within lake systems. In general, a combination of intensive geophysical investigations to characterize the lake basin, talik and catchment together with detailed information from sediment cores or outcrops is desirable when investigating thermokarst dynamics and landscape evolution. However, upscaling thermokarst landscape processes from regional case studies into global perspectives should be conducted with caution (Edwards et al. 2016).

Further investigations on thermokarst lakes should focus on improving knowledge on how previously frozen organic matter gets degraded by thermokarst processes. Little is known about transport pathways and decomposition patterns of organic matter by degrading permafrost. Even though data sets of carbon pools in yedoma regions are currently expanding, the carbon pools of unfrozen lake and talik sediments, and re-frozen deposits from DTLBs are largely unknown. As TOC is a parameter commonly measured in paleolimnological investigations, it would be highly interesting to compare TOC values of thermokarst lake with non-thermokarst lake sediments to better assess the role of Arctic lakes in global biogeochemical cycles. Recently, a database of > 1,200 basal or minimum lake ages extracted from the literature was developed with the help of the thesis' author. This data-set represents a great source to further investigate carbon accumulation rates that could be calculated from lake data sets which include carbon analyses and a reliable age-depth model. Carbon decomposition within complex thermokarst dynamics of several lake cycles should be further studied by analyzing sediment cores from thermokarst basins where remotely sensed data revealed multiple lake generations superimposed on each other.

The studies presented in this thesis and further investigations are essential to improve our understanding of Arctic landscape changes which are expected to intensify in the coming decades.

Bibliography

Abbott, M. B., M. E. Edwards, and B. P. Finney (2010), A 40,000-yr record of environmental change from Burial Lake in Northwest Alaska, *QR*, *74*(1), 156-165.

Ager, T. A. (2003), Late Quaternary vegetation and climate history of the central Bering land bridge from St. Michael Island, western Alaska, *QR*, *60*(1), 19-32.

Alley, R. B. (2000), The Younger Dryas cold interval as viewed from central Greenland, *QSR*, *19*(1), 213-226.

Alley, R. B., and A. M. Ágústsdóttir (2005), The 8k event: cause and consequences of a major Holocene abrupt climate change, *QSR*, *24*(10), 1123-1149.

Alm, G. (1914), Beiträge zur Kenntnis der nördlichen und arktischen Ostracodenfauna, *Arkiv f r Zoologi*, *9*, 1-20 (in German).

Anderson, L., M. B. Abbott, B. P. Finney, and S. J. Burns (2007), Late Holocene moisture balance variability in the southwest Yukon Territory, Canada, *QSR*, *26*(1), 130-141.

Anderson, P. M. (1985), Late quaternary vegetational change in the Kotzebue sound area, northwestern Alaska, *QR*, *24*(3), 307-321.

Anderson, P. M., and L. B. Brubaker (1994), Vegetation history of northcentral Alaska: a mapped summary of late-Quaternary pollen data, *QSR*, *13*(1), 71-92.

Anderson, P. M., and A. V. Lozhkin (2001), The Stage 3 interstadial complex (Karginskii/middle Wisconsinan interval) of Beringia: variations in paleoenvironments and implications for paleoclimatic interpretations, *QSR*, *20*(1-3), 93-125.

Andreev, A. A., et al. (2009), Weichselian and Holocene palaeoenvironmental history of the

Bol'shoy Lyakhovsky Island, New Siberian Archipelago, Arctic Siberia, *Boreas*, *38*(1), 72-110.

Appleby, P. G., P. J. Nolan, D. W. Gifford, M. J. Godfrey, F. Oldfield, N. J. Anderson, and R. W. Battarbee (1986), 210Pb dating by low background gamma counting, *Hydrobiologia*, *114*, 21-27.

Appleby, P. G., N. Richardson, and P. J. Nolan (1992), Self-absorption corrections for well-type germanium detectors, *Nuclear Instruments and Methods in Physics Research Section B: Beam Interactions with Materials and Atoms*, *71*(2), 228-233.

Arp, C. D., and B. M. Jones (2009), Geography of Alaska Lake Districts: Identification, description, and analysis of lake-rich regions of a diverse and dynamic state, *U.S. Geological Survey Scientific Investigations Report 2008-5215*(2008-5215), 40.

Arp, C. D., B. M. Jones, A. K. Liljedahl, K. M. Hinkel, and J. A. Welker (2015), Depth, ice thickness, and ice-out timing cause divergent hydrologic responses among Arctic lakes, *Water Resources Research*, *51*, 9379-9401.

Arp, C. D., B. M. Jones, Z. Lu, and M. S. Whitman (2012), Shifting balance of thermokarst lake ice regimes across the Arctic Coastal Plain of northern Alaska, *Geophysical Research Letters*, *39*(16), L16503.

Arp, C. D., B. M. Jones, F. E. Urban, and G. Grosse (2011), Hydrogeomorphic processes of thermokarst lakes with grounded-ice and floating-ice regimes on the Arctic coastal plain, Alaska, *Hydrological Processes*, *25*(15), 2422-2438.

Bartlein, P. J., K. H. Anderson, P. M. Anderson, M. E. Edwards, C. J. Mock, R. S. Thompson, R. S. Webb, T. Webb Iii, and C. Whitlock (1998), Paleoclimate simulations for

North America over the past 21,000 years: features of the simulated climate and comparisons with paleoenvironmental data, *QSR*, *17*(6), 549-585.

Beget, J. E., D. M. Hopkins, and S. D. Charron (1996), The Largest Known Maars on Earth, Seward Peninsula, Northwest Alaska, *Arctic*, *49*(1), 62-69.

Berger, G. W., and P. M. Anderson (1994), Thermoluminescence dating of an Arctic lake core from Alaska, *QSR*, *13*(5), 497-501.

Beug, H.-J. (1961), Leitfaden der pollenbestimmung, *Fischer, Stuttgart*, 63pp.

Bigelow, N. H., et al. (2003), Climate change and Arctic ecosystems: 1. Vegetation changes north of 55°N between the last glacial maximum, mid-Holocene, and present, *J. Geophys. Res.*, *108*(D19), 8170.

Bigelow, N. H., and M. E. Edwards (2001), A 14,000 yr paleoenvironmental record from Windmill Lake, Central Alaska: Lateglacial and Holocene vegetation in the Alaska range, *QSR*, *20*(1-3), 203-215.

Billings, W. D., and K. M. Peterson (1980), Vegetational Change and Ice-Wedge Polygons through the Thaw-Lake Cycle in Arctic Alaska, *Arctic and Alpine Research*, *12*(4), 413-432.

Bird, B. W., M. B. Abbott, B. P. Finney, and B. Kutchko (2009), A 2000 year varve-based climate record from the central Brooks Range, Alaska, *Journal of Paleolimnology*, *41*(1), 25-41.

Biskaborn, B. K., U. Herzschuh, D. Bolshiyanov, L. Savelieva, R. Zibulski, and B. Diekmann (2012), Late Holocene thermokarst variability inferred from diatoms in a lake sediment record from the Lena Delta, Siberian Arctic, *Journal of Paleolimnology*, 1-16.

Biskaborn, B. K., U. Herzschuh, D. Y. Bolshiyanov, G. Schwamborn, and B. Diekmann (2013), Thermokarst Processes and Depositional Events in a Tundra Lake, Northeastern Siberia, *Permafrost and Periglacial Processes*, *24*(3), 160-174.

Blaauw, M., and J. A. Christen (2011), Flexible paleoclimate age-depth models using an autoregressive gamma process, *Bayesian Analysis*, *6*(3), 457-474.

Black, R. F., and W. L. Barksdale (1949), Oriented lakes of northern Alaska, *Journal of Geology*, *57*(2), 105-118.

Bockheim, J. G., L. R. Everett, K. M. Hinkel, F. E. Nelson, and J. Brown (1999), Soil Organic Carbon Storage and Distribution in Arctic Tundra, Barrow, Alaska, *Soil Sci. Soc. Am. J.*, *63*(4), 934-940.

Bockheim, J. G., K. M. Hinkel, W. R. Eisner, and X. Y. Dai (2004), Carbon pools and accumulation rates in an age-series of soils in drained thaw-lake basins, Arctic Alaska, *Soil Sci Soc Am J*, *68*(2), 697-704.

Boike, J., T. Grau, B. Heim, F. Günther, M. Langer, S. Muster, I. Gouttevin, and S. Lange (2016), Satellite-derived changes in the permafrost landscape of central Yakutia, 2000–2011: Wetting, drying, and fires, *Global and Planetary Change*, *139*, 116-127.

Bouchard, M. (1974), Surficial Geology of Herschel Island, Yukon Territory, 77 pp, University of Montréal.

Bowden, W. B., M. N. Gooseff, A. Balser, A. Green, B. J. Peterson, and J. Bradford (2008), Sediment and nutrient delivery from thermokarst features in the foothills of the North Slope, Alaska: Potential impacts on headwater stream ecosystems, *J. Geophys. Res.*, *113*, G02026.

Bradley, R. S., and J. H. England (2008), The Younger Dryas and the sea of ancient ice, *QR*, *70*(1), 1-10.

Brewer, M. C. (1958), The thermal regime of an Arctic lake, *Trans. Am. Geophys. Union*, *39*(2), 278-284.

Brigham-Grette, J., and L. D. Carter (1992), Pliocene marine transgressions of northern Alaska: circumarctic correlations and paleoclimatic interpretations, *Arctic*, 74-89.

Brigham-Grette, J., and D. M. Hopkins (1995), Emergent Marine Record and Paleoclimate of the Last Interglaciation along the Northwest Alaskan Coast, *QR*, *43*(2), 159-173.

Briner, J. P., N. Michelutti, D. R. Francis, G. H. Miller, Y. Axford, M. J. Wooller, and A. P. Wolfe (2006), A multi-proxy lacustrine record of Holocene climate change on northeastern Baffin Island, Arctic Canada, *QR*, *65*(3), 431-442.

Brosius, L. S., K. M. Walter Anthony, G. Grosse, J. P. Chanton, L. M. Farquharson, P. P. Overduin, and H. Meyer (2012), Using the deuterium isotope composition of permafrost meltwater to constrain thermokarst lake contributions to atmospheric CH4 during the last deglaciation, *J. Geophys. Res.*,*117*(G1), G01022.

Brown, J., O. J. Ferrians Jr, J. A. Heginbottom, and E. S. Melnikov (1997), *Circum-Arctic map of permafrost and ground-ice conditions*, US Geological Survey.

Brown, J., O. J. Ferrians, J. A. J. Heginbottom, and E. S. Melnikov (2001), Circum-Arctic Map of Permafrost and Ground Ice Conditions, National Snow and Ice Data Center/World Data Center for Glaciology: Boulder, CO.

Bunbury, J., and K. Gajewski (2009), Postglacial climates inferred from a lake at treeline, southwest Yukon Territory, Canada, *QSR*, *28*(3), 354-369.

Burgess, M., A. Judge, A. Taylor, and V. Allen (1982), Ground temperature studies of permafrost growth at a drained lake site, Mackenzie Delta, *Proceedings 4th Canadian Permafrost Conference*, 3-11.

Burn, C. R. (1997), Cryostratigraphy, paleogeography, and climate change during the early Holocene warm interval, western Arctic coast, Canada, *Canadian Journal of Earth Sciences*, *34*(7), 912-925.

Burn, C. R. (2009), After Whom is Herschel Island Named?, *Arctic*, 317-323.

Burn, C. R., F. A. Michel, and M. W. Smith (1986), Stratigraphic, isotopic and mineralogical evidence for an early Holocene thaw unconformity at Mayo, Yukon Territory, *Canadian Journal of Earth Sciences = Journal Canadien des Sciences de la Terre*, *23*(6), 794-803.

Burn, C. R., and M. W. Smith (1990), Development of thermokarst lakes during the Holocene at sites near Mayo, Yukon territory, *Permafrost and Periglacial Processes*, *1*(2), 161-175.

Burn, C. R., and Y. Zhang (2009), Permafrost and climate change at Herschel Island (Qikiqtaruq), Yukon Territory, Canada, *Journal of Geophysical Research: Earth Surface*, *114*(F2).

Calmels, F., L.-P. Roy, C. Laurent, M. Pelletier, L. Kinnear, B. Benkert, B. Horton, and J. Pumple (2015), A practical guide to permafrost vulnerability for Yukon's North Alaska Highway, paper presented at GeoQuébec 2015, Québec City, Canada.

Carson, C. E., and K. M. Hussey (1962), The oriented lakes of arctic Alaska, *Journal of Geology*, *70*(4), 417-439, doi:10.1086/626834.

Carter, L. D. (1988), Loess and deep thermokarst basins in Arctic Alaska, paper presented at 5th International Conference on Permafrost, Tapir, Trondheim.

Chardez, D. (1965), Ecologie generale des Thecamoebiens (Rhizopoda, testacea), *Bulletin de l'Institut Agronomigue et des Stations de Recherches Gembloux*, *3*, 306-341.

Chen, M., J. C. Rowland, C. J. Wilson, G. L. Altmann, and S. P. Brumby (2014), Temporal and spatial pattern of thermokarst lake area changes at Yukon Flats, Alaska, *Hydrological Processes*, *28*(3), 837-852.

Cohen, A. V. (2003), *Paleoclimatology: the History and Evolution of Lake Systems*, 525 pp., Oxford University Press, Oxford.

Colinvaux, P. A. (1964), The environment of the Bering Land Bridge, *Ecological Monographs*, *34*(3), 297-329.

Coulombe, O., F. Bouchard, and R. Pienitz (2016), Coupling of sedimentological and limnological dynamics in subarctic thermokarst ponds in Northern Québec (Canada) on an interannual basis, *Sedimentary Geology, 249*, 15-24.

Craig, H. (1961), Isotopic variations in meteoric waters, *Science*, *133*(3465), 1702-1703.

Croudace, I. W., A. Rindby, and R. G. Rothwell (2006), ITRAX: description and evaluation of a new multi-function X-ray core scanner, *Geological Society, London, Special Publications*, *267*(1), 51-63.

Crutzen, P. J. (2002), Geology of mankind, *Nature*, *415*(6867), 23-23.

Cwynar, L. C. (1982), A late-Quaternary vegetation history from Hanging Lake, northern Yukon, *Ecological Monographs*, 2-24.

Cwynar, L. C., and R. W. Spear (1995), Paleovegetation and paleoclimatic changes in the Yukon at 6 ka BP, *Geogr Phys Quatern*, *49*(1), 29-35.

Czudek, T., and J. Demek (1970), Thermokarst in Siberia and its influence on the development of lowland relief, *QR*, *1*(1), 103-120.

Dallimore, A., C. J. Schröder-Adams, and S. R. Dallimore (2000), Holocene environmental history of thermokarst lakes on Richards Island, Northwest Territories, Canada: Thecamoebians as paleolimnological indicators, *Journal of Paleolimnology*, *23*(3), 261-283.

Dansgaard, W. (1964), Stable isotopes in precipitation, *Tellus*, *16*(4), 436-468.

De Deckker, P. (1981), Ostracods of athalassic saline lakes, *Hydrobiologia*(81-82), 131-144.

Detterman, R. L. (1970), Early Holocene Warm Interval In Northern Alaska, *Arctic*, *23*, 130-132.

Douglas, M. S. V., P. B. Hamilton, R. Pienitz, and J. P. Smol (2004), Algal indicators of environmental change in arctic and antarctic lakes and ponds, in *Long-term Environmental Change in Arctic and Antarctic Lakes*, edited by R. Pienitz, M. S. V. Douglas, J. P. Smol and P. B. Hamilton, pp. 117-157, Springer, Netherlands.

Dutta, K., E. A. G. Schuur, J. C. Neff, and S. A. Zimov (2006), Potential carbon release from permafrost soils of Northeastern Siberia, *Global Change Biology*, *12*(12), 2336-2351.

Dyke, A. S., J. T. Andrews, P. U. Clark, J. H. England, G. H. Miller, J. Shaw, and J. J. Veillette (2002), The Laurentide and Innuitian ice sheets during the last glacial maximum, *QSR*, *21*(1), 9-31.

Dyke, A. S., A. Moore, and L. Robertson (2003), *Deglaciation of North America*, Geological Survey of Canada Ottawa, Ontario, Canada.

Dyke, A. S., and V. K. Prest (1987), Late Wisconsinan and Holocene history of the Laurentide ice sheet, *Geogr Phys Quatern*, *41*(2), 237-263.

Edwards, M., G. Grosse, B. M. Jones, and P. McDowell (2016), The evolution of a thermokarst-lake landscape: Late Quaternary permafrost degradation and stabilization in interior Alaska, *Sedimentary Geology*, *340*, 3-14.

Edwards, M. E., C. J. Mock, B. P. Finney, V. A. Barber, and P. J. Bartlein (2001), Potential analogues for paleoclimatic variations in eastern interior Alaska during the past 14,000 yr: atmospheric-circulation controls of regional temperature and moisture responses, *QSR*, *20*(1-3), 189-202.

Edwards, T. L., M. Crucifix, and S. P. Harrison (2007), Using the past to constrain the future: how the palaeorecord can improve estimates of global warming, *Progress in Physical Geography*, *31*(5), 481-500.

Eisner, W. R., J. G. Bockheim, K. M. Hinkel, T. A. Brown, F. E. Nelson, K. M. Peterson, and B. M. Jones (2005), Paleoenvironmental analyses of an organic deposit from an erosional landscape remnant, Arctic Coastal Plain of Alaska, *Paleo3*, *217*(3-4), 187-204.

Elberling, B., A. Michelsen, C. Schädel, E. A. G. Schuur, H. H. Christiansen, L. Berg, M. P. Tamstorf, and C. Sigsgaard (2013), Long-term CO2 production following permafrost thaw, *Nature Climate Change*, *3*(10), 890-894.

Elias, S. A. (2000), Late Pleistocene climates of Beringia, based on analysis of fossil beetles, *QR*, *53*(2), 229-235.

Elias, S. A. (2001), Beringian paleoecology: results from the 1997 workshop, *QSR*, *20*(1-3), 7-13.

Elias, S. A., S. K. Short, and H. H. Birks (1997), Late Wisconsin environments of the Bering Land Bridge, *Paleo3*, *136*(1-4), 293-308.

Engstrom, D. R., and H. E. Wright Jr (1984), Chemical stratigraphy of lake sediments as a record of environmental change, in *Lake sediments and environmental history: studies in palaeolimnology and palaeoecology in honour of Winifred Tutin*, edited by E. Y. Haworth and J. W. G. Lund, p. 411, Leicester University Press, Leicester.

Environment Canada (2015), http://climate.weather.gc.ca/index_e.html (accessed October 2015).

Everdingen, R. O. v. (1998, revised 2005), *Multi-language glossary of permafrost and related ground-ice terms*, revised 2002 ed., National Snow and Ice Data Center/World Data Center for Glaciology, Boulder, CO.

Faegri, K., P. E. Kaland, and K. Krzywinski (1989), *Textbook of pollen analysis*, John Wiley & Sons Ltd.

Farquharson, L., K. W. Anthony, N. Bigelow, M. Edwards, and G. Grosse (2016), Facies analysis of yedoma thermokarst lakes on the northern Seward Peninsula, Alaska, *Sedimentary Geology, 340*, 25-37.

Farquharson, L. M., D. H. Mann, G. Grosse, B. M. Jones, and V. E. Romanovsky (under review), Spatial distribution of thaw-influenced terrain in arctic Alaska, *Geomorphology*.

Folk, R. L., and W. C. Ward (1957), Brazos River bar: a study in the significance of grain size parameters, *Journal of Sedimentary Research*, *27*(1), 3-27.

Forster, P., V. Ramaswamy, P. Artaxo, T. Berntsen, R. Betts, D. W. Fahey, J. Haywood, J. Lean, D. C. Lowe, and G. Myhre (2007), *Changes in atmospheric constituents and in radiative forcing. Chapter 2*.

Francis, D. R., A. P. Wolfe, I. R. Walker, and G. H. Miller (2006), Interglacial and Holocene temperature reconstructions based on midge remains in sediments of two lakes from Baffin Island, Nunavut, Arctic Canada, *Paleo3*, *236*(1), 107-124.

Francus, P., R. S. Bradley, M. B. Abbott, W. Patridge, and F. Keimig (2002), Paleoclimate studies of minerogenic sediments using annually resolved textural parameters, *Geophysical Research Letters*, *29*(20).

French, H., and Y. Shur (2010), The principles of cryostratigraphy, *ESR*, *101*(3-4), 190-206.

French, H. M. (1974), Active Thermokarst Processes, Eastern Banks Island, Western Canadian Arctic, *Canadian Journal of Earth Sciences = Journal Canadien des Sciences de la Terre*, *11*(6), 785-794.

French, H. M. (2007), *The Periglacial Environment*, 3 ed., 458 pp., John Wiley & Sons Ltd., London.

French, H. M., and S. W. S. Millar (2013), Permafrost at the time of the Last Glacial Maximum (LGM) in North America, *Boreas*, *43*, 667–677.

Fritz, M., U. Herzschuh, S. Wetterich, H. Lantuit, G. P. De Pascale, W. H. Pollard, and L. Schirrmeister (2012a), Late glacial and Holocene sedimentation, vegetation, and climate history from easternmost Beringia (northern Yukon Territory, Canada), *QR*, *78*(3), 549-560.

Fritz, M., I. Unkel, J. Lenz, K. Gajewski, P. Frenzel, N. Paquette, H. Lantuit, L. Körte, and S. Wetterich (under review), Regional environmental change versus local signal preservation in Holocene thermokarst lake sediments: A case study from Herschel Island, Yukon (Canada), *Journal of Paleolimnology*.

Fritz, M., S. Wetterich, H. Meyer, L. Schirrmeister, H. Lantuit, and W. H. Pollard (2011), Origin and characteristics of massive ground ice on Herschel Island (western Canadian Arctic) as revealed by stable water isotope and Hydrochemical signatures, *Permafrost and Periglacial Processes*, *22*(1), 26-38.

Fritz, M., S. Wetterich, L. Schirrmeister, H. Meyer, H. Lantuit, F. Preusser, and W. H. Pollard (2012b), Eastern Beringia and beyond: Late Wisconsinan and Holocene landscape dynamics along the Yukon Coastal Plain, Canada, *Paleo3*, *319–320*, 28-45.

Fritz, M., J. Wolter, N. Rudaya, O. Palagushkina, L. Nazarova, J. Obu, J. Rethemeyer, H. Lantuit, and S. Wetterich (in press), Holocene ice-wedge polygon development in northern Yukon permafrost peatlands (Canada), *QSR*, doi:10.1016/j.quascirev.2016.02.008.

Froese, D. G., G. D. Zazula, J. A. Westgate, S. J. Preece, P. T. Sanborn, A. V. Reyes, and N. J. G. Pearce (2009), The Klondike goldfields and Pleistocene environments of Beringia, *GSA Today*, *19*(8), 4-10.

Frohn, R. C., K. M. Hinkel, and W. R. Eisner (2005), Satellite remote sensing classification of thaw lakes and drained thaw lake basins on the North Slope of Alaska, *Remote Sensing of Environment*, *97*, 116-126.

Gaglioti, B. V., D. H. Mann, B. M. Jones, J. W. Pohlman, M. L. Kunz, and M. J. Wooller (2014), Radiocarbon age-offsets in an arctic lake reveal the long-term response of permafrost carbon to climate change, *Journal of Geophysical Research: Biogeosciences*, *119*(8), 2014JG002688.

Gajewski, K. (2002), Modern pollen assemblages in lake sediments from the Canadian Arctic, *Arctic, Antarctic, and Alpine Research*, 26-32.

Gajewski, K. (2015a), Quantitative reconstruction of Holocene temperatures across the Canadian Arctic and Greenland, *Global and Planetary Change*, *128*, 14-23.

Gajewski, K. (2015b), Impact of Holocene climate variability on Arctic vegetation, *Global and Planetary Change*, *133*, 272-287.

Godin, E., and D. Fortier (2012), Geomorphology of a thermo-erosion gully, Bylot Island, Nunavut, Canada, *Canadian Journal of Earth Sciences*, *49*(8), 979-986.

Goetcheus, V. G., and H. H. Birks (2001), Full-glacial upland tundra vegetation preserved under tephra in the Beringia National Park, Seward Peninsula, Alaska, *QSR*, *20*(1-3), 135-147.

Grimm, E. C. (1987), CONISS: a FORTRAN 77 program for stratigraphically constrained cluster analysis by the method of incremental sum of squares, *Computers & Geosciences*, *13*(1), 13-35.

Grosse, G., et al. (2011), Vulnerability of high-latitude soil organic carbon in North America to disturbance, *J. Geophys. Res.*, *116*, G00K06.

Grosse, G., B. Jones, and C. Arp (2013a), 8.21 Thermokarst Lakes, Drainage, and Drained Basins, in *Treatise on Geomorphology*, edited by F. S. Editor-in-Chief: John, pp. 325-353, Academic Press, San Diego.

Grosse, G., J. E. Robinson, R. Bryant, M. D. Taylor, W. Harper, A. DeMasi, E. Kyker-Snowman, A. Veremeeva, L. Schirrmeister, and J. Harden (2013b), Distribution of late Pleistocene ice-rich syngenetic permafrost of the Yedoma Suite in east and central Siberia, Russia, *US Geological Survey Open File Report*, *2013*(1078), 1-37.

Grosse, G., V. Romanovsky, T. Jorgenson, K. W. Anthony, J. Brown, and P. P. Overduin (2011), Vulnerability and feedbacks of permafrost to climate change, *Eos Trans. AGU, Fall Meeting*, *9*(1), 73-74.

Grosse, G., L. Schirrmeister, V. V. Kunitsky, and H.-W. Hubberten (2005), The use of CORONA images in remote sensing of periglacial geomorphology: an illustration from the NE Siberian coast, *Permafrost and Periglacial Processes*, *16*(2), 163-172.

Grosse, G., L. Schirrmeister, C. Siegert, V. V. Kunitsky, E. A. Slagoda, A. A. Andreev, and A. Y. Dereviagyn (2007), Geological and geomorphological evolution of a sedimentary periglacial landscape in Northeast Siberia during the Late Quaternary, *Geomorphology*, *86*(1-2), 25-51.

Guyard, H., E. Chapron, G. St-Onge, F. S. Anselmetti, F. Arnaud, O. Magand, P. Francus, and M.-A. Mélières (2007), High-altitude varve records of abrupt environmental changes and mining activity over the last 4000 years in the Western French Alps (Lake Bramant, Grandes Rousses Massif), *QSR*, *26*(19), 2644-2660.

Hammer, Ø., D. A. T. Harper, and P. D. Ryan (2001), PAST-PAlaeontological STatistics, ver. 1.89, *Palaeontologia electronica*, *4*(1), 1-9.

Harris, S. A. (2002), Causes and consequences of rapid thermokarst development in permafrost or glacial terrain, *Permafrost and Periglacial Processes*, *13*(3), 237-242.

Harry, D. G., and H. M. French (1983), The orientation and evolution of thaw lakes, southwest Banks Island, Canadian Arctic, paper presented at Fourth International Conference on Permafrost, National Academy Press, Fairbanks, Alaska, July 17-22.

Havel, J. E., P. D. N. Hebert, and L. D. Delorme (1990), Genetics of sexual Ostracoda from a low Arctic site, *Journal of Evolutionary Biology*, *3*(1-2), 65-84.

Heslop, J. K., K. M. Walter Anthony, A. Sepulveda-Jauregui, K. Martinez-Cruz, A. Bondurant, G. Grosse, and M. C. Jones (2015), Thermokarst lake methanogenesis along a complete talik profile, *Biogeosciences*, *12*(14), 4317-4331, doi:10.5194/bg-12-4317-2015.

Hill, P. R., P. J. Mudie, K. Moran, and S. M. Blasco (1985), A sea-level curve for the Canadian Beaufort Shelf, *Canadian Journal of Earth Sciences*, *22*(10), 1383-1393.

Hinkel, K. M., W. R. Eisner, J. G. Bockheim, E. N. Frederick, K. M. Peterson, and X. Dai (2003), Spatial extent, age, and carbon stocks in drained thaw lake basins on the Barrow Peninsula, Alaska, *Arctic, Antarctic and Alpine Research*, *35*(3), 291-300.

Hinkel, K. M., R. C. Frohn, F. E. Nelson, W. R. Eisner, and R. A. Beck (2005), Morphometric and Spatial Analysis of Thaw Lakes and Drained Thaw Lake Basins in the Western Arctic Coastal Plain, Alaska, *Permafrost and Periglacial Processes*, *16*, 327-341.

Hinkel, K. M., B. M. Jones, W. R. Eisner, C. J. Cuomo, R. A. Beck, and R. Frohn (2007), Methods to assess natural and anthropogenic thaw lake drainage on the western Arctic coastal plain of northern Alaska, *Journal of Geophysical Research*, *112*, F02S16.

Hinkel, K. M., J. D. Lenters, Y. Sheng, E. A. Lyons, R. A. Beck, W. R. Eisner, E. F. Maurer, J. Wang, and B. L. Potter (2012), Thermokarst Lakes on the Arctic Coastal Plain of Alaska: Spatial and Temporal Variability in Summer Water Temperature, *Permafrost and Periglacial Processes*, *23*, 207-217.

Hinzman, L. D., et al. (2005), Evidence and Implications of Recent Climate Change in Northern Alaska and Other Arctic Regions, *Climatic Change*, *72*(3), 251-298.

Hoefle, C., M. E. Edwards, D. M. Hopkins, D. H. Mann, and C.-L. Ping (2000), The Full-Glacial Environment of the Northern Seward Peninsula, Alaska, Reconstructed from the 21,500-Year-Old Kitluk Paleosol, *QR*, *53*(2), 143-153.

Höfle, C., M. E. Edwards, D. M. Hopkins, D. H. Mann, and C.-L. Ping (2000), The full-glacial environment of the northern Seward Peninsula, Alaska, reconstructed from the 21,500-year-old Kitluk paleosol, *QR*, *53*(2), 143-153.

Höfle, C., C.-L. Ping, and J. M. Kimble (1998), Properties of Permafrost Soils on the Northern Seward Peninsula, Northwest Alaska, *Soil Sci Soc Am J*, *62*(6), 1629-1639.

Hopkins, D. M. (1959a), Cenozoic History of the Bering Land Bridge, *Science*, *129*(3362), 1519-1528.

Hopkins, D. M. (1959b), History of Imuruk Lake, Seward Peninsula, Alaska, *Bulletin of the Geological Society of America*, *70*, 1033-1046.

Hopkins, D. M. (1963), Geology of the Imuruk Lake area, Seward Peninsula, Alaska, *US Geological Survey Bulletin*, 101.

Hopkins, D. M. (1967), *The Bering land bridge*, Stanford University Press.

Hopkins, D. M. (1973), Sea level history in Beringia during the past 250,000 years, *QR*, *3*(4), 520-540.

Hopkins, D. M. (1982), Aspects of the paleogeography of Beringia during the late Pleistocene, *Paleoecology of Beringia*, 3-28.

Hopkins, D. M. (1988), The Espenberg Maars: a record of explosive volcanic activity in the Devil Mountain-Cape Espenberg area, Seward Peninsula, Alaska, in *The Bering Sea Land Bridge National Preserve: an archeological survey*, edited by J. M. Schaaf, pp. 262-321, National Park Service, Alaska Regional Office.

Hopkins, D. M., R. E. Giterman, and J. V. Matthews (1976), Interstadial mammoth remains and associated pollen and insect fossils, Kotzebue Sound area, northwestern Alaska, *Geology*, *4*(3), 169-172.

Hopkins, D. M., and J. G. Kidd (1988), Thaw lake sediments and sedimentary environments, paper presented at 5th International Permafrost Conference, Tapir, Trondheim.

Hopkins, D. M., P. A. Smith, and J. V. Matthews (1981), Dated wood from Alaska and the Yukon: Implications for forest refugia in Beringia, *QR*, *15*(3), 217-249.

Hugelius, G., et al. (2014), Estimated stocks of circumpolar permafrost carbon with quantified uncertainty ranges and identified data gaps, *Biogeosciences*, *11*(23), 6573-6593.

Hughen, K. A., J. T. Overpeck, R. F. Anderson, and K. M. Williams (1996), The potential for palaeoclimate records from varved Arctic lake sediments: Baffin Island, Eastern Canadian Arctic, *Geological Society, London, Special Publications*, *116*(1), 57-71.

Hughes, A. L. C., R. Gyllencreutz, Ø. S. Lohne, J. Mangerud, and J. I. Svendsen (2016), The last Eurasian ice sheets–a chronological database and time-slice reconstruction, DATED-1, *Boreas*, *45*(1), 1-45.

Hunt, J. B., and P. G. Hill (1996), An inter-laboratory comparison of the electron probe microanalysis of glass geochemistry, *QI*, *34*, 229-241.

Hunt, S., Z. Yu, and M. Jones (2013), Lateglacial and Holocene climate, disturbance and permafrost peatland dynamics on the Seward Peninsula, western Alaska, *QSR*, *63*(0), 42-58.

Irvine, F., L. Cwynar, J. Vermaire, and A. H. Rees (2012), Midge-inferred temperature reconstructions and vegetation change over the last ~15,000 years from Trout Lake, northern Yukon Territory, eastern Beringia, *Journal of Paleolimnology*, *48*(1), 133-146.

Jeppesen, E., J. P. Jensen, S. Amsinck, F. Landkildehus, T. Lauridsen, and S. F. Mitchell (2002), Reconstructing the historical changes in Daphnia mean size and planktivorous fish abundance in lakes from the size of Daphnia ephippia in the sediment, *Journal of Paleolimnology*, *27*(1), 133-143.

Jin, Z., S. Wang, J. Shen, E. Zhang, F. Li, J. Ji, and X. Lu (2001), Chemical weathering since the Little Ice Age recorded in lake sediments: a high-resolution proxy of past climate, *Earth Surface Processes and Landforms*, *26*(7), 775-782.

Jones, B. M., and C. D. Arp (2015), Observing a Catastrophic Thermokarst Lake Drainage in Northern Alaska, *Permafrost and Periglacial Processes*, *26*(2), 119–128.

Jones, B. M., G. Grosse, C. D. Arp, M. C. Jones, K. M. Walter Anthony, and V. E. Romanovsky (2011), Modern thermokarst lake dynamics in the continuous permafrost zone, northern Seward Peninsula, Alaska, *J. Geophys. Res.*, *116*, G00M03.

Jones, B. M., G. Grosse, C. D. Arp, E. Miller, L. Liu, D. J. Hayes, and C. F. Larsen (2015), Recent Arctic tundra fire initiates widespread thermokarst development, *Scientific Reports*, *5*, 15865, doi:10.1038/srep15865

http://www.nature.com/articles/srep15865#supplementary-information.

Jones, M. C., G. Grosse, B. M. Jones, and K. Walter Anthony (2012), Peat accumulation in drained thermokarst lake basins in continuous, ice-rich permafrost, northern Seward Peninsula, Alaska, *J. Geophys. Res.*, *117*, G00M07.

Jones, M. C., and Z. Yu (2010), Rapid deglacial and early Holocene expansion of peatlands in Alaska, *Proceedings of the National Academy of Sciences*, *107*(16), 7347-7352.

Jordan, J. W., and O. K. Mason (1999), A 5000 year record of intertidal peat stratigraphy and sea level change from northwest Alaska, *QI*, *60*(1), 37-47.

Jorgenson, M. T., V. Romanovsky, J. Harden, Y. Shur, rsquo, J. Donnell, E. A. G. Schuur, M. Kanevskiy, and S. Marchenko (2010), Resilience and vulnerability of permafrost to climate change, *Canadian Journal of Forest Research*, *40*(7), 1219-1236.

Jorgenson, M. T., J. E. Roth, S. F. Schlentner, and T. C. Cater (2003), Ecological land evaluation for the Yukon Training Area on Fort Wainwright: permafrost and disturbance, *ABR, Fairbanks, Alaska and US Army, Anchorage, Alaska*.

Jorgenson, M. T., and Y. Shur (2007), Evolution of lakes and basins in northern Alaska and discussion of the thaw lake cycle, *Journal of Geophysical Research*, *112*, F02S17.

Jorgenson, M. T., Y. Shur, and T. Osterkamp (2008), Thermokarst in Alaska, in *Proceedings of the 9th International Conference on Permafrost*, edited by K. M. Hinkel and D. L. Kane, pp. 869-876, Institute of Northern Engineering, University of Alaska Fairbanks, Fairbanks.

Jorgenson, M. T., Y. L. Shur, and E. R. Pullman (2006), Abrupt increase in permafrost degradation in Arctic Alaska, *Geophysical Research Letters*, *33*, L02503.

Jorgenson, M. T., K. Yoshikawa, M. Kanevskiy, Y. Shur, V. Romanovsky, S. Marchenko, G. Grosse, J. Brown, and B. Jones (2008), Permafrost characteristics of Alaska, in *Proceedings of the 9th International Conference on Permafrost*, edited by D. L. Kane and K. M. Hinkel, pp. 121-122, Institute of Northern Engineering, University of Alaska Fairbanks.

Kanevskiy, M., T. Jorgenson, Y. Shur, J. A. O'Donnell, J. W. Harden, Q. Zhuang, and D. Fortier (2014), Cryostratigraphy and Permafrost Evolution in the Lacustrine Lowlands of West-Central Alaska, *Permafrost and Periglacial Processes*, *25*(1), 14-34.

Kanevskiy, M., Y. Shur, D. Fortier, M. T. Jorgenson, and E. Stephani (2011), Cryostratigraphy of late Pleistocene syngenetic permafrost (yedoma) in northern Alaska, Itkillik River exposure, *QR*, *75*(3), 584-596.

Kanevskiy, M., Y. Shur, M. T. Jorgenson, C. L. Ping, G. J. Michaelson, D. Fortier, E. Stephani, M. Dillon, and V. Tumskoy (2013), Ground ice in the upper permafrost of the Beaufort Sea coast of Alaska, *Cold Regions Science and Technology*, *85*(0), 56-70.

Kao-Kniffin, J., B. J. Woodcroft, S. M. Carver, J. G. Bockheim, J. Handelsman, G. W. Tyson, K. M. Hinkel, and C. W. Mueller (2015), Archaeal and bacterial communities across a chronosequence of drained lake basins in arctic alaska, *Scientific reports*, *5*.

Kaplina, T. N., and A. V. Lozhkin (1979), Age of alass deposits of Yakutian coastal lowlands (radiocarbon dating), *Izv RAS Geology*, *2*, 69-76.

Kaplina, T. N., and A. V. Lozhkin (1980), Age of alass deposits of the Maritime Lowland of Yakutia, *International Geology Review*, *22*(4), 470-476.

Kaufman, D. S., et al. (2004), Holocene thermal maximum in the western Arctic (0-180°W), *QSR*, *23*(5-6), 529-560.

Kaufman, D. S., R. S. Anderson, F. S. Hu, E. Berg, and A. Werner (2010), Evidence for a variable and wet Younger Dryas in southern Alaska, *QSR*, *29*(11), 1445-1452.

Kaufman, D. S., Y. L. Axford, A. C. G. Henderson, N. P. McKay, W. W. Oswald, C. Saenger, R. S. Anderson, H. L. Bailey, B. Clegg, and K. Gajewski (in press), Holocene climate changes in eastern Beringia (NW North America)–A systematic review of multi-proxy evidence, *QSR*.

Kaufman, D. S., and D. M. Hopkins (1985), Late Cenozoic radiometric dates, Seward and Baldwin Peninsulas, and adjacent continental shelf, Alaska, *USGS Open-File Report 85-374*, 28.

Kaufman, D. S., and D. M. Hopkins (1986), Glacial history of the Seward Peninsula, in *Glaciation in Alaska: The Geologic Record*, edited by T. D. Hamilton, K. M. Reed and R. M. Thorsen, pp. 51-78, Alaska Geological Society, Anchorage, Alaska.

Kaufman, D. S., W. F. Manley, E. J, and P. L. Gibbard (2004), *Pleistocene Maximum and Late Wisconsinan glacier extents across Alaska, U.S.A*, 9-27 pp., Elsevier.

Keigwin, L. D., J. P. Donnelly, M. S. Cook, N. W. Driscoll, and J. Brigham-Grette (2006), Rapid sea-level rise and Holocene climate in the Chukchi Sea, *Geology*, *34*(10), 861-864.

Kennedy, K. E., D. G. Froese, G. D. Zazula, and B. Lauriol (2010), Last Glacial Maximum age for the northwest Laurentide maximum from the Eagle River spillway and delta complex, northern Yukon, *QSR*, *29*(9-10), 1288-1300.

Kessler, M. A., L. J. Plug, and K. M. Walter Anthony (2012), Simulating the decadal- to millennial-scale dynamics of morphology and sequestered carbon mobilization of two thermokarst lakes in NW Alaska, *J. Geophys. Res.*, *117*, G00M06.

Klein, E. S., Z. Yu, and R. K. Booth (2013), Recent increase in peatland carbon accumulation in a thermokarst lake basin in southwestern Alaska, *Paleo3*, *392*(0), 186-195.

Kling, G. W., G. W. Kipphut, and M. C. Miller (1992), The flux of CO2 and CH4 from lakes and rivers in arctic Alaska, *Hydrobiologia*, *240*(1-3), 23-36.

Kokelj, S., R. Jenkins, and D. Milburn (2005), The influence of thermokarst disturbance on the water quality of small upland lakes, Mackenzie Delta region, Northwest Territories, Canada, *Permafrost and Periglacial Processes*, *16*(4), 343-353.

Kokelj, S. V., and M. T. Jorgenson (2013), Advances in Thermokarst Research, *Permafrost and Periglacial Processes*, *24*(2).

Kokelj, S. V., T. C. Lantz, J. Kanigan, S. L. Smith, and R. Coutts (2009), Origin and polycyclic behaviour of tundra thaw slumps, Mackenzie Delta region, Northwest Territories, Canada, *Permafrost and Periglacial Processes*, *20*(2), 173-184.

Kokelj, S. V., C. A. S. Smith, and C. R. Burn (2002), Physical and chemical characteristics of the active layer and permafrost, Herschel Island, western Arctic Coast, Canada, *Permafrost and Periglacial Processes*, *13*, 171-185.

Kokorowski, H. D., P. M. Anderson, C. J. Mock, and A. V. Lozhkin (2008), A re-evaluation and spatial analysis of evidence for a Younger Dryas climatic reversal in Beringia, *QSR*, *27*(17-18), 1710-1722.

Koven, C. D., B. Ringeval, P. Friedlingstein, P. Ciais, P. Cadule, D. Khvorostyanov, G. Krinner, and C. Tarnocai (2011), Permafrost carbon-climate feedbacks accelerate global warming, *Proceedings of the National Academy of Sciences*, *108*(36), 14769-14774.

Kuehn, S. C., D. G. Froese, P. A. R. Shane, and I. I. Participants (2011), The INTAV intercomparison of electron-beam microanalysis of glass by tephrochronology laboratories: results and recommendations, *QI*, *246*(1), 19-47.

Kurek, J., L. C. Cwynar, T. A. Ager, M. B. Abbott, and M. E. Edwards (2009), Late Quaternary paleoclimate of western Alaska inferred from fossil chironomids and its relation to vegetation histories, *QSR*, *28*(9-10), 799-811.

Kurek, J., L. C. Cwynar, and J. C. Vermaire (2009), A late Quaternary paleotemperature record from Hanging Lake, northern Yukon Territory, eastern Beringia, *QR*, *72*(2), 246-257.

Kuzmina, S., S. Elias, P. Matheus, J. E. Storer, and A. Sher (2008), Paleoenvironmental reconstruction of the Last Glacial Maximum, inferred from insect fossils from a tephra buried soil at Tempest Lake, Seward Peninsula, Alaska, *Paleo3*, *267*(3-4), 245-255.

Lamoureux, S. F., and R. Gilbert (2004), A 750-yr record of autumn snowfall and temperature variability and winter storminess recorded in the varved sediments of Bear Lake, Devon Island, Arctic Canada, *QR*, *61*(2), 134-147.

Lamoureux, S. F., and R. Gilbert (2004), Physical and chemical properties and proxies of high latitude lake sediments, in *Long-term Environmental Change in Arctic and Antarctic Lakes*, edited by J. P. Smol, R. Pienitz and M. S. V. Douglas, pp. 53-87, Springer Netherlands.

Lantuit, H., and W. H. Pollard (2008), Fifty years of coastal erosion and retrogressive thaw slump activity on Herschel Island, southern Beaufort Sea, Yukon Territory, Canada, *Geomorphology*, *95*(1-2), 84-102.

Lantuit, H., W. H. Pollard, N. Couture, M. Fritz, L. Schirrmeister, H. Meyer, and H. W. Hubberten (2012), Modern and Late Holocene Retrogressive Thaw Slump Activity on the Yukon Coastal Plain and Herschel Island, Yukon Territory, Canada, *Permafrost and Periglacial Processes*, *23*(1), 39-51.

Lenz, J., M. Fritz, L. Schirrmeister, H. Lantuit, M. J. Wooller, W. H. Pollard, and S. Wetterich (2013), Periglacial landscape dynamics in the western Canadian Arctic: Results from a thermokarst lake record on a push moraine (Herschel Island, Yukon Territory), *Paleo3*, *381–382*(0), 15-25.

Lenz, J., G. Grosse, B. M. Jones, K. M. Walter Anthony, A. Bobrov, S. Wulf, and S. Wetterich (2016), Mid-Wisconsin to Holocene Permafrost and Landscape Dynamics based on a Drained Lake Basin Core from the Northern Seward Peninsula, Northwest Alaska, *Permafrost and Periglacial Processes*, *27*, 56-75.

Lenz, J., B. M. Jones, S. Wetterich, R. Tjallingii, M. Fritz, C. D. Arp, and G. Grosse (under review), Impacts of shore expansion and catchment characteristics on lacustrine thermokarst records in permafrost lowlands, Alaska Arctic Coastal Plain, *Arktos*.

Lenz, J., S. Wetterich, B. M. Jones, H. Meyer, A. Bobrov, and G. Grosse (in press), Evidence of multiple thermokarst lake generations from an 11 800-year-old permafrost core on the northern Seward Peninsula, Alaska, *Boreas*, pp. 20, doi:10.1111/bor.12186.

Ling, F., and T. Zhang (2003), Numerical simulation of permafrost thermal regime and talik development under shallow thaw lakes on the Alaskan Arctic Coastal Plain, *J Geophys Res-Atmos*, *108*(D16), 4511.

Löwemark, L., H. F. Chen, T. N. Yang, M. Kylander, E. F. Yu, Y. W. Hsu, T. Q. Lee, S. R. Song, and S. Jarvis (2011), Normalizing XRF-scanner data: a cautionary note on the interpretation of high-resolution records from organic-rich lakes, *Journal of Asian Earth Sciences*, *40*(6), 1250-1256.

MacDonald, L. A., K. W. Turner, A. M. Balasubramaniam, B. B. Wolfe, R. I. Hall, and J. N. Sweetman (2012), Tracking hydrological responses of a thermokarst lake in the Old Crow Flats (Yukon Territory, Canada) to recent climate variability using aerial photographs and paleolimnological methods, *Hydrological Processes*, *26*(1), 117-129.

Mackay, J. R. (1959), Glacier ice-thrust features of the Yukon coast, *Geographical Bulletin*, *13*, 5-21.

Mackay, J. R. (1978), Freshwater shelled invertebrate indicators of paleoclimate in northwestern Canada during late glacial times: Discussion, *Canadian Journal of Earth Sciences*, *15*(3), 461-462.

Mackay, J. R. (1988), Catastrophic lake drainage, Tuktoyaktuk Peninsula area, District of Mackenzie, in *Current Research, Part D*, edited, pp. 83-90, Geological Survey of Canada.

Mackay, J. R. (1990), Some observations on the growth and deformation of epigenetic, syngenetic and anti-syngenetic ice wedges, *Permafrost and Periglacial Processes*, *1*(1), 15-29.

Mackay, J. R. (1997), A full-scale field experiment (1978-1995) on the growth of permafrost by means of lake drainage, western Arctic coast; a discussion of the method and some results, *Canadian Journal of Earth Sciences*, *34*(1), 17-33.

Mackay, J. R., and C. R. Burn (2002), The first 20 years (1978-1979 to 1998-1999) of ice-wedge growth at the Illisarvik experimental drained lake site, western Arctic coast, Canada, *Canadian Journal of Earth Sciences = Revue Canadienne des Sciences de la Terre*, *39*(1), 95-111.

Mackay, J. R., and S. R. Dallimore (1992), Massive ice of the Tuktoyaktuk area, western Arctic coast, Canada, *Canadian Journal of Earth Sciences*, *29*(6), 1235-1249.

Mann, D. H., P. Groves, R. E. Reanier, and M. L. Kunz (2010), Floodplains, permafrost, cottonwood trees, and peat: What happened the last time climate warmed suddenly in arctic Alaska?, *QSR*, *29*(27–28), 3812-3830.

Mann, D. H., P. A. Heiser, and B. P. Finney (2002b), Holocene history of the Great Kobuk Sand Dunes, Northwestern Alaska, *QSR*, *21*(4-6), 709-731.

Mann, D. H., D. M. Peteet, R. E. Reanier, and M. L. Kunz (2002a), Responses of an arctic landscape to Lateglacial and early Holocene climatic changes: the importance of moisture, *QSR*, *21*(8-9), 997-1021.

Marsh, P., M. Russell, S. Pohl, H. Haywood, and C. Onclin (2009), Changes in thaw lake drainage in the Western Canadian Arctic from 1950 to 2000, *Hydrological Processes*, *23*(1), 145-158.

Matthews Jr., J. V. (1974), Quaternary Environments at Cape Deceit (Seward Peninsula, Alaska): Evolution of a tundra ecosystem, *Geological Society of America Bulletin*, *85*, 1353-1384.

McCulloch, D., and D. Hopkins (1966), Evidence for an early recent warm interval in Northwestern Alaska, *Geological Society of America Bulletin*, *77*, 1089-1108.

Meisch, C. (2000), Freshwater Ostracoda in Western and Central Europe, in *S wasserfauna von Mitteleuropa*, edited by J. Schwoerbel and P. Zwick, p. 522, Spektrum Akademischer Verlag, Heidelberg, Berlin.

Meyer, H., T. Opel, T. Laepple, A. Y. Dereviagin, K. Hoffmann, and M. Werner (2015), Long-term winter warming trend in the Siberian Arctic during the mid- to late Holocene, *Nature Geosci*, 8, 122–125

Meyer, H., L. Schirrmeister, K. Yoshikawa, T. Opel, S. Wetterich, H.-W. Hubberten, and J. Brown (2010), Permafrost evidence for severe winter cooling during the Younger Dryas in northern Alaska, *Geophys. Res. Lett.*, *37*(3), L03501.

Meyer, H., L. Schönicke, U. Wand, H.-W. Hubberten, and H. Friedrichsen (2000), Isotope studies of hydrogen and oxygen in ground ice – Experiences with the equilibration technique, *Isotopes in Environmental and Health Studies*, *36*, 133-149.

Meyers, P. A. (1994), Preservation of elemental and isotopic source identification of sedimentary organic matter, *Chemical Geology*, *114*(3-4), 289-302.

Meyers, P. A. (1997), Organic geochemical proxies of paleoceanographic, paleolimnologic, and paleoclimatic processes, *Organic geochemistry*, *27*(5), 213-250.

Meyers, P. A., and E. Lallier-Vergès (1999), Lacustrine sedimentary organic matter records of Late Quaternary paleoclimates, *Journal of Paleolimnology*, *21*(3), 345-372.

Meyers, P. A., and K. Takemura (1997), Quaternary changes in delivery and accumulation of organic matter in sediments of Lake Biwa, Japan, *Journal of Paleolimnology*, *18*(3), 211-218.

Michel, F. A., P. Fritz, and R. J. Drimmie (1989), Evidence of climatic change from oxygen and carbon isotope variations in sediments of a small arctic lake, Canada, *Journal of Quaternary Science*, *4*(3), 201-209.

Mischke, S., M. Kramer, C. Zhang, H. Shang, U. Herzschuh, and J. Erzinger (2008), Reduced early Holocene moisture availability in the Bayan Har Mountains, northeastern Tibetan Plateau, inferred from a multi-proxy lake record, *Paleo3*, *267*(1), 59-76.

Mook, W. G., and J. Van Der Plicht (1999), Reporting (super 14) C activities and concentrations, *Radiocarbon*, *41*(3), 227-239.

Moore, P. D., J. A. Webb, and M. E. Collison (1991), *Pollen analysis*, Blackwell scientific publications, Oxford.

Moorman, B. J., F. A. Michel, and A. Wilson (1996), 14C dating of trapped gases in massive ground ice, Western Canadian Arctic, *Permafrost and Periglacial Processes*, *7*(3), 257-266.

Morgenstern, A., G. Grosse, F. Günther, I. Fedorova, and L. Schirrmeister (2011), Spatial analyses of thermokarst lakes and basins in Yedoma landscapes of the Lena Delta, *The Cryosphere*, *5*(4), 849-867.

Morgenstern, A., M. Ulrich, F. Günther, S. Roessler, I. V. Fedorova, N. A. Rudaya, S. Wetterich, J. Boike, and L. Schirrmeister (2013), Evolution of thermokarst in East Siberian ice-rich permafrost: A case study, *Geomorphology*, *201*, 363-379.

Morlan, R. E., and J. Cinq-Mars (1982), Ancient Beringians: human occupation in the late Pleistocene of Alaska and the Yukon Territory, *Paleoecology of Beringia*, 353-381.

Mueller, C. W., J. Rethemeyer, J. Kao-Kniffin, S. Löppmann, K. Hinkel, and J. Bockheim (2015), Large amounts of labile organic carbon in permafrost soils of Northern Alaska, *Global Change Biology*, *21*(7), 2804–2817.

Munsell (1994), Munsell Soil Color Charts. Macbeth Division of Kollmorgen Instruments Corporation, *New Windsor, NY*, *12553*.

Murton, J. B. (1996), Thermokarst-lake-basin sediments, Tuktoyaktuk Coastlands, western arctic Canada, *Sedimentology*, *43*(4), 737-760.

Murton, J. B. (2001), Thermokarst sediments and sedimentary structures, Tuktoyaktuk Coastlands, western Arctic Canada, *Global and Planetary Change*, *28*(1-4), 175-192.

Murton, J. B., M. D. Bateman, S. R. Dallimore, J. T. Teller, and Z. Yang (2010), Identification of Younger Dryas outburst flood path from Lake Agassiz to the Arctic Ocean, *Nature*, *464*(7289), 740-743.

Murton, J. B., M. Frechen, and D. Maddy (2007), Luminescence dating of mid-to Late Wisconsinan aeolian sand as a constraint on the last advance of the Laurentide Ice Sheet across the Tuktoyaktuk Coastlands, western Arctic Canada, *Canadian Journal of Earth Sciences*, *44*(6), 857-869.

Murton, J. B., and H. M. French (1994), Cryostructures in permafrost, Tuktoyaktuk coastlands, western Arctic Canada, *Canadian Journal of Earth Sciences = Journal Canadien des Sciences de la Terre*, *31*(4), 737-747.

Murton, J. B., H. M. French, and M. Lamothe (1997), Late Wisconsinan erosion and eolian deposition, Summer Island area, Pleistocene Mackenzie Delta, Northwest Territories; optical dating and implications for glacial chronology., *Canadian Journal of Earth Sciences*, *34*.

Murton, J. B., H. M. French, and M. Lamothe (1998), The dating of thermokarst terrain, Pleistocene Mackenzie Delta, Canada, *Collection Nordicana*, *57*, 777-782.

Murton, J. B., C. A. Whiteman, R. I. Waller, W. H. Pollard, I. D. Clark, and S. R. Dallimore (2005), Basal ice facies and supraglacial melt-out till of the Laurentide Ice Sheet, Tuktoyaktuk Coastlands, western Arctic Canada, *QSR*, *24*(5), 681-708.

Nelson, R. E., and L. D. Carter (1987), Paleoenvironmental Analysis of Insects and Extralimital Populus from an Early Holocene Site on the Arctic Slope of Alaska, U.S.A, *Arctic and Alpine Research*, *19*(3), 230-241.

Nowacki, G., P. Spencer, M. Fleming, T. Brock, and T. Jorgenson (2002), *Unified ecoregions of Alaska: 2001*, USGS open file report

Nowaczyk, N. R., E. M. Haltia, D. Ulbricht, V. Wennrich, M. A. Sauerbrey, P. Rosén, H. Vogel, A. Francke, C. Meyer-Jacob, and A. A. Andreev (2013), Chronology of Lake El'gygytgyn sediments – A combined magnetostratigraphic, palaeoclimatic and orbital tuning study based on multi-parameter analyses, *Climate of the Past*, *9*(6), 2413-2432.

Obu, J., H. Lantuit, I. Myers-Smith, B. Heim, J. Wolter, and M. Fritz (2015), Effect of Terrain Characteristics on Soil Organic Carbon and Total Nitrogen Stocks in Soils of Herschel Island, Western Canadian Arctic, *Permafrost and Periglacial Processes*, doi:10.1002/ppp.1881.

Olthof, I., R. H. Fraser, and C. Schmitt (2015), Landsat-based mapping of thermokarst lake dynamics on the Tuktoyaktuk Coastal Plain, Northwest Territories, Canada since 1985, *Remote Sensing of Environment*, *168*, 194-204, doi:http://dx.doi.org/10.1016/j.rse.2015.07.001

Osterkamp, T. E. (2007), Characteristics of the recent warming permafrost in Alaska, *Journal of Geophysical Research F: Earth Surface*, *112*(2).

Oswald, W. W., L. B. Brubaker, and P. M. Anderson (1999), Late Quaternary vegetational history of the Howard Pass area, northwestern Alaska, *Canadian Journal of Botany*, *77*(4), 570-581.

Overpeck, J., et al. (1997), Arctic Environmental Change of the Last Four Centuries, *Science*, *278*, 1251-1256.

Peltier, W. R., and R. G. Fairbanks (2006), Global glacial ice volume and Last Glacial Maximum duration from an extended Barbados sea level record, *QSR*, *25*(23-24), 3322-3337.

Péwé, T. L. (1975), Quaternary geology of Alaska, *US Govt. Print. Off.*

Pienitz, R., M. S. V. Douglas, and J. P. Smol (2004), Paleolimnological research in polar regions: An introduction, in *Long-term Environmental Change in Arctic and Antarctic Lakes*, edited by J. P. Smol, R. Pienitz and M. S. V. Douglas, pp. 1-17, Springer Netherlands.

Pienitz, R., J. P. Smol, W. M. Last, P. R. Leavitt, and B. F. Cumming (2000), Multi-proxy Holocene palaeoclimatic record from a saline lake in the Canadian Subarctic, *The Holocene*, *10*(6), 673-686.

Pienitz, R., I. R. Walker, B. A. Zeeb, J. P. Smol, and P. R. Leavitt (1992), Biomonitoring past salinity changes in an athalassic subarctic lake, *International Journal of Salt Lake Research*, *1*(2), 91-123.

Pint, A., P. Frenzel, R. Fuhrmann, B. Scharf, and V. Wennrich (2012), Distribution of Cyprideis torosa (Ostracoda) in Quaternary athalassic sediments in Germany and its application for palaeoecological reconstructions, *International Review of Hydrobiology*, *97*(4), 330-355.

Plug, L. J., and J. J. West (2009), Thaw lake expansion in a two-dimensional coupled model of heat transfer, thaw subsidence, and mass movement, *J. Geophys. Res.*, *114*, F01002.

Pollard, W. H. (1990), The nature and origin of ground ice in the Herschel Island area, Yukon Territory, paper presented at 5th Canadian Permafrost Conference, Nordicana, Québec, 1990.

R Core Team (2014), A language and environment for statistical computing. R Foundation for Statistical Computing, Vienna, Austria. URL: http://www.R-project.org/, edited.

Rampton, V. N. (1974), The influence of ground ice and thermokarst upon the geomorphology of the Mackenzie-Beaufort region, in *Research in Polar and Alpine Geomorphology: Proceedings of the 3rd Guelph Symposium on Geomorphology. Geo-Abstracts*, edited by B. D. Fahey and R. D. Thompson, pp. 43-59, Norwich.

Rampton, V. N. (1982), Quaternary Geology Yukon Coastal Plain, *Geological Survey of Canada, Bulletin*, *317*, 49pp.

Rampton, V. N. (1988), *Quaternary geology of the Tuktoyaktuk Coastlands, Northwest Territories*, Geological Survey of Canada: Energy, Mines and Resources Canada.

Ramsey, C. B. (2008), Deposition models for chronological records, *QSR*, *27*(1), 42-60.

Ramsey, C. B. (2009a), Bayesian analysis of radiocarbon dates, *Radiocarbon*, *51*(1), 337-360.

Ramsey, C. B. (2009b), Dealing with outliers and offsets in radiocarbon dating, *Radiocarbon*, *51*(3), 1023-1045.

Raynolds, M. K., D. A. Walker, and H. A. Maier (2005), Alaska Arctic Vegetation Map, Scale 1: 4 000 000, U.S. Fish and Wildlife Service, Anchorage, Alaska.

Regmi, P., G. Grosse, M. Jones, B. Jones, and K. Anthony (2012), Characterizing Post-Drainage Succession in Thermokarst Lake Basins on the Seward Peninsula, Alaska with TerraSAR-X Backscatter and Landsat-based NDVI Data, *Remote Sensing*, *4*(12), 3741-3765.

Reille, M. (1992), Pollen et spores d'Europe et d'Afrique du nord: Laboratoire de botanique historique et palynologie, *URA CNRS, Marseille, France*.

Reille, M. (1998), Pollen et spores d'Europe et d'Afrique du Nord: Supplément 2 P: Laboratoire de botanique historique et palynologie, *URA CNRS, Marseille, France*.

Reimer, P. J., et al. (2009), IntCal13 and Marine13 radiocarbon age calibration curves 0–50,000 years cal BP, *Radiocarbon*, *51*, 1111-1150.

Reimer, P. J., et al. (2013), IntCal13 and Marine13 radiocarbon age calibration curves 0–50,000 years cal BP, *Radiocarbon*, *55*(4), 1869-1887.

Ricketts, R. D., T. C. Johnson, E. T. Brown, K. A. Rasmussen, and V. V. Romanovsky (2001), The Holocene paleolimnology of Lake Issyk-Kul, Kyrgyzstan: Trace element and stable isotope composition of ostracodes, *Paleo3*, *176*(1), 207-227.

Ritchie, J. C. (1984), *Past and Present Vegetation of the Far Northwest Canada*, 251 pp., University of Toronto Press, Toronto

Ritchie, J. C., L. C. Cwynar, and R. W. Spear (1983), Evidence from north-west Canada for an early Holocene Milankovitch thermal maximum, *Nature*, *305*, 126-128.

Ritchie, J. C., and F. K. Hare (1971), Late-quaternary vegetation and climate near the arctic tree line of northwestern North America, *QR*, *1*(3), 331-342.

Roach, J., B. Griffith, D. Verbyla, and J. Jones (2011), Mechanisms influencing changes in lake area in Alaskan boreal forest, *Global Change Biology*, *17*(8), 2567-2583.

Roach, J. K., B. Griffith, and D. Verbyla (2013), Landscape influences on climate-related lake shrinkage at high latitudes, *Global Change Biology*, *19*, 2276–2284,.

Røen, U. (1962), Studies on freshwater Entomostraca in Greenland II, *Meddr Gr nland*, *170*(2), 1-240.

Røen, U. (1968), Studies on freshwater Entomostraca in Greenland III. Entomostraca from Peary Land with notes on their biology, *Meddr Gr nland*, *184*(4), 1-59.

Röhl, U., and L. J. Abrams (2000), High resolution, downhole, and nondestructive core measurements from sites 999 and 1001 in the Caribbean Sea: Application to the late Paleocene thermal maximum, *Ocean Drilling Program, Scientific Results*, *165*, 191-203.

Romanovskii, N. N. (1993), *Fundamentals of cryogenesis of the lithosphere. (Osnowi kriogenesa litosfery)*, 336 pp., University Press. Moscow State University, Moscow.

Romanovskii, N. N., H.-W. Hubberten, A. V. Gavrilov, V. E. Tumskoy, G. S. Tipenko, M. N. Grigoriev, and C. Siegert (2000), Thermokarst and Land-Ocean Interactions, Laptev Sea Region, Russia, *Permafrost and Periglacial Processes*, *11*, 137-152.

Romanovsky, V. E., and T. E. Osterkamp (1995), Interannual variations of the thermal regime of the active layer and near-surface permafrost in northern Alaska, *Permafrost and Periglacial Processes*, *6*(4), 313-335.

Romanovsky, V. E., T. S. Sazonova, V. T. Balobaev, N. I. Shender, and D. O. Sergueev (2007), Past and recent changes in air and permafrost temperatures in eastern Siberia, *Global and Planetary Change*, *56*(3–4), 399-413.

Romanovsky, V. E., S. L. Smith, and H. H. Christiansen (2010), Permafrost thermal state in the polar Northern Hemisphere during the international polar year 2007-2009: a synthesis, *Permafrost and Periglacial Processes*, *21*(2), 106-116.

Rowland, J. C., et al. (2010), Arctic Landscapes in Transition: Responses to Thawing Permafrost, *Eos, Transactions American Geophysical Union*, *91*(26), 229-230.

Rühland, K., J.-M. S. Jacques, B. D. Beierle, S. F. Lamoureux, A. S. Dyke, and J. P. Smol (2009), Lateglacial and Holocene paleoenvironmental changes recorded in lake sediments, Brock Plateau (Melville Hills), Northwest Territories, Canada, *The Holocene*, *19*(7), 1005-1016.

Sancetta, C., and S. W. Robinson (1983), Diatom evidence on Wisconsin and Holocene events in the Bering Sea, *QR*, *20*(2), 232-245.

Sars, G. O. (1898), The Cladocera, Copepoda and Ostracoda of the Jana Expedition *Annual Zoology Museum RAS, Sankt-Peterburg*(3), 324-358.

Schädel, C., E. A. G. Schuur, R. Bracho, B. Elberling, C. Knoblauch, H. Lee, Y. Luo, G. R. Shaver, and M. R. Turetsky (2014), Circumpolar assessment of permafrost C quality and its vulnerability over time using long-term incubation data, *Global Change Biology*, *20*(2), 641-652.

Schaefer, K., H. Lantuit, V. E. Romanovsky, E. A. G. Schuur, and R. Witt (2014), The impact of the permafrost carbon feedback on global climate, *Environmental Research Letters*, *9*(8), 085003.

Schirrmeister, L., D. G. Froese, V. Tumskoy, G. Grosse, and S. Wetterich (2013), Yedoma: Late Pleistocene ice-rich syngenetic permafrost of Beringia, in *Encyclopedia of Quaternary Sciences*, edited by S. A. Elias, Elsevier, Amsterdam.

Schirrmeister, L., G. Grosse, S. Wetterich, P. P. Overduin, J. Strauss, E. A. G. Schuur, and H.-W. Hubberten (2011), Fossil organic matter characteristics in permafrost deposits of the northeast Siberian Arctic, *J. Geophys. Res.*, *116*, G00M02.

Schirrmeister, L., H. Meyer, S. Wetterich, C. Siegert, V. V. Kunitsky, G. Grosse, T. V. Kuznetsova, and A. Y. Derevyagin (2008), The Yedoma Suite of the Northeastern Siberian Shelf Region: Characteristics and Concept of Formation, paper presented at 9th International Conference on Permafrost, Institute of Northern Engineering, University of Alaska Fairbanks, Fairbanks, USA.

Schleusner, P., B. K. Biskaborn, F. Kienast, J. Wolter, D. Subetto, and B. Diekmann (2014), Basin evolution and palaeoenvironmental variability of the thermokarst lake El'gene-Kyuele, Arctic Siberia, *Boreas*, *44*, 216–229.

Schneider, A., S. Wetterich, L. Schirrmeister, U. Herzschuh, H. Meyer, and L. A. Pestryakova (2016), Freshwater ostracods (Crustacea) and environmental variability of polygon ponds in the tundra of the Indigirka Lowland, north-east Siberia, *Polar Research*, *35*.

Schuur, E. A. G., et al. (2015), Climate change and the permafrost carbon feedback, *Nature*, *520*(7546), 171-179.

Schuur, E. A. G., J. G. Vogel, K. G. Crummer, H. Lee, J. O. Sickman, and T. E. Osterkamp (2009), The effect of permafrost thaw on old carbon release and net carbon exchange from tundra, *Nature*, *459*(7246), 556-559.

Schwamborn, G., H. Meyer, L. Schirrmeister, and G. Fedorov (2014), Past freeze and thaw cycling in the margin of the El'gygytgyn crater deduced from a 141 m long permafrost record, *Climate of the Past*, *10*, 1109-1123.

Schweger, C. E. (1997), Late Quaternary palaeoecology of the Yukon: a review, in *Insects of the Yukon, Biological Survey of Canada (Terrestrial Arthropods), Ottawa*, edited by H. V. Danks and J. A. Downes, pp. 59-72, Biological Survey of Canada, Ottawa.

Schweger, C. E., and J. V. Matthews (1985), Early and Middle Wisconsinan environments of eastern Beringia: stratigraphic and paleoecological implications of the Old Crow tephra, *Geogr Phys Quatern*, *39*(3), 275-290.

Scott, D. B., T. Schell, G. St-Onge, A. Rochon, and S. Blasco (2009), Foraminiferal assemblage changes over the last 15,000 years on the Mackenzie-Beaufort Sea Slope and Amundsen Gulf, Canada: Implications for past sea ice conditions, *Paleoceanography*, *24*(2).

Séjourné, A., F. Costard, A. Fedorov, J. Gargani, J. Skorve, M. Massé, and D. Mège (2015), Evolution of the banks of thermokarst lakes in Central Yakutia (Central Siberia) due to retrogressive thaw slump activity controlled by insolation, *Geomorphology*, *241*(0), 31-40.

Sellmann, P. V., J. Brown, R. I. Lewellen, H. L. McKim, and C. J. Merry (1975), The classification and geomorphic implications of thaw lakes on the Arctic Coastal Plain, Alaska*Rep. CRREL ID: RR 344*, 21 pp, U.S. Army Cold Regions Research and Engineering Laboratory, Hanover, New Hampshire.

Serreze, M. C., J. E. Walsh, F. S. Chapin, T. Osterkamp, M. Dyurgerov, V. Romanovsky, W. C. Oechel, J. Morison, T. Zhang, and R. G. Barry (2000), Observational Evidence of Recent Change in the Northern High-Latitude Environment, *Climatic Change*, *46*(1-2), 159-207.

Shepard, F. P. (1954), Nomenclature based on sand-silt-clay ratios, *Journal of Sedimentary Research*, *24*(3), 151-158.

Shur, Y., M. Z. Kanevskiy, M. T. Jorgenson, D. Fortier, M. Dillon, E. Stephani, and M. Bray (2009), Yedoma and thermokarst in the northern part of Seward Peninsula, Alaska, paper presented at AGU Fall Meeting, San Fransico, USA.

Shur, Y. L., and M. T. Jorgenson (2007), Patterns of permafrost formation and degradation in relation to climate and ecosystems, *Permafrost and Periglacial Processes*, *18*(1), 7-19.

Smith, C. A. S., C. E. Kennedy, A. E. Hargrave, and K. M. McKenna (1989), Soil and vegetation of Herschel Island, Yukon Territory. Yukon Soil Survey Report, vol. 1. Land Resource Research Centre, *Agriculture Canada, Ottawa*.

Smith, L. C., Y. Sheng, and G. M. MacDonald (2007), A first pan-Arctic assessment of the influence of glaciation, permafrost, topography and peatlands on northern hemisphere lake distribution, *Permafrost and Periglacial Processes*, *18*(2), 201-208.

Smith, L. C., Y. Sheng, G. M. MacDonald, and L. D. Hinzman (2005), Disappearing Arctic Lakes, *Science*, *308*(5727), 1429.

Smith, S. L., and M. M. Burgess (2002), *A digital database of permafrost thickness in Canada*, Geological Survey of Canada Ottawa.

Smith, S. L., V. E. Romanovsky, A. G. Lewkowicz, C. R. Burn, M. Allard, G. D. Clow, K. Yoshikawa, and J. Throop (2010), Thermal state of permafrost in North America: a contribution to the international polar year, *Permafrost and Periglacial Processes*, *21*(2), 117-135.

Soloviev, P. A. (1962), Alass relief and its origin in Central Yakutia, in *Mnogoletnemerzlye porody I soputstvuscie im yavleniya na territorii Yakutskoj ASSR*, Akademi Nauk SSSR, Moscow.

Spear, R. W. (1993), The palynological record of Late-Quaternary arctic tree-line in northwest Canada, *Review of Palaeobotany and Palynology*, *79*(1), 99-111.

Staubwasser, M., F. Sirocko, P. M. Grootes, and M. Segl (2003), Climate change at the 4.2 ka BP termination of the Indus valley civilization and Holocene south Asian monsoon variability, *Geophysical Research Letters*, *30*(8).

Strauss, J., L. Schirrmeister, G. Grosse, S. Wetterich, M. Ulrich, U. Herzschuh, and H.-W. Hubberten (2013), The deep permafrost carbon pool of the Yedoma region in Siberia and Alaska, *Geophysical Research Letters*, *40*(23), 2013GL058088.

Strauss, J., L. Schirrmeister, K. Mangelsdorf, L. Eichhorn, S. Wetterich, and U. Herzschuh (2015), Organic-matter quality of deep permafrost carbon – a study from Arctic Siberia, *Biogeosciences*, *12*(7), 2227-2245, doi:10.5194/bg-12-2227-2015.

Strauss, J., L. Schirrmeister, S. Wetterich, A. Borchers, and S. P. Davydov (2012), Grain-size properties and organic-carbon stock of Yedoma Ice Complex permafrost from the Kolyma lowland, northeastern Siberia, *Global Biogeochem. Cycles*, *26*(3), GB3003.

Szeicz, J. M., and G. M. MacDonald (2001), Montane climate and vegetation dynamics in easternmost Beringia during the Late Quaternary, *QSR*, *20*(1-3), 247-257.

Team, C. (2003), Circumpolar Arctic Vegetation Map, Map No.1, *US Fish and Wildlife Service, Anchorage, Alaska*.

Tedrow, J. C. F. (1969), Thaw lakes, thaw sinks and soils in northern Alaska, *Biuletyn Peryglacjalny*, *20*, 337-345.

Thieler, E. R., D. Martin, and A. Ergul (2003), Digital Shoreline Analysis System (DSAS) version 2.0 - An ArcView extension for calculating shoreline change, *U.S. Geological Survey Open-File Report*, *2008-1278*.

Thompson, R., R. W. Battarbee, P. E. O'Sulliuan, and F. Oldfield (1975), Magnetic susceptibility of lake sediments, *Limnology and Oceanography*, *20*, 688-698.

Tjallingii, R., U. Röhl, M. Kölling, and T. Bickert (2007), Influence of the water content on X-ray fluorescence core-scanning measurements in soft marine sediments, *Geochemistry, Geophysics, Geosystems*, *8*(2).

Tomirdiaro, S. V. (1982), Evolution of lowland landscape in northeastern Asia during late Quaternary time, *Paleoecology of Beringia.*, 29-37.

van Everdingen, R. O. (2005), *Multi-Language Glossary of Permafrost and Related Ground-Ice Terms*, International Permafrost Association, University of Calgary, Calgary, Canada.

van Geel, B., H. Heijnis, D. J. Charman, G. Thompson, and S. Engels (2014), Bog burst in the eastern Netherlands triggered by the 2.8 kyr BP climate event, *The Holocene*, *24*, 1465-1477.

van Huissteden, J., C. Berrittella, F. J. W. Parmentier, Y. Mi, T. C. Maximov, and A. J. Dolman (2011), Methane emissions from permafrost thaw lakes limited by lake drainage, *Nature Clim. Change*, *1*(2), 119-123.

Vandenberghe, J., H. M. French, A. Gorbunov, S. Marchenko, A. A. Velichko, H. Jin, Z. Cui, T. Zhang, and X. Wan (2014), The Last Permafrost Maximum (LPM) map of the Northern Hemisphere: permafrost extent and mean annual air temperatures, 25–17 ka BP, *Boreas*, *43*(3), 652-666.

Vandenberghe, J., and A. Pissart (1993), Permafrost changes in Europe during the last glacial, *Permafrost and Periglacial Processes*, *4*(2), 121-135.

Vardy, S. R., B. G. Warner, and R. Aravena (1997), Holocene climate effects on the development of a peatland on the Tuktoyaktuk Peninsula, Northwest Territories, *QR*, *47*(1), 90-104.

Vaughan, D. G., et al. (2013), Observations: Cryosphere, in *Climate Change 2013: The Physical Science Basis. Contribution of Working Group I to the 5th Assessment Report of the Intergovernmental Panel on Climate Change*, edited by T. F. Stocker, D. Qin, G. K. Plattner, M. Tignor, A. SK, J. Boschung, A. Nauels, Y. Xia, V. Bex and P. M. Midgley, pp. 317-382, Cambridge University Press, Cambridge and New York.

Viau, A. E., and K. Gajewski (2009), Reconstructing millennial-scale, regional paleoclimates of boreal Canada during the Holocene, *Journal of Climate*, *22*(2), 316-330.

Viau, A. E., K. Gajewski, M. C. Sawada, and J. Bunbury (2008), Low-and high-frequency climate variability in eastern Beringia during the past 25 000 years, *Canadian Journal of Earth Sciences*, *45*(11), 1435-1453.

Viereck, L. A., K. Van Cleve, and C. T. Dyrness (1986), Forest ecosystem distribution in the taiga environment, in *Forest ecosystems in the Alaskan taiga*, pp. 22-43, Springer.

Wahl, H. E., D. B. Fraser, R. C. Harvey, and J. B. Maxwell (1987), Climate of Yukon. Environment Canada, *Atmospheric Environment Service, Climatological Studies*, *40*, 1-323.

Walker, D. A., M. K. Raynolds, F. J. A. Daniëls, E. Einarsson, A. Elvebakk, W. A. Gould, A. E. Katenin, S. S. Kholod, C. J. Markon, and E. S. Melnikov (2005), The circumpolar Arctic vegetation map, *Journal of Vegetation Science*, *16*(3), 267-282.

Walter Anthony, K. M., et al. (2014), A shift of thermokarst lakes from carbon sources to sinks during the Holocene epoch, *Nature*, *511*, 452–456.

Walter, K. M., M. E. Edwards, G. Grosse, S. A. Zimov, and F. S. Chapin, III (2007), Thermokarst Lakes as a Source of Atmospheric CH4 During the Last Deglaciation, *Science*, *318*(5850), 633-636.

Walter, K. M., S. A. Zimov, J. P. Chanton, D. Verbyla, and F. S. Chapin (2006), Methane bubbling from Siberian thaw lakes as a positive feedback to climate warming, *Nature*, *443*(7107), 71-75.

Washburn, A. L. (1980), Permafrost features as evidence of climatic change, *ESR*, *15*(4), 327-402.

Weltje, G. J., and R. Tjallingii (2008), Calibration of XRF core scanners for quantitative geochemical logging of sediment cores: theory and application, *EPSL*, *274*(3), 423-438.

West, J. J., and L. J. Plug (2008), Time-dependent morphology of thaw lakes and taliks in deep and shallow ground ice, *Journal of Geophysical Research*, *113*, F01009.

Wetterich, S., G. Grosse, L. Schirrmeister, A. A. Andreev, A. A. Bobrov, F. Kienast, N. H. Bigelow, and M. E. Edwards (2012), Late Quaternary environmental and landscape dynamics revealed by a pingo sequence on the northern Seward Peninsula, Alaska, *QSR*, *39*, 26-44.

Wetterich, S., U. Herzschuh, H. Meyer, L. Pestryakova, B. Plessen, C. Lopez, and L. Schirrmeister (2008a), Evaporation effects as reflected in freshwaters and ostracod calcite from modern environments in Central and Northeast Yakutia (East Siberia, Russia), *Hydrobiologia*, *614*(1), 171-195.

Wetterich, S., S. Kuzmina, A. A. Andreev, F. Kienast, H. Meyer, L. Schirrmeister, T. Kuznetsova, and M. Sierralta (2008b), Palaeoenvironmental dynamics inferred from late Quaternary permafrost deposits on Kurungnakh Island, Lena Delta, Northeast Siberia, Russia, *QSR*, *27*(15-16), 1523-1540.

Wetterich, S., N. Rudaya, V. Tumskoy, A. A. Andreev, T. Opel, L. Schirrmeister, and H. Meyer (2011), Last Glacial Maximum records in permafrost of the East Siberian Arctic, *QSR*, *30*(21-22), 3139-3151.

Wetterich, S., L. Schirrmeister, A. A. Andreev, M. Pudenz, B. Plessen, H. Meyer, and V. V. Kunitsky (2009), Eemian and Late Glacial/Holocene palaeoenvironmental records from permafrost sequences at the Dmitry Laptev Strait (NE Siberia, Russia), *Paleo3*, *279*(1-2), 73-95.

Wetterich, S., L. Schirrmeister, H. Meyer, F. Viehberg, and A. Mackensen (2008a), Arctic freshwater ostracods from modern periglacial environments in the Lena River Delta (Siberian Arctic, Russia): geochemical applications for palaeoenvironmental reconstructions, *Journal of Paleolimnology*, *39*(4), 427-449.

Wetterich, S., L. Schirrmeister, and E. Pietrzeniuk (2005), Freshwater Ostracodes in Quaternary Permafrost Deposits in the Siberian Arctic, *Journal of Paleolimnology*, *34*(3), 363-376.

Whitmore, J., K. Gajewski, M. Sawada, J. W. Williams, B. Shuman, P. J. Bartlein, T. Minckley, A. E. Viau, T. Webb, and S. Shafer (2005), Modern pollen data from North America and Greenland for multi-scale paleoenvironmental applications, *QSR*, *24*(16), 1828-1848.

Willemse, N. W., O. van Dam, P.-J. van Helvoort, R. Dankers, M. Brommer, J. Schokker, T. E. Valstar, and H. de Wolf (2004), Physical and chemical limnology of a subsaline athalassic lake in West Greenland, *Hydrobiologia*, *524*(1), 167-192.

Williams, J. R., L. D. Carter, and W. Yeend (1978), Coastal plain deposits of NPRA. B20-22. In: Johnson KM (ed), The United States geological survey in Alaska: Accomplishments during 1977 (No. 772-B), *Branch of Distribution, US Geological Survey*.

Williams, J. R., and W. E. Yeend (1978), Deep thaw lake basins of the inner Arctic Coastal Plain, Alaska, *USGS*, B35-B37.

Wolter, J., H. Lantuit, M. Fritz, M. Macias-Fauria, I. Myers-Smith, and U. Herzschuh (in press), Vegetation composition and shrub extent on the Yukon coast, Canada, are strongly linked to ice-wedge polygon degradation, *Polar Research*.

Wooller, M., J. Pohlman, B. Gaglioti, P. Langdon, M. Jones, K. Walter Anthony, K. Becker, K.-U. Hinrichs, and M. Elvert (2012), Reconstruction of past methane availability in an Arctic Alaska wetland indicates climate influenced methane release during the past ~12,000 years, *Journal of Paleolimnology*, *48*(1), 27-42.

Yershov, E. D. (1998), *General Geocryology. Studies in Polar research*, 580 pp., Cambridge University Press, Cambridge.

Zabenskie, S., and K. Gajewski (2007), Post-glacial climatic change on boothia peninsula, Nunavut, Canada, *QR*, *68*(2), 261-270.

Zabenskie, S., M. Peros, and K. Gajewski (2006), The use of heavy-liquid in the separation of pollen from Arctic lake sediments, *Can. Assoc. Palynologists*, *29*, 5-7.

Zazula, G. D., P. G. Hare, and J. E. Storer (2009), New Radiocarbon-Dated Vertebrate Fossils from Herschel Island: Implications for the Palaeoenvironments and Glacial Chronology of the Beaufort Sea Coastlands, *Arctic*, *62*(3), 273-280.

Zhang, T., R. G. Barry, K. Knowles, J. A. Heginbottom, and J. Brown (2008), Statistics and characteristics of permafrost and ground-ice distribution in the Northern Hemisphere, *Polar Geography*, *31*(1-2), 47-68.

Zimov, S. A., E. A. G. Schuur, and F. S. Chapin III (2006), Permafrost and the Global Carbon Budget, *Science*, *312*, 1612-1613.

Zona, D., W. C. Oechel, K. M. Peterson, R. J. Clements, K. T. Paw U, and S. L. Ustin (2010), Characterization of the carbon fluxes of a vegetated drained lake basin chronosequence on the Alaskan Arctic Coastal Plain, *Global Change Biology*, *16*(6), 1870-1882.

Appendix I:

Periglacial landscape dynamics in the western Canadian Arctic: Results from a thermokarst lake record on a push moraine (Herschel Island, Yukon)

Josefine Lenz[1,2], Michael Fritz[1], Lutz Schirrmeister[1], Hugues Lantuit[1], Matthew J. Wooller[3,4], Wayne H. Pollard[5] and Sebastian Wetterich[1]

[1] Department of Periglacial Research, Alfred Wegener Institute Helmholtz Center for Polar and Marine Research, Potsdam, Germany

[2] Institute of Earth and Environmental Sciences, University of Potsdam, Germany

[3] University of Alaska Fairbanks, Water & Environmental Research Center and School of Fisheries & Ocean Sciences, Fairbanks, Alaska, U.S.A.

[4] University of Alaska Fairbanks, Alaska Quaternary Center, Fairbanks, Alaska, U.S.A.

[5] McGill University, Department of Geography, Montréal, Quebec, Canada

Published in: Palaeogeography, Palaeoclimatology, Palaeoecology,

DOI: 10.1016/j.palaeo.2013.04.009

Key words: Paleolimnology, Holocene Thermal Maximum, thermokarst, permafrost, Canadian Arctic, Herschel Island

I-1 Abstract

Ice-rich permafrost landscapes are sensitive to climate and environmental change due to the melt-out of ground ice during thermokarst development. Thermokarst processes in the northern Yukon are currently not well-documented. Lake sediments from Herschel Island (69°36'N; 139°04'W) in the western Canadian Arctic provide a record of thermokarst lake development since the early Holocene. A 727-cm long lake sediment core was analyzed for radiographic images, magnetic susceptibility, granulometry, and biogeochemical parameters (organic carbon, nitrogen, and stable carbon isotopes). Based on eight calibrated AMS radiocarbon dates, the sediment record covers the last ~ 11,500 years and was divided into four lithostratigraphic units (A to D) reflecting different thermokarst stages. Thermokarst initiation at the study area began ~ 11.5 cal ka BP. From ~ 11.5 to 10.0 cal ka BP, lake sediments of Unit A started to accumulate in an initial lake basin created by melt-out of massive ground ice and thaw subsidence. Between 10.0 and 7.0 cal ka BP (Unit B) the lake basin expanded in size and depth, attributed to talik formation during the

Holocene Thermal Maximum. Higher-than-modern summer air temperatures led to increased lake productivity and widespread terrain disturbances in the lake's catchment. Thermokarst lake development between 7.0 and 1.8 cal ka BP (Unit C) was characterized by a dynamic equilibrium, where lake basin and talik steadily expanded into ambient ice-rich terrain through shoreline erosion. Once lakes become deeper than the maximum winter lake ice thickness, thermokarst lake sediments show a great preservation potential. However, site-specific geomorphic factors such as episodic bank-shore erosion or sudden drainage through thermo-erosional valleys or coastal erosion breaching lake basins can disrupt continuous deposition. A hiatus in the record from 1.8 to 0.9 cal ka BP in Lake Herschel likely resulted from lake drainage or allochthonous slumping due to collapsing shore lines before continuous sedimentation of Unit D recommenced during the last 900 years.

I-2 Introduction

Beginning with the Pleistocene-Holocene transition, the waning of the Laurentide Ice Sheet (LIS) led to a complete reorganization of landscapes that were formerly ice-covered or situated in proximity to the ice margin (Kaufman & Manley 2004). Ice-rich permafrost landscapes like moraine belts quickly changed their morphology, hydrology, and depositional dynamics due to thermokarst processes related to the melt-out of ground ice and thaw settlement (e.g. Czudek & Demek 1970, Rampton 1974, 1982, 1988, Murton et al. 1998). Periglacial landscapes are sensitive to climate and environmental changes (e.g. Burn & Zhang 2009) and these changes can be recorded in thermokarst lake sediments (Murton 1996). So far, there exist only a few paleoenvironmental datasets from push moraines in the western Canadian Arctic that aim at reconstructing the variety of environmental responses from a periglacial perspective taking into account thermokarst onset, lake basin development, and limnogeological succession (Rampton 1988, Spear 1993, Murton 1996, 2001).

Rapidly ameliorating temperatures during the Bølling/Allerød interstadial (~ 14.7 to 13 cal ka BP) are documented in the northern Yukon, inferred from pollen spectra and chironomid assemblages (Viau et al. 2008, Kurek et al. 2009, Fritz et al. 2012a, Irvine et al. 2012). However, regional lake development was probably still suppressed due to sustained dry conditions caused by continentality effects (Burn 1997) of a lower glacio-eustatic sea level (Hill et al. 1985, Keigwin et al. 2006) and an almost permanent sea-ice cover (Bradley & England 2008, Scott et al. 2009). Between 13 and 8 cal ka BP thermokarst activity occurred widely on the arctic coastal plains of Canada (Rampton 1974, 1982, 1988) and Alaska (Williams & Yeend 1979, Carter 1988, Hopkins & Kidd 1988) and on the plains of northeast Siberia (Tomirdiaro 1982, Romanovskii et al. 2000) during the Holocene Thermal Maximum (HTM, Kaufman et al. 2004). Thermokarst activity was extremely intense at 10–9 cal ka BP, causing widespread terrain disturbance, regional

active-layer deepening (Mackay 1978, Burn 1997, Murton et al. 1997), numerous retrogressive thaw slumps, and the development of thermokarst basins in ice-rich terrain (Rampton 1974). Ponds formed at locations with high relief, incomplete deglaciation, or postglacial ground ice aggradation, and developed into thermokarst lakes as the basins expanded. As climate warming ceased during the middle Holocene (e.g. Ritchie 1984), thermokarst activity diminished (Rampton 1974). Today, thermokarst lakes in continuous permafrost regions are actively and rather constantly expanding as a result of surface permafrost degradation (Smith et al. 2005, Jones et al. 2011). In coastal areas, thermal degradation of permafrost occurs locally and episodically, for example in areas of coastal erosion (Lantuit et al. 2012). Records documenting postglacial landscape evolution and paleoenvironmental change at the northwestern LIS margin in a coastal setting are rare and often focus on vegetation changes (e.g. Ritchie & Hare, 1971, Ritchie et al. 1983, Spear 1993, Vardy et al. 1997). Thermokarst lakes and their sedimentary records often go unrecognized (Hopkins & Kidd 1988, Murton 1996) though they have a high preservation potential (Murton 2001).

Here, we present a multi-proxy paleoenvironmental reconstruction using sediments from a thermokarst lake located on a push moraine that makes up Herschel Island. This study highlights the limnogeological succession of a thermokarst lake in an ice-rich arctic periglacial environment since the beginning of the Holocene. Our dataset represents the northernmost postglacial paleoenvironmental archive of the Yukon and one of the northernmost in the western Canadian Arctic, where multi-proxy analyses on lacustrine sequences are rare. We put this dataset into context with existing regional records covering the last glacial–interglacial transition and the Holocene to assess the paleoenvironmental significance of thermokarst lake sediment records for portraying regional climate evolution and to distinguish this from effects of local permafrost conditions leaving their imprint in the sedimentary record.

I-3 Study area

The Coastal Plain of the Yukon in Canada (Figure I-1) extends north–south over approximately 24 km and spans 200 km from west to east, from the Alaska–Yukon border to the Mackenzie River delta (Bouchard 1974). Signs of glacigenic deformation and glacial deposits, such as morainic ridges and erratic boulders, attest to the presence of a major glacial advance in the area extending from Shingle Point westward beyond Herschel Island (Rampton 1982). Herschel Island (69°36’N; 139°04’W), the northernmost part of the Yukon, is located 250 km northwest of Inuvik (Northwest Territories), 60 km east of the Alaska–Yukon border, and 3 km off the mainland coast

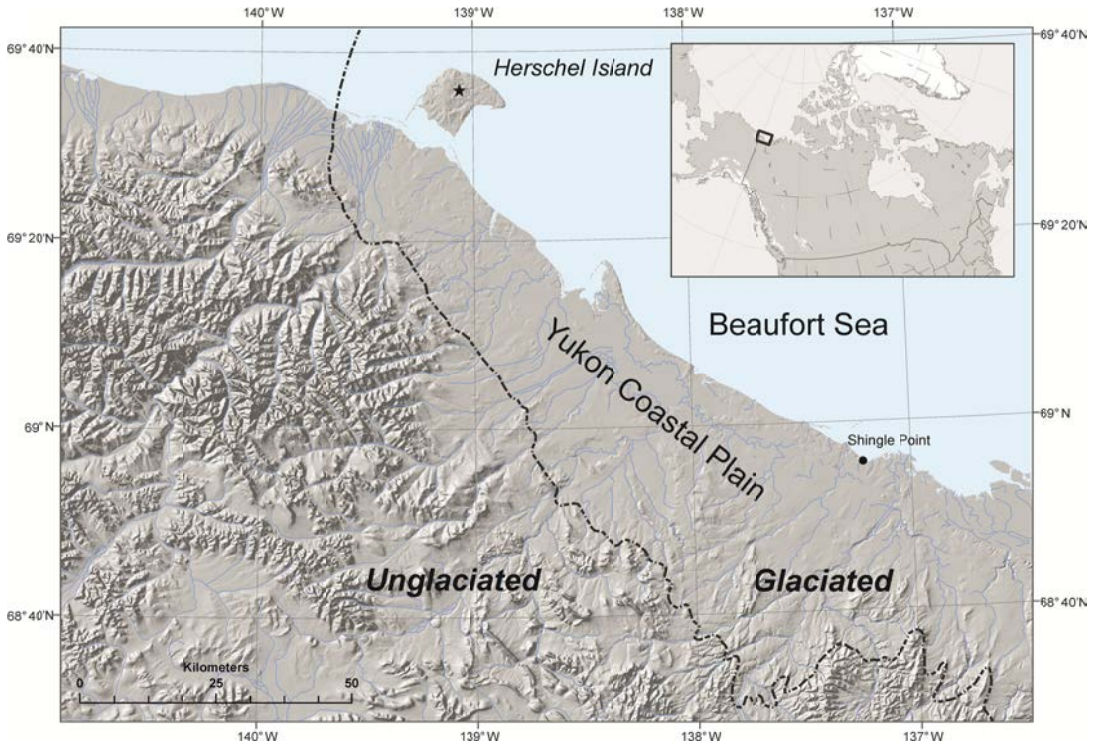

Figure I-1: Study area map. Coring location on Herschel Island (Lake Herschel) is marked with an asterisk. Glacial limit along the Yukon coast according to Smith et al. (1989), adapted from Rampton (1982) and Dyke & Prest (1987).

(Figure I-1). This rhombic-shaped island has an area of 108 km^2 and a maximum elevation of 183 m above sea level (m asl) (de Krom 1990). The push moraine of Herschel Island ridge is of Pleistocene origin and was formed by LIS glacier ice-thrusting of material from the subaerially exposed continental shelf that later became Herschel Island and the offshore Herschel Basin after Holocene sea level rise (Mackay 1959, Burn 2009). The island is primarily composed of upthrust beds of shell-bearing and salty marine sands, silts, and silty clays containing different forms of ground ice. Ground ice on Herschel Island constitutes up to 70 % of the upper 10 to 15 m of permafrost and occurs as segregated ice lenses, ice-wedges, pore ice, and massive tabular ice bodies in the form of buried glacier ice, snow bank ice, and massive segregated ice (Pollard 1990). Ice-wedge polygons have formed since deglaciation in flat areas of the island; some have evolved into thermokarst ponds.

Lake Herschel (informal name) is about 0.126 km^2 in area and is located in the center of Herschel Island at an elevation of about 75 m asl (Figure I-2). The lake is subcircular and 400 m in diameter, with a maximum water depth of about 6 m (Figure I-2). The main part of the relatively small catchment area (~ 0.5 km^2) is situated west of the lake where the hinterland elevation is as high as 100 m asl and where influent water is supplied. Groundwater flow to the lake is controlled by a shallow permafrost table; an active-layer depth of about 25 cm was

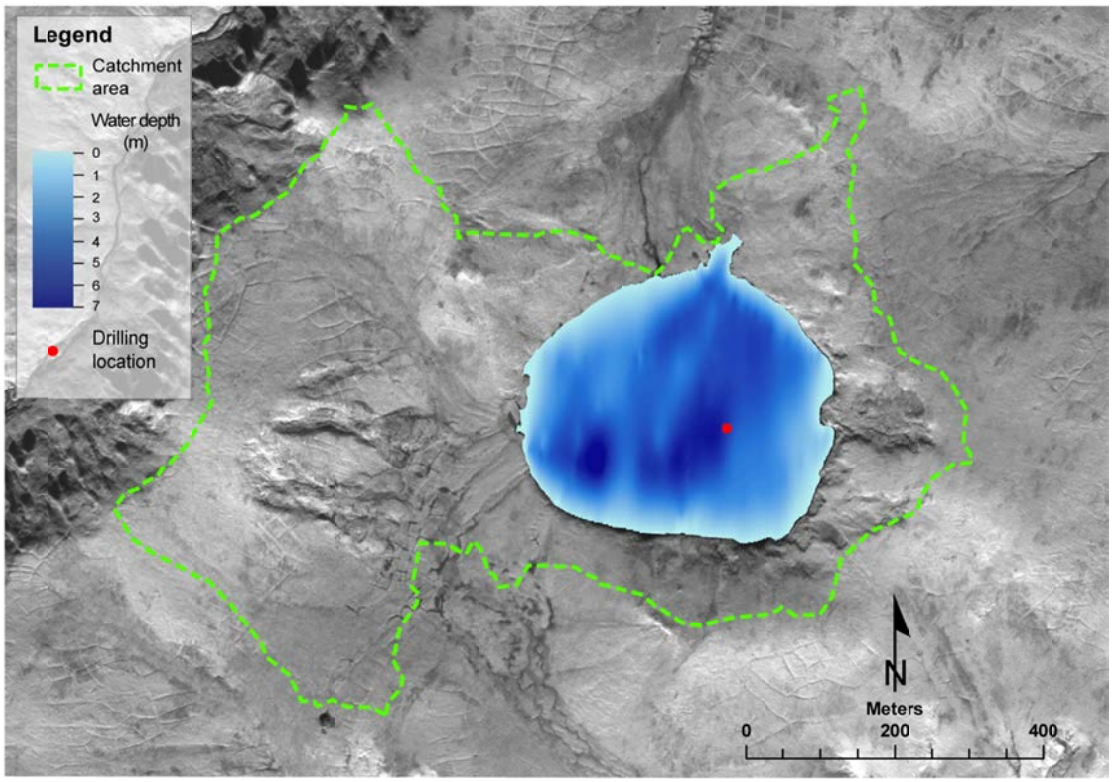

Figure I-2: Bathymetry and catchment area of Lake Herschel. Coring location is marked by a red dot. Bathymetry was created by interpolation of individual soundings using ArcGIS and displayed in an IKONOS (2000) satellite image.

measured adjacent to the lake. Spatial variations in active-layer thickness and near-surface ground ice conditions are described in detail by Burn & Zhang (2009). Lake water temperatures ranged from about 8 °C in summers 2006, 2008, 2009, and 2010 to about 1 °C below the ice cover in spring 2009 (Table I-1). Uniform values of temperature, electrical conductivity (EC) and pH measured in summer 2008 at depths of 150, 350, and 500 cm indicate a mixed water body in summer and confirm a cold-monomictic lake circulation. The relatively high modern lake water EC of about 1000 µS/cm is typical for an athalassic brackish environment. The major lake water ion source is likely the salty upthrust marine sediments (Kokelj et al. 2002, Fritz et al. 2012b). The increased EC in winter is explained by a ~ 2 m thick ice cover (April 2009) that concentrates ions in the liquid phase.

Table I-1: Hydrochemical characteristics of water samples taken from Lake Herschel at different depths and from different seasons.

Date of sampling	Water depth (cm)	pH	EC (µS cm^{-1})	T (°C)
August 2008	0	-	1095	-
April 2009	0	7.50	2303	1.2
July 2010	0	7.22	1119	-
July 2006	40	8.31	1096	8.3
August 2008	150	8.34	1095	8.5
August 2008	350	8.27	1093	8.4
August 2008	500	8.32	1098	8.4

I-4 Material and methods

The bathymetry of Lake Herschel was measured with echo sounding through drill holes in the lake ice in 2009. Pre-site surveys in 2008 yielded global positioning data (Garmin GPS 12) from the shoreline and echo-sounding data (hand-held depth sounder) from the lake basin as well as water samples from different depths. Surface water samples were taken during the summers of 2006, 2008, 2009, and 2010. EC and pH values were determined using a pH-conductivity meter (MultiLab 540, WTW).

A 727-cm long sediment core (core code: PG1967) was retrieved from Lake Herschel in April 2009 with a piston corer (UWITEC) in a water depth of 527 cm. The piston corer was operated with a tripod on the ~2 m thick lake ice. The PVC liner filled with sediments was cut into pieces of up to 100 cm and stored cold, but unfrozen, until laboratory analysis. The working half was used for destructive analyses (e.g. granulometry and biogeochemical analyses), whereas nondestructive analyses (e.g. radiographic images and mass-specific magnetic susceptibility [MS]) were conducted using the archive half of the core.

Radiography profiles based on X-ray were used to display density differences and to describe bedding, bioturbation, and deformation structures. The ITRAX core scanner at the University of Cologne (Germany) operates at 55 kV and 50 mA and creates 2D positive radiographic images with a resolution of 200 µm without automatic gray level adjustments as well as high-definition photographs with an optical camera system (Croudace et al. 2006).

The mass-specific MS was measured with a Multi-Sensor Core Logger (GEOTEK, MSCL) and is expressed in SI units (10^{-5} m^3 kg^{-1}). The water content was calculated using the weight difference between fresh and freeze-dried bulk sediment samples and is expressed as weight percentage (wt%). The grain size distribution was measured (according to EN ISO 14688) using a laser particle size analyzer (Coulter LS 200) from which the organic matter had been previously removed with hydrogen peroxide (H_2O_2, 30 %).

Total nitrogen (TN), total carbon (TC), and total organic carbon (TOC) were measured with an elemental analyzer (Elementar Vario EL III, with an analytical accuracy of ± 0.1 wt%). The total inorganic carbon (TIC) content was calculated using the TC and TOC data (TIC = TC − TOC). The calcium carbonate content was calculated from the TIC using the molar mass ratio of calcium carbonate and carbon ($CaCO_3$ = 8.33*TIC). The C/N-ratio (TOC/TN) was calculated as an indicator for organic matter origin and $\delta^{13}C$ values of TOC were measured using an elemental analyzer (Carlo-Erba CN2500) attached to a stable isotope ratio mass spectrometer (DELTAplusXL, Finnigan) at the German Research Centre of Geosciences (GFZ) in Potsdam,

Germany. $\delta^{13}C_{TOC}$ values are expressed relative to the Vienna Pee Dee Belemnite (V-PDB) standard in per mill (‰) and the analytical precision was ≤ ± 0.02 % (1σ).

Accelerator Mass Spectrometry (AMS) radiocarbon age determination of macroscopic plant remains and mollusk shells was carried out on wet-sieved and hand-picked samples (> 250 µm). Nine samples of plant detritus including moss, leaves, and wood remains, and one sample of two connected mollusk valves (*Pisidium* sp.) were dated at the Poznan Radiocarbon Laboratory (Poland). The AMS dates were calibrated using CALIB 6.0 and INTCAL09 (Reimer et al. 2009). All geochronological dates in this study are reported in calibrated years before 1950 AD, referred as before present (cal ka BP).

I-5 Results

I-5.1 Core lithology

The sediment from Lake Herschel core PG1967 is characterized by gray, consolidated, fine-grained deposits with irregularly interbedded strata. Based on lithological descriptions, radiographic images, photographs, and the analyzed sedimentary parameters, the core is divided into four lithostratigraphic units:

- Unit A: 727–700 cm
- Unit B: 700–600 cm
- Unit C: 600–200 cm
- Unit D: 200–0 cm

The boundaries at 700 cm (between Units A and B) and 200 cm (between Units C and D) are evident from changes in sediment texture and structure, and are confirmed by variations in grain size parameters, density, water content, MS, and biogeochemical parameters, whereas the boundary at 600 cm (between Units B and C) is primarily based on changes of biogeochemical parameters.

Unit A is composed of light-gray, compact, fine-grained clayey sediment that does not contain any visible biogenic fossil matter. The material is compact and weakly bedded (Figure I-3). The transition to Unit B is marked by minerogenic material with embedded wood remains at 697, 703, and 705 cm depth. Alternations of organic-rich dark-gray and minerogenic light-gray beds occur in Unit B every 6 to 17 cm. A peaty layer at 683 to 684 cm depth was sampled for radiocarbon dating. Plant and mollusk remains are present at 646 to 647 cm core depth. Unit C sediment is gray and is less moist and less consolidated than Unit B sediment, with frequent recurring layers. Mollusk remains are present at 572 to 574 cm, wood remains at 498 cm, and

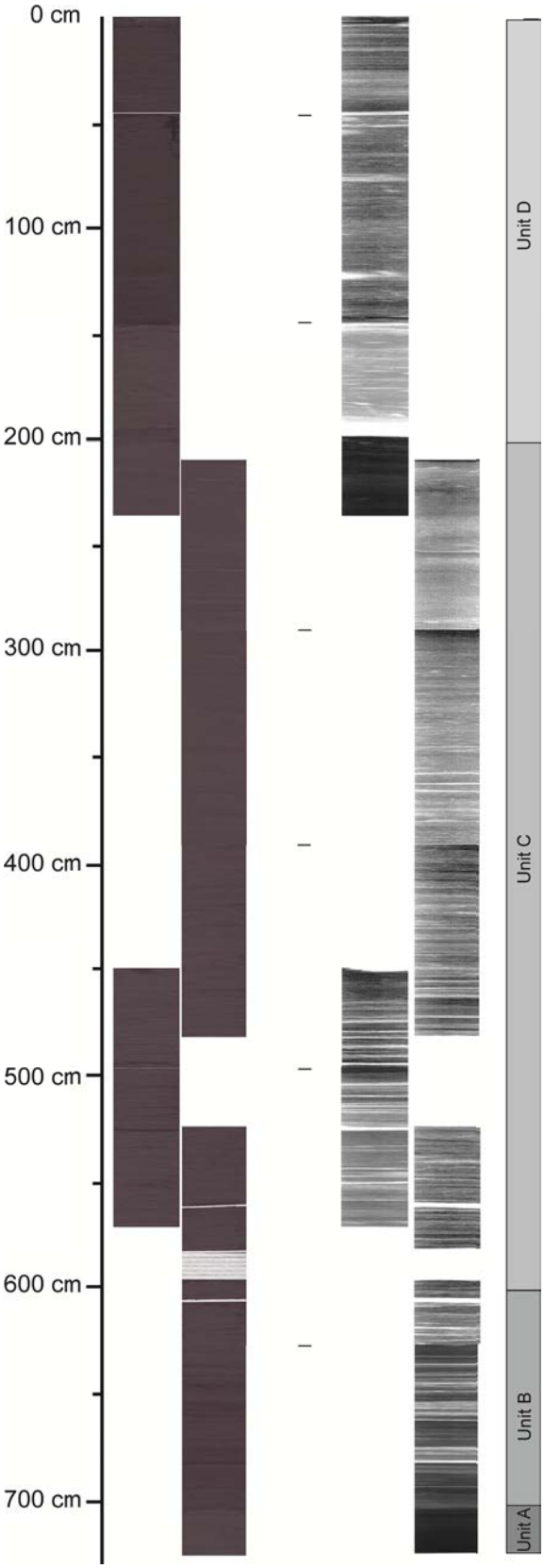

Figure I-3: Down-core high-resolution photographs (left), radiographic images (right) and lithostratigraphic units (far right) of Lake Herschel sediment core PG1967.

plant fragments at 528 and 366 to 367 cm. Material extrusion upon core recovery due to degassing of methane after decompression likely caused gaps of 2 to 15 cm between 515 and 610 cm core depth. Small-scale crevices (< 1 mm) with brown discoloration due to iron oxidation are located at organic-rich layers between 468 and 527 cm. A distinct light-gray sandy bed of coarser grain size from 197 to 204 cm is followed by an organic-rich and more fine-grained dark-gray layer at 194 to 197 cm. This marks the boundary between Unit C and Unit D. A pebble of 1 cm in diameter is present at 198 cm. Within Unit D, minerogenic light-gray layers (about 4 mm thick) alternate with dark-gray organic-rich sandy layers (about 2 mm thick). Unit D sediment is less compact than the sediments of the units below. Dark organic-rich material is visible at 126 cm and between 145 and 148 cm depth; mollusk shells occur at 57 to 61 cm.

I-5.2 Radiography

The positive radiographic images show a distinct change in sediment structure along the core (Figure I-3). Except for the weakly bedded and rather dense material composing Unit A, the sediments are laminated, as indicated by areas of lower and higher density. Between 700 and 350 cm (Unit B and the lower half of Unit C) the sediment core shows stronger contrast between thin layers less than 1 mm thick. The upper half of the core (350 cm to the top) is also layered but with less contrast between individual layers. The boundary between Units C and D is marked by a distinct high density area below 200 cm and a

very low density area from above 200 cm to the top. Besides this boundary, and apart from the described gaps in Unit C, low density areas are visible at 10, 70, 120, and 360 cm. Distinct low density layers are present at 530 and 690 cm within the layered Units C and B.

I-5.3 Magnetic susceptibility and water content

The MS data vary between 6.4 and 19.7 (Figure I-4). The Unit A MS is nearly constant, ranging between 14.0 and 15.0, whereas the Unit B MS ranges from 7.3 to 13.2 and exhibits the highest variability of all the core units. A step towards lower values at 480 to 500 cm and a general trend of declining values, from about 15.0 to 10.0, with depth are notable in Unit C. At the boundary between Units C and D, a significant change in MS is evident where values decrease from 14.2 to 6.4; they remain at a low level (7.2 to 9.0) in Unit D.

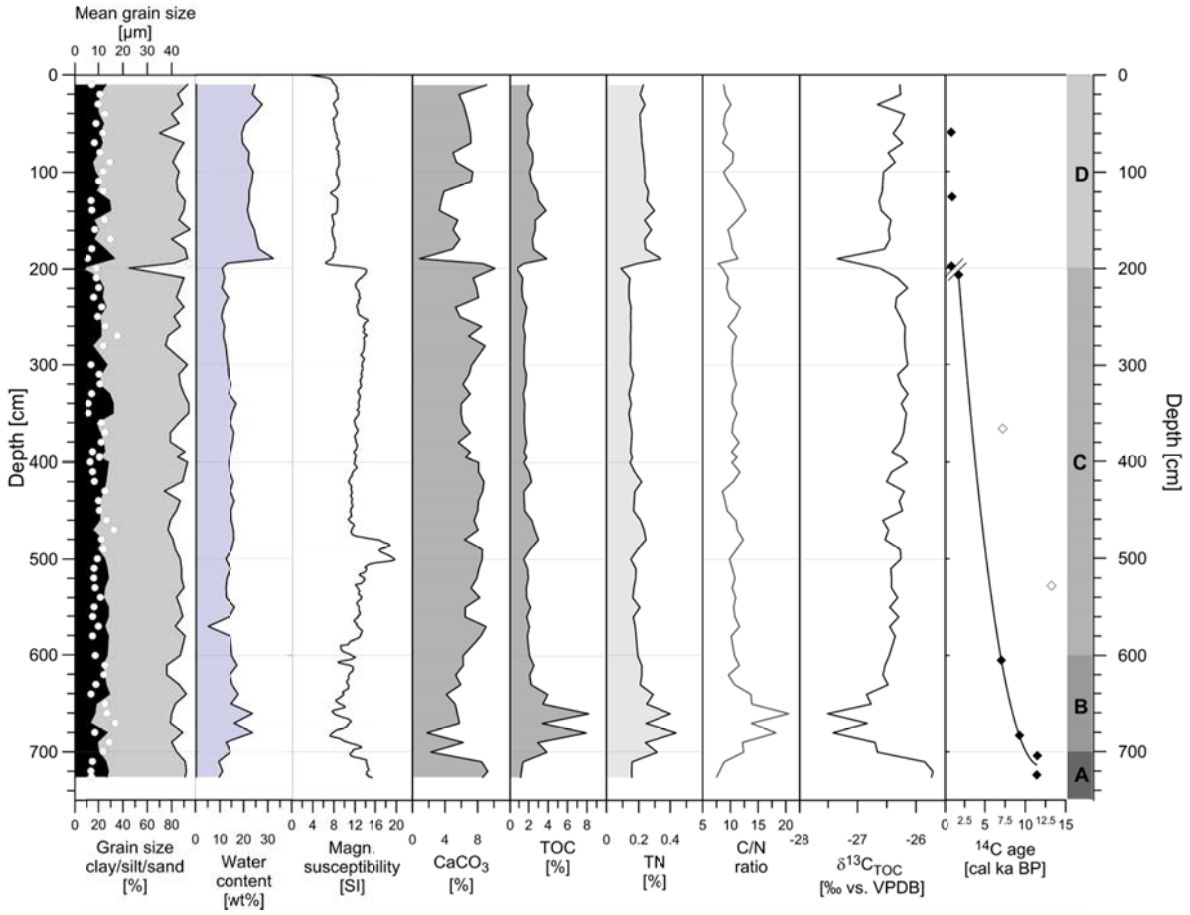

Figure I-4: Results of grain size analyses, water content, magnetic susceptibility, $CaCO_3$, TOC, TN, C/N ratio, values of $\delta^{13}C_{TOC}$, and AMS radiocarbon ages of the Lake Herschel sediment core. AMS dates marked with open rhombs were excluded from the age-depth relationship because the material is likely reworked. A summary table of sedimentological parameters from lake sediment core #PG1967 (Herschel Island, Yukon) can be found in the digital appendix table I-1 to this article.

The water content of the sediment core ranges from 5.2 to 32.3 wt% (Figure I-4). A low average water content of 11.2 wt% was measured in Unit A. In Unit B, values vary between

12.6 wt% and 23.7 wt% with higher water content in organic-rich layers. The average water content in Unit C is about 14.1 wt% with values ranging from 10.7 to 16.9 wt%, except for a significant minimum of 5.2 wt% at 570 cm. At the transition from Unit C to D a significant increase in water content was measured. With the exception of the relatively high value (32.3 wt%) at 190 cm, the Unit D water content is uniform, but at 21.9 wt% on average it is almost twice as high as in Unit C.

I-5.4 Grain size distribution

The observed 2 to 5 mm thick laminations are not resolved by our sampling interval of 10 cm. Therefore, the granulometrical results integrate the laminations and general trends in sedimentological variations. According to the nomenclature used by Shephard (1954), the sediment core is dominated by clayey to sandy silt (Figure I-5). The mean grain size ranges from 5.7 µm (fine silt) to 17.8 µm (coarse silt) with a sandy outlier at 200 cm (Figure I-4). The pattern of grain-size distribution usually shows bimodal to trimodal curves with a major peak in the fine-silt fraction and a minor peak in the fine-sand fraction reflecting the observed fine lamination. There is a distinct peak of very-poorly-sorted fine sand from 200 to 201 cm. The sediment of the whole core is poorly to very-poorly sorted (3.5 to 6.4, 4.8 on average, after Folk & Ward 1957).

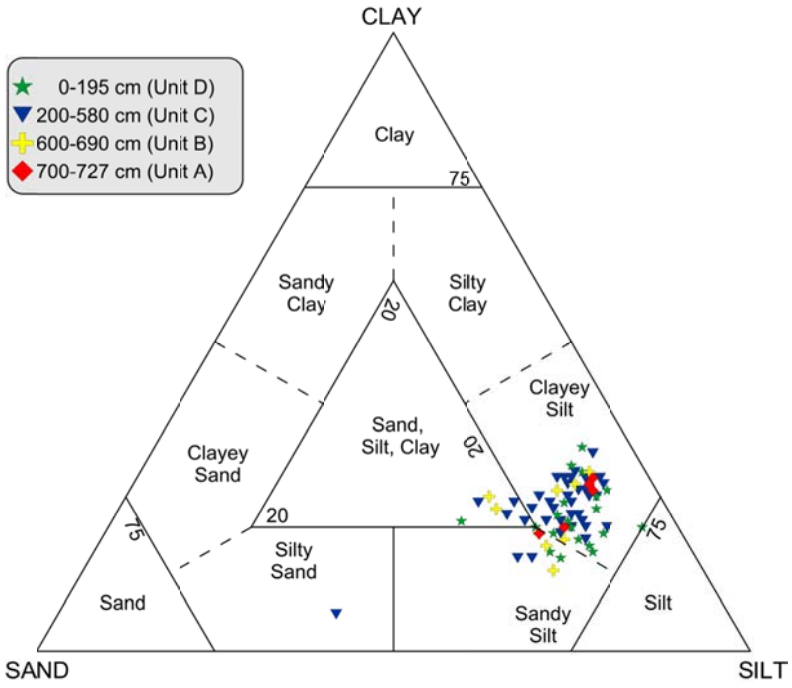

Figure I-5: Grain size characteristics from Lake Herschel sediment core displayed in a sediment triangle according to Shephard (1954).

I-5.5 Biogeochemical characteristics

In Unit A, the TN is 0.2 %, the TOC is 1.9 %, and the mean C/N ratio is 9.2. The calculated $CaCO_3$ content is relatively high (median = 7.2 %) in Unit A. Unit B exhibits the highest content and largest variance of TN and $CaCO_3$ values (TN_{max} of 0.4 %, $CaCO3_{min}$ of 1.8 %). TOC content in Unit B is between 2.1 and 8.2 %. C/N ratios range between 20.5 at 660 cm and 9.6 at 620 cm depth. Less variation in the biogeochemical parameters is found in Unit C. TN values are low (TN_{max} of 0.2 %) and slightly decrease upwards to the device-specific accuracy of 0.1 %. TOC values show minimal changes (median = 1.8 %). The C/N ratio (median = 10.5) is moderate without major variations. The $CaCO_3$ content ranges from 5.3 to 9.1 % (median = 7.5 %). Except for increases in TN and TOC at 430 cm and at 470 to 480 cm, respectively, the values are almost constant. At the boundary between Units C and D (at 200 cm) all biogeochemical parameters indicate a distinct change. After a decrease in TN and TOC at 200 cm (TN < 0.1 %; TOC 0.8 %) an increase follows (TN 0.3 %; TOC 8.9 %). At this transition the $CaCO_3$ content decreases by 9.2 % (from 10.1 to 0.9 %). Unit D shows minor variations. TN varies from 0.2 to 0.3 % from 140 to 170 cm and TOC values are between 2.4 and 3.8 %.

The $\delta^{13}C_{TOC}$ values from core PG1967 range between -27.5 and -25.7 ‰, reflecting mostly a lacustrine organic carbon source deriving from C3 photosynthesis (Meyers 1994). In Unit A, $\delta^{13}C_{TOC}$ values are between -26.7 and -25.7 ‰. $\delta^{13}C_{TOC}$ values in Unit B have a mean value of -26.8 ‰ with a maximum of -26.5‰ at 600 to 610 cm depth (upper boundary of Unit B) and minima of -27.5 ‰ and -27.4 ‰ at 660 cm and 680 cm (lower boundary of Unit B). Almost no $\delta^{13}C_{TOC}$ variation was found in Unit C; values range between -26.6 and -26.1 ‰. The boundary between Units C and D coincides with a decrease in $\delta^{13}C_{TOC}$ values from -26.7 to -27.3 ‰ at 190 cm. In Unit D the $\delta^{13}C_{TOC}$ values range between -27.3 and -26.2 ‰.

I-5.6 Geochronology

An age-depth relationship was established using eight out of ten AMS radiocarbon dates from the sediment core (Figure I-4, Table I-2). A squared regression model ($y = -5.1721*10^{-6}x^2 + 0.1205x + 12.1237$; $r^2 = 0.99$) was used for age interpolation between Units A, B, and C. No interpolation was applied between individual Unit D datings as they show concordant ages of about 900 years BP within two standard deviations. According to the dating results, the sediment record covers the last ~ 11,500 years. The basal part of the sediment sequence (Unit A) was deposited between ≥ 11.5 and 10.0 cal ka BP (Figure I-4). Unit B covers the time span from 10.0 to 7.0 cal ka BP. Unit C was dated at 7.0 to 1.8 cal ka BP. Finally, Unit D represents the most recent 900 years, indicating rapid sedimentation of the uppermost ~ 200 cm. Dating of organic macro remains directly below and above the lithostratigraphic boundary between Units C and D revealed a hiatus between 1.8 and 0.9 cal ka BP, probably due to lake drainage or slumping of bankside material. Both hypotheses are discussed below in section I-6. Two age determinations of ~ 13.2 cal ka BP

and 7.2 cal ka BP at 525 cm and 367 cm, respectively, yielded anomalously old dates compared to ambient ages. These dates are considered to originate from material that has been reworked and are not used for further interpretation. Re-deposition of terrestrial organic matter by slumping of bankside material could cause the deviation from superposition, which is quite common in sediments of thermokarst lakes (Murton 1996) that formed by thaw subsidence and were influenced by active shore erosion within older deposits (Wetterich et al. 2009).

Table I-2: AMS-^{14}C age determination and calibrated ^{14}C ages using the CALIB 6.0 software with the terrestrial radiocarbon age calibration INTCAL09 (Reimer et al. 2009) of material from Lake Herschel sediment core PG1967. [a] Poz = Poznan Radiocarbon Laboratory, [b] not used for reasons explained in the text.

Core depth (cm)	Dated material	Mass (mg C)	δ^{13}C (‰)	Uncalibrated ^{14}C age (a BP)	Calibrated 2σ-age range (cal a BP)	Mean 2σ-age (cal a BP)	Lab. No.[a]
57-61	Mollusc shell (*Pisidium* sp.)	0.2	-8.4	920 ± 40	759-923	840	Poz-36423
126	Undefined moss and wood fragments	> 1	-27.9	985 ± 30	895-959	930	Poz-36425
197-199	*Drapanocladus* sp.	0.5	-32.0	950 ± 35	788-930	860	Poz-49515
206-208	Vascular plant fragments	0.7	-25.7	179 ± 30	1,687-1,818	17,50	Poz-49516
366-367	Undefined moss fragments	> 1	-27.8	6,230 ± 40 [b]	7,144-7,255	7,200	Poz-36426
528	Vascular plant fragments	> 1	-27.4	11,370 ± 70 [b]	13,111-13,363	13,240	Poz-36427
604-606	*Homalothecium nitens*	0.6	-29.9	6,160 ± 50	6,906-7,175	7,040	Poz-49517
683	Undefined wood fragments	> 1	-30.4	8,290 ± 50	9,127-9,438	9,280	Poz-36428
703-705	*Homalothecium nitens*, *Carex* sp.	0.5	-34.1	9,990 ± 60	11,252-11,717	11,490	Poz-49519
723-725	undefined wood fragments	> 1	-31.9	9,980 ± 50	11,253-11,633	11,440	Poz-49520

I-6 Discussion

I-6.1 Evolution of Lake Herschel

An extensive Late Wisconsin advance of the LIS towards the northern Yukon and Northwest Territories is documented by Dyke et al. (2002) and Kennedy et al. (2010). Relatively young ages are assumed for this last regional advance (Zazula et al. 2009: 20.0 cal ka BP, Mackay and Dallimore 1992: 18.0 to 17.0 cal ka BP, Murton et al. 2007: 17.0 to 15.0 cal ka BP, and Fritz et al. 2012a,b: ~ 16.0 cal ka BP). Glacial push-up of pre-existing ice-rich permafrost formed the Herschel ridge and incomplete glaciation left behind a landscape with high relief energy and abundant basal glacier ice among other types of massive ground ice. This is illustrated in Figure I-6a as the pre-lake stage.

Initial lake phase

Thermokarst in general and thermokarst lake development in particular commenced after deglaciation. Rapidly rising air temperatures at the Pleistocene-Holocene transition led to the melt-out of massive ground ice, accompanied by surface subsidence and water pooling in depressions underlain by permafrost and a semi-permeable clayey diamicton. We consider Unit A to represent the initial phase of lake genesis, and thus, the minimum age of thermokarst onset is at or prior to 11.5 cal ka BP (Figure I-6b). This is in agreement with studies from the northern Yukon and Northwest Territories where the frequency distribution of basal dates from thaw lake sediments and in-situ rootlets from the base of a regional paleo-active-layer indicate a thermokarst onset at around 10 ka BP (i.e. ~ 11.7 to 11.2 cal ka BP) (Rampton 1974, 1982, 1988, Mackay 1978, Burn 1997, Murton et al. 1997). Herschel Island is highly susceptible to thermokarst processes and thermal erosion (Mackay 1959, Lantuit & Pollard 2008), as indicated by the occurrence of numerous retrogressive thaw slumps at coastal sites. This fact is due to the widespread occurrence of ice-rich permafrost (Bouchard 1974), near-surface ground ice (Burn & Zhang 2009), and large bodies of massive ice to depths of more than 30 m below surface (Pollard 1990, Fritz et al. 2011).

Since Lake Herschel is currently the largest lake on Herschel Island, the site was particularly susceptible to ground ice melting. Surface subsidence was likely followed by the accumulation of water in an initial depression within a landscape of undulating morphology. Massive ground ice bodies of nearly pure ice are known from permafrost outcrops along the coast (Pollard 1990, Moorman et al. 1996, Fritz et al. 2011). Herschel Island is mainly composed of a frozen marine and clayey diamicton (Mackay 1959, Bouchard 1974, Fritz et al. 2012b). Therefore, suitable preconditions for pooling of water are provided by this compact semi-permeable to impermeable basal material.

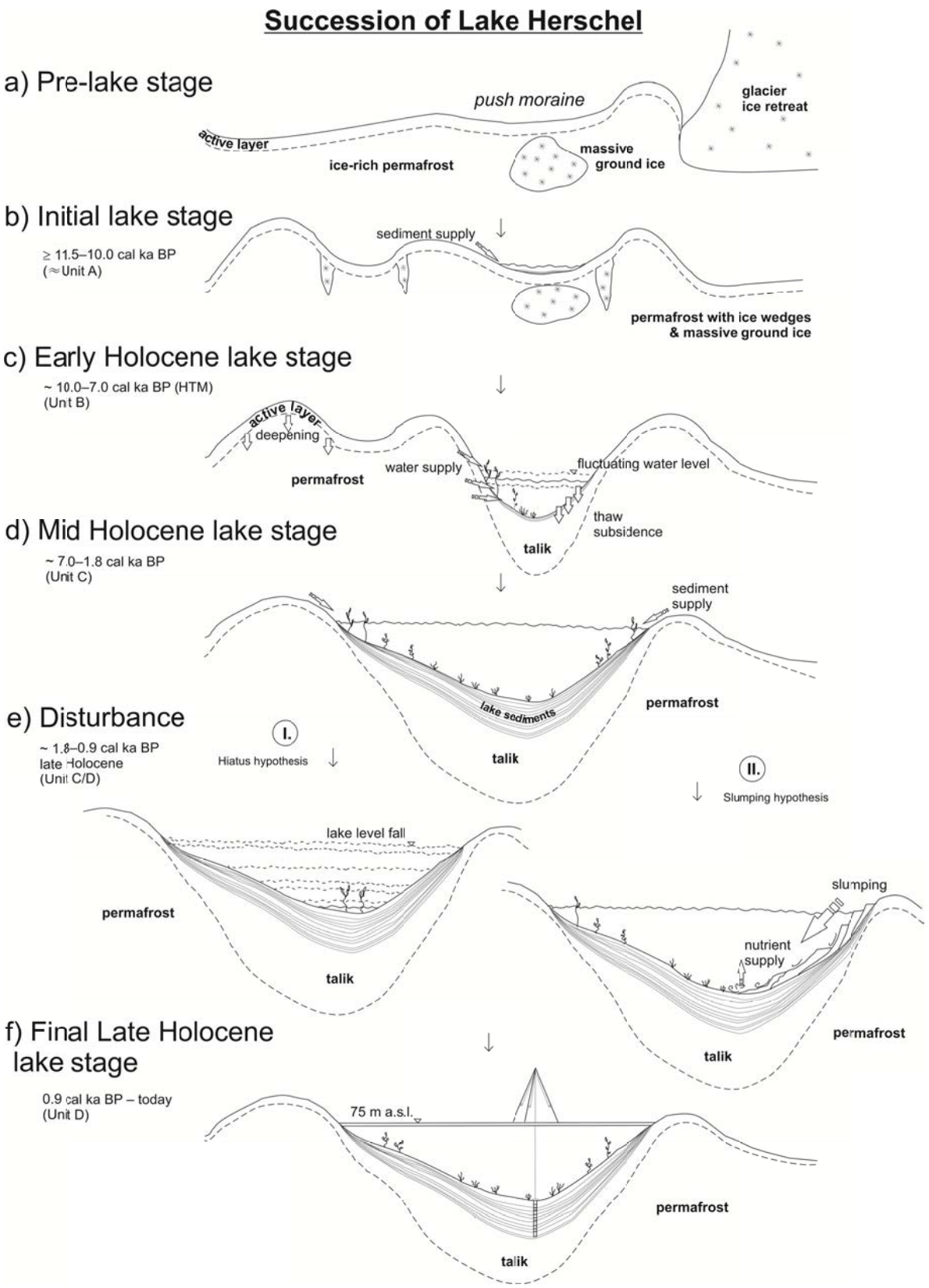

Figure I-6: Schematic synthesis of the evolution of thermokarst lakes on Herschel Island under conditions of ice-rich permafrost as discussed in this paper.

Thermokarst lakes will not develop if the warmed water percolates through the ground and only deepens the active-layer (Harris 2002). But if the water from melting ground ice or snow pools in basins and remains on the surface, absorption of incoming radiation is increased compared to the surrounding surface. Increased thawing of ice-rich permafrost and thaw subsidence form a positive feedback mechanism (Harris 2002).

Early Holocene lake phase

The Pleistocene–Holocene transition was a period of rapid environmental change. In this context, the evolution of Lake Herschel started as a thermokarst basin. Thermokarst development likely peaked during the HTM, which is a post-glacial warm period with warmer-than-modern summer air temperatures lasting from about 10.6 to 6 cal ka BP in northwestern Canada (Kaufman et al. 2004). Maximum Holocene summer air temperatures caused maximum active-layer deepening accompanied by intense ground ice melt-out and thaw subsidence (e.g. Burn 1997). Lateral lake basin expansion caused shore-line erosion which in turn led to higher lake productivity due to increased nutrient input (Kokelj et al. 2005).

The growing Lake Herschel basin was possibly characterized by a fluctuating lake level (Figure I-6c) and alternation in the relative inputs of lacustrine vs. terrestrial organic matter, as evident from the variable C/N-ratios and $\delta^{13}C_{TOC}$ values (Figure I-7). High bioproductivity inferred by up to 0.4 % TN and 8.2 % TOC content could be explained by a shorter duration of lake-ice coverage and a longer growing season during the early Holocene warming.

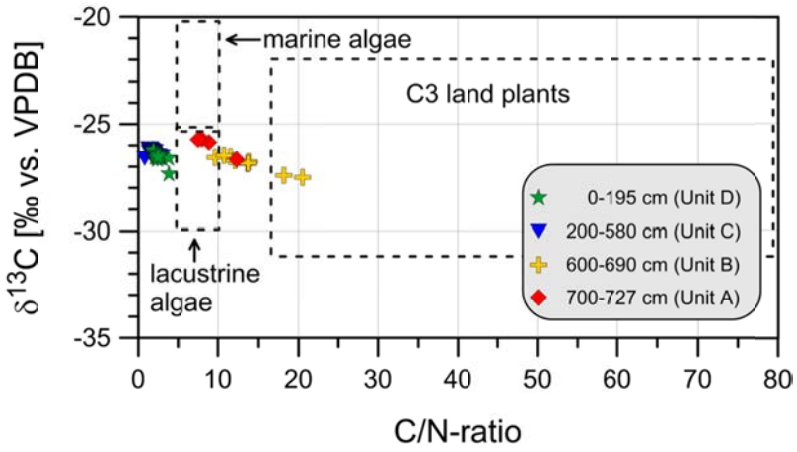

Figure I-7: $\delta^{13}C_{TOC}$ values and C/N-ratios of bulk organic matter from Units A (red diamonds), B (yellow crosses), C (blue triangles) and D (green stars) presented relative to the ranges for organic matter produced by C3 land plants, marine algae, and lacustrine algae (according to Meyers 1994 and Meyers & Lallier-Verges 1999).

Similar characteristics (MS, water content, C/N) of lake sediments deposited during the HTM are described for Lake CF3 (Briner et al. 2006) and for Brother Lake and Fog Lake (Francis et al. 2006) on Baffin Island (Canadian Arctic Archipelago). We suggest that the Lake Herschel became deep enough (> ~ 2 m depth) to avoid freezing to the bottom in winter. The heat storage effect of an unfrozen water body leads to continuous thawing of underlying permafrost and creates a talik (Figure I-6c), which is a layer or body of unfrozen ground within permafrost that forms due to a local anomaly in thermal, hydrological, hydrogeological, or hydrochemical conditions (van Everdingen 2005). Any disturbance of the heat balance results in further permafrost thawing and deepening of the thermokarst lake basin. Additionally, the movement of water by wind and wave action can further contribute to thawing and shoreline erosion.

The Mid Holocene thermokarst lake phase

We consider a dynamic equilibrium of thermokarst lake development between 7.0 and 1.8 cal ka BP. The lake and the talik steadily expanded into ambient ice-rich terrain through shoreline erosion and an increase of aquatic accommodation space (Figure I-6d). The sedimentological parameters of Unit C do not indicate distinct events in terms of sediment supply or lake level fluctuations. The invariability of measured parameters (Figure I-4) reflects stable accumulation conditions with a uniform and likely lacustrine source of organic carbon (Figure I-7). A growing distance between the shoreline and our coring location might have occurred over time with lake expansion. Therefore, a directed or abrupt sediment input close to shore changed into a more continuous and diffuse input of particles as the coring location became more distal to the sediment source with lake expansion (Murton 1996).

The final Late Holocene lake stage

Unit D represents accumulation during the last 900 years (Figure I-6f). This uppermost unit is characterized by sediments with higher organic matter content as indicated by increased TOC and water contents, and by decreased MS and bulk density (Figure I-4). Here, depositional conditions differ significantly from those of the previous stage. We consider two hypotheses to explain the facies change at the transition between Units C and D that left behind a hiatus between 1.8 and 0.9 cal ka BP (Figure I-6e):

a) Hiatus hypothesis: the lake dried out or drained, causing a hiatus in sedimentation.
b) Slumping hypothesis: allochthonous slumping disturbed the continuous sedimentation.

a) Hiatus hypothesis

A hiatus between 1.8 and 0.9 cal ka BP might be explained by subaerial sedimentation after the lake dried out or rapidly drained. In this case, the last 900 years of lake development might have happened as follows. Due to increased evaporation or subsidence, reactivation, and modified inflow or drainage conditions, the water level fell and caused a higher morphological gradient. This in turn led to increased transport energy allowing coarser sediments to become deposited as recognized at 190 cm core depth. The lake at 0.9 cal ka BP was either shallow with a rising lake level that continued to rise until today, or the lake basin dried out or drained completely causing a hiatus (Figure I-6e). Thermokarst lakes can drain catastrophically within a few hours due to melt-out of ground ice (Mackay 1990, Jones et al. 2011). For example, lakes on northern Richards Island (Northwest Territories) drain because they are breached shorelines that are retreating due to coastal erosion (Dallimore et al. 2000). However, the mechanisms and interrelations, of thermokarst lake growth, expansion, and eventual drainage are still not completely understood (French 2007).

A distinct organic-rich layer directly above the minerogenic layer at the transition from Unit C to D supports the drainage hypothesis. A lake level fall could have produced the higher energy required to transport coarser sediment grains, followed by an increasing productivity of lacustrine organisms in a shallow small lake; and finally, the re-start of lacustrine deposition may have induced the accumulation of nutrient and organic-rich layers in Unit D. The high water content of up to 32.3 wt% coupled with the low density in Unit D indicates a completely different depositional environment and high accumulation rates compared with Units C and B.

(b) *Slumping hypothesis*

A slumping hypothesis is supported by differences in water content, MS, $CaCO_3$, TOC, TN, C/N ratio, and $\delta^{13}C_{TOC}$ values between Units C and D (Figure I-4). According to Kokelj et al. (2002), the geomorphological activity of mass movements could promote salt concentration due to evaporation from the surface of exposed sediments. Slumping provides not only sediments but also nutrients and soluble elements that could cause higher primary productivity, as indicated in Unit D by the relatively high TN (up to 0.3 %) and TOC content (up to 3.9 %). Organic-rich layers are also less dense compared with minerogenic sediments, as visible in the radiographic images (Figure I-3). This probably explains the higher water content measured in organic-rich layers, especially in the thick organic-rich horizon at 190 cm covering the coarser sand layer at the boundary between Unit C and Unit D.

Expanding thermokarst lakes are often characterized by frequently collapsing shore lines (Burn & Smith 1990). A corresponding inactive landslide site, currently stabilized and vegetated, is located east of the drilling location on the eastern shore (Figure I-2). Higher precipitation and higher pore-water pressures in surface sediments could have caused mass wasting processes and thaw slumps along lake shore slopes (Figure I-6). Increasing effective moisture during the late Holocene is reported from Marcella Lake in the southwest Yukon (Anderson et al. 2007). The abrupt occurrence of testate amoebae indicating freshwater to slightly brackish conditions in thermokarst lakes on Richards Island indicates eutrophic conditions within the last 3,000 years (Dallimore et al. 2000). According to Dallimore et al. (2000), higher productivity does not necessarily indicate a warming climate trend but could have been caused by changes in local limnological conditions due to morphological instability of thermokarst lakes and nutrient input (Kokelj et al. 2005). The last 900 years of thermokarst lake history demonstrate that local events such as slumping or drainage are most likely responsible for facies changes during the late Holocene.

I-6.2 Paleoenvironmental implications of the Lake Herschel record

The Herschel ridge was formed by glacier-ice thrust and the responsible ice advance has recently been timed to as late as ~ 16 cal ka BP (Fritz et al. 2012b). Nevertheless, the Herschel area remained ice-free during the late glacial period and was affected by periglacial processes under harsh continental climate conditions in close vicinity to the LIS (Rampton 1982, Schweger 1997, Fritz et al. 2012b). Northwest Canada experienced the HTM between approximately 11.6 and 6.0 cal ka BP and the Yukon and the westernmost Mackenzie Delta area experienced warmer-than-present summer temperatures by that time (Ritchie et al. 1983, Ritchie 1984, Kaufman et al. 2004). Paleoenvironmental controls included orbital, climatic and geographical effects: (1) high precessional forcing resulted in summer insolation at 60°N of 10 % above modern conditions; (2) atmospheric water vapor content increased due to postglacial warming; (3) reduced snow and ice cover caused positive albedo–ground temperature feedbacks (Kaufman et al. 2004); and (4) a lower glacio-eustatic sea level displaced the coastline northward leading to greater continentality (Burn 1997).

Rapid climate warming in the western Canadian Arctic at about 11.0 cal ka BP is indicated by a northwards-moving tree line (e.g. Ritchie & Hare 1971, Spear 1993, Szeicz & MacDonald 2001, Bigelow et al. 2003). Pollen records from South Lake (Northwest Territories; Rühland et al. 2009) and Hanging Lake (northern Yukon; Cwynar 1982) provide evidence for a pronounced HTM. Cwynar (1982) inferred wet heath communities in the period from 11.1 to 8.9 cal ka BP as a response to a warmer and wetter climate. Between 11.0 and 8.5 cal ka BP climate conditions progressively ameliorated and could have induced a period of thermokarst development (French

1974, Ritchie et al. 1983, Ritchie 1984, Rampton 1988, Murton 2001, Fritz et al. 2012b). Lake Herschel is probably one of the numerous lakes along the western Arctic coast that initiated as a result of the HTM. According to Rampton (1982, 1988), the formation of thermokarst lakes along the Yukon Coastal Plain and the Tuktoyaktuk Coastlands peaked between 11.6 and 10.3 cal ka BP. Murton (1996, 2001) and Dallimore et al. (2000) assigned the onset of thermokarst lake development on the Tuktoyaktuk Coastlands to the HTM. At the same time, several lakes in the Yukon seem to have dried out (Pienitz et al. 1992). According to Kaufman et al. (2004), local HTM summer temperatures in the western Arctic regions were on average 1.6 °C (± 0.8) higher than the 20th century mean annual air temperatures. The HTM was time-transgressive because Alaska and the western Canadian Arctic were most distant from the waning LIS and therefore warmed earlier (11.3 ± 1.5 cal ka BP) than continental Canada and the Canadian Arctic Archipelago (7.3 ± 1.6 cal ka BP), which were still under the cooling influence of the LIS (Kaufman et al. 2004).

Between 11.6 and 5.6 cal ka BP several plant taxa indicating wetter and warmer climate conditions (*Populus*, *Typha*, *Myrica*) spread north of their present ranges, and *Picea* forest advanced 75 km beyond the present tree line on the Tuktoyaktuk Peninsula (Ritchie & Hare 1971, Cwynar 1982, Ritchie et al. 1983, Spear 1993). Near-modern temperatures were reached between 6.7 and 5.6 cal ka BP (Cwynar & Spear 1995, Kaufman et al. 2004). Cooler and moister conditions have prevailed since the middle Holocene at ~6.0 cal ka BP, as indicated by increases of green alder (*Alnus crispa*) and black spruce (*Picea mariana*) pollen percentages in the Yukon (Cwynar & Spear 1995, Fritz et al. 2012a).

The continuous Holocene sedimentation into Lake Herschel progressed uninterrupted until about 1.8 cal ka BP. This may account for the absence of strong changes in depositional conditions or the low sensitivity of the lake to environmental change. Wetter conditions at this time are evident from the southern Yukon (Pienitz et al. 2000, Anderson et al., 2007), but no significant changes in climate conditions in the Mackenzie Delta and the northern Yukon have been identified from pollen records representing the last 6.0 cal ka BP (Ritchie 1984, Fritz et al. 2012a). The majority of thermokarst lakes in the Mayo area (central Yukon) have been expanding since their inception a few hundred years ago and warm summers, as in 1989, could have reactivated slumping even along formerly stable shorelines (Burn & Smith 1990). Comparing the late Holocene lake evolution on Herschel Island with the early Holocene development indicates that thermokarst lake development is not solely controlled by global and regional climate dynamics, but is also driven by site-specific factors like permafrost dynamics, geomorphology and local climate effects.

I-7 Conclusions

Lake sediments from Herschel Island represent the northernmost paleoenvironmental record of thermokarst activity from the Yukon. A multidisciplinary approach allowed us to reconstruct thermokarst lake evolution since the early Holocene on a late Wisconsin push moraine. The following conclusions can be drawn from this study:

1. Thermokarst lake development started around 11.5 cal ka BP on Herschel Island and probably at the same time in other parts of the northern Yukon.
2. The onset of Lake Herschel correlates with the Holocene Thermal Maximum and is therefore in good agreement with thermokarst lake formation in other parts of the western Canadian Arctic.
3. Lake basin development on a push moraine is apparently the result of ground subsidence due to thawing of ice-rich permafrost and melt-out of massive ground ice, which is abundant in areas of incomplete glaciation like the formerly glaciated parts of the Yukon Coastal Plain.
4. Positive feedback mechanisms operating between the heat capacity of the growing water body and the ice-rich permafrost catchment likely led to thermokarst lake growth during the Early and Mid Holocene.

Abrupt events like sudden lake drainage or collapsing lake shores may leave their imprints in the sedimentary record. Though thermokarst lake sediments have a high preservation potential and may capture regional environmental change, this study also shows that site-specific processes can disturb continuous sedimentation under otherwise fairly constant climate conditions. This study provides a record of thermokarst lake dynamics on a heterogenic push moraine where geomorphological processes are driven by relief energy and high ground ice content.

Acknowledgments

We wish to express our thanks to the Yukon Territorial Government, the Yukon Parks (Herschel Island Qiqiktaruk Territorial Park), and especially to chief ranger R. Gordon. The authors acknowledge the support of the Polar Continental Shelf Program (PCSP/ÉPCP) and the Aurora Research Institute (ARI, Inuvik) for the field component. This study was partly funded by the German Federal Ministry of Education and Research (BMBF, Project No. CAN 09/001) and by a doctoral fellowship awarded to M. Fritz by the German Federal Environmental Foundation (DBU). Field support was provided by G. Müller, G. De Pascale, and S. McLeod. Analytical work was supported with $\delta^{13}C_{TOC}$ determination by B. Plessen (GFZ Potsdam), measurement of magnetic susceptibility by C. Gebhardt (AWI Bremerhaven), radiographic images and photographs by V. Wennrich (University of Cologne), plant macrofossil determination by R. Zibulski (AWI Potsdam), D.Michaelis and A. Teltewskoi (University of Greifswald) and general laboratory assistance by U. Bastian (AWI Potsdam). We thank N.J. Couture (Geological Survey of Canada), P. Frenzel (University of Jena), and S. Lorenz (University of Greifswald) for discussions on earlier versions of the manuscript and C. O'Connor (UAF, Fairbanks, Alaska) for language correction. Two anonymous reviewers and the editor (T. Corrège) are thanked for constructive comments that helped to improve the paper.

Appendix II:

Regional environmental change versus local signal preservation in Holocene thermokarst lake sediments: A case study from Herschel Island, Yukon (Canada)

Michael Fritz[1,2], Ingmar Unkel[3], Josefine Lenz[1,4], Konrad Gajewski[5], Peter Frenzel[6], Nathalie Paquette[5], Hugues Lantuit[1,4], Lisa K rte[3] and Sebastian Wetterich[1]

[1] Department of Periglacial Research, Alfred Wegener Institute Helmholtz Center for Polar and Marine Research, Potsdam, Germany

[2] Department of Earth Sciences, Utrecht University, Utrecht, The Netherlands

[3] Institute for Ecosystem Research, Christian-Albrechts-Universität zu Kiel, Germany

[4] Institute of Earth and Environmental Sciences, University of Potsdam, Germany

[5] Laboratory for Paleoclimatology and Climatology, Department of Geography, Environment and Geomatics, University of Ottawa, Canada

[6] Institute of Earth Sciences, Friedrich Schiller University of Jena, Germany

Under review in: Journal of Paleolimnology

Key words: Arctic, permafrost, athalassic subsaline lake, xrf scanning, pore-water hydrochemistry, ostracods

II-1 Abstract

Thermokarst lakes cover nearly one fourth of ice-rich permafrost lowlands in the Arctic. Sediments from an athalassic subsaline thermokarst lake on Herschel Island (69°36'N; 139°04'W, Canadian Arctic) were used to understand regional changes in climate and in sediment transport, hydrology, nutrient availability and permafrost disturbance. The sediment record spans the last ~ 11,700 years and the basal date is in good agreement with the Holocene onset of thermokarst initiation in the region. Electrical conductivity in pore-water continuously decreases, thus indicating desalinization and continuous increase of lake size and water level. The inc/coh ratio of XRF scans provides a high-resolution organic-carbon proxy which correlates with TOC measurements. XRF-derived Mn/Fe ratios indicate aerobic versus anaerobic conditions which moderate the preservation potential of organic matter in lake sediments. The coexistence of marine, brackish and freshwater ostracods and foraminifera is explained by (1) oligohaline to

mesohaline water chemistry of the past lake and (2) re-deposition of Pleistocene specimens found within upthrusted marine sediments around the lake. Episodes of catchment disturbance are identified when calcareous fossils and allochthonous material were transported into the lake by thermokarst processes such as active-layer detachments, slumping and erosion of ice-rich shores. The pollen record does not show major variations and the pollen-based climate record does not match well with other summer air temperature reconstructions from this region. Local vegetation patterns in small catchments are strongly linked to morphology and sub-surface permafrost conditions rather than to climate. Multidisciplinary studies can identify the onset, and life cycle of thermokarst lakes as they play a crucial role in Arctic freshwater ecosystems and in the global carbon cycle of the past, present and future.

II-2 Introduction and study area

Thermokarst lakes cover nearly 25 % of the ice-rich permafrost lowlands of Arctic Canada (Marsh et al. 2009), Alaska (Hinkel et al. 2005) and Siberia (Grosse et al. 2005). For example, on the Arctic Coastal Plain of northern Alaska, thermokarst lakes presently occupy 22.5 % of the surface area, and drained thermokarst lake basins occupy 61.8 % (Jones & Arp 2015). Thermokarst lakes form upon a thermal disequilibrium of ice-rich permafrost. Permafrost thaw and ground-ice melt lead to ground subsidence. Precipitation and gravitational subsurface flow let water pool in an initial depression where vertical drainage is inhibited by permafrost. The resulting lakes are usually shallow (< 5 m), sometimes oriented and rapidly changing in terms of size, water level, and sediment input.

Walter Anthony et al. (2014) documented the large quantities of organic carbon (up to 159 ± 24 Pg C) stored in thermokarst lake basins of Holocene age in the yedoma region. As the terrestrial Arctic warms, permafrost soils, including those located in drained lake basins, are expected to release substantial greenhouse gas emissions that will generate a positive feedback to global warming (Dutta et al. 2006, Koven et al. 2011, Schaefer et al. 2014). Walter-Anthony et al. (2014) indicated that widespread permafrost thaw could ultimately result in reduced lake and wetland abundance caused by drainage and drying, facilitating rapid sediment carbon decomposition.

Thermokarst lakes in Arctic tundra landscapes are dynamic features with highly variable timing in terms of life cycle (Morgenstern et al. 2011, 2013, Lenz et al. 2015) that includes initiation, expansion, drainage and eventual re-initiation (Mackay 1988, van Huissteden et al. 2011). The initiation of thermokarst lakes in northwest Canada, Alaska, and Siberia is related to increasing air temperatures, available moisture and permafrost thaw in response to warming during the late glacial period or later during the Holocene thermal maximum (Rampton 1988, Walter Anthony et al. 2014). In this context, thermokarst lakes provide valuable

paleoenvironmental information preserved in the sedimentary, geochemical and paleontological properties of lacustrine deposits. Since the aggradation and degradation of permafrost are controlled by both large-scale climate variations and local conditions such as vegetation, substrate, precipitation and hydrology, the paleoenvironmental information preserved in permafrost deposits is biased by interrelated processes and dependencies. The use of thermokarst deposits in paleoenvironmental research, therefore, needs a clear understanding of signal sources and careful interpretation.

This study combines sedimentological data, pore-water hydrochemistry and paleontological proxy data such as pollen and ostracods from a Holocene thermokarst lake core from Herschel Island (69°36'N; 139°04''W) in the northern Yukon, Canada. Herschel Island in the Southern Beaufort Sea is part of the Yukon Coastal Plain in the western Canadian Arctic (Figure II-1). The modern climate of northernmost Yukon is subarctic maritime in summer during the open-water season, and continental in winter (Wahl et al. 1987). The mean annual air temperature (1971-2000) is −11 °C at Komakuk Beach, the closest weather station ~ 40 km west of Herschel Island, with an average July maximum of 7.8 °C (Environment Canada 2015). Mean annual total

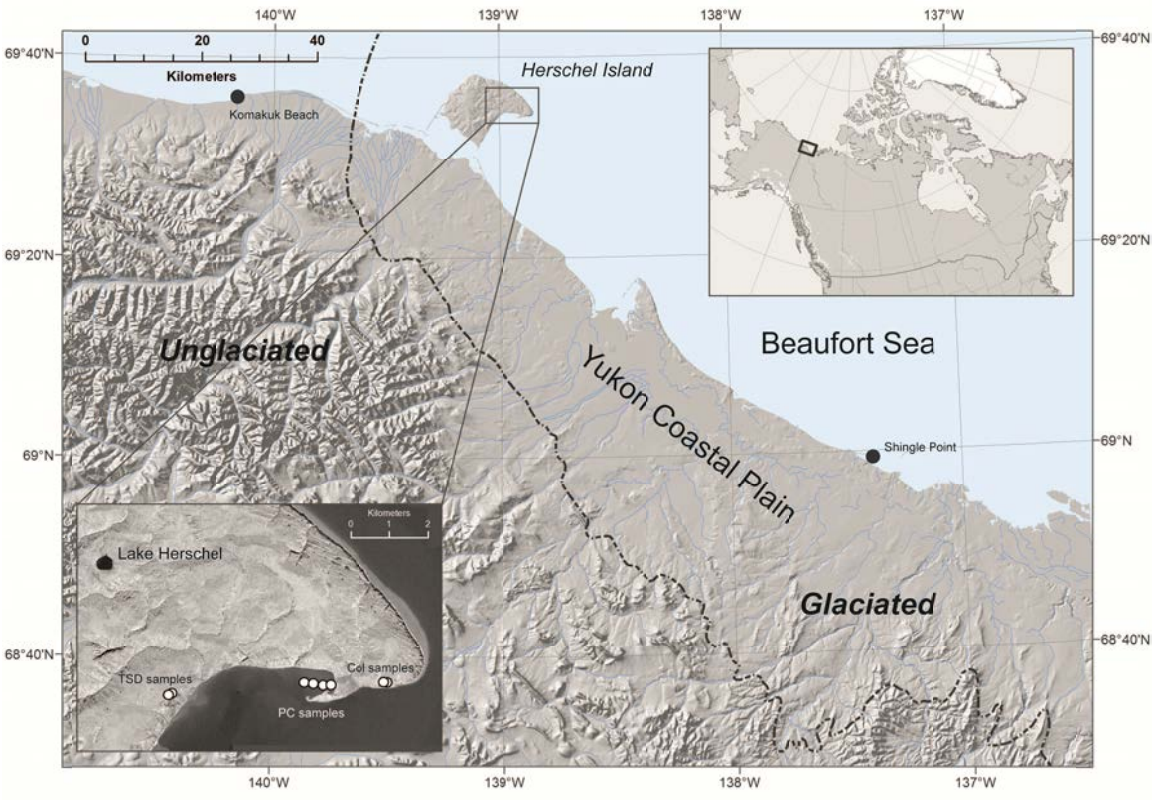

Figure II-1: Map of study area showing location of Lake Herschel on Herschel Island in the western Canadian Arctic (Ikonos image, 2001). Detailed map (lower left inset) shows location of Lake Herschel and fossil reference samples from Colinson Head (Col samples) and samples from Thaw Slump D (TSD samples) as well as modern marine reference samples from Pauline Cove (PC samples).

precipitation is between 161 mm a^{-1} at Komakuk Beach and 254 mm a^{-1} at Shingle Point (~ 100 km southeast of Herschel Island) and is almost equally divided between rain and snow

(Environment Canada 2015). The typical vegetation of Herschel Island is tussock tundra dominated by grasses, herbs, dwarf shrubs and various mosses and lichens (Smith et al. 1989). Herschel Island is primarily composed of marine sands, silts and silty clays with incorporated carbonate fossils from the continental shelf as it was formed as a Pleistocene push moraine that emerged from the last regional advance of the Laurentide Ice Sheet (Mackay 1959) between around 20.0 cal ka BP (Zazula et al. 2009) and 16.0 cal ka BP (Fritz et al. 2012a, b). Since the Holocene sea level rise, Herschel Island reaches the highest elevation along the Yukon Coastal Plain with 183 m asl (meter above sea level) whereas the carved out Herschel Basin southeast of Herschel Island reaches depths of about 70 m below sea level (Mackay 1959, Figure II-1). The island is characterized by continuous, ice-rich permafrost with up to 70 % ground ice content in the upper 10-15 m occurring as segregated ice lenses, ice-wedges, pore-ice, and massive tabular ice bodies in the form of buried glacier ice, snow bank ice, and massive segregated ice (Fritz et al. 2011; 2012b). Polygonal patterned ground and ponds have formed in flat areas since deglaciation (Fritz et al. in press).

A larger thermokarst lake is located in the center of Herschel Island (69°36′03′′N, 139°03′47′′W; Lenz et al. 2013). The studied subcircular thermokarst lake is about 400 m in diameter, 0.126 km² in area and up to 6 m deep (Lenz et al. 2013; Figure II-1). The lake circulation is cold-monomictic. The water body is mixed in summer with a water temperature of ~ 8 °C, electrical conductivity (EC) of 1.1 mS cm^{-1} and a pH of 7.2 to 8.3. Under the winter ice cover of 2 m the EC of lake water increased to 2.3 mS cm^{-1} and water temperatures of about 1 °C were measured (Lenz et al. 2013).

The goal of this study is to show that thermokarst lake sediment records are a valuable environmental archive in permafrost landscapes which captures large-scale climate variations and local landscape changes. We seek to provide a better understanding on which environmental proxies reflect large-scale changes in climate and which are more related to local changes in sediment transport, hydrology, nutrient availability and surface disturbance. The specific objectives of this manuscript are:

1. to show that episodic permafrost disturbance in the catchment leaves an imprint in the sedimentological record of the lake,
2. to relate the chemical predisposition of an athalassic subsaline lake to habitat conditions for calcareous microfossil taxa,
3. to reconstruct the response of the calcareous microfossil record to past changes in lake-water hydrochemistry and sediment-input patterns,
4. to assess the ability of pollen assemblages to provide quantitative climate reconstructions in thermokarst settings, and

5. to distinguish between climatically-relevant information on large scales and local conditions.

II-3 Material and methods

II-3.1 Sediment core

The sedimentological and biogeochemical properties of the 727-cm-long lake sediment core (core ID: PG1967) of Lake Herschel were described in detail by Lenz et al. (2013). Four sedimentary units were distinguished which resembled the four phases of lake development during the Holocene by variations in grain size, biogeochemical parameters, density, water content, and magnetic susceptibility: Unit A (727-700 cm), Unit B (700-600 cm), Unit C (600-200 cm) and Unit D (200-0 cm). The clayish to sandy matrix contained bedding structures and organic layers in places. Total organic carbon (TOC) contents varied between about 2 and 9 wt%, and total nitrogen contents between about < 0.1 and 0.4 wt%. Largest variations were observed within the early Holocene Unit B. Calcium carbonate was present throughout the core. The radiocarbon-based core chronology, which is re-evaluated in this study, included eight dates and the age-depth relationship used a squared regression model for Unit A to C assuming continuous sedimentation between < 11.5 and 1.8 cal ka BP and excluded the hiatus between Units C and D. Unit D was dated to 0.9 cal ka BP to today (Lenz et al. 2013).

II-3.2 Radiocarbon dating and age modelling

Nine samples of plant material (mosses, sedges, and wood fragments) and one bivalve mollusk sample were recovered from the core and measured for radiocarbon (^{14}C AMS) ages (digital appendix table II-1) at the Poznan Radiocarbon Laboratory, Poland. All ^{14}C samples were calibrated with respect to IntCal13 (Reimer et al. 2013). An age-depth-model was calculated using the OxCal 4.2.3 calibration software (Bronk Ramsey 2009a). This software combines the probability distributions of the calibrated radiocarbon ages with certain assumptions on depositional processes to obtain an age-depth-curve with 1σ (68.2 %) probability margins of the radiocarbon ages. We applied the *P_Sequence* model of OxCal 4.2.3 to our data which assumes the deposition to be random (meaning no regular annual layers), although with an approximate proportionality to depth z (Bronk Ramsey 2008). We adopted a *k*-value of 150, which gives an estimate of the variation from a constant sedimentation rate equivalent to 7 mm calculation increments. An age-depth curve was directly extracted from the OxCal model, returning maximal and minimal ages for every centimeter (Figure II-2). For plotting our proxy data, a curve based on the mean age values was then extracted from OxCal and interpolated to 2 mm and 5 mm steps using the *interpol*-function (method "*linear*") of R version 3.1.2 (R Core Team 2014). Calibrated years are denoted as *cal BP* (i.e. before AD 1950) (Mook & van der Plicht 1999). Outlier ^{14}C

dates that differed significantly from the general age-depth-model were assessed using the *Outlier "charcoal"* model of OxCal (Bronk Ramsey 2009b). Outliers were excluded from the calculation of the age-depth-curve if no agreement with the model could be achieved.

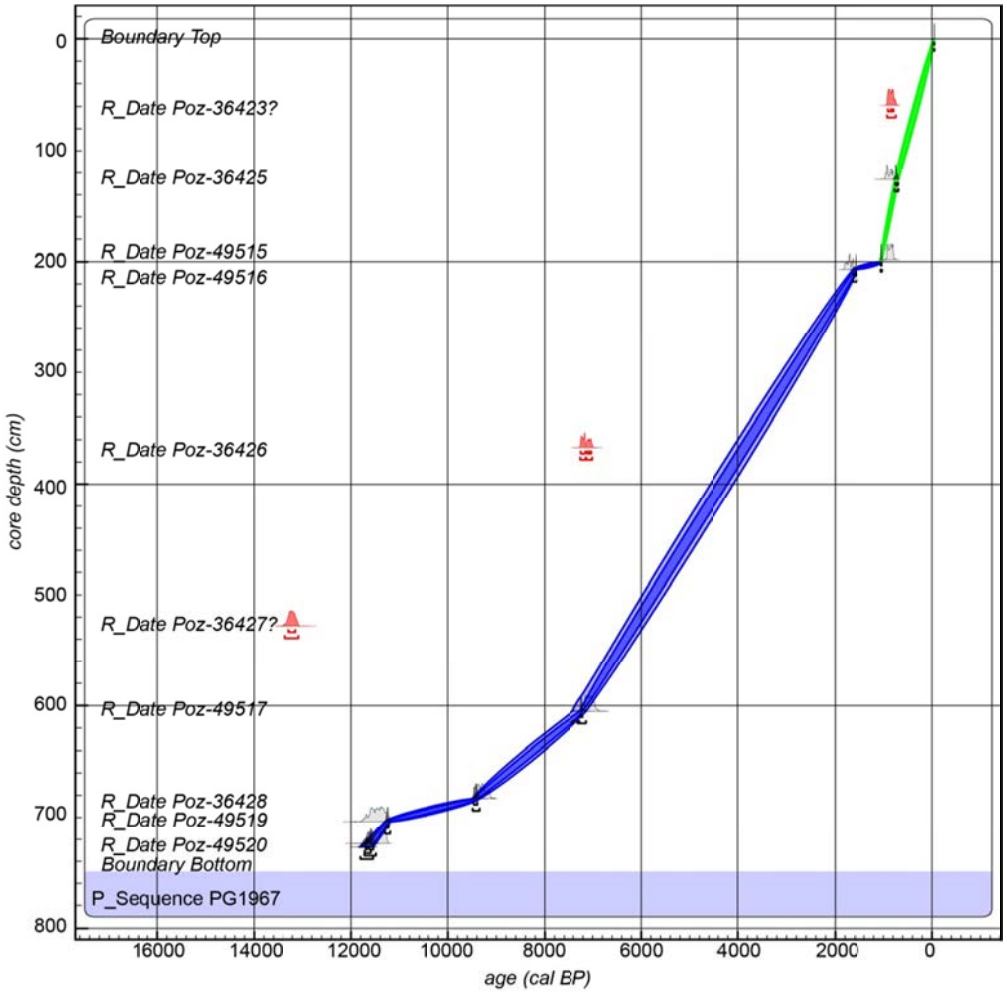

Figure II-2: Age-depth-model of core PG1967 from Lake Herschel calculated and plotted using the software OxCal 4.2.3 (Bronk Ramsey 2009a). Blue lines are used for the aged-depth-range before the hiatus, green lines for the range after the hiatus. The inner ranges reflect 1σ (68.2 %) probability ranges, the outer ranges 2σ (95.4 %) probability. Outliers are marked in red.

II-3.3 Pore-water chemistry

Pore-water was obtained using rhizon soil moisture samplers (Rhizon SMS, Eijkelkamp) which have mean pore size of 0.15 µm. Hydrochemical characterization included pH, electrical conductivity (EC), major anions and cations. The cation content was analyzed by inductively coupled plasma-optical emission spectrometry (ICP-OES, Perkin-Elmer Optima 3000 XL), while the anion content was determined by ion chromatography (IC, Dionex DX-320). Hydrogen carbonate concentrations were measured by titration with 0.01 M HCl using an automatic titrator (Metrohm 794 Basic Titrino). Not every parameter was measured continuously down-core because of sample volume restrictions. Where measurements gave values below the detection limit, we display half of the detection limit. This was sometimes the case for Fe (throughout the core), NO_3 (in units A-C), Ba (in unit D), Mn (in units B and D).

II-3.4 X-ray fluorescence (XRF) scanning

XRF scanning was carried out at a resolution of 2 mm until 290 cm core depth and thereafter at a resolution of 5 mm until 727 cm. The XRF scans were performed at Cologne University (Germany) using an ITRAX core scanner with a molybdenum X-ray source (Croudace et al. 2006). The XRF-scanning results represent element intensities in "counts per second" (cps) which are proportional to chemical concentrations but depend also on sediment properties (Röhl & Abrams 2000), water content (Tjallingii et al. 2007), and element-element interaction (matrix effect) during measurement (Weltje & Tjallingii 2008). We report the XRF-scanning results as log-ratios to avoid statistical analysis of data sensitive to the closed-sum effect (dilution by organic material) (Weltje & Tjallingii 2008, Löwemark et al. 2011).

II-3.5 Micropaleontology

Calcareous microfossils

The micropaleontological material comprised 77 samples from core PG 1967. For comparing the lacustrine record with modern and Pleistocene faunas additional six recent surface sediment samples (four littoral marine and two from Lake Herschel) and four samples from strata from Pleistocene permafrost outcrops with an age of more than 16.0 cal ka BP, according to Fritz et al. (2012b), were analyzed (Figure II-1). Sediments were washed through a 63 µm sieve, air-dried and picked for microfossils under a stereomicroscope. Specimens were identified and their number counted if rare or estimated if highly abundant to produce semi-quantitative abundance data for each group. For revealing factors influencing the distribution of microfossils and for comparing core samples with reference material, a PCA based on abundance data was applied using the program package PAST (Hammer et al. 2001).

Palynology

Two cm^3 of sediment were processed to concentrate the pollen from the sediment using standard chemical treatment with the addition of heavy liquid separation (Zabenskie et al. 2006, Zabenskie & Gajewski 2007) and mounted in silicone oil. Pollen counting was difficult due to low concentrations and the presence of many poorly preserved grains; an average of 270 grains was counted per level, with the range from 237 to 312 grains. Climate estimates were based on the modern analogue technique (MAT) and modern pollen samples from North America (Whitmore et al. 2005). Only samples from the tundra and forest-tundra from the modern database were retained as possible analogues; for the climate reconstruction our pollen sum consisted of 26 NAP taxa (digital appendix table II-2).

II-4 Results

II-4.1 Chronostratigraphy: The revised age model

The age-depth model (Figure II-2) shows continuous sedimentation from the core bottom until 197 cm depth, which covers the period from 11.67 to 1.59 cal ka BP. The bivalve sample (*Pisidium* sp., Poz-36423) taken at 57-61 cm shows an apparent age of 920 ± 40 ^{14}C years. However, individuals living at the lake bottom included a substantial amount of dead carbon in their carbonate shell and therefore this date was excluded from the age-depth model. Two ^{14}C dates (Poz-36426, 36427, digital appendix table II-1) obtained at 366 and 528 cm depth were also detected as outliers and excluded. The respective plant material was most probably eroded in the catchment and transported into the lake by water or ice. Two ^{14}C dates were obtained immediately below and above a distinct light-gray sandy layer of coarser grain size at 207 and 198 cm depth, respectively (Poz-49515, 49516, digital appendix table II-1). These two dates, only 9 cm apart, show mean ages of 1.59 and 1.04 cal ka BP respectively, with a minimum distance of their 1-σ ranges of 490 years. It is not clear at what point of time the sandy layer between these dates was deposited, but the ^{14}C ages support a chronological hiatus between them. Based on this age model we consider the sediment units to represent the following periods:

- Unit A (727-700 cm: > 11.66 to 10.93 cal ka BP)
- Unit B (700-600 cm: ~ 10.93 to 7.17 cal ka BP)
- Unit C (600-200 cm: ~ 7.17 to 1.59 cal ka BP)
- Hiatus (1.59 cal ka BP to 1.04 cal ka BP, approximately 550 years);
- Unit D (200-0 cm: 1.04 cal ka BP to 2009 AD)

The deposition periods of the sediment units (A-D) of the Lake Herschel core PG1967 previously established by Lenz et al. (2013) are mainly confirmed by the refined age model presented here. Differences occur due to application of the updated calibration data set by Reimer et al. (2013) and the newly applied age modelling as described above.

II-4.2 XRF chemistry

We here focus on four selected element ratios which are most suitable for comparison with the other proxies reported in this study: (1) the incoherent (inc) and coherent (coh) electron scattering which is recorded by ITRAX-XRF scanners in addition to the element counts; (2) the Mn/Fe ratio (Figure II-3) providing information on redox conditions and alkalinity and thus on preservation conditions for organic matter; (3) the Sr/Ca ratio (Figure II-4) which changes in carbonate shells in reaction to changes in lake-water salinity (Ricketts et al. 2001); (4) the Rb/Sr ratio which is an indicator for weathering in the catchment and is sensitive to temperature variations (Jin et al. 2001).

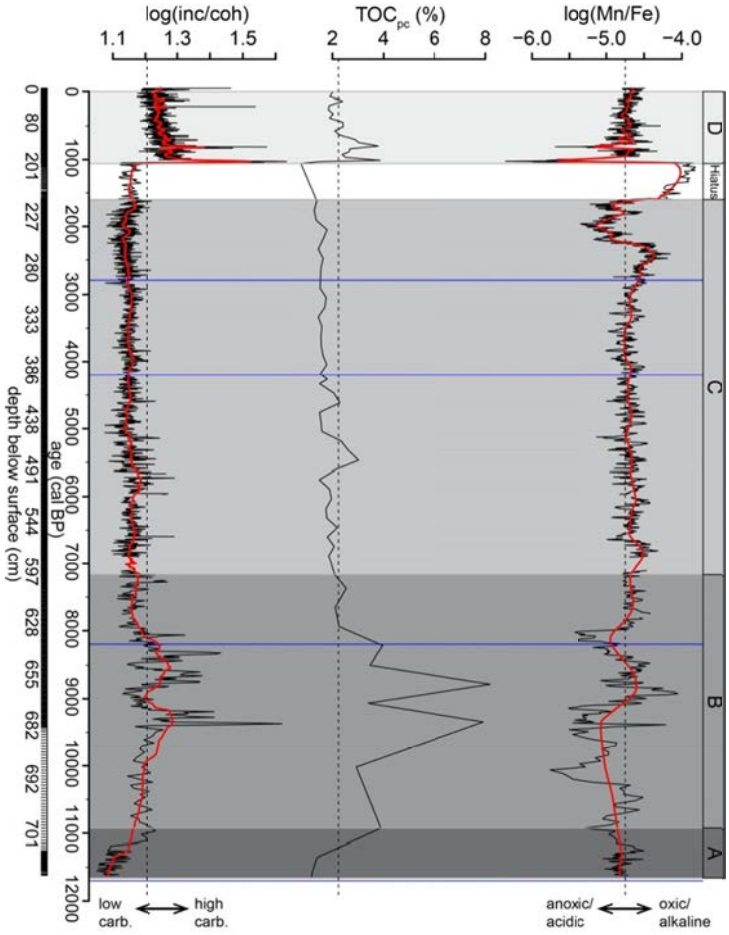

Figure II-3: XRF-based proxy log-ratios (inc/coh, Mn/Fe) compared to absolute TOC measurements from Lake Herschel (TOC taken from Lenz et al. 2013). All proxies plotted against age (cal a BP). Measured values plotted in black, red lines for inc/coh and Mn/Fe are a 30pt running mean for visualizing more general trends in the data. Dashed lines indicate the mean value for each proxy calculated from the entire sequence. Blue lines indicate the approximate time of major Holocene climate events for facilitating comparison: 8.2 ka event (Alley & Ágústsdóttir 2005), 4.2 ka event (Staubwasser et al. 2003) and 2.8 ka event (van Geel 2014).

Inc/coh ratio and total organic carbon (TOC)

Incoherent scattering is higher for elements with low atomic mass like carbon. Hence, the ratio incoherent to coherent (inc/coh) scattering can be used as an indicator for the organic carbon content (Guyard et al. 2007). Here, the inc/coh ratio correlates well with the measurements of TOC ($r = 0.42$, $p < 0.001$), and therefore provides a high-resolution proxy for organic carbon content in comparison to the TOC measurements performed at coarser resolution (Figure II-3). The inc/coh ratio is lowest at the very bottom of the core sequence. It then increases moderately until 11.2 cal ka BP and more strongly until approx. 11.0 cal ka BP (Figure II-3). Between 9.4 and 8.2 cal ka BP there are three peaks in inc/coh ratio that broadly correspond to high values in TOC. After 8.2 cal ka BP, inc/coh and TOC never reach the same high values as before. With the onset of unit D (after the sedimentation hiatus) the inc/coh ratio is generally higher than before in unit C. Two distinct peaks around 0.9 cal ka BP are also reflected in the TOC record.

Manganese / iron (Mn/Fe) ratio

The Mn/Fe ratio is negatively correlated with the inc/coh ratio ($r = -0.37$, $p < 0.001$) and the TOC ($r = -0.26$, $p < 0.001$) over the entire sequence, especially notable in Unit B (Figure II-3). A decreasing Mn/Fe ratio (more anaerobic conditions) during unit A is accompanied by rising inc/coh and TOC, which indicates higher preservation of organic material. While there are no significant variations in Mn/Fe or inc/coh in unit C, the "hiatus layer" shows the highest Mn/Fe ratios of the entire sequence, contrasting to minimal TOC. Variation of Fe and Mn in lake sediments are difficult to interpret (Engstrom & Wright Jr 1984) since a number of independent environmental factors control their supply and sedimentation, such as alkalinity and acidity (pH) as well as reduction potential (Eh). Anaerobic conditions and lowered pH favor mobility of iron. As the pH is generally high in our pore-water record (Figure II-5), the Mn/Fe ratio could be regarded as a proxy for aerobic versus anaerobic conditions.

Strontium / calcium (Sr/Ca) ratio

Sr/Ca strongly increases between 11.7 and 10.3 cal ka BP, only interrupted by a negative peak between 10.8 and 10.3 cal ka BP (Figure II-4). The Sr/Ca ratio decreases gradually towards 8.9 cal ka BP, then this trend is inversed until 8.2 cal ka BP before the ratio decreases again until approximately 6.8 cal ka BP. After 6.8 cal ka BP the Sr/Ca ratio fluctuates around the mean value of the entire sequence before it shows a clear decrease in the "hiatus" layer followed by a sharp rise at the onset of unit D. Strontium (Sr) can substitute calcium (Ca) in carbonate minerals and co-precipitates in lakes (Cohen 2003). This results in a strong correlation ($r = 0.60$ to 0.86) between these two elements (digital appendix table II-3). The Sr/Ca ratio of carbonate shells is related to the Sr/Ca ratio of the lake water. While the ratio in ostracod shells seems independent

from the temperature of formation it is sensitive to changes in salinity of the lake water (Mischke et al. 2008, Ricketts et al. 2001).

Rubidium / strontium (Rb/Sr) ratio

Through most of the sediment sequence the Rb/Sr ratio fluctuates around its mean value (Figure II-4). Only at 8.2 cal ka BP there is a significant shift to a higher Rb/Sr ratio indicating cooler conditions which lasted approximately until 7.0 cal ka BP. The strong deviation to a lower Rb/Sr ratio in the "hiatus layer" is not due to a climatic cause. The Rb/Sr ratio can be used as a proxy for chemical weathering in the catchment (Jin et al. 2001). High Rb/Sr ratios in lake sediments are related to reduced catchment weathering under cooler climatic conditions, hence, reduced catchment precipitation. Accordingly, a low Rb/Sr ratio might correspond to relatively warm climatic conditions.

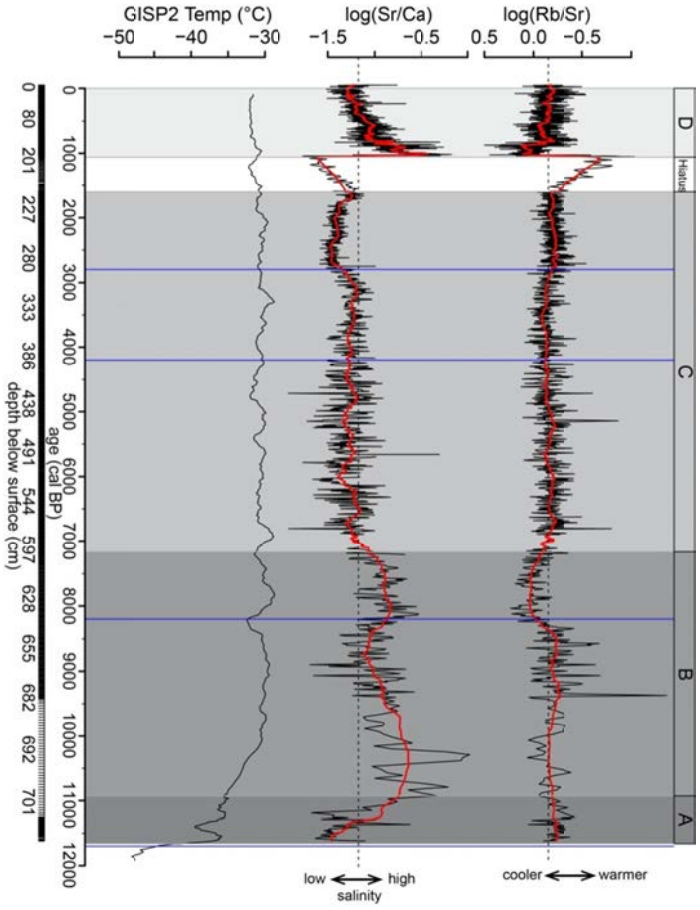

Figure II-4: XRF geochemistry from Lake Herschel vs. GISP2. Greenland GISP2 temperature record for Younger Dryas and Holocene (Alley 2000) compared to XRF-based proxy log-ratios (Sr/Ca) and (Rb/Sr) indicating changes in salinity and temperature, respectively. All proxies plotted against age (cal a BP). Measured values plotted in black, red lines for Sr/Ca and Rb/Sr are a 30pt running mean for visualizing more general trends in the data. Dashed lines indicate the mean value for each proxy calculated from the entire sequence. Blue lines indicate the approximate time of major Holocene climate events (see Figure II-3)

II-4.3 Pore-water chemistry

Pore-water throughout the core is characterized by high EC values between 13.7 and 2.7 mS cm^{-1} (Figure II-5). Lenz et al. (2013) have shown modern lake water EC values between 1.1 mS cm^{-1} in summer and 2.3 mS cm^{-1} in winter, which is typical for an athalassic brackish environment in the Arctic (Willemse et al. 2004). A trend of decreasing EC from lake initiation in the early Holocene until about 1.6 cal ka BP is significant. Desalinization by increasing freshwater input into the brackish system was interrupted at the hiatus with slightly increasing EC values from 4.4 to 6.0 mS cm^{-1}. The last 1,000 years were again characterized by decreasing EC towards values close to modern winter bottom lake water; although the modern lake water is chemically dissimilar from the pore-water, due to the lower proportion of HCO_3^- in the pore water (digital appendix II-4). Variation of pH throughout the core was between 7.0 and 7.8. It was stable (7.3-7.4) in the early Holocene until 7.15 cal ka BP and more variable and slightly higher (7.2-7.6) until the hiatus at 1.59 cal ka BP. The pH dropped to the overall minimum (7.0) at the hiatus and showed values between 7.5 and 7.8 until today.

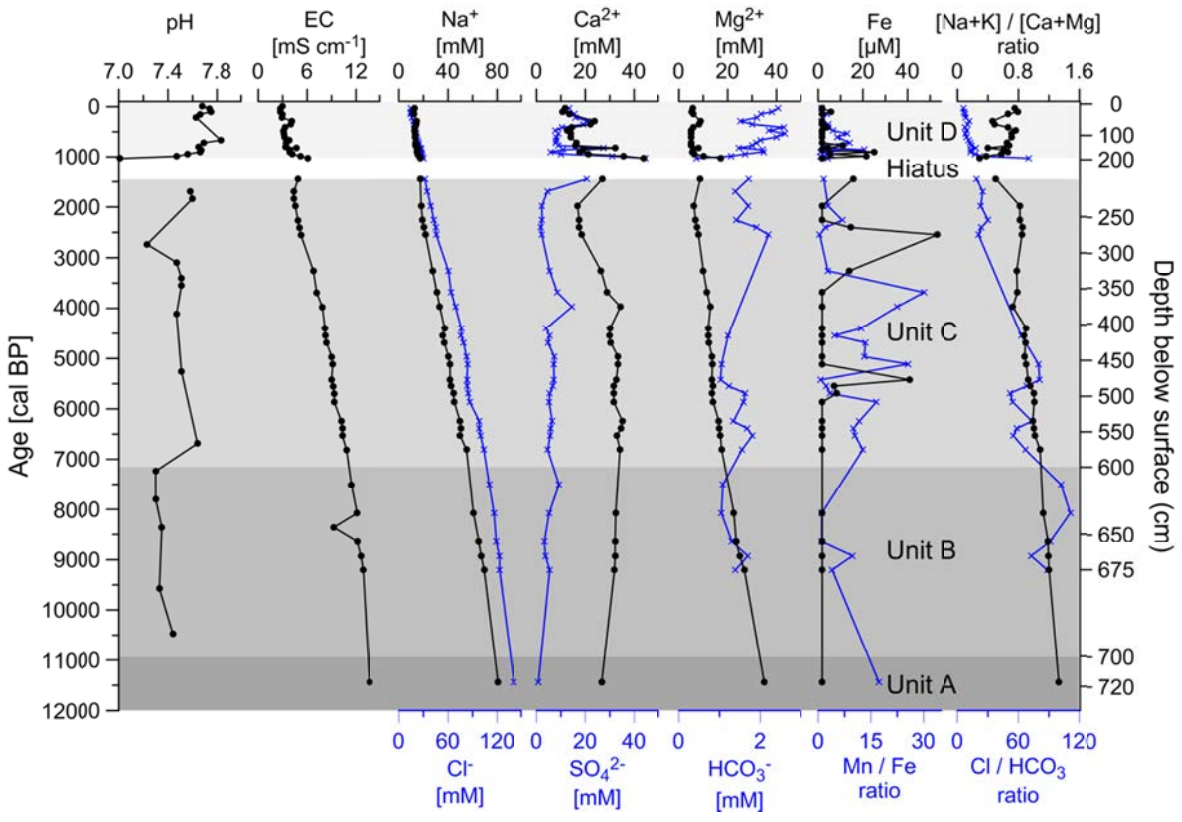

Figure II-5: Pore-water hydrochemistry of Lake Herschel sediments according to age with regard to sedimentary units A-D including the hiatus. Concentrations are displayed in mol eq. per liter [mM, µM]. For individual data points see data table in digital appendix (Table II-5).

Na^+ and Cl^- follow the generally decreasing trend in EC. Na^+ and Cl^- dominated the ion composition with high concentrations until the hiatus at 1.59 cal ka BP, where Ca^{2+}, Mg^{2+} and SO_4^{2-} occurred at maximum concentrations and thus changed the overall ion composition completely (Figure II-5). A decreasing trend in Ca^{2+} concentration is visible between 4.0 cal ka BP and the hiatus at 1.59 cal ka BP, where Ca^{2+} concentrations suddenly rose towards a maximum of 44 mM and then decreased again until today. Fe in measurable concentrations (> 3.6 µM) is documented in sediment pore-water younger than 5.7 cal ka BP. Mn decreased from 11.5 until 8.0 cal ka BP and then increased, reaching maximum concentrations above 40 µM between 4.0 and 3.0 cal ka BP. A decreasing trend in Mn concentrations followed towards the hiatus, where Mn varied strongly and decreased until today. SO_4^{2-} had its minimum (0.8 mM) in the oldest core part and remained relatively constant at a low level until the hiatus at 1.6 cal ka BP, where it suddenly reached its maximum concentration of 45 mM. Subsequently, SO_4^{2-} remained at relatively high concentrations with an average value of 15 mM until today. Although we do not have data on HCO_3^- from the oldest core part, a generally increasing trend upwards is detected. The overall HCO_3^- minimum occurred at the hiatus with 0.4 mM. All hydrochemical data is available in the digital appendix (Table II-5).

II-4.4 Calcareous microfossils

Reference samples

The four modern marine littoral samples contain the highest number of microfossils. Dominating are the foraminifers *Haynesina orbiculare* and *Cribroelphidium excavatum* and the brackish water ostracods *Heterocyprideis sorbyana*, *Paracyprideis fennica* and *Palmoconcha russelensis* (digital appendix table II-6). The same species also occur in the Pleistocene permafrost outcrop samples although less frequently. Marine or brackish ostracods or foraminifers are completely missing in the two modern Lake Herschel sediment samples. Mollusk fragments are rare and limited to the marine and outcrop samples, sometimes comprising freshwater taxa as well. All microfossil groups encountered within the reference samples (digital appendix table II-6) are also represented in the core (digital appendix table II-7).

Distribution of microfossils in Lake Herschel sediments

Ostracods and foraminifers are present throughout the core, in contrast to only occasional findings of bivalve fragments (Figure II-6). Unit A is characterized by abundant marine to brackish foraminifers and ostracods, including a few marine and a number of freshwater bivalve fragments. Terrestrial microfossils are rare in all samples of the basal Unit A. In general, frequencies of occurrence of marine and brackish microfossils are low in Unit B with marine mollusks remains in the lower part whereas freshwater ostracods are more abundant than in Unit A. The overlying Units C to D are characterized by constant abundance of freshwater

ostracods and a varying number of marine to brackish microfossils with absence of marine-brackish and brackish ostracods from 5.0 to 2.0 cal ka BP (Figure II-6). Marine foraminifers are abundant within Unit C but absent from 3.5 to 2.5 cal ka BP. In Unit D freshwater ostracods and freshwater bivalves show constant abundance with 10 to 100 specimens, whereas brackish-marine microfossils show less frequent occurrence. The abundance of terrestrial taxa such as insect remains, oribatid mites and plant remains varies throughout the sediment sequence; they are most abundant in Unit D (Figure II-6). Marine mollusks are missing from this part of the core whereas the freshwater bivalve *Pisidium* is quite common. A list of taxa with their main habitats and distribution is given in digital appendix table II-7, where also selected taxa are illustrated.

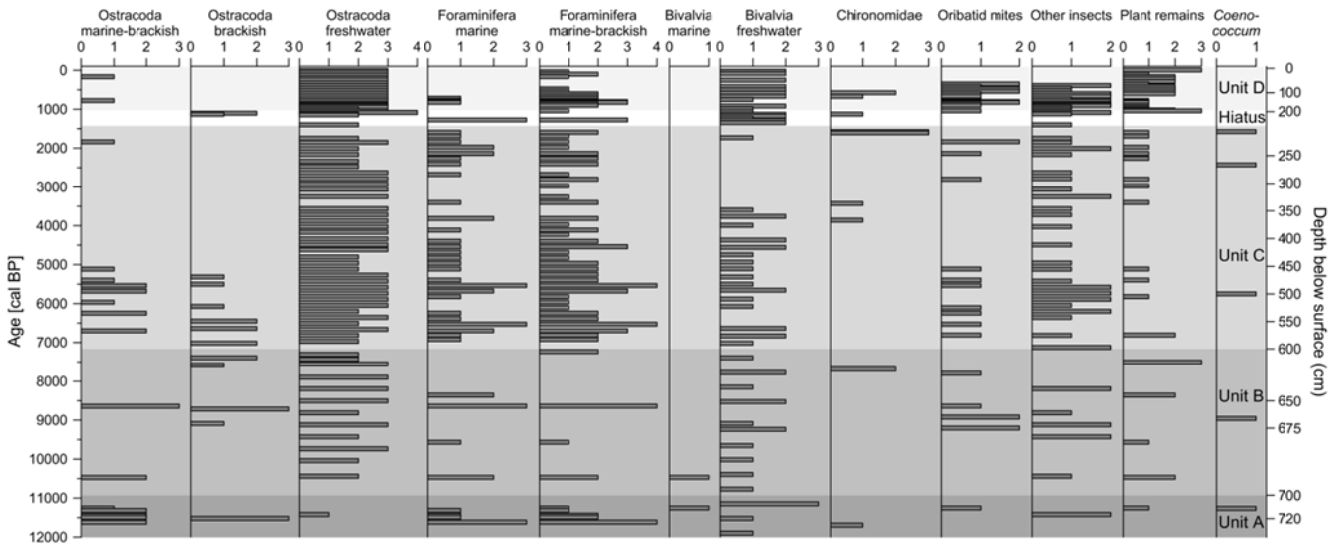

Figure II-6: Semi-quantitative distribution of microfossil groups in sediments from Lake Herschel shown according to age. Abundance classes: 1 = 1-2 specimens; 2 = 3-10 specimens; 3 = 11-100 specimens; 4 = 101-1000 specimens. For a species list digital appendix (Table II-7).

II-4.5 Pollen

There were few changes through time in the pollen assemblages. Pollen of Cyperaceae and Poaceae were the most abundant taxa (Figure II-7); Cyperaceae pollen were more abundant in sediments older than 2.0 cal ka BP (Units A-C), and decreased in the past 1,000 years. Between 7.0-2.0 cal ka BP, Cyperaceae percentages were variable but generally high. Poaceae pollen percentages steadily increased between 9.0-3.5 cal ka BP, and more rapidly in the past 3,000 years. Pollen from several shrubs is found in relatively high quantities, including *Alnus, Betula* and *Juniperus*. *Salix* pollen percentages are high in the lowermost and uppermost sediments. Tree taxa comprise 3-20 % of the total pollen grains, with little change through time (Figure II-7).

Pollen concentrations and influx were low prior to 6.0 cal ka BP. They then increased and remained high, although somewhat variable for the past 5,500 years, and total pollen influx was especially high in the past 1,000 years. Reconstructed mean July air temperatures varied around

present-day values (Komakuk meteorological station, Figure II-1) but were typically below the present-day value during the past 3,500 years (Figure II-8). Values of squared chord distance (SQD) are relatively high and change little through time.

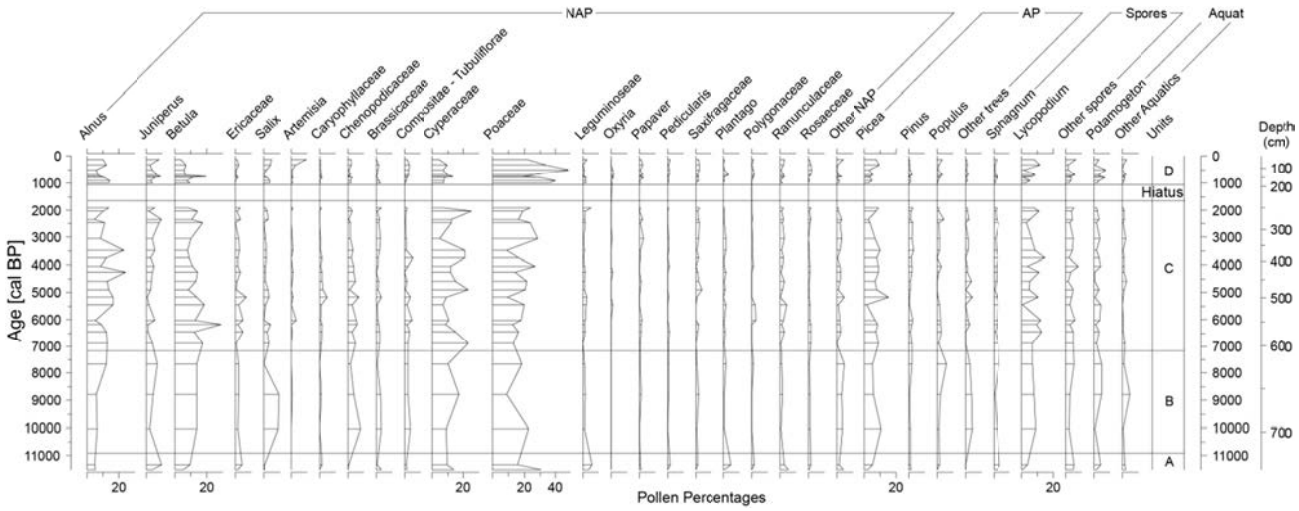

Figure II-7: Percentage pollen diagram from Lake Herschel, Herschel Island, Yukon.

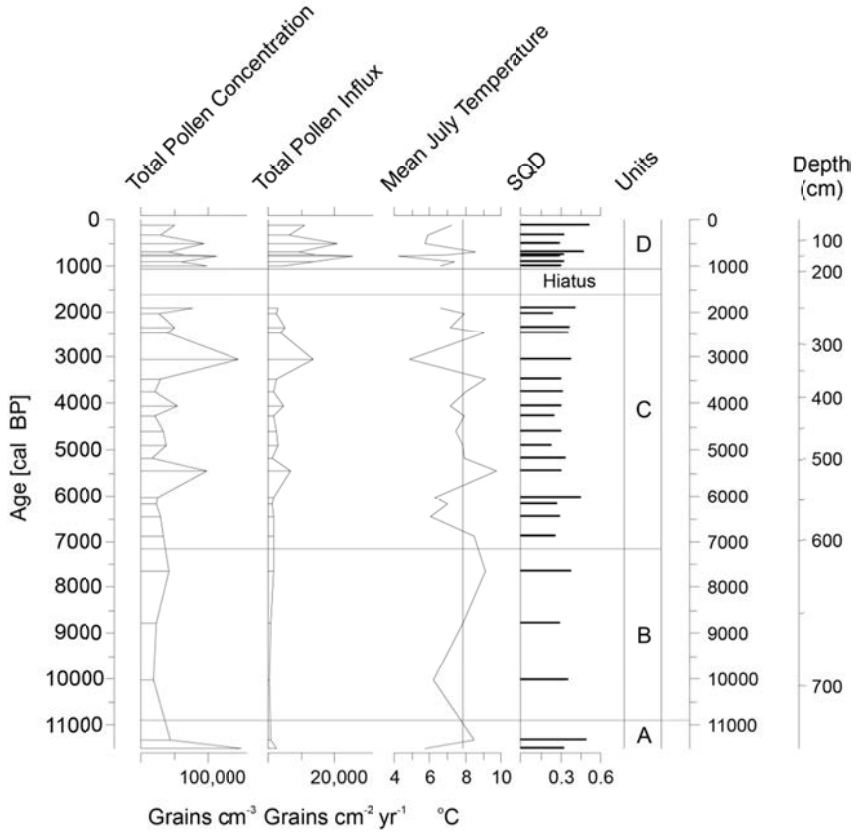

Figure II-8: Total pollen concentration, pollen influx and reconstructed July air temperatures based on the top analogues, and squared chord distance (SQD) of the top analogue from Lake Herschel. The axis of the temperature reconstruction is placed at the mean July air temperature at Komakuk Beach which is 7.8 °C (Environment Canada 2015)

II-5 Discussion

II-5.1 Sedimentation history of Lake Herschel

The evolution of Lake Herschel deduced from multi-parameter analyses of the sedimentary record (Lenz et al. 2013) differentiates into four lake stages covering the entire Holocene since about 11.7 cal ka BP. A late Holocene hiatus is identified by radiocarbon dating and sediment properties, and occurred between about 1.59 and 1.04 cal ka BP.

The lake onset started in response to thermokarst processes between >11.5 and 10.0 cal ka BP by melting of massive ground ice and subsequent surface subsidence which shaped the lake's basin. Favorable climate conditions (warmer and wetter than today) during the Holocene thermal maximum from 10.6 to 7.0 cal ka BP in northwestern Canada (Kaufman et al. 2004, Gajewski 2015a) encouraged this lake development. Between about 10.0 and 7.0 cal ka BP, ongoing ground-ice melting deepened the lake to a depth exceeding 2 m so that the water body did not freeze to the bottom in winter, ensuring that a continuously unfrozen zone (talik) developed below the lake The Mid Holocene lake phase between about 7.0 and 1.8 cal ka BP is considered as dynamic equilibrium of lake development. High sedimentation rates indicate that the lake steadily expanded and that lateral extension of the basin by shore erosion surrounding ice-rich terrain took place. A disturbance in sedimentation is obvious in the late Holocene lake phase between about 1.59 and 1.04 cal ka BP. This coincides with the coldest period of the Holocene in the western Arctic (Gajewski 2015a). Two hypotheses to explain the hiatus are outlined by Lenz et al. (2013) as either allochthonous slumping disturbed the continuous sedimentation or abrupt lake level fall interrupted the accumulation of lacustrine sediments. After about 1.0 cal ka BP until today the lake is considered to reach its modern dimensions.

Due to the position and development of Lake Herschel in ice-rich preglacial deposits of marine origin that have undergone ice-thrust deformation (Fritz et al. 2012b), brackish conditions are assumed and indicated by the inventory of calcareous fossils (foraminifera, mollusks and ostracods) and by XRF geochemistry (Sr/Ca ratio). Lake expansion by degrading marine ice-rich deposits increased the supply of solutes into the evolving lake. This rather uncommon setting requires special attention in interpreting the fossil record of Lake Herschel in terms of paleoecology and paleoclimate.

II-5.2 Limnological, sedimentary and geochemical properties predefine the habitat

Decreasing EC and Sr/Ca ratio from lake initiation in the Early Holocene until about 1.6 cal ka BP indicates desalinization, which points to a lake-level rise with increasing freshwater input. A trend towards freshwater conditions is supported by decreasing [Na+K]/[Ca+Mg] and Cl/HCO_3 ratios (Figure II-5). However, the general salinity always was and still is elevated compared to typical Arctic freshwaters. Lake Herschel as athalassic subsaline lake represents a rare lake type that has been only occasionally studied in Arctic environments (Pienitz et al. 1992, 2000, Willemse et al. 2004). Continuous desalinization suggests continuously increasing lake size and rising water level together with relatively decreasing material input or reduced leaching of salt-rich solutes from surrounding sediments. Nevertheless, the major lake water ion source is still likely to be the salt-rich upthrusted marine sediments (Kokelj et al. 2002, Fritz et al. 2012b). A hydrochemical regime shift from marine-derived ions (Na^+, Cl^-) to terrestrial-dominated ion composition (Ca^{2+}, Mg^{2+}) at the hiatus is apparent (Figure II-5). While marine-derived ions continued to decrease, terrestrial derived ions increased sharply at the sedimentary hiatus together with a slight increase in EC. Ion concentrations remain elevated throughout the pore-water record. XRF-derived sediment geochemistry and pore-water hydrochemistry indicate a strong input and fast accumulation of terrestrial material leading to the hiatus. This might be derived from active-layer detachments, lake-shore erosion and large slumping events sometime between 1.59 and 1.04 cal ka BP. Lenz et al. (2013) already suggested an episodic and catastrophic sediment input from the catchment by thermal shoreline erosion based on a sandy layer - coarser material indicates higher transport energy - and a shift in biogeochemical sediment properties such as low $\delta^{13}C_{TOC}$ ratios. Sediments originating from disturbance are organic-poor, relatively coarse-grained and show a maximum in Mn/Fe ratio and low Sr/Ca ratios indicate little authigenic carbonate production. In a graded sequence, fine particles and organic matter deposit last. At the upper end of the disturbed sequence, the drop in pore-water pH and a sharply decreasing Mn/Fe ratio indicate more anaerobic conditions which are supported by good organic-matter preservation. The minimum in HCO_3^- at the uppermost part of the disturbed sequence also suggests elevated bioproductivity and an uptake of HCO_3^- from the lake water, for example by algae which then in turn lowered pH and oxygen availability.

Warmer air temperatures together with higher precipitation or higher runoff would be also an appropriate trigger for more intensive thermokarst processes and sediment mobilization. However, thermokarst is a process that is not solely linked to climate so that this linkage remains speculative. More interesting than a relation to climate might be the geochemical predisposition of the lacustrine system for calcareous organisms.

II-5.3 Autochthonous versus allochthonous deposition of calcareous microfossils

Sediments of Unit A older than 11.0 cal ka BP are composed of thawed upthrusted glacial sediments, which have a marine origin on the Beaufort Shelf, as indicated by the presence of marine and marine-brackish foraminifers, ostracods and remains of marine mollusks. The latter are completely missing in the other core sections and harder to transport than microfossils. A comparison of faunal assemblages in Unit A with our reference samples shows closest relations to the modern marine and Pleistocene fauna (Figure II-9a). This similarity points to lake expansion in Pleistocene marine material in response to thaw subsidence and with little autochthonous lake sediments. In general, we conclude that increasing similarity with Pleistocene permafrost samples indicates increased reworking of calcareous fossils and allochthonous transport into the lake by thermokarst and shore erosion.

High abundance of freshwater ostracods in the upper units from about 10.0 cal ka BP until today indicates at least oligohaline conditions (Meisch 2000). The majority of the samples yield also marine to brackish microfossils, partly in high numbers. Their coexistence can be explained by erosion of Pleistocene upthrusted marine sediments in the catchment, transportation and deposition of easily transportable foraminifers, and, to a lesser degree, of ostracods into the lake basin. There is a general trend towards lower numbers of marine components over time which can be explained by changing water chemistry towards less marine-derived ions as indicated by the pore-water record. Based on the similarity between core-based microfossils and marine and Pleistocene marine reference samples, reworking phases are most prominent between 8.7 and 8.3 cal ka BP, 6.9 and 5.3 cal ka BP, and at the hiatus between 1.59 and 1.04 cal ka BP (Figure II-9b), due to higher allochthonous input from the catchment. Stronger geomorphic disturbance due to thermokarst, and possibly higher precipitation and runoff, are considered to be the most likely reasons. As the brackish microfossils are abundant and partly well-preserved, we cannot exclude that some of the brackish taxa actually lived in the lake if its water chemistry was oligohaline to mesohaline and relatively stable. Athalassic foraminifera and ostracod faunas are a common phenomenon in inland salt-water bodies (de Deckker 1981, Pint et al. 2012); hence, presence of brackish foraminifers or ostracods in Lake Herschel would not be surprising. Short distance to the sea makes an avian-mediated introduction of marginal marine taxa easy as long as salinity is high enough and relatively stable. Modern and Pleistocene marine reference samples show a trend towards lower similarity with the core over time (Figure II-9b). This trend might reflect stabilizing surface conditions around the lake towards the late Holocene; with the exception of the event being responsible for the hiatus.

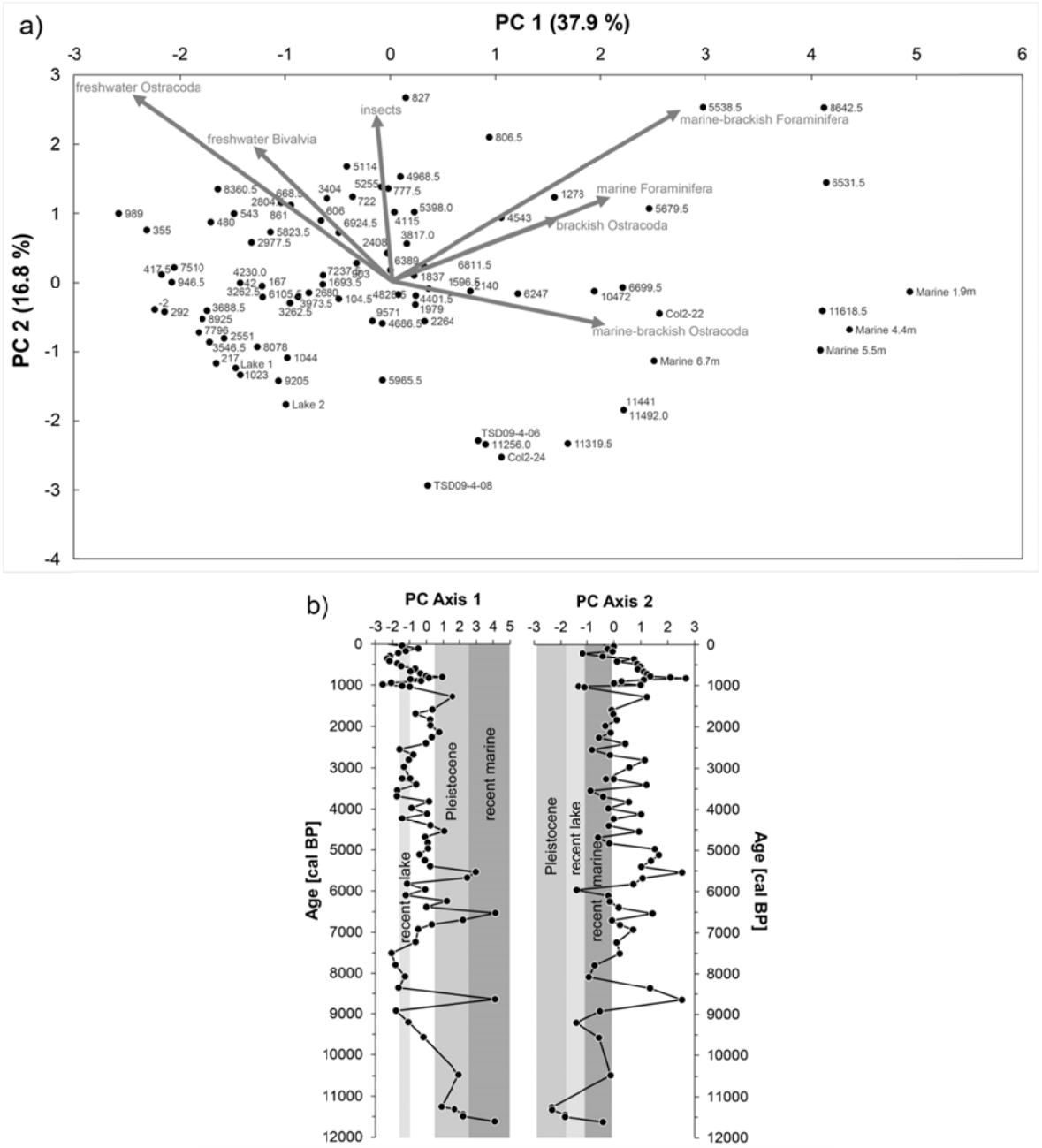

Figure II-9: Principal component analysis (PCA) of fauna assemblages in sediments of Lake Herschel. (a) The first two axes explain 54.7 % of the variance. Lake sediment samples from the core are compared to endmembers of recent littoral samples (Lake 1 and 2), recent marine samples (Marine 1.9 m, 4.4 m, 5.5 m and 6.7 m) and Pleistocene samples in permafrost (Col2-22 and -24 and TSD09-4-06). (b) Samples scores of the first (PC Axis 1) and second axis (PC Axis 2) from fauna assemblages in sediments of Lake Herschel are compared to sample scores to the endmembers of recent lake samples, recent marine samples and Pleistocene samples in permafrost to illustrate similarity and dissimilarity.

The lower proportion of freshwater taxa at the hiatus suggests higher mobilization of permafrost-derived marine and brackish taxa. Thereafter, the lake stabilized and freshwater taxa, especially ostracods, occur steadily and in relatively high numbers. Plant fragments including submersed taxa such as *Potamogeton* are frequent in sediments covering the last 1,000 years pointing to higher productivity and good preservation conditions. Higher productivity could have been caused by higher temperatures and less saline water conditions. Improved organic-matter preservation may also have occurred under anaerobic conditions and at episodes of rapid sedimentation and burial. Neither the calcareous microfossil record nor the XRF geochemical record shows any significant reaction to major Holocene climate fluctuations like the 8.2 ka event (Alley & Ágústsdóttir 2005), the 4.2 ka event (Staubwasser et al. 2003) or the 2.8 ka event (van Geel 2014), indicated as blue marker lines in figures II-3 and II-4. We therefore suggest that episodic thermokarst processes and changes in lake-water properties are the main drivers of ecosystem change, calcareous microfossil assemblages and geochemical processes in the lake catchment.

II-5.4 Regional pollen-based reconstruction of vegetation and climate

Our pollen-based climate record does not match well with other summer air temperature reconstructions from the region (Viau et al. 2008, Bunbury & Gajewski 2009, Kurek et al. 2009, Viau & Gajewski 2009, Fritz et al. 2012a, Gajewski, 2015a). First, the value of the squared chord distance in the reconstruction is rather high (Figure II-8; Gajewski 2015a) so the fossil samples from the Herschel core do not find good analogues in the modern dataset (Whitmore et al. 2005). Second, the resolution in the lower part is not high enough to clearly detect an early Holocene warming (Kaufman et al. 2004, Gajewski 2015a). The typical modern vegetation on Herschel Island consists of sedges, mosses and erect dwarf shrubs or low shrubs (CAVM Team 2003), and these conditions may not be well enough represented in the modern dataset.

Even during the Holocene, the mediating effect of sea-level rise on summer air temperatures seems to have changed the local climate very little. In contrast to other locations at the Arctic Ocean facing a broad and shallow shelf, Herschel Island is located close to the steep slopes of the Mackenzie Trough directly north of the island. As pointed out by Fritz et al. (2012b), the distance to the sea was not much farther than today, even at times of low sea level at the early phases of the Holocene.

Obu et al. (2015) and Wolter et al. (in press) have shown that vegetation on Herschel Island is closely related to morphology und sub-surface conditions, which cover a very broad range on the high-relief island. Wolter et al. (in press) demonstrated that even small-scale vegetation patterns vary within a single ecological unit such as polygonal wetlands depending on active-layer thickness and soil temperatures. The lake is surrounded by such ice-wedge polygons that are

dominated by *Cyperaceae*. This may help explain the excess of *Cyperaceae* in the pollen spectrum, which points to wet and cool climate conditions. Fritz et al. (in press) have used the *Cyperaceae*/*Poaceae* ratio from a peat core in ice-wedge polygon terrain on Herschel Island as an indicator of wetland development on the local scale rather than climate variation. However, high *Cyperaceae* values are also indicative of middle-Arctic conditions and *Poaceae* percentages are greater in High-Arctic pollen assemblages (Gajewski 2002). The mixing of a temperature and moisture signal may be contributing to the muted variation in the reconstruction.

Pollen concentrations and influx were higher during the past 5,500 years when the climate reconstruction indicates lower values of July temperature (Figure II-8), again contrary to the usual pattern in Arctic pollen diagrams (Gajewski 2015b). This suggests that pollen input to the sediment is more controlled by sedimentation patterns within the lake than due to pollen production in the catchment. The cooler temperatures in the late Holocene are in good agreement with a reconstruction of July temperatures based on pollen records from Banks, Victoria and Melville Island (Gajewski 2015a), in both cases showing an abrupt cooling that started between 4.0 and 3.5 cal ka BP.

II-6 Conclusions

Lake Herschel (Yukon, Canada) is an athalassic subsaline lake, a lake type that has rarely been studied in Arctic environments. Geochemical, hydrochemical, and paleoecological investigations of lake sediments in a thermokarst setting provided environmental conditions reconstructed on a local to regional scale.

1. The inc/coh ratio of XRF core scans provides a high-resolution semi-quantitative organic carbon proxy record that correlates well with TOC measurements performed at coarser resolution. XRF-derived Mn/Fe ratios are a robust indicator of aerobic vs. anaerobic conditions that moderate the preservation potential of organic matter in lake sediments.
2. Continuous desalinization is indicated by pore-water hydrochemistry and the XRF-derived Sr/Ca ratio. This implies increasing lake size and lake level together with a relatively decreasing input of solute-rich material.
3. The chemical composition of catchment sediments provides a predisposition for the living conditions of calcareous microfaunal communities in Lake Herschel. Elevated salinity allows the settlement of brackish taxa in an athalassic setting. The onset of the lacustrine sequence was characterized by reworking of older marine sediments and their associated microfauna as well as saline conditions that provided a habitat for autochthonous brackish ostracods and foraminifers. Intermittent similarities with reference samples from Pleistocene permafrost and low numbers of freshwater taxa indicate reworking phases of calcareous fossils and allochthonous transport into the lake by active thermokarst

processes and shore erosion.

4. Quantitative climate reconstruction based on pollen is not recommended for thermokarst lakes with actively eroding shore lines and small catchments. First, older pollen might be reworked from catchment sediments and reworking might not be clearly recognized due to short transport pathways. Second, small catchments may lead to an over-representation of local vegetation in the pollen assemblage, which is possibly not solely related to climate but to permafrost conditions regulating microtopography, nutrient availability and moisture regime.

With this multidisciplinary study, we have shown that thermokarst lake sediments represent a valuable environmental archive and that such aquatic ecosystems are extremely vulnerable to disturbances in the catchment. Projected permafrost thaw in the future will increase the lateral material transport into aquatic ecosystem, thus making thermokarst lakes an important net sink and location for carbon and nutrient turnover in terrestrial Arctic environments.

Acknowledgements

We wish to express our thanks to the Yukon Territorial Government and the Yukon Parks (Herschel Island Qiqiktaruk Territorial Park). The authors acknowledge the support of the Aurora Research Institute (ARI, Inuvik) for the field component. This study was partly funded by the German Federal Ministry of Education and Research (BMBF grant no. CAN 09/001, 01DM12002), the German Science Foundation (DFG grant no. LA 2399/3-1), the Helmholtz Association (grant no. VH-NG-801), a dissertation stipend by the Potsdam University and a fellowship by the Association for Canadian Studies awarded to J. Lenz, and by a fellowship awarded to M. Fritz by the German Federal Environmental Foundation (DBU). K. Gajewski and N. Paquette were supported by a Discovery Grant from the Natural Sciences and Engineering Research Council of Canada (NSERC). The study contributes to the *Arctic Ecological Network* (Arc-EcoNet) funded by the BMBF (grant no. 01DJ14003). Field support was provided by B. Radosavljevic, G. Müller, G. De Pascale, and S. McLeod. Analytical support was provided by L. Schirrmeister (AWI) for modern marine ostracods, by A. Eulenburg (AWI) with hydrochemical analyses and by V. Wennrich and Sonja Berg (University of Cologne, Germany) with XRF scanning.

Acknowledgements

I'm grateful for numerous experiences and increase of knowledge during my PhD study which was possible due to many people's support. Although not fully exhaustive, I wish to thank some of them by name:

First of all, I wish to thank Prof. Hans-Wolfgang Hubberten who enabled me to conduct my research at the Alfred Wegener Institute (AWI) in Potsdam and supported not only my proposal for a PhD stipend but helped realizing all other things I planned within my research study and on the side at AWI. The University Potsdam granted me a 3-years scholarship without this dissertation would not have been possible. Additional financial support was gratefully received by the Christiane Nüsslein-Volhard Foundation and the Alfred Wegener Institute. Finally, numerous travels to conferences, field work and a research stay in Iceland was enabled by funding from the Helmholtz Graduate School for Polar and Marine Research (POLMAR) and the Potsdam Graduate School (PoGS) who also offered an excellent program with courses to develop personal skills outside research.

Further on, I wish to thank my PhD committee including Prof. Hans-Wolfgang, Dr. Sebastian Wetterich, Prof. Guido Grosse, Prof. Ulrike Herzschuh, and Dr. Michael Fritz for sharing their valuable experiences and giving good advices during and outside our committee meetings. Dr. Sebastian Wetterich and Prof. Guido Grosse were great supervisors, advisors and mentors who were always within reach for me. I appreciated Sebastian's structural thinking and clear thoughts in organizing a manuscript and finding solutions in challenging situations. With Guido I started to work as a collaboration partner at the University of Alaska Fairbanks, who shared core material with me which resulted in two manuscripts. When I came back from maternity leave he turned into my colleague at AWI and adopted me in his ERC PETA-CARB group and finally I finish my PhD with Guido as a Professor at the University of Potsdam and soon successor of my supervisor Prof. Hubberten and leader of the Periglacial Research section at AWI. He was especially important to me because he is not only a local expert and "door opener" to Alaskan study sites but also offered unlimited professional guidance, global perspectives and great personal motivation. I have to say that I feel exceptional privileged by the professional people who surrounded me during the last years!

Another Alaskan expert was of great importance: Dr. Ben Jones enabled field work on the North Slope, Alaska, which was also supported with the help and man power of Dr. Chris Arp, Carson Baughman and pilot Jim Webster. I´m grateful for Ben`s advices, feedback and friendship.

Two manuscripts presented in the appendix were enabled by field work in the western Canadian Arctic led by Prof. Hugues Lantuit and Dr. Michael Fritz. The enthusiasm and initial support of both of them opened the fascinating world of Arctic Research to me.

POLMAR and an invitation by Prof. Steffen Mischke helped to finalize the second manuscript in this thesis at the University of Iceland.

I especially wish to thank all my co-authors for their valuable contributions. Their timely feedback allowed me to finish this dissertation in due time.

Further on, I thank all staff in logistics, administration and particularly in laboratories I was able to use at the Alfred Wegener Institute and Germany Research Center for Geosciences (GFZ) in Potsdam. I thank Caroline Coch for map preparation in this thesis; and I thank Béatrice Frank-Fahle and Alison Beamish for English language corrections. Cover and spine of this dissertation was designed by my sister Juliane Lenz.

Experiences outside my actual research project included engagement in the Permafrost Young Researchers Network (PYRN), in organizing committees of small workshops and big conferences and finally a Fellowship in the International Arctic Science Committee (IASC). I'm very grateful for these additional experiences which allowed me to develop specific skills and meet very special people.

Many awesome colleagues and valuable friends are working at the Alfred Wegener Institute in Potsdam; some of them have always been there (from my perspective) - some of them came and some of them went during my time in the department which has been several years. I wouldn't be able to give a complete list here and hope that you feel addressed when I say: Thank you for having spent an awesome time with me! Thanks for your support during less awesome periods and for many joyful moments which will always stay with me.

Finally I wish to thank my friends and family outside this insane science life:
I'm very grateful for having you in my life, for your open ears and different perspectives – whether you're nearby or very far away. For different reasons this has been a very exciting and sometimes exhausting period in my life and I highly acknowledge that you accompanied me.

I wish to close by expressing my special thanks to my mom and my sister, and to Christian and Jakob: I'm grateful for being strongly connected to you which enabled this work in many ways. Mein kleiner Jakob, Du wurdest in die Zeit dieser Arbeit hineingeboren und hast eine gute Portion Gewürz hinzugefügt. Du bereicherst mein Leben seitdem unendlich und daher sei diese Arbeit Dir gewidmet.

Eidesstattliche Erklärung

Hiermit versichere ich, dass ich die vorliegende Arbeit selbstständig verfasst und keine anderen als die angegebenen Quellen und Hilfsmittel verwendet habe.

Ich habe diese kumulative Dissertation am Alfred-Wegener-Institut, Helmholtz Zentrum für Polar und Meeresforschung in Potsdam erarbeitet und in englischer Sprache angefertigt. Diese Dissertation wird erstmalig und ausschließlich an der Universität Potsdam eingereicht.

Die dem Promotionsverfahren zugrundeliegende Promotionsordnung vom 18.09.2013 ist mir bekannt.

Potsdam, den 15.06.2016

Josefine Lenz